GENETIC AND TRANSCRIPTOMIC INSIGHTS INTO DISSIMILATORY ANTIMONATE REDUCTION BY AN OBLIGATELY ANAEROBIC BACTERIUM

by

CHRISTOPHER ANTHONY ABIN

(Under the Direction of James T. Hollibaugh)

ABSTRACT

Antimony (Sb) is an industrially significant metalloid that has been exploited by humans for the last 3,000 years. Although Sb is more toxic than its well-known group 15 neighbor, arsenic, relatively little is known about the fate and transport of Sb in the environment, especially with respect to the involvement of microorganisms in mediating redox transformations. The isolation and description of the first microorganism capable of using antimonate [Sb(V)] as a terminal electron acceptor to support growth was accomplished. The microorganism, designated *Desulfuribacillus stibiiarsenatis* MLFW-2^T, was an obligately anaerobic member of the order *Bacillales* of the phylum *Firmicutes*. It was isolated from anoxic sediments collected from the drainage area of a geothermal spring near the southern shore of alkaline, hypersaline Mono Lake, CA. MLFW-2^T was capable of using formate, lactate, pyruvate, or H_2 as electron donors with nitrate, nitrite, dimethyl sulfoxide (DMSO), selenate [Se(VI)], selenite [Se(IV)], arsenate [As(V)], or Sb(V) as electron acceptors. Consistent with the environment from which it was isolated, MLFW-2^T was found to be mesophilic, slightly alkaliphilic, and halotolerant. Dissimilatory Sb(V) reduction by MLFW-2^T was accompanied by the precipitation of antimonite [Sb(III)] as microcrystals of antimony trioxide.

The draft genome of MLFW-2^T contains 14 genes that encode the catalytic subunits of anaerobic respiratory reductases of the DMSO reductase (DMSOR) family of complex iron-sulfur molybdoenzymes. The involvement of each of these genes in the anaerobic respiratory chain of MLFW-2^T was evaluated by monitoring their relative expression during growth on nitrate, Se(VI), As(V), and Sb(V) using reverse transcription-quantitative polymerase chain reaction (RT-qPCR). The analyses identified the most probable terminal reductase for each of the oxyanions tested. Homologs of an operon encoding the putative terminal Sb(V) reductase were found to occur in microorganisms belonging to six described phyla and two candidate phyla across both prokaryotic domains of life. Lastly, the physiological response of MLFW-2^T to growth on Sb(V) and As(V) was examined using RNA sequencing. Sb was found to elicit a stronger oxidative stress response in comparison to As, with DNA, proteins, cofactors, and components of the cell envelope as the primary targets of damage.

INDEX WORDS: Antimony; Antimony Trioxide; Arsenic; Selenium; Anaerobic Respiration; Electron Acceptor; DMSO Reductase Family; Complex Iron-Sulfur Molybdoenzymes; Biogeochemistry; Mono Lake; *Desulfuribacillus*

GENETIC AND TRANSCRIPTOMIC INSIGHTS INTO DISSIMILATORY ANTIMONATE REDUCTION BY AN OBLIGATELY ANAEROBIC BACTERIUM

by

CHRISTOPHER ANTHONY ABIN

B.S., Florida International University, 2011

A Dissertation Submitted to the Graduate Faculty of The University of Georgia in Partial Fulfillment of the Requirements for the Degree

DOCTOR OF PHILOSOPHY

ATHENS, GEORGIA

2018

GENETIC AND TRANSCRIPTOMIC INSIGHTS INTO DISSIMILATORY ANTIMONATE REDUCTION BY AN OBLIGATELY ANAEROBIC BACTERIUM

by

CHRISTOPHER ANTHONY ABIN

Major Professor:	James T. Hollibaugh
Committee:	William B. Whitman
	Robert J. Maier
	Joy Doran Peterson

Electronic Version Approved:

Suzanne Barbour
Dean of the Graduate School
The University of Georgia
May 2018

DEDICATION

To my wife, Samantha, and our beautiful son, Jacob

ACKNOWLEDGEMENTS

I would like to express my deepest gratitude to my advisor, Tim Hollibaugh, for his guidance and support throughout my tenure as a doctoral student at UGA. From the moment I became a member of his lab, he made me feel welcome and appreciated. Rather than assign me to work on a specific project, he encouraged me to create my own based on what I found interesting and exciting. Over the years, he has taught me how to become a better and more efficient scientist. He has an infectious and unrivaled passion for science that I hope to achieve one day in my career. I will always be grateful to him for allowing me to take time off to be with my family after my son was born. He has shown that he is not only a great mentor, but an even better friend. I will truly miss my interactions with him, but I know that he will always be there for me if I ever need any advice.

I would also like to thank the members of my advisory committee – Barny Whitman, Rob Maier, and Joy Doran Peterson – for the advice and input they have provided to help strengthen my thesis work. I could not thank Barny enough for all of the advice he provided about microbial metabolism and techniques for the cultivation of anaerobes. He was always more than happy to allow me to use his facilities, even taking time out of his busy schedule to help me build a gassing station to grow anaerobes more efficiently. I will always be grateful to Rob and Joy for keeping me focused and excited about my research, especially when I became discouraged about challenging experiments. It was their bright and positive attitudes that made my annual committee meetings comfortable and fun. I would like to thank Joy for providing advice about

non-academic careers in science. It was her encouragement that led me to seriously reconsider the academic route.

I also owe many thanks to past and present members of the Hollibaugh laboratory, including Julian Damashek, Christian Edwardson, Bradley Tolar, Qian Liu, Carrie Givens, Meredith Ross, Aimee Okotie-Oyekan, Drew Duckett, Jelani Cheek, Corinne Sweeney, Annie Bratcher, and Erica Malagón. I want to especially recognize Christian for many helpful conversations about metalloids and microbes over the years. He was immensely helpful in providing advice on how to analyze my next-generation sequencing data. Additionally, he explained protocols and helped me troubleshoot laboratory equipment on countless occasions. Most of all, he was a great friend and someone that I felt comfortable sharing ideas with. Although Julian has only been a member of the lab for less than two years, I hope to always remain friends. He assumed a mentorship role with me that I am extremely appreciative of. Whether it was fielding questions about job hunting or life, in general, Julian was always willing to help. He is the perfect example of what a postdoc should be. I like to think that a greater power brought our two families together. My family and I will forever cherish our friendship with Julian, his wife Kendahl, and their two sons, August and Arlo.

My project would not have been possible without the help of various people and institutions at UGA. I would like to thank John Shields at Georgia Electron Microscopy for his continued help in preparing samples for electron microscopy. Becky Auxier, the former lab manager at the Chemical Analysis Laboratory at CAIS, performed most of the dissolved Sb analyses on our culture samples, often having the results back within a few hours. I would also like to thank the Sierra Nevada Aquatic Research Laboratory (SNARL) and Camp Valentine for hosting us on our sampling trip to Mono Lake during the Summer of 2012. I am grateful to five

members of the Moran Lab – Shalabh Sharma, Brent Nowinski, Frank Ferrer González, Courtney Thomas, and Christa Smith – for providing help with my project. Shalabh and Courtney provided timely help with bioinformatics. Christa, Brent, and Frank let me borrow equipment and reagents from the Moran lab on multiple occasions and provided advice on the best practices for RNA extraction.

Lastly, I would like to thank eight special people in my life. My parents, Juan Carlos and Yospa, have always been there for me, fostering my love for science from a young age. They are such wonderful people and words cannot begin to describe how much I love them. Without their care and support, I would not be the person that I am today. My brother, Kevin, is someone who has my deepest respect and admiration. Although he is younger than me, I often look up to him as a role model, as he shares my passion for science and discovery. I'm so glad that I was able to grow up with someone like him at my side. My in-laws – Armando, Maggie, and Cassie – have been like a second family to me. They have always been extremely generous and supportive, treating me like the son they never had. Lastly, I would like to thank my wife, Samantha, and my son, Jacob, for the love and encouragement they have provided on a daily basis. The two happiest days in my life were the day that I got married and the day that my son was born. Jacob has an infectious smile and a playful disposition that gets me through each day. My wife has provided such an immense amount of emotional support over the last fourteen years. She has kept me motivated throughout graduate school, helping to keep my spirits high when things did not go as planned. She is equally deserving of all of the honors I receive from this degree.

TABLE OF CONTENTS

Page

CHAPTER 1

INTRODUCTION AND LITERATURE REVIEW

Antimony Redox Chemistry

Antimony (Sb) is a naturally occurring, toxic metalloid that occupies group 15 of the periodic table along with nitrogen (N), phosphorus (P), arsenic (As), and bismuth (Bi). Sb can exist in a variety of oxidation states (-III, 0, III, and V), but is most commonly found in either the +3 or +5 oxidation states in biological and geochemical samples (Filella *et al.* 2002a). Equilibrium thermodynamics predict that Sb(V) and Sb(III) should be the favored forms in oxic and anoxic environments, respectively (Bard *et al.* 1985, Filella *et al.* 2002b). Like other metalloids, Sb(III) and Sb(V) do not exist as free ions in aqueous solution, but instead undergo spontaneous hydrolysis to form oxyanions. As a result of its larger ionic radius and lower charge density, Sb(V) coordinates octahedrally with oxygen, as opposed to P(V) and As(V), which both display tetrahedral coordination (Pauling 1933). On the other hand, both As(III) and Sb(III) coordinate trihedrally with oxygen (Sadiq 1997, Filella and May 2003). At environmentally relevant pH values, Sb(V) and Sb(III) are predominantly present as $Sb(OH)_6^-$ and $Sb(OH)_3$, respectively (Pitman *et al.* 1957, Baes and Mesmer 1986). While $Sb(OH)_6^-$ is readily soluble in solutions containing low concentrations of alkali metals, the neutral species $Sb(OH)_3$ precipitates at micromolar concentrations to yield antimony trisulfide (Sb_2S_3) in the presence of free sulfide or antimony trioxide (Sb_2O_3) in non-euxinic, aqueous solutions (Tourky and Mousa 1948, Gayer and Garrett 1952, Blandamer *et al.* 1974, Zotov *et al.* 2003). Like As, Sb is a strongly

chalcophilic element, although its affinity for sulfur is comparatively higher owing to its increased metallic character (Gebel 1997).

Industrial Uses for Antimony

It is estimated that the total amount of Sb currently in circulation is approximately 2-4 million metric tons (Mt), with global reserves totaling 1.5 Mt in 2017 (USGS 2018). China dominates the global Sb mining market, with the large Xikuangshan mine in Hunan Province producing a majority of the Sb ore (He *et al.* 2012). In order to meet increasing industrial demand, global production of Sb has more than doubled in the last 50 years from an estimated value of 70,000 Mt yr^{-1} in 1960 to 150,000 Mt yr^{-1} today (USGS 2018). Sb-containing compounds have wide ranging applications in a number of different industries. Sb is used to form alloys with other metals such as lead and tin in order to increase their hardness and strength (Filella *et al.* 2002a). Sb-containing alloys are used for the manufacture of castings, bearings, metal sheeting and piping, cable sheathing, and solders (ATSDR 2017). In recent years, Sb has been used as a dopant for silicon wafers in the manufacture of infrared detectors, diodes, and Hall-effect devices (Chin *et al.* 2010). Sb_2O_3 is a versatile compound that is used as a flame retardant, pigment, ceramic opacifier, glass decolorizing agent, mordant, PVC stabilizer, and catalyst for the production of polyethyleneterephthalate (PET) plastic for bottles, films, and food packaging (Filella *et al.* 2002a, Anderson 2012). Lastly, soluble compounds such as tartar emetic (potassium antimonyl tartrate) and pentavalent antimonials have historically been used to treat a variety of diseases and digestive ailments (Christopherson 1918, Marsden 1985). In fact, the Sb(V)-containing drugs Pentostam and Glucantime are still the treatments of choice for

several tropical protozoan diseases, including leishmaniasis, schistosomiasis, ascariasis, trypanosomiasis, and bilharziasis (Frézard *et al.* 2009, Frézard *et al.* 2013).

Antimony Toxicity

Sb and its compounds are considered to be pollutants of priority interest by both the U.S. Environmental Protection Agency and the Council of the European Communities (CEC 1976, Callahan *et al.* 1979). Sb has no known biological function and its toxicity closely mirrors that of its group 15 neighbor, As (Gebel 1997). In general, the toxicity of Sb stems from its propensity to bind sulfur- or oxygen-bearing ligands on cellular biomolecules. For example, both Sb(III) and Sb(V) form highly stable complexes with biomolecules containing adjacent carboxylic or hydroxyl groups, such as RNA and free ribonucleosides (Demicheli *et al.* 2002, Filella and May 2005, Hansen and Pergantis 2006, Tella and Pokrovski 2009). Sb(III) disrupts cellular redox homeostasis and protein function by reacting with the cytosolic and protein-associated pool of thiols (De Wolff 1995, Tirmenstein *et al.* 1997). Depletion of the cytosolic pools of major antioxidants such as glutathione, cysteine, and thioredoxin leads to oxidative stress through the accumulation of reactive oxygen species (Tirmenstein *et al.* 1995, Hashemzaei *et al.* 2015, Jiang *et al.* 2016). The binding of Sb(III) to thiol groups in proteins can disrupt normal functioning and the ability to coordinate cofactors such as metals, Fe-S clusters, and heme. For example, recent evidence has demonstrated that irreversible thiol-binding by Sb(III) indirectly induces DNA damage by deactivating proteins involved in DNA damage repair (Grosskopf *et al.* 2010, Koch *et al.* 2017).

Antimony in the Environment

Sb is present in aquatic and terrestrial environments as a result of mineral weathering, soil runoff, and anthropogenic sources such as mining and smelting, waste incineration, sewage sludge, vehicular emissions, and chemical fertilizers (Herath *et al.* 2017). In natural, unpolluted freshwater systems, dissolved Sb concentrations are typically less than 8 nM, while in geothermal waters such as hot springs and geysers, concentrations can be several orders of magnitude higher (Reimann *et al.* 2010). Analysis of cores from Arctic ice and ombrotrophic peat bogs in Switzerland, Scotland, and the Shetland Islands have revealed significant enrichments of atmospheric Sb extending back to the Roman period, indicating that anthropogenic fluxes have exceeded natural inputs for the past 2,000 years of human history (Shotyk *et al.* 1996, Shotyk *et al.* 2004, Krachler *et al.* 2005). In fact, the intensity of atmospheric Sb loading in Europe since the Roman period closely mirrors that of lead, another element that is highly detrimental to human health (Cloy *et al.* 2005, Shotyk *et al.* 2005). These findings, along with highly publicized studies demonstrating significant leaching of Sb from plastic drinking water bottles and fruit juice containers, have led some to question whether Sb has "become the new lead" (Fox 2006, Hansen and Pergantis 2006, Shotyk *et al.* 2006, Hansen *et al.* 2010).

Biogeochemical Cycling of Antimony: Antimonite Oxidation

Relatively little information exists on the biogeochemical cycling of Sb by living organisms. Due to an increased focus on Sb(III) oxidation, most of the literature relates to the oxidative side of the Sb cycle. The first microorganism to be shown to conserve energy from the oxidation of Sb(III) to Sb(V) was *Stibiobacter senarmontii*, a Gram-positive, chemoautotrophic

bacterium isolated from an Sb ore deposit in the former Yugoslavia (Lyalikova 1972, Lyalikova 1974, Lyalikova *et al.* 1976). *S. senarmontii* was shown to use oxygen as a terminal electron acceptor for the oxidation of the minerals sénarmontite (Sb_2O_3) and cervantite (Sb_2O_4) to stibiconite [$Sb_3O_6(OH)$]. Unfortunately, the strain was never preserved in an international culture collection or biorepository, thus eliminating any possibility for further study of its novel physiology. The Sb(III)-oxidizing strains that have been described in the four decades since then are generally aerobic heterotrophs that oxidize Sb(III) as a cellular detoxification method rather than as a means to support growth. Only one of these strains, *Variovorax paradoxus* IDSBO-4, has been shown to grow chemoautotrophically by coupling the aerobic oxidation of Sb(III) to CO_2 fixation (Terry *et al.* 2015). There are currently no known microorganisms capable of using Sb(III) as an electron donor to support anoxygenic photosynthetic growth.

At present, 76 strains of Sb(III)-oxidizing bacteria have been isolated from Sb-rich mining soils and contaminated sediments (Hamamura *et al.* 2013, Li *et al.* 2013, Shi *et al.* 2013, Nguyen and Lee 2015, Terry *et al.* 2015, Nguyen *et al.* 2017), As-rich sediments (Fan *et al.* 2008), and As-amended soils (Macur *et al.* 2004). These strains belong to 19 different genera (number of strains in parentheses): *Pseudomonas* (26), *Comamonas* (11), *Acinetobacter* (9), *Agrobacterium* (8), *Stenotrophomonas* (3), *Variovorax* (3), *Cupriavidus* (2), *Paracoccus* (2), *Sphingopyxis* (2), *Aminobacter* (1), *Arthrobacter* (1), *Bacillus* (1), *Ensifer* (1), *Hydrogenophaga* (1), *Janibacter* (1), *Sinorhizobium* (1), *Shinella* (1), *Stibiobacter* (1), and *Thiobacillus* (1). All of these Sb(III)-oxidizing bacteria can be classified into five phylogenetic groups: *Gammaproteobacteria* (51%), *Betaproteobacteria* (24%), *Alphaproteobacteria* (21%), *Actinobacteria* (3%), and *Firmicutes* (1%). Members of the *Betaproteobacteria* have displayed the highest rates of Sb(III) oxidation measured thus far. For example, cultures of *V. paradoxus*

IDSBO-4 and *Comamonas testosteroni* S44 oxidize Sb(III) at a rate of 50 and 16.7 μM day^{-1}, respectively (Li *et al.* 2013, Terry *et al.* 2015).

Historically, it was thought that aerobic oxidation of As(III) and Sb(III) could be catalyzed by the same enzyme, the aerobic As(III) oxidase AioAB. This theory stemmed from the fact that As(III) and Sb(III) share very similar chemical structures and properties. Additionally, the *ars* operon, which confers As resistance in phylogenetically-diverse bacteria, is transcriptionally responsive to Sb(III) and the ATP-driven efflux pump ArsAB can transport both As(III) and Sb(III) out of the cell (Ji and Silver 1992, Wu and Rosen 1993, Carlin *et al.* 1995, Cai *et al.* 1998, Sato and Kobayashi 1998, López-Maury *et al.* 2003, Meng *et al.* 2004). However, the notion that AioAB was responsible for Sb(III) oxidation was challenged by several findings. For example, an *aioA*-deficient mutant of the As(III) and Sb(III)-oxidizing bacterium *Agrobacterium tumefaciens* 5A was observed to oxidize Sb(III) at a rate equivalent to the wild-type strain (Lehr *et al.* 2007). Additionally, the Sb(III)-oxidizing bacterium *C. testosteroni* S44 cannot oxidize As(III) (Li *et al.* 2013), while the As(III)-oxidizing bacterium *Sinorhizobium* sp. A2 cannot oxidize Sb(III) (Hamamura *et al.* 2013). Indeed, only a minor proportion of Sb(III)-oxidizing bacteria encode homologues of *aioAB*, providing additional evidence that both species may be oxidized by separate and distinct mechanisms (Shi *et al.* 2013).

Recently, at least two enzymes have been shown to be directly involved in aerobic Sb(III) oxidation in *A. tumefaciens*. In contradiction to previous observations, *in vivo* experiments with *A. tumefaciens* 5A showed that AioAB was responsible for 34% of the Sb(III) oxidation activity in this organism (Wang *et al.* 2015). The authors argued that the previous failure to detect any difference in Sb(III) oxidation between the *aioA*-deficient mutant and the wild type strain was due to suboptimal culture and assay conditions. Experiments with AioAB purified from

Rhizobium sp. NT-26 showed that it could oxidize Sb(III) *in vitro*, albeit with a significantly decreased V_{max} relative to As(III) oxidation (Wang *et al.* 2015). Unlike the case for *A. tumefaciens* 5A, deletion of the *aioA* gene in *A. tumefaciens* GW4 had no effect on the efficiency of Sb(III) oxidation (Li *et al.* 2017). Using a proteomics approach, a protein belonging to the short-chain dehydrogenase/reductase family, coined AnoA, was induced significantly in the presence of Sb(III) (Li *et al.* 2015). Disruption of the *anoA* gene in *A. tumefaciens* GW4 resulted in a 27% decrease in Sb(III) oxidation efficiency relative to the wild type strain. *In vitro* experiments showed that AnoA could oxidize Sb(III) more efficiently than AioAB. Subsequent genomic analyses revealed that several Sb(III)-oxidizing bacteria, including all of the As(III)-oxidizing *Agrobacterium* and *Comamonas* strains isolated thus far, encode a homolog of the *anoA* gene (Li *et al.* 2016).

Biogeochemical Cycling of Antimony: Antimonate Reduction

In comparison to Sb(III) oxidation, the reductive side of the biogeochemical cycle has received relatively little attention. Based on the $\Delta G_f°$ values provided in the literature for $Sb(OH)_{6\,(aq)}^-$ (Diemar *et al.* 2009) and $Sb(OH)_{3(aq)}$ (Zotov *et al.* 2003), the midpoint potential of the Sb(V)/Sb(III) redox couple is +94 mV at pH 7. Therefore, the reduction of Sb(V) should be thermodynamically favored over the reduction of other commonly used electron acceptors such as fumarate (+33 mV), arsenate (+21 mV), sulfate (-216 mV), and elemental sulfur (-269 mV). *Shewanella oneidensis* MR-1 was the first bacterium to be shown to potentially use Sb(V) as an electron acceptor for growth (Ackermann 2008). However, the author did not provide evidence for Sb(V)-dependent consumption of lactate, so it is unknown whether *S. oneidensis* MR-1 can actually conserve energy from Sb(V) reduction. The first unequivocal evidence for microbially-

mediated Sb(V) reduction came from experiments involving Sb-rich anoxic sediments collected from a defunct stibnite mine (Kulp *et al.* 2014). Incubation of the sediments with Sb(V) and lactate under anoxic conditions led to the complete conversion of Sb(V) to Sb(III) within 100 hours. Kulp *et al.* (2014) also observed a similar phenomenon for sediments collected from an unpolluted lake, suggesting that Sb(V) reduction is a ubiquitous, microbially-mediated process.

Several reports of dissimilatory Sb(V)-reducing bacteria or enrichment cultures have surfaced over the last five years. An Sb(V)-reducing bacterium, *Sinorhizobium* sp. JUK-1, was isolated from Sb-contaminated sediment samples collected from the water outlet of a South Korean Sb refinery (Nguyen and Lee 2014). This bacterium was shown to grow heterotrophically by coupling acetate oxidation to the reduction of Sb(V), precipitating Sb(III) in the form of a complex mineral phase. Extensive investigations into the range of electron donors that can be coupled to Sb(V) reduction are currently underway. Using Sb-contaminated sediments as inocula for enrichment cultures, it was shown that Sb(V) reduction could not only be coupled to the oxidation of acetate and lactate, but to H_2, glucose, and inositol as well (Lai *et al.* 2016, Nguyen *et al.* 2018). The discovery of H_2-linked Sb(V) reduction is significant because it shows that the reductive side of the Sb cycle can proceed chemoautotrophically in the absence of organic carbon. Interestingly, the common organic acids propionate and butyrate have not yet been shown to serve as electron donors for Sb(V) reduction.

Sb(V)-reducing enrichment cultures grown on acetate and lactate have been dominated by members of the *Proteobacteria*, especially those belonging to the genera *Pseudomonas*, *Geobacter*, and *Thauera* (Lai *et al.* 2016, Nguyen *et al.* 2018, Zhu *et al.* 2018). While H_2-fed enrichments have also been dominated by *Proteobacteria*, the microbial communities are fundamentally different from cultures supplied with organic carbon. In one study, the

chemoautotrophic consortium consisted largely of *Rhizobiales* (Lai *et al.* 2016), while another community was dominated by *Rhodocyclales* and *Pseudomonadales* (Nguyen *et al.* 2018). Consistent with their capacity for fermentative growth, members of the genus *Clostridium* dominate enrichments supplied with fermentable substrates, such as glucose and inositol, as electron donors (Nguyen *et al.* 2018). With the exception of one report, the majority of Sb(III) produced by chemoautotrophic or chemoheterotrophic reduction of Sb(V) has been shown to precipitate as amorphous or crystalline Sb_2O_3 or Sb_2S_3.

Antimonate Reduction as a Bioremediation Strategy

In addition to supporting microbial growth, dissimilatory Sb(V) reduction may serve as a promising bioremediation strategy. In sulfidic environments, Sb(III) formed as a product of Sb(V) reduction can be immobilized by precipitation with free sulfide to yield Sb_2S_3. This phenomenon has been observed previously in an anoxic, Sb(V)-reducing enrichment culture containing sulfide as a reducing agent, where an amorphous orange precipitate formed as Sb(III) was produced (Kulp *et al.* 2014). Some researchers have employed this strategy for the removal of Sb from anoxic mine drainage (Wang *et al.* 2013) and wastewater (Zhu *et al.* 2018). In these cases, sulfate-reducing bacteria have been used to convert sulfate to sulfide, which then reacts with Sb(III) to form insoluble Sb_2S_3. In non-sulfidic environments, Sb(III) can either precipitate as Sb_2O_3, or become strongly adsorbed to the surface of iron, manganese, or aluminum (hydr)oxides (Thanabalasingam and Pickering 1990, Rauf *et al.* 1994, Guo *et al.* 2014). For example, the onset of anoxic conditions in Sb-contaminated, water-logged soils has been shown to lead to a decrease in dissolved Sb due to microbial Sb(V) reduction and immobilization of Sb(III) onto the surface of iron hydr(oxide) mineral phases (Hockmann *et al.* 2014). Therefore,

microbial Sb(V) reduction may be a promising strategy for the treatment of anoxic sediments, groundwaters, and wastewaters contaminated with toxic Sb.

OBJECTIVES

The objective of this dissertation was to isolate and describe a microorganism capable of using Sb(V) as a terminal electron acceptor for anaerobic respiration. Once isolated, the primary goal was to study the physiology of the Sb(V)-reducing microorganism, with particular emphasis placed on the identification of the metabolic pathway(s) involved in the process. At the time of this undertaking, unequivocal evidence for microbial growth by dissimilatory Sb(V) reduction did not yet exist. Previous authors reported active, biologically-linked Sb(V) reduction by mixed microbial communities from both natural and Sb-contaminated sediments, but not for a microorganism in pure culture.

In Chapter 2, the isolation and growth of a microorganism capable of using Sb(V) as a terminal electron acceptor is presented for the first time. A sample of anoxic, As-rich sediments collected from the outflow of a geothermal spring along the southern shore of Mono Lake, CA, was used as an inoculum for an enrichment culture in a chemically-defined medium. The enrichment culture was supplied with lactate as the electron donor and carbon source, and Sb(V) as the sole electron acceptor. Once the enrichment culture came to be dominated by a single morphotype, the microorganism, designated strain MLFW-2^T, was isolated using classical techniques and classified phylogenetically. A growth experiment demonstrated that Sb(V) reduction by MLFW-2^T was linked to lactate oxidation and growth. Lastly, the morphology, composition, and spectroscopic properties of the crystalline Sb(III) precipitate produced by

MLFW-2^T were examined using scanning electron microscopy, energy dispersive X-ray spectroscopy, X-ray diffraction, UV-Vis spectroscopy, and fluorescence spectroscopy.

Chapter 3 presents a formal description of the morphological, phylogenetic, physiological, and chemotaxonomic properties of strain MLFW-2^T. The cellular morphology of the strain was investigated using light, epifluorescence, and scanning electron microscopy, while the structure of the cell envelope was observed using transmission electron microscopy. The phylogeny of the strain was evaluated by comparing the sequence of the 16S ribosomal RNA gene with that of other bacteria using the neighbor-joining, maximum likelihood, and maximum parsimony methods. Average nucleotide identity, average amino acid identity, and percent of conserved proteins analyses were performed to refine the phylogenetic relationship between strain MLFW-2^T and other closely related microorganisms. The metabolic versatility of strain MLFW-2^T was explored by testing the range of electron donors and acceptors that could be used to support growth. Other aspects of its physiology and biochemistry, such as growth optima (temperature, salinity, and pH), polar lipids, fatty acids, dominant respiratory quinones, genomic G+C content, and antibiotic sensitivity were studied and compared with phylogenetically-related microorganisms. A draft genome of the novel strain obtained by paired-end sequencing on the Illumina MiSeq platform is provided. Lastly, the strain was deposited into two international culture collections and given a formal name, *Desulfuribacillus stibiiarsenatis* MLFW-2^T, in accordance with the Rules of the *Bacteriological Code* (1990 Revision).

Genomic and transcriptomic approaches were used to identify complex iron-sulfur molybdoenzymes of the DMSO reductase (DMSOR) family functioning as possible anaerobic respiratory reductases in MLFW-2^T in Chapter 4. For the most part, the DMSOR family is composed of reductases or oxidases that catalyze two-electron redox reactions. Genes encoding

enzymes of the DMSOR family were identified in the draft genome of MLFW-2^T using BLAST searches with known members of the family as queries. In order to assign functions to some of these genes, reverse transcription-quantitative PCR (RT-qPCR) was used to monitor the relative transcription of each target gene during growth of MLFW-2^T on nitrate, selenate [Se(VI)], As(V), and Sb(V). With the exception of Sb(V), all of these oxyanions are known substrates for anaerobic reductases of the DMSOR family. There was a high likelihood that the dissimilatory Sb(V) reductase was a member of the DMSOR family because As and Sb share chemical properties and Sb(V) reduction involves a two-electron redox reaction. The most likely terminal reductases for each of the substrates tested were identified based on the RT-qPCR data. In addition to these experiments, RNA sequencing was used to detect differences in the physiological response of strain MLFW-2^T to growth on Sb(V) and As(V).

REFERENCES

Ackermann S (2008). The interaction of iron oxides and sulfates with antimony, aqueous solutions, and bacteria: a mineralogical and geochemical study. PhD Thesis: Albert-Ludwigs-Universität, Freiburg im Breisgau, Germany.

Anderson CG (2012). The metallurgy of antimony. *Chem Erde Geochem* **72:** 3-8.

Agency for Toxic Substances & Disease Registry (ATSDR) (2017). *Toxicological profile for antimony and compounds*. Atlanta, GA: U.S. Department of Health and Human Services.

Baes CF, Mesmer RE (1986). *The Hydrolysis of Cations*. Malabar, FL: Krieger.

Bard AJ, Parsons R, Jordan J (1985). *Standard Potentials in Aqueous Solutions*. New York, NY: Marcel Dekker.

Blandamer MJ, Burgess J, Peacock RD (1974). Solubility of sodium hexahydroxoantimonate in water and in mixed aqueous solvents. *J Chem Soc (Dalton Trans)* **0:** 1084-1086.

Cai J, Salmon K, DuBow MS (1998). A chromosomal *ars* operon homologue of *Pseudomonas aeruginosa* confers increased resistance to arsenic and antimony in *Escherichia coli*. *Microbiol* **144:** 2705-2729.

Callahan MA, Slimak MW, Gabel NW, May IP, Fowler CF, Freed JR *et al.* (1979). *Water related fate of the 129 priority pollutants*. Washington D.C., USA: U.S. Environmental Protection Agency.

Carlin A, Shi W, Dey S, Rosen BP (1995). The *ars* operon of *Escherichia coli* confers arsenical and antimonial resistance. *J Bacteriol* **177:** 981-986.

Council of the European Communities (CEC) (1976). Council directive 76/464/EEC of 4 May 1976 on pollution caused by certain dangerous substances discharged into the aquatic environment of the community. *Off J Euro Commun* **L129:** 23-29.

Chin HS, Cheong KY, Razak KA (2010). Review on oxides of antimony nanoparticles: synthesis, properties, and applications. *J Mater Sci* **45:** 5993-6008.

Christopherson JB (1918). The successful use of antimony in bilharziosis administered as intravenous injections of anti-monium tartaratum (tartar emetic). *Lancet* **192:** 325-327.

Cloy JM, Farmer JG, Graham MC, MacKenzie AB, Cook GT (2005). A comparison of antimony and lead profiles over the past 2,500 years in Flanders Moss ombrotrophic peat bog, Scotland. *J Environ Monit* **7:** 1137-1147.

De Wolff FA (1995). Antimony and health. *Brit Med J* **310:** 1216-1217.

Demicheli C, Frézard F, Lecouvey M, Garnier-Suillerot A (2002). Antimony(V) complex formation with adenine nucleosides in aqueous solution. *Biochim Biophys Acta Gen Subj* **1570:** 192-198.

Diemar GA, Filella M, Leverett P, Williams PA (2009). Dispersion of antimony from oxidizing ore deposits. *Pure Appl Chem* **81:** 1547-1553.

Fan H, Su C, Wang Y, Yao J, Zhao K, Wang Y *et al.* (2008). Sedimentary arsenite-oxidizing and arsenate-reducing bacteria associated with high arsenic groundwater from Shanyin, Northwestern China. *J Appl Microbiol* **105:** 529-539.

Filella M, Belzile N, Chen YW (2002a). Antimony in the environment: a review focused on natural waters: I. Occurrence. *Earth-Sci Rev* **57:** 125-176.

Filella M, Belzile N, Chen YW (2002b). Antimony in the environment: a review focused on natural waters: II. Relevant solution chemistry. *Earth-Sci Rev* **59:** 265-285.

Filella M, May PM (2003). Computer simulation of the low-molecular-weight inorganic species distribution of antimony(III) and antimony(V) in natural waters. *Geochim Cosmochim Acta* **67:** 4013-4031.

Filella M, May PM (2005). Critical appraisal of available thermodynamic data for the complexation of antimony(III) and antimony(V) by low molecular mass organic ligands. *J Environ Monit* **7:** 1226-1237.

Fox M (2006). Is antimony the new lead? In *Highlights in Chemical Science*. Cambridge: RCS Publishing.

Frézard F, Demicheli C, Kato KC, Reis PG, Lizarazo-Jaimes EH (2013). Chemistry of antimony-based drugs in biological systems and studies of their mechanism of action. *Rev Inorg Chem* **33:** 1-12.

Frézard F, Demicheli C, Ribeiro R (2009). Pentavalent antimonials: new perspectives for old drugs. *Molecules* **14:** 2317-2336.

Gayer KH, Garrett AB (1952). The equilibria of antimonous oxide (rhombic) in dilute solutions of hydrochloric acid and sodium hydroxide at 25°. *J Am Chem Soc* **74:** 2353-2354.

Gebel T (1997). Arsenic and antimony: comparative approach on mechanistic toxicology. *Chem-Biol Interact* **107:** 131-144.

Grosskopf C, Schwerdtle T, Mullenders LHF, Hartwig A (2010). Antimony impairs nucleotide excision repair: XPA and XPE as potential molecular targets. *Chem Res Toxicol* **23:** 1175-1183.

Guo X, Wu Z, He M, Meng X, Jin X, Qiu N *et al.* (2014). Adsorption of antimony onto iron oxyhydroxides: adsorption behavior and surface structure. *J Hazard Mater* **276:** 339-345.

Hamamura N, Fukushima K, Itai T (2013). Identification of antimony- and arsenic-oxidizing bacteria associated with antimony mine tailing. *Microbes Environ* **28:** 257-263.

Hansen C, Tsirigotaki A, Bak SA, Pergantis SA, Sturup S, Gammelgaard B *et al.* (2010). Elevated antimony concentrations in commercial juices. *J Environ Monit* **12:** 822-824.

Hansen HR, Pergantis SA (2006). Mass spectrometric identification and characterization of antimony complexes with ribose-containing biomolecules and an RNA oligomer. *Anal Bioanal Chem* **385:** 821-833.

Hansen HR, Pergantis SA (2006). Detection of antimony species in citrus juices and drinking water stored in PET containers. *J Anal At Spectrom* **21:** 731-733.

Hashemzaei M, Pourahmad J, Safaeinejad F, Tabrizian K, Akbari F, Bagheri G *et al.* (2015). Antimony induces oxidative stress and cell death in normal hepatocytes. *Toxicol Environ Chem* **97:** 256-265.

He M, Wang X, Wu F, Fu Z (2012). Antimony pollution in China. *Sci Tot Environ* **421-422:** 41-50.

Herath I, Vithanage M, Bundschuh J (2017). Antimony as a global dilemma: geochemistry, mobility, fate and transport. *Environ Pollut* **223:** 545-559.

Hockmann K, Lenz M, Tandy S, Nachtegaal M, Janousch M, Schulin R (2014). Release of antimony from contaminated soil induced by redox changes. *J Hazard Mater* **275:** 215-221.

Ji G, Silver S (1992). Regulation and expression of the arsenic resistance operon from *Staphylococcus aureus* plasmid pI258. *J Bacteriol* **174:** 3684-3694.

Jiang X, An Z, Lu C, Chen Y, Du E, Qi S *et al.* (2016). The protective role of Nrf2-Gadd45b against antimony-induced oxidative stress and apoptosis in HEK293 cells. *Toxicol Lett* **256:** 11-18.

Koch B, Maser E, Hartwig A (2017). Low concentrations of antimony impair DNA damage signaling and the repair of radiation-induced DSB in HeLa S3 cells. *Arch Toxicol* **91:** 3823-3833.

Krachler M, Zheng J, Koerner R, Zdanowicz C, Fisher D, Shotyk W (2005). Increasing atmospheric antimony contamination in the northern hemisphere: snow and ice evidence from Devon Island, Arctic Canada. *J Environ Monit* **7:** 1169-1176.

Kulp TR, Miller LG, Braiotta F, Webb SM, Kocar BD, Switzer Blum J *et al.* (2014). Microbiological reduction of Sb(V) in anoxic freshwater sediments. *Environ Sci Technol* **48:** 218-226.

Lai C, Wen L, Zhang Y, Luo S, Wang Q, Luo Y *et al.* (2016). Autotrophic antimonate bio-reduction using hydrogen as the electron donor. *Water Res* **88:** 467-474.

Lehr CR, Kashyap DR, McDermott TR (2007). New insights into microbial oxidation of antimony and arsenic. *Appl Environ Microbiol* **73:** 2386-2389.

Li J, Wang Q, Li M, Yang B, Shi M, Guo W *et al.* (2015). Proteomics and genetics for identification of a bacterial antimonite oxidase in *Agrobacterium tumefaciens*. *Environ Sci Technol* **49:** 5980-5989.

Li J, Wang Q, Oremland RS, Kulp TR, Rensing C, Wang G (2016). Microbial antimony biogeochemistry: enzymes, regulation, and related metabolic pathways. *Appl Environ Microbiol* **82:** 5482-5495.

Li J, Wang Q, Zhang S, Qin D, Wang G. (2013). Phylogenetic and genome analyses of antimony-oxidizing bacteria isolated from antimony mined soil. *Int Biodeterior Biodegrad* **76:** 76-80.

Li J, Yang B, Shi M, Yuan K, Guo W, Wang Q *et al.* (2017). Abiotic and biotic factors responsible for antimonite oxidation in *Agrobacterium tumefaciens* GW4. *Sci Rep* **7:** 43225.

López-Maury L, Florencio FJ, Reyes JC (2003). Arsenic sensing and resistance system in the cyanobacterium *Synechocystis* sp. strain PCC 6803. *J Bacteriol* **185:** 5363-5371.

Lyalikova NN (1972). Oxidation of trivalent antimony up to higher oxides as an energy source for the development of a new autotrophic organism, *Stibiobacter* gen. nov. *Dokl Akad Nauk SSSR* **205:** 1228-1229.

Lyalikova NN (1974). *Stibiobacter senarmontii* - a new microorganism oxidizing antimony. *Mikrobiol* **43:** 941-948.

Lyalikova NN, Vedenina L, Romanova AK (1976). Assimilation of carbon dioxide by Stibiobacter senarmontii. *Mikrobiol* **45:** 552-554.

Macur RE, Jackson CR, Botero LM, McDermott TR, Inskeep WP (2004). Bacterial populations associated with the oxidation and reduction of arsenic in an unsaturated soil. *Environ Sci Technol* **38:** 104-111.

Marsden PD (1985). Pentavalent antimonials: old drugs for new diseases. *Rev Soc Bras Med Trop* **18:** 187-198.

Meng YL, Liu Z, Rosen BP (2004). As(III) and Sb(III) uptake by GlpF and efflux by ArsB in *Escherichia coli*. *J Biol Chem* **279:** 18334-18341.

Nguyen VK, Choi W, Park Y, Yu J, Lee T (2018). Characterization of diversified Sb(V)-reducing bacterial communities by various organic or inorganic electron donors. *Bioresour Technol* **250:** 239-246.

Nguyen VK, Choi W, Yu J, Lee T (2017). Microbial oxidation of antimonite and arsenite by bacteria isolated from antimony-contaminated soils. *Int J Hydrog Energy* **42:** 27832-27842.

Nguyen VK, Lee JU (2014). Isolation and characterization of antimony-reducing bacteria from sediments collected in the vicinity of an antimony factory. *Geomicrobiol J* **31:** 855-861.

Nguyen VK, Lee JU (2015). Antimony-oxidizing bacteria isolated from antimony-contaminated sediment – a phylogenetic study. *Geomicrobiol J* **32:** 50-58.

Pauling L (1933). The formulas of antimonic acid and the antimonates. *J Am Chem Soc* **55:** 1895-1900.

Pitman AL, Pourbaix M, de Zoubov N (1957). Potential-pH diagram of the antimony-water system: its applications to properties of the metal, its compounds, its corrosion, and antimony electrodes. *J Electrochem Soc* **104:** 594-600.

Rauf MA, Ikram M, Hasany SM, Najam-ud-Din SM (1994). Adsorption studies of antimony on manganese dioxide using radiometric techniques. *Adsorpt Sci Technol* **11:** 41-50.

Reimann C, Matschullat J, Birke M, Salminen R (2010). Antimony in the environment: Lessons from geochemical mapping. *Appl Geochem* **25:** 175-198.

Sadiq M (1997). Arsenic chemistry in soils: an overview of thermodynamic predictions and field observations. *Water Air Soil Pollut* **93:** 117-136.

Sato T, Kobayashi Y (1998). The *ars* operon in the *skin* element of *Bacillus subtilis* confers resistance to arsenate and arsenite. *J Bacteriol* **180:** 1655-1661.

Shi Z, Cao Z, Qin D, Zhu W, Wang Q, Li M *et al.* (2013). Correlation models between environmental factors and bacterial resistance to antimony and copper. *PLoS ONE* **8:** e78533.

Shotyk W, Cheburkin AK, Appleby PG, Fankhauser A, Kramers JD (1996). Two thousand years of atmospheric arsenic, antimony, and lead deposition recorded in an ombrotrophic peat bog profile, Jura Mountains, Switzerland. *Earth Planet Sci Lett* **145:** E1-E7.

Shotyk W, Krachler M, Chen B (2004). Antimony in recent, ombrotrophic peat from Switzerland and Scotland: comparison with natural background values (5,320 to 8,020 14C yr BP) and implications for the global atmospheric Sb cycle. *Global Biogeochem Cycles* **18:** GB1016.

Shotyk W, Krachler M, Chen B (2005). Antimony: global environmental contaminant. *J Environ Monit* **7:** 1135-1136.

Shotyk W, Krachler M, Chen B (2006). Contamination of Canadian and European bottled waters with antimony from PET containers. *J Environ Monit* **8:** 288-292.

Tella M, Pokrovski GS (2009). Antimony(III) complexing with O-bearing organic ligands in aqueous solution: an x-ray absorption fine structure spectroscopy and solubility study. *Geochim Cosmochim Acta* **73:** 268-290.

Terry LR, Kulp TR, Wiatrowski H, Miller LG, Oremland RS (2015). Microbiological oxidation of antimony(III) with oxygen or nitrate by bacteria isolated from contaminated mine sediments. *Appl Environ Microbiol* **81:** 8478-8488.

Thanabalasingam P, Pickering WF (1990). Specific sorption of antimony (III) by the hydrous oxides of Mn, Fe, and Al. *Water Air Soil Pollut* **49:** 175-185.

Tirmenstein MA, Mathias PI, Snawder JE, Wey HE, Toraason M (1997). Antimony-induced alterations in thiol homeostasis and adenine nucleotide status in cultured cardiac myocytes. *Toxicology* **119:** 203-211.

Tirmenstein MA, Plews PI, Walker CV, Woolery MD, Wey HE, Toraason MA (1995). Antimony-induced oxidative stress and toxicity in cultured cardiac myocytes. *Toxicol Appl Pharmacol* **130:** 41-47.

Tourky AR, Mousa AA (1948). Studies on some metal electrodes. Part V. The amphoteric properties of antimony tri- and pent-oxide. *J Chem Soc* **0:** 759-763.

U.S. Geological Survey (USGS) (2018). Antimony. In *Mineral Commodities Summaries 2018*. Reston, VA: U.S. Department of the Interior.

Wang H, Chen F, Mu S, Zhang D, Pan X, Lee DJ *et al.* (2013). Removal of antimony (Sb(V)) from Sb mine drainage: biological sulfate reduction and sulfide oxidation–precipitation. *Bioresour Technol* **146:** 799-802.

Wang Q, Warelow TP, Kang YS, Romano C, Osborne TH, Lehr CR *et al.* (2015). Arsenite oxidase also functions as an antimonite oxidase. *Appl Environ Microbiol* **81:** 1959-1965.

Wu J, Rosen BP (1993). Metalloregulated expression of the *ars* operon. *J Biol Chem* **268:** 52-58.

Zhu Y, Wu M, Gao N, Chu W, An N, Wang Q *et al.* (2018). Removal of antimonate from wastewater by dissimilatory bacterial reduction: role of the coexisting sulfate. *J Hazard Mater* **341:** 36-45.

Zotov AV, Shikina ND, Akinfiev NN (2003). Thermodynamic properties of the Sb(III) hydroxide complex $Sb(OH)_{3(aq)}$ at hydrothermal conditions. *Geochim Cosmochim Acta* **67:** 1821-1836.

CHAPTER 2

DISSIMILATORY ANTIMONATE REDUCTION AND PRODUCTION OF ANTIMONY TRIOXIDE MICROCRYSTALS BY A NOVEL MICROORGANISM[1]

[1]Abin C.A. and J.T. Hollibaugh. 2014. *Environ. Sci. Technol.* 48(1): 681-688. Reprinted here with permission of publisher.

ABSTRACT

Antimony (Sb) is a metalloid that has been exploited by humans since the beginning of modern civilization. The importance of Sb to such diverse industries as nanotechnology and health is underscored by the fact that it is currently the ninth-most mined metal worldwide. Although its toxicity mirrors that of its Group 15 neighbor arsenic, its environmental chemistry is very different and, unlike arsenic, relatively little is known about the fate and transport of Sb, especially with regard to biologically-mediated redox reactions. To further our understanding of the interactions between microorganisms and Sb, we have isolated a bacterium that is capable of using antimonate [Sb(V)] as a terminal electron acceptor for anaerobic respiration, resulting in the precipitation of antimonite [Sb(III)] as microcrystals of antimony trioxide. The bacterium, designated strain MLFW-2, is a sporulating member of a deeply-branching lineage within the order *Bacillales* (phylum *Firmicutes*). This report provides the first unequivocal evidence that a bacterium is capable of conserving energy for growth and reproduction from the reduction of antimonate. Moreover, microbiological antimonate reduction may serve as a novel route for the production of antimony trioxide microcrystals of commercial significance to the nanotechnology industry.

INTRODUCTION

Antimony (Sb) is a toxic metalloid that belongs to Group 15 of the periodic table along with nitrogen, phosphorus, arsenic, and bismuth. Sb can exist in a variety of oxidation states (-3, 0, +3, and +5) in nature, but is most commonly found in either the +3 or +5 states (Filella *et al.* 2002a). In aqueous solution at neutral pH, Sb(III) and Sb(V) do not exist as free ions, but instead undergo hydrolysis to form $Sb(OH)_3^0$ ("antimonite") and $Sb(OH)_6^-$ ("antimonate"), respectively (Filella *et al.* 2002b). Under oxic to slightly reducing conditions, Sb(V) is the thermodynamically favored form, while Sb(III) is predicted to predominate only under anoxic conditions. Sb is a strongly chalcophilic element and most often occurs as the mineral stibnite (Sb_2S_3) or in close association with sulfide-bearing ores of copper, lead, gold, silver, and arsenic (Filella *et al.* 2002a). Several oxygen-bearing mineral phases such as cervantite (Sb_2O_4), stibiconite [$Sb_3O_6(OH)$], sénarmontite (cubic Sb_2O_3), and valentinite (orthorhombic Sb_2O_3) comprise the principal weathering products of stibnite (Biver and Shotyk 2013). Sb and its compounds have been classified as pollutants of priority interest by the U.S. Environmental Protection Agency (Callahan *et al.* 1979) and European Union (CEC 1976) for the past four decades.

Antimony was once the ninth-most mined metal worldwide (Scheinost *et al.* 2006), with commercial importance to a diverse array of industries. For example, it is used in the semiconductor industry as a doping agent in the manufacture of infrared detectors, diodes, and Hall-effect devices (Filella *et al.* 2002a). It also forms alloys with lead that are used in the manufacture of lead-acid automobile batteries, type-metal for printing presses, small arms bullets, cable sheathing, and solders. The most important compound of commercial interest is antimony trioxide (Sb_2O_3) (Oorts *et al.* 2008). It is used as a flame retardant, pigment, ceramic

opacifier, glass decolorizing agent, mordant, PVC stabilizer, and catalyst for the production of polyethyleneterephthalate (PET) used in plastic drinking water bottles and fruit juice containers (Westerhoff *et al.* 2008, Wang *et al.* 2009). Compounds such as potassium antimonyl tartrate and pentavalent antimonials have historically been used to treat a variety of digestive ailments and tropical protozoan diseases such as leishmaniasis (Frézard *et al.* 2009, Frézard *et al.* 2013).

Although a great deal of literature exists concerning the interactions between microorganisms and metalloids such as arsenic (van Lis *et al.* 2013) and selenium (Stolz *et al.* 2006), microbe-Sb interactions remain poorly understood. Sb(III) has been shown to be unstable in the presence of oxygen, yet several studies have detected it in aerobic freshwater (Cutter *et al.* 1991, Sun *et al.* 1993), marine (Cutter *et al.* 1991, Sun and Yang 1999), and groundwater (Willis *et al.* 2011) systems. Similarly, Sb(V) has been found to constitute as much as 50% of total dissolved Sb in the anoxic bottom waters of the Baltic (Andreae and Froelich 1984) and Black Seas (Cutter 1991). While a variety of abiotic mechanisms have been put forth to account for these observations, biological activity remains as a plausible explanation for the geochemical disequilibria. The only microorganism shown to conserve energy from Sb(III) oxidation is the chemoautotrophic bacterium *Stibiobacter senarmontii* (Lyalikova 1972, Lyalikova 1974). The capacity to oxidize Sb(III) has also been documented for a strain of *Agrobacterium tumefaciens*, as well as a species of eukaryotic alga belonging to the order *Cyanidiales*, but it was not clear if these processes were tied to energy conservation (Lehr *et al.* 2007).

To our knowledge, unequivocal evidence for dissimilatory reduction of Sb(V) by a microorganism in pure culture has not yet been provided in the literature. Using the thermodynamic values for aqueous Sb species provided by Zotov *et al.* (2003) and Diemar *et al.* (2009), the Sb(V)/Sb(III) redox couple is expected to have a favorable standard midpoint

potential (E°') of +94 mV at neutral pH. Therefore, the opportunity exists for microorganisms to derive useable energy from the reduction of Sb(V) coupled to the oxidation of organic and inorganic compounds. Indeed, evidence for microbiological Sb(V) reduction was recently borne out of experiments with Sb-rich, anoxic sediments collected from a defunct stibnite mine near Yellow Pine, Idaho, USA (Kulp *et al.* 2014). When the sediments were amended with 1 mM Sb(V), incubation under anaerobic conditions resulted in the complete reduction of Sb(V) to Sb(III) within 100 hours. Absence of Sb(V) reduction in heat-killed controls suggested that this process was not governed by abiotic reactions. Hockmann *et al.* (2014) also showed that incubation of Sb-contaminated soils under waterlogged (and presumably anoxic) conditions resulted in the rapid conversion of endogenous Sb(V) to Sb(III).

Although these studies provide evidence for a robust Sb biogeochemical cycle, the role of microbes in Sb(V) reduction is not yet clear due to a lack of pure culture studies. The identification and isolation of Sb(V)-respiring microorganisms is therefore a priority if we wish to enhance our understanding of the processes responsible for the transformation of this highly toxic element in nature. Here, we report the enrichment and isolation of a bacterium capable of respiring Sb(V) as a terminal electron acceptor (TEA) for anaerobic respiration, producing crystalline Sb_2O_3 as a by-product. This discovery not only establishes a definitive link between microorganisms and the reductive side of the Sb biogeochemical cycle, but may provide a novel route for the synthesis of Sb_2O_3 microcrystals potentially suitable for commercial applications.

MATERIALD AND METHODS

Study Site and Sample Collection

The site of sample collection was located at Navy Beach, on the southwestern shore of Mono Lake, California, USA (Figure 2.S1A). Mono Lake is an alkaline, hypersaline lake that occupies a hydrographically closed and volcanically active basin on the eastern edge of the Sierra Nevada mountain range (Bischoff *et al.* 1993). Shoreline springs are prominent along the northwestern, western, and southwestern shores of the lake, where they occur as either diffuse seepages from littoral sands or as artesian features with clearly defined orifices at or below lake level (Lee 1969, Basham 1988). The Navy Beach Warm Springs (NBWS) consist of three interconnected geothermal springs that occupy a 150 m trend oriented from SW to NE relative to the shoreline at Navy Beach. Previous studies have demonstrated that the waters issuing from these springs are deeply circulating groundwaters that do not originate from within the lake and have a radiocarbon age in excess of 22,000 years (Oremland *et al.* 1987, Neumann and Dreiss 1995). The temperature and pH of the NBWS waters have remained fairly constant at 35.2 ± 3.4°C and 6.6 ± 0.2, respectively, since sampling began in 1967 (Bischoff *et al.* 1993).

Anoxic sediments were collected during June 2012 by extracting a 35 cm core from an area receiving hydrological inputs from NBWS-1, the northernmost feature of the NBWS closest to the shoreline of Mono Lake (37°56'28.7" N, 119°1'22.4" W; Figure 2.S1B). The core was sectioned aseptically at intervals of approximately 5 cm and sediment subsamples (200 mL) were stored in sealed mason jars and maintained at 4°C during transport to the University of Georgia (UGA). The total metal content of a section of the core from 5 – 10 cm depth was determined following acid digestion according to previously published methods (Imperato *et al.* 2003). Whole sediment was dried in an oven overnight at 75°C and a 5 g subsample was added to 100

mL of 3:1 concentrated HCl:HNO_3 and refluxed for 1 hour at 100°C. After cooling to room temperature, the supernatant was separated from undigested solids by centrifugation and diluted to 200 mL with deionized water. The Center for Applied Isotope Studies (CAIS) at UGA determined the elemental composition of the sediment extracts using a VG PlasmaQuad 3 inductively coupled plasma mass spectrometer (Thermo Scientific, Waltham, MA).

Enrichment Culture

The basal salts medium (BSM) used for enrichment cultures contained the following ingredients (in grams per liter of deionized H_2O): K_2CO_3 x $1.5H_2O$, 0.240; KH_2PO_4, 0.100; K_2HPO_4, 0.150; NH_4Cl, 0.075; vitamin solution (Oremland *et al.* 1994), 10 mL; and SL-10 trace metals solution (Widdel *et al.* 1983) supplemented with 14 mM $MgCl_2$ and 700 µM $CaCl_2$, 1 mL. The pH of the medium was adjusted to 7.0 with HCl and it was made anaerobic by incubating in a Coy anaerobic chamber (Coy Laboratory Products, Grass Lake, MI) containing an atmosphere of 95% N_2 + 5% H_2 for at least 96 hours prior to use. Sterile stock solutions of ACS reagent-grade sodium L-lactate, $KSb(OH)_6$, and Na_2S x $9H_2O$ were prepared in deionized water and made anaerobic in the same fashion as described above. All subsequent manipulations were performed within the anaerobic chamber.

Inocula for enrichment cultures were taken from a depth of 5–10 cm within the sediment core. The enrichments were initiated by adding ~1.0 g (wet weight) of sediment to a total of 100 mL BSM amended with 2 mM $KSb(OH)_6$, 1 mM sodium L-lactate, and 100 µM Na_2S x $9H_2O$ (as reducing agent and sulfur source) in sterile 160-mL glass serum bottles. The serum bottles were then closed with sterilized butyl rubber stoppers and crimp-sealed with aluminum caps before being placed in the dark at 30°C without shaking. Every week, or after the medium had

become noticeably turbid to the naked eye, enrichments were sub-cultured by dispensing 10 mL of culture into 90 mL of fresh BSM and incubating as described above. A pure culture of a candidate Sb(V)-reducing microorganism was obtained by three successive rounds of dilution streaking onto anaerobic BSM agar plates (1.5% w/v) supplemented with 2 mM Sb(V), 1 mM lactate, and 100 μM Na_2S x $9H_2O$.

Growth Experiments

The isolate was systematically tested for the ability to use Sb(V) as a TEA for anaerobic respiration with lactate as the sole carbon and energy source. Cells grown to mid-log phase were collected by centrifugation under an atmosphere of 95% N_2 + 5% H_2 and re-suspended in fresh BSM. Aliquots of this suspension were dispensed in triplicate into each of three sets of 200 mL glass serum bottles containing BSM medium. The first set of serum bottles contained BSM amended with 2 mM Sb(V) alone; the second set, 1 mM lactate alone; and the third set, both 2 mM Sb(V) and 1 mM lactate but with a heat-killed inoculum that had been subjected to two successive rounds of autoclaving. These first three sets of triplicate incubations served as negative controls. To a fourth set of triplicate serum bottles, an aliquot of washed, live cells was added to BSM medium amended with 2 mM Sb(V) and 1 mM lactate. The bottles were then closed with butyl rubber stoppers and sealed with aluminum crimp caps before incubating at 30 °C in the dark without shaking. At regular intervals, an aliquot of culture was extracted using a sterile needle and syringe for analysis of cell density, Sb(V)/Sb(III) concentrations, and lactate/acetate concentrations.

Phylogenetic Analysis

Genomic DNA was extracted from a cell pellet using a phenol-chloroform method as described elsewhere (Ferrari and Hollibaugh 1999). The concentration and purity of extracted DNA was measured on a NanoDrop 2000c UV-Vis spectrophotometer (Thermo Fisher Scientific). The polymerase chain reaction (PCR) was used to amplify a large region of the 16S rRNA gene using universal bacterial primers 27F and 1492R (Lane 1991). Bands corresponding to PCR products of the expected size were excised from a 1% agarose gel and purified using a QiaQuik Gel Extraction Kit (Qiagen, Valencia, CA) according to the manufacturer's instructions. The amplicons were sequenced in both directions using a BigDye Terminator Cycle Sequencing Kit (Applied Biosystems, Foster City, CA) and the primers given above by the Georgia Genomics Facility at UGA. The 16S rRNA gene sequence was assembled using Geneious v6.1 (Biomatters Ltd., Auckland, New Zealand), resulting in a consensus sequence of 1,446 bp with ~250 bp of overlap. The consensus sequence was compared to others in the GenBank database using the BLASTn algorithm (Altschul *et al.* 1990) and subsequently aligned with related sequences using ClustalW (Thompson *et al.* 1994). A phylogenetic tree based on 1,440 bp of the 16S rRNA gene sequence was generated with bootstrap values (1,000 replicates) using the neighbor-joining method (Saitou and Nei 1987) and Jukes-Cantor evolutionary distances (Jukes and Cantor, 1969). The partial 16S rRNA gene sequence obtained in this study has been deposited in NCBI Genbank under accession number KF387535.

Microscopy

Light and epifluorescence microscopy were performed using a Leica DM RXA microscope (Leica, Wetzlar, Germany). The Gram stain reaction was performed according to

standard methods (Gerhardt *et al.* 1981). Changes in cell density during growth experiments were measured by epifluorescence microscopy after staining with 0.01% (w/v) acridine orange (Hobbie *et al.* 1977). For scanning electron microscopy (SEM), cells were harvested by filtration onto a 0.22 µm polycarbonate membrane filter, successively fixed with 2.5% glutaraldehyde and 1% osmium tetroxide, and visualized on a Zeiss 1450EP scanning electron microscope (Carl Zeiss NTS, Peabody, MA) at the Center for Advanced Ultrastructural Research (CAUR) at UGA. Sb_2O_3 microcrystals were separated from spent culture medium by centrifugation at 1,000 x g for 1 minute and then rinsed successively with distilled water, 100% acetone, and distilled water. The supernatant was removed after each rinse by centrifugation at 2,000 x g for 2 minutes. This series was repeated for a total of three cycles. The microcrystals were then dried overnight in an oven at 65°C.

EDS, XRD, and UV-Vis/Photoluminescence Spectroscopy

Sb_2O_3 microcrystals were harvested and washed using the method described above. We assumed that the microcrystals were substantially free of cells and cellular debris after the final washing step, as cells were not evident when the preparations were examined using SEM. Elemental analysis of Sb_2O_3 microcrystals by energy dispersive x-ray spectroscopy (EDS) was performed using an Oxford Instruments X-Act 10mm^2 Silicon Drift Detector (Oxford Instruments, Concord, MA) attached to a Zeiss 1450EP SEM at the CAUR. The microcrystal samples were spread onto a conductive carbon tab and a thin carbon fiber coating was applied in preparation for EDS. X-ray powder diffraction (XRD) analysis was performed at the X-ray Diffraction Lab at UGA using a Bruker D8 Advance X-ray powder diffractometer (Bruker AXS, Karlsruhe, Germany) with CoKα radiation (λ = 1.789 Å) operating at 40 kV and 40 mA. The

room temperature UV-visible absorption spectrum of a suspension of Sb_2O_3 microcrystals in ethanol was recorded on an Evolution 201 UV-Vis spectrophotometer (Thermo Fisher Scientific) equipped with a xenon flash lamp. The room temperature photoluminescence spectrum was measured with an Aqualog spectrofluorometer (Horiba Scientific, Edison, NJ) at an excitation wavelength of 325 nm.

Chemical Analyses

Lactate and acetate concentrations were measured by high performance liquid chromatography (HPLC) using a mobile phase of 0.016 N sulfuric acid and a UV detector set at a wavelength of 210 nm (Culbertson *et al.* 1988). Sb(III) and Sb(V) concentrations were determined after selective removal of Sb(III) by a liquid-liquid extraction technique (Han-wen *et al.* 1982, Garboś *et al.* 2000). Briefly, a 2 mL aliquot of culture was dispensed into a 5 mL centrifuge tube and acidified with 0.5 mL of 4.5 M HCl. Following acidification, 0.5 mL of a 100 mM solution of N-benzoyl-N-phenylhydroxylamine (BPHA) in chloroform was added to the tube and the mixture was vortexed for 15 minutes at room temperature. Between pH 0.3 - 6, Sb(III) forms a non-ionic complex with poorly water-soluble BPHA, quantitatively extracting Sb(III) into the organic phase, whereas no extraction of Sb(V) occurs within this range (Lyle and Shendrikar 1966, Chen and Tsai 1983). Following extraction, the concentration of Sb remaining in the aqueous phase [corresponding to Sb(V)] was measured by the CAIS at UGA using a Thermo Jarrell-Ash 965 inductively coupled argon plasma optical emission spectrometer (Thermo Jarrell-Ash, Franklin, MA) at an emission wavelength of 206.83 nm. The Sb(III) concentration was then determined by subtracting the measured Sb(V) concentration from the total amount of Sb(V) initially added to the culture medium. This subtractive method was used

because direct measurement of Sb(III) proved extremely difficult due to precipitation of Sb_2O_3 along the inner surfaces of serum bottles.

RESULTS AND DISCUSSION

Sediment Analysis

The total metal content of the NBWS-1 subsurface sediments is presented in Table 2.S1. The sediments were enriched in several metal(loid)s, including arsenic, molybdenum, selenium, tellurium, and Sb relative to average concentrations obtained for the upper continental crust (Wedepohl 1995, Hu and Gao 2008). It is important to note, however, that the Sb concentration measured in these sediments fell within the background range of 0.06 – 8.8 ppm observed for a variety of unpolluted soils from the United States, Europe, and Australia (Wilson *et al.* 2010). Sb concentrations in contaminated soils have been reported to be as high as 80,200 mg kg^{-1} at an historic Sb smelting site in New Zealand (Wilson *et al.* 2004), 15,100 mg kg^{-1} for a site in Italy impacted by past Sb mining activities (Baroni *et al.* 2000), and 17,500 ppm for shooting ranges in Switzerland (Johnson *et al.* 2005, Scheinost *et al.* 2006).

Enrichment Culture and Isolation of an Sb(V)-Respiring Bacterium

Incubation of NBWS-1 sediments under anoxic conditions with millimolar concentrations of lactate and Sb(V) as the electron donor and acceptor pair, respectively, resulted in the stimulation of microbial growth relative to un-amended controls (data not shown). The enrichment culture was transferred repeatedly over a period of six months until it was observed to be dominated by a single Gram positive, motile, endospore-forming, and rod-shaped morphotype. The organism, which formed small, off-white colonies on agar media, was isolated

into pure culture and designated strain MLFW-2. SEM visualization of a culture of strain MLFW-2 grown on Sb(V) and lactate showed that cells form filaments of highly variable length during growth (Figure 2.1).

Growth Experiments

Strain MLFW-2 was capable of completely respiring a 2 mM amendment of Sb(V) in approximately 80 hours at 30 ^{o}C using lactate as the sole carbon and energy source (Figure 2.2). Sb(V) reduction was accompanied by an equivalent rise in the concentration of Sb(III), while lactate was stoichiometrically oxidized to acetate and presumably HCO_3^- according to the reaction: $Lactate^- + 2Sb(OH)_6^- + H^+ \rightarrow Acetate^- + HCO_3^- + 2Sb(OH)_3^0 + 4H_2O$ ($\Delta G°' = -199.7$ kJ mol^{-1}). These activities coincided with a roughly 100-fold increase in cell density, indicating that strain MLFW-2 conserved energy from this process. This reaction was biological in nature, as Sb(V) reduction was not observed in controls lacking lactate or in which cells were heat-killed prior to inoculation, and no growth was obtained on lactate alone (Figure 2.2).

Sb(V) reduction was followed by the precipitation and accumulation of a white, crystalline substance (Figure 2.S2). Visualization of the precipitate by SEM showed that it consisted of an unequal mixture of two crystal phases, a less common cubic phase and a more prevalent prismatic phase displaying complex "bowtie" morphology. The cubic crystals were fairly uniform and ranged in size from 5 – 20 μm (Figure 2.3A). The "bowtie"-shaped crystals were generally 10 – 60 μm long and composed of blade-like projections radiating outward from each end of a central bundle (Figure 2.3B). Elemental analysis of both crystal phases by EDS showed that they were comprised of Sb and O in atomic ratios consistent with antimony trioxide (Sb_2O_3) (Figure 2.S3A and B). The EDS spectrum of commercially-available, ≥99% pure Sb_2O_3

was identical to the spectrum of the precipitate from our cultures (Figure 2.S3C). Sb_2O_3 naturally occurs as either one of two polymorphs, cubic (sénarmontite) and orthorhombic (valentinite). While sénarmontite is the most stable polymorph at temperatures up to 570°C, valentinite is metastable and can be synthesized in the laboratory at room temperature (Biver and Shotyk 2013). XRD analysis confirmed that the precipitate from our cultures consisted of a mixture of cubic and orthorhombic Sb_2O_3 (Figures 2.3C and D). In light of these observations, the immediate product of Sb(V) reduction is likely the amphoteric hydroxide $Sb(OH)_3^0$, which subsequently loses water and precipitates as sénarmontite and valentinite according to the reaction: $Sb(OH)_3^0 \rightarrow Sb_2O_{3(s)} + 3H_2O$ (Zotov *et al.* 2003).

Phylogenetic Analysis

Phylogenetic analysis of a ~1,450 bp region of the 16S rRNA gene of strain MLFW-2 revealed the isolate to be a member of a novel, deeply branching family within the order *Bacillales* of the phylum *Firmicutes* (Figure 2.4). The MLFW-2 16S rRNA gene shared only 94% nucleotide identity with that of its closest described relative, *Desulfuribacillus alkaliarsenatis* AHT28, an obligately anaerobic, dissimilatory sulfur- and arsenate-reducing haloalkaliphile isolated from a Russian soda lake (Sorokin *et al.* 2012). Like strain MLFW-2, *D. alkaliarsenatis* exhibits a curved, rod-shaped morphology and forms round, terminal endospores. The 16S rRNA gene of strain MLFW-2 also shared 93% sequence identity with two low G+C Gram-positive sequences, "clone ML-S-9" and "clone mixed culture A-1", retrieved from enrichments of Mono Lake water samples amended with arsenate and sulfide (Hollibaugh *et al.* 2006).

Optical Properties of Sb_2O_3 Microcrystals

We analyzed the optical properties of Sb_2O_3 precipitated in cultures of strain MLFW-2 to compare them with those of crystals prepared by chemical syntheses. The room temperature UV-Vis absorption spectrum measured from 200 – 800 nm showed that the biologically-produced Sb_2O_3 provide a broad absorption within this range with two prominent maxima at 255 nm and 364 nm (Figure 2.5A). These values are in close proximity to those reported in the literature for artificially-synthesized Sb_2O_3 nano-rods (Deng *et al.* 2007), nano-wires (Deng *et al.* 2006), and nano-belts (Li *et al.* 2013), as well as "bowtie"- (Ge *et al.* 2010) and "flower"-shaped (Ge *et al.* 2013) microstructures. The peak at 255 nm corresponds to a λ_{onset} of 372.6 nm and a calculated optical band gap (E_g)of 3.33 eV, which is very similar to that of bulk orthorhombic phase Sb_2O_3 (λ_{onset} = 375 nm; E_g = 3.30 eV) (Geng *et al.* 2011). Moreover, the room temperature photoluminescence spectrum recorded at an excitation wavelength of 325 nm showed that the Sb_2O_3 microcrystals exhibit a strong photoluminescence maximum at ~378 nm (Figure 2.5B). Once again, this value was in agreement with others reported in the literature for Sb_2O_3 nano- and micro-crystals of diverse morphologies synthesized using chemical methods (Deng *et al.* 2006, Deng *et al.* 2007, Ge *et al.* 2010, Li *et al.* 2013).

Taken together, our data demonstrate that the Sb_2O_3 microcrystals produced in cultures of strain MLFW-2 possess properties that may be of commercial significance to the nanotechnology, optics, and electronics industries. As an important member of the Group V- VI semiconductors, Sb_2O_3 has been proposed as a promising material for optical applications due to its wide optical band gap, low melting point, low phonon energy, and high refractive index (Cebriano *et al.* 2012). In recent years, a series of Sb_2O_3 crystals with novel morphologies have been synthesized using various strategies, of which the solvothermal and hydrothermal routes

remain the most popular. However, these processes can be expensive and often require elevated temperatures or the use of noxious reagents, thus leading to the creation of toxic waste streams (Jha *et al.* 2009). We have now demonstrated that commercially significant Sb_2O_3 microstructures can be synthesized using a potentially inexpensive, relatively non-toxic, and sustainable method. Thus, dissimilatory Sb(V) reduction has the potential to serve as an alternative to chemical routes for the controlled synthesis of such microstructures.

In conclusion, the results presented here demonstrate for the first time that microorganisms are capable of anaerobic respiration using Sb(V) as a TEA. This discovery completes the biogeochemical cycle of Sb through the oxidized and reduced forms and adds Sb to the growing list of metals and metalloids whose oxidized species are capable of serving as electron acceptors for microbial respiration – a list that already includes Fe, Mn, Cr, U, V, Co, Tc, Np, Pu, As, Se, and Te. Importantly, the insoluble product of Sb(V) reduction, Sb_2O_3, is a versatile compound that may be of commercial significance to the emerging nanotechnology industry.

ACKNOWLEDGEMENTS

We thank Christian Edwardson, Meredith Ross, and Robert Jellison for assistance with field work and sample collection; Rebecca Auxier for assistance with chemical analyses; John Shields for help with SEM and EDX analyses; and Paul Schroeder for assistance with XRD. We are also grateful to the Sierra Nevada Aquatic Research Laboratory (SNARL) for allowing us to use their facilities for sample processing. This work was supported by National Science Foundation grant EAR 09-52271 (JTH); NSF Graduate Research Fellowship DGE-0903734 (CAA); and an Alfred P. Sloan Minority PhD Program scholarship (CAA). With regards to author contributions, CAA and JTH planned the project; CAA conducted the experiments and performed data analyses; and CAA and JTH interpreted the results and wrote the manuscript.

REFERENCES

Altschul SF, Gish W, Miller W, Myers EW, Lipman DJ (1990). Basic local alignment search tool. *J Mol Biol* **215:** 403-410.

Andreae MO, Froelich PN (1984). Arsenic, antimony, and germanium biogeochemistry in the Baltic Sea. *Tellus B Chem Phys Meteorol* **36:** 101-117.

Baroni F, Boscagli A, Protano G, Riccobono F (2000). Antimony accumulation in *Achillea ageratum, Plantago lanceolata* and *Silene vulgaris* growing in an old Sb-mining area. *Environ Pollut* **109:** 347-352.

Basham SL (1988). Analyses of the shoreline springs in the Mono Basin, California: with applications to the groundwater system. MS Thesis: University of California, Santa Cruz, CA.

Bischoff JL, Stine S, Rosenbauer RJ, Fitzpatrick JA, Stafford Jr TW (1993). Ikaite precipitation by mixing of shoreline springs and lake water, Mono Lake, California, USA. *Geochim Cosmochim Acta* **57:** 3855-3865.

Biver M, Shotyk W (2013). Stibiconite (Sb_3O_6OH), senarmontite (Sb_2O_3) and valentinite (Sb_2O_3): dissolution rates at pH 2–11 and isoelectric points. *Geochim Cosmochim Acta* **109:** 268-279.

Callahan MA, Slimak MW, Gabel NW, May IP, Fowler CF, Freed JR *et al.* (1979). *Water related fate of the 129 priority pollutants*. Washington D.C., USA: U.S. Environmental Protection Agency.

Cebriano T, Méndez B, Piqueras J (2012). Micro- and nanostructures of Sb_2O_3 grown by evaporation–deposition: self assembly phenomena, fractal and dendritic growth. *Mater Chem Phys* **135:** 1096-1103.

Council of the European Communities (CEC) (1976). Council directive 76/464/EEC of 4 May 1976 on pollution caused by certain dangerous substances discharged into the aquatic environment of the community. *Off J Euro Commun* **L129:** 23-29.

Chen SG, Tsai HT (1983). Using NAA for the determination of antimony in trichlorosilane with substoichiometric extraction. *J Chinese Chem Soc* **30:** 249-253.

Culbertson CW, Strohmaier FE, Oremland RS (1988). Acetylene as a substrate in the development of primordial bacterial communities. *Orig Life Evol Biosph* **18:** 397-407.

Cutter GA (1991). Dissolved arsenic and antimony in the Black Sea. *Deep Sea Res Part A Oceanogr Res Pap* **38:** S825-S843.

Cutter LS, Cutter GA, San Diego-McGlone MLC (1991). Simultaneous determination of inorganic arsenic and antimony species in natural waters using selective hydride generation with gas chromatography/photoionization detection. *Anal Chem* **63:** 1138-1142.

Deng Z, Chen D, Tang F, Meng X, Ren J, Zhang L (2007). Orientated attachment assisted self-assembly of Sb_2O_3 nanorods and nanowires: end-to-end versus side-by-side. *J Phys Chem C* **111:** 5325-5330.

Deng Z, Tang F, Chen D, Meng X, Cao L, Zou B (2006). A simple solution route to single-crystalline Sb_2O_3 nanowires with rectangular cross sections. *J Phys Chem B* **110:** 18225-18230.

Diemar GA, Filella M, Leverett P, Williams PA (2009). Dispersion of antimony from oxidizing ore deposits. *Pure Appl Chem* **81:** 1547-1553.

Ferrari VC, Hollibaugh JT (1999). Distribution of microbial assemblages in the Central Arctic Ocean Basin studied by PCR/DGGE: analysis of a large data set. *Hydrobiologia* 401, 55-68.

Filella M, Belzile N, Chen YW (2002a). Antimony in the environment: a review focused on natural waters: I. Occurrence. *Earth-Sci Rev* **57:** 125-176.

Filella M, Belzile N, Chen YW (2002b). Antimony in the environment: a review focused on natural waters: II. Relevant solution chemistry. *Earth-Sci Rev* **59:** 265-285.

Frézard F, Demicheli C, Ribeiro R (2009). Pentavalent antimonials: new perspectives for old drugs. *Molecules* **14:** 2317-2336.

Frézard F, Demicheli C, Kato KC, Reis PG, Lizarazo-Jaimes EH (2013). Chemistry of antimony-based drugs in biological systems and studies of their mechanism of action. *Rev Inorg Chem* **33:** 1-12.

Garboś S, Bulska E, Hulanicki A, Fijałek Z, Sołtyk K (2000). Determination of total antimony and antimony(V) by inductively coupled plasma mass spectrometry after selective separation of antimony(III) by solvent extraction with N-benzoyl-N-phenylhydroxylamine. *Spectrochim Acta B* **55:** 795-802.

Ge S, Wang Q, Li J, Shao Q, Wang X (2010). Controllable synthesis and formation mechanism of bow-tie-like Sb_2O_3 nanostructures via a surfactant-free solvothermal route. *J Alloys Comp* **494:** 169-174.

Ge S, Yang X, Shao Q, Liu Q, Wang T, Wang L *et al.* (2013). Self-assembled flower-like antimony trioxide microstructures with high infrared reflectance performance. *J Solid State Chem* **200:** 136-142.

Geng A, Cao L, Wan C, Ma Y (2011). High-pressure Raman investigation of the semiconductor antimony oxide. *Phys Status Solidi C* **8:** 1708-1711.

Gerhardt P, Costilow RN, Krieg NR, Murray RGE, Nester EW, Phillips GB *et al.* (1981). *Manual of methods for general bacteriology*. Washington D.C.: ASM Press.

Han-wen S, Xiao-quan S, Zhe-ming N (1982). Selective separation and differential determination of antimony(III) and antimony(V) by solvent extraction with N-benzoyl-N-phenylhydroxylamine and graphite-furnace atomic-absorption spectrometry using a matrix-modification technique. *Talanta* **29:** 589-593.

Hobbie JE, Daley RJ, Jasper S (1977). Use of nuclepore filters for counting bacteria by fluorescence microscopy. *Appl Environ Microbiol* **33:** 1225-1228.

Hockmann K, Lenz M, Tandy S, Nachtegaal M, Janousch M, Schulin R (2014). Release of antimony from contaminated soil induced by redox changes. *J Hazard Mater* **275:** 215-221.

Hollibaugh JT, Budinoff C, Hollibaugh RA, Ransom B, Bano N (2006). Sulfide oxidation coupled to arsenate reduction by a diverse microbial community in a soda lake. *Appl Environ Microbiol* **72:** 2043-2049.

Hu Z, Gao S (2008). Upper crustal abundances of trace elements: a revision and update. *Chem Geol* **253:** 205-221.

Imperato M, Adamo P, Naimo D, Arienzo M, Stanzione D, Violante P (2003). Spatial distribution of heavy metals in urban soils of Naples city (Italy). *Environ Pollut* **124:** 247-256.

Jha AK, Prasad K, Prasad K (2009). A green low-cost biosynthesis of Sb_2O_3 nanoparticles. *Biochem Eng J* **43:** 303-306.

Johnson CA, Moench H, Wersin P, Kugler P, Wenger C (2005). Solubility of antimony and other elements in samples taken from shooting ranges. *J Environ Qual* **34:** 248-254.

Jukes TH, Cantor CR (1969). Evolution of protein molecules. In *Mammalian Protein Metabolism*. New York, NY: Academic Press.

Kulp TR, Miller LG, Braiotta F, Webb SM, Kocar BD, Switzer Blum J, Oremland RS (2014). Microbiological reduction of Sb(V) in anoxic freshwater sediments. *Environ Sci Technol* **48:** 218-226.

Lane DJ (1991). 16S/23S rRNA sequencing. In *Nucleic Acid Techniques in Bacterial Systematics*. New York, NY: John Wiley and Sons.

Lee K (1969). Infrared exploration for shoreline springs at Mono Lake, California. PhD Thesis: Stanford University, Palo Alto, CA.

Lehr CR, Kashyap DR, McDermott TR (2007). New insights into microbial oxidation of antimony and arsenic. *Appl Environ Microbiol* **73:** 2386-2389.

Li BJ, Xu XM, Zhao YB, Zhang ZJ (2013). Fabrication of Sb_2O_3 nanobelt bundles via a facile ultrasound-assisted room temperature liquid phase chemical route and evaluation of their optical properties. *Mater Res Bull* **48:** 1281-1287.

Lyalikova NN (1972). Oxidation of trivalent antimony up to higher oxides as an energy source for the development of a new autotrophic organism, *Stibiobacter* gen. nov. *Dokl Akad Nauk SSSR* **205:** 1228-1229.

Lyalikova NN (1974). *Stibiobacter senarmontii* - a new microorganism oxidizing antimony. *Mikrobiol* **43:** 941-948.

Lyle SJ, Shendrikar AD (1966). Some aspects of n-benzoylphenylhydroxylamine and cupferron reactions with tin, antimony and other selected elements. *Anal Chim Acta* **36:** 286-297.

Neumann K, Dreiss S (1995). Strontium 87/strontium 86 ratios as tracers in groundwater and surface waters in Mono Basin, California. *Water Resour Res* **31:** 3183-3193.

Oorts K, Smolders E, Degryse F, Buekers J, Gascó G, Cornelis G *et al.* (2008). Solubility and toxicity of antimony trioxide (Sb_2O_3) in soil. *Environ Sci Technol* **42:** 4378-4383.

Oremland RS, Switzer Blum J, Culbertson CW, Visscher PT, Miller LG, Dowdle P *et al.* (1994). Isolation, growth, and metabolism of an obligately anaerobic, selenate-respiring bacterium, strain SES-3. *Appl Environ Microbiol* **60:** 3011-3019.

Oremland RS, Miller LG, Whiticar MJ (1987). Sources and flux of natural gases from Mono Lake, California. *Geochim Cosmochim Acta* **51:** 2915-2929.

Saitou N, Nei M (1987). The neighbor-joining method: a new method for reconstructing phylogenetic trees. *Mol Biol Evol* **4:** 406-425.

Scheinost AC, Rossberg A, Vantelon D, Xifra I, Kretzschmar R, Leuz AK *et al.* (2006). Quantitative antimony speciation in shooting-range soils by EXAFS spectroscopy. *Geochim Cosmochim Acta* **70:** 3299-3312.

Sorokin DY, Tourova TP, Sukhacheva MV, Muyzer G (2012). *Desulfuribacillus alkaliarsenatis* gen. nov. sp. nov., a deep-lineage, obligately anaerobic, dissimilatory sulfur and arsenate-reducing, haloalkaliphilic representative of the order *Bacillales* from soda lakes. *Extremophiles* **16:** 597-605.

Stolz JF, Basu P, Santini JM, Oremland RS (2006). Arsenic and selenium in microbial metabolism. *Ann Rev Microbiol* **60:** 107-130.

Sun YC, Yang JY (1999). Simultaneous determination of arsenic(III,V), selenium(IV,VI), and antimony(III,V) in natural water by coprecipitation and neutron activation analysis. *Anal Chim Acta* **395:** 293-300.

Sun YC, Yang JY, Lin YF, Yang MH, Alfassi ZB (1993). Determination of antimony(III,V) in natural waters by coprecipitation and neutron activation analysis. *Anal Chim Acta* **276:** 33-37.

Thompson JD, Higgins DG, Gibson TJ (1994). CLUSTAL W: improving the sensitivity of progressive multiple sequence alignment through sequence weighting, position-specific gap penalties and weight matrix choice. *Nucleic Acids Res* **22:** 4673-4680.

van Lis R, Nitschke W, Duval S, Schoepp-Cothenet B (2013). Arsenics as bioenergetic substrates. *Biochim Biophys Acta Bioenerg* **1827:** 176-188.

Wang D, Zhou Y, Song C, Shao M (2009). Phase and morphology controllable synthesis of Sb_2O_3 microcrystals. *J Cryst Growth* **311:** 3948-3953.

Wedepohl KH (1995). The composition of the continental crust. *Geochim Cosmochim Acta* **59:** 1217-1232.

Westerhoff P, Prapaipong P, Shock E, Hillaireau A (2008). Antimony leaching from polyethylene terephthalate (PET) plastic used for bottled drinking water. *Water Res* **42:** 551-556.

Widdel F, Kohring GW, Mayer F (1983). Studies on dissimilatory sulfate-reducing bacteria that decompose fatty acids. III. Characterization of the filamentous gliding *Desulfonema limnicola* gen. nov., sp. nov., and *Desulfonema magnum* sp. nov. *Arch Microbiol* **134:** 286-294.

Willis S, Haque S, Johannesson K (2011). Arsenic and antimony in groundwater flow systems: a comparative study. *Aquat Geochem* **17:** 775-807.

Wilson NJ, Craw D, Hunter K (2004). Antimony distribution and environmental mobility at an historic antimony smelter site, New Zealand. *Environ Pollut* **129:** 257-266.

Wilson SC, Lockwood PV, Ashley PM, Tighe M (2010). The chemistry and behaviour of antimony in the soil environment with comparisons to arsenic: a critical review. *Environ Pollut* **158:** 1169-1181.

Zotov AV, Shikina ND, Akinfiev NN (2003). Thermodynamic properties of the Sb(III) hydroxide complex $Sb(OH)_{3(aq)}$ at hydrothermal conditions. *Geochim Cosmochim Acta* **67:** 1821-1836.

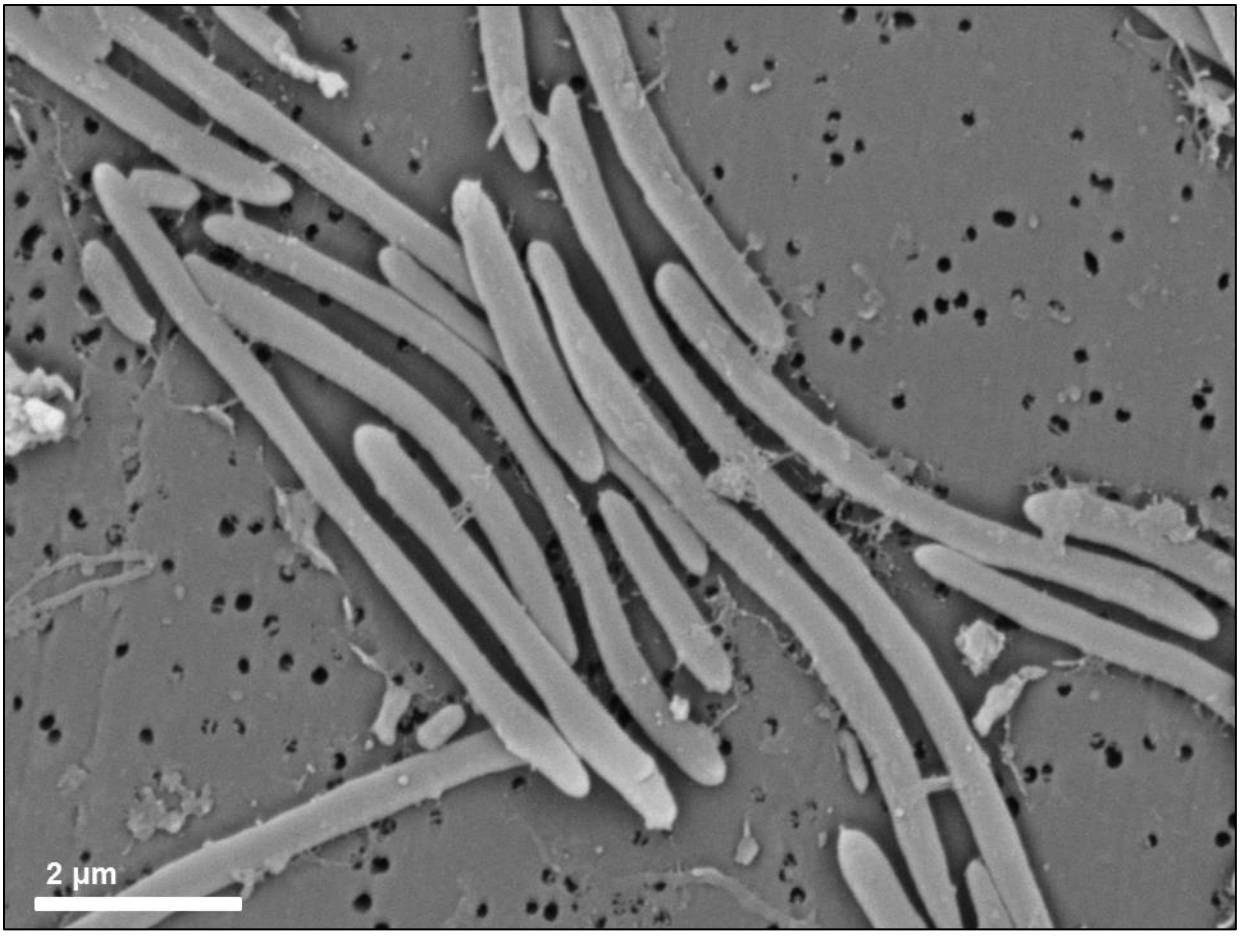

Figure 2.1. Scanning electron micrograph of cells of strain MLFW-2 grown on Sb(V) and lactate in a basal salts medium.

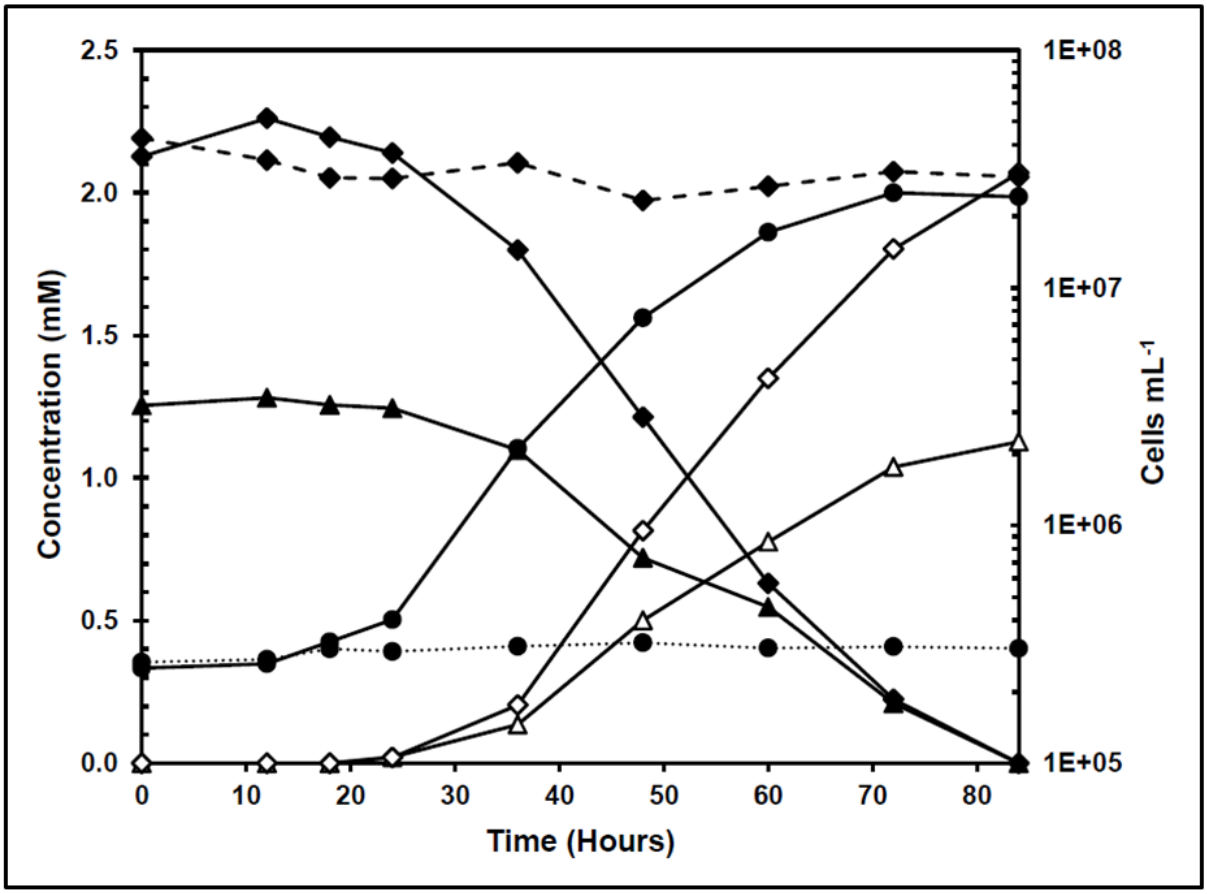

Figure 2.2. Anaerobic growth of strain MLFW-2 at 30 °C with 2 mM Sb(V) and 1 mM lactate as electron acceptor and donor, respectively. Symbols are as follows: Sb(V) (◆); Sb(III) (◇); lactate (▲); acetate (△); cells (●). The dashed line corresponds to the Sb(V) concentration in a control lacking lactate. The dotted line corresponds to the cell density in a control containing lactate but lacking Sb(V).

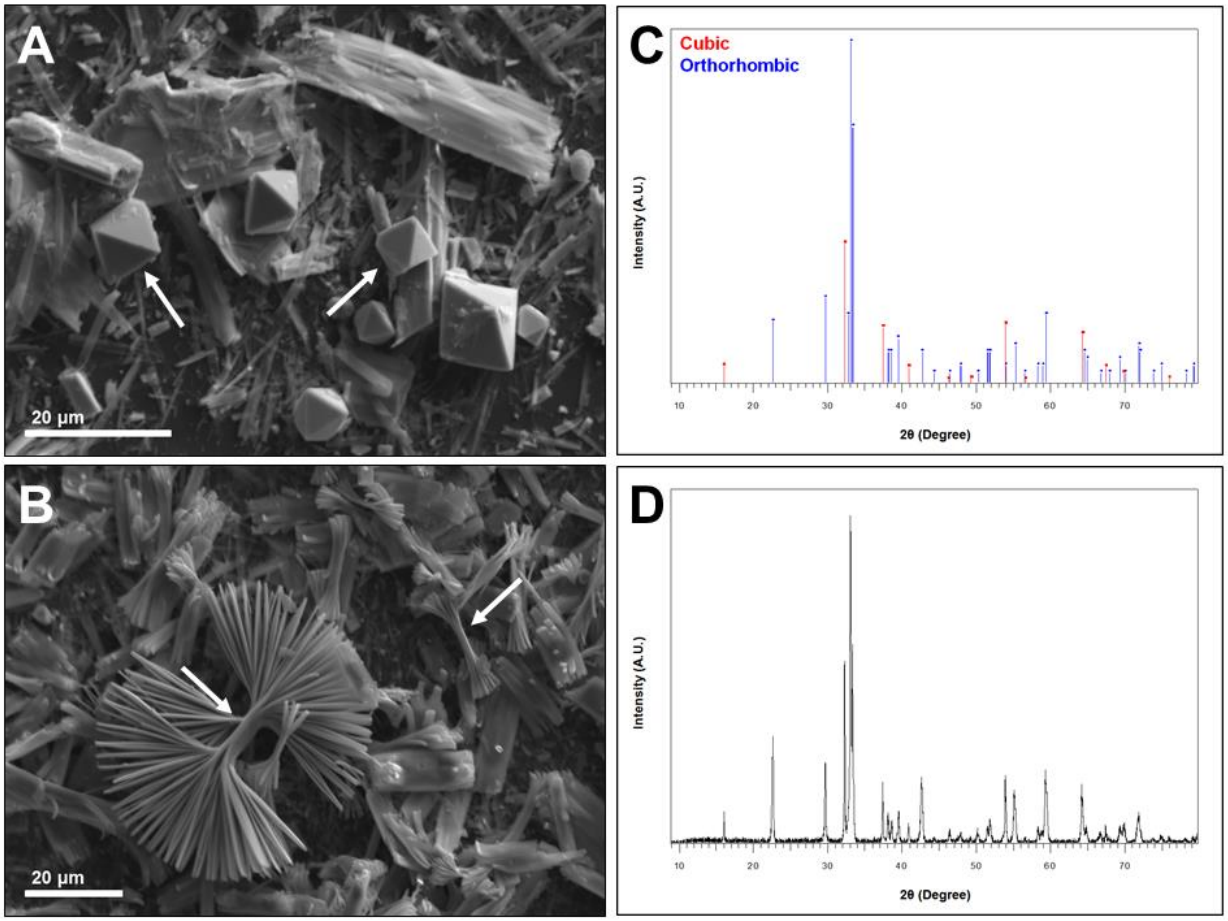

Figure 2.3. (A and B) Scanning electron micrographs of the microcrystals produced by strain MLFW-2 during dissimilatory Sb(V) reduction in a basal salts medium. **(C)** Standard X-ray diffraction patterns associated with the cubic (red; JCPDS 05-0534) and orthorhombic (blue; JCPDS 11-689) polymorphs of Sb_2O_3. **(D)** X-ray diffraction pattern of the microcrystals produced by strain MLFW-2.

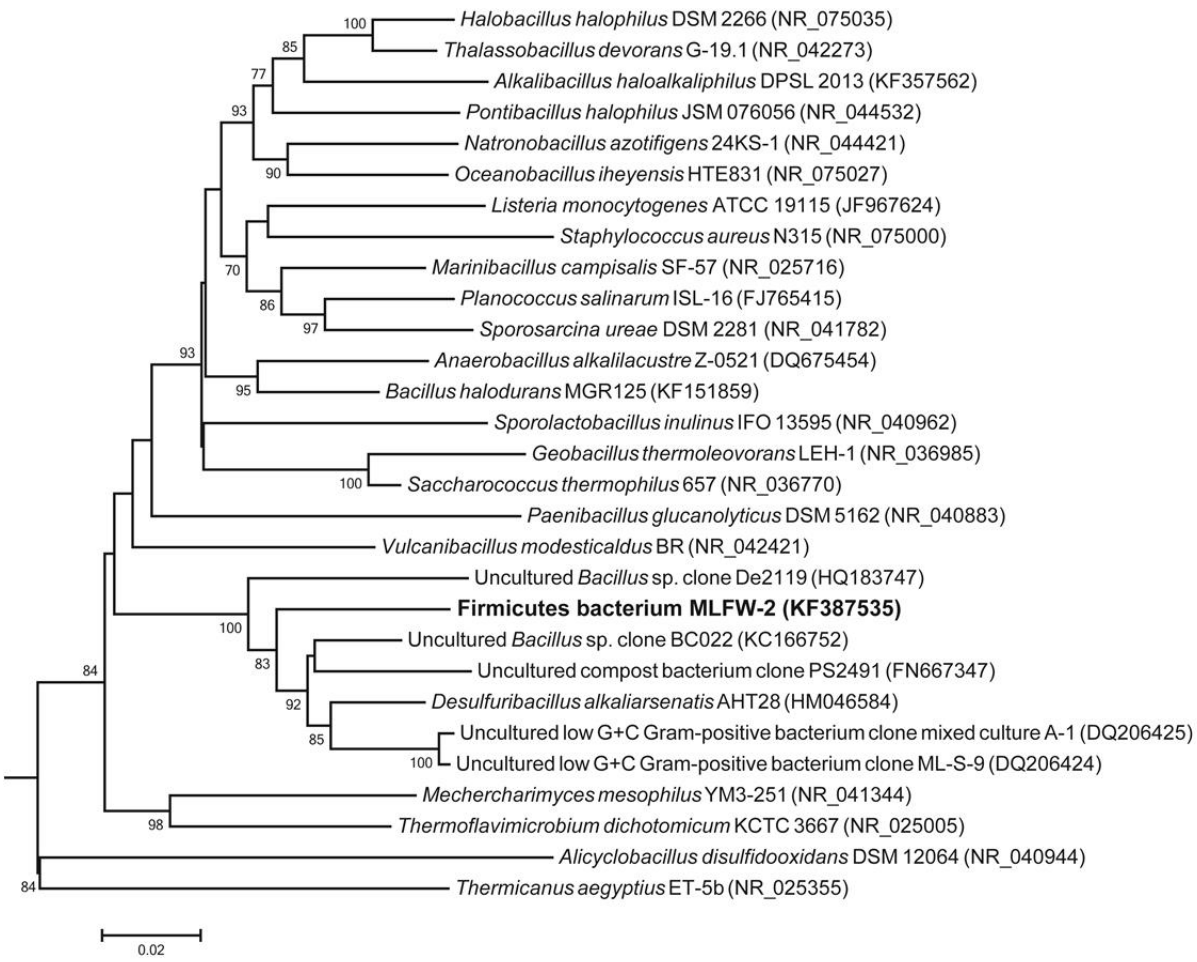

Figure 2.4. Phylogenetic tree based on 16S rRNA gene sequence analysis showing the relationship between strain MLFW-2 and other members of the order *Bacillales*. Tree topology and evolutionary distances were obtained by the neighbor-joining method with Jukes-Cantor evolutionary distances. Numbers at the nodes give bootstrap support for the node as a percentage of 1,000 replicates. GenBank and RefSeq accession numbers are given in parentheses. Scale bar, 0.02 substitutions per nucleotide position.

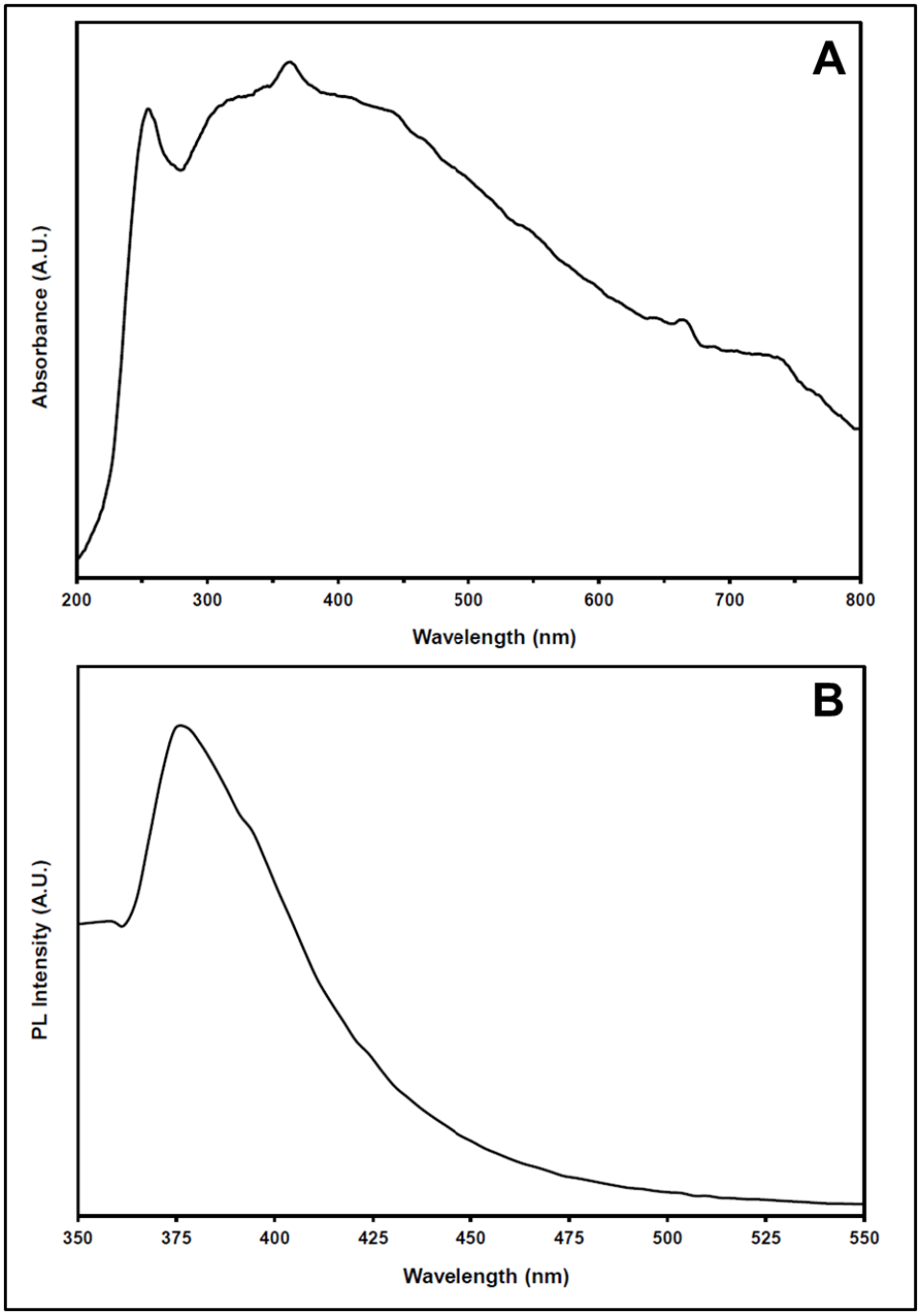

Figure 2.5. **(A)** UV-Vis absorption spectrum and **(B)** photoluminescence spectrum of the Sb_2O_3 microcrystals produced by strain MLFW-2.

CHAPTER 3

DESULFURIBACILLUS STIBIIARSENATIS SP. NOV., AN OBLIGATELY ANAEROBIC, DISSIMILATORY ANTIMONATE- AND ARSENATE-REDUCING BACTERIUM ISOLATED FROM ANOXIC SEDIMENTS, AND EMENDED DESCRIPTION OF THE GENUS *DESULFURIBACILLUS*[2]

[2]Abin C.A. and J.T. Hollibaugh. 2017. *Int. J. Syst. Evol. Microbiol.* 67(4): 1011-1017. Reprinted here with permission of publisher.

ABSTRACT

A novel anaerobic, Gram-stain-negative, endospore-forming bacterium, designated strain MLFW-2^T, was isolated from anoxic sediments collected from the drainage area of a geothermal spring near Mono Lake, CA, USA. Optimal growth was achieved at 34°C and pH 8.25 – 8.50 in medium containing 0.75% (w/v) NaCl. Catalase, but not oxidase, was produced. Strain MLFW-2^T was an obligate anaerobe capable of respiring with nitrate, nitrite, DMSO, arsenate, antimonate, selenate, and selenite as terminal electron acceptors. Lactate, pyruvate, formate, and H_2 could serve as electron donors to support growth. The isolate was incapable of fermentation. The predominant fatty acids were $C_{16:0}$, $C_{16:1}\omega9c$, $C_{16:1}\omega7c$, $C_{18:1}\omega9c$, and $C_{18:1}\omega7c$. The major polar lipids were phosphatidylglycerol and phosphatidylethanolamine. The only isoprenoid quinone detected was MK-7. The DNA G+C content was 38.2 mol%. Phylogenetic analysis based on the 16S rRNA gene sequence demonstrated that strain MLFW-2^T was a member of the order *Bacillales* and was most closely related to *Desulfuribacillus alkaliarsenatis* AHT28^T (93.9%). On the basis of phenotypic and phylogenomic evidence, strain MLFW-2^T represents a novel species of the genus *Desulfuribacillus*, for which the name *Desulfuribacillus stibiiarsenatis* sp. nov. is proposed. The type strain is MLFW-2^T (=DSM 28709^T=JCM 30866^T). An emended description of the genus *Desulfuribacillus* is also provided.

INTRODUCTION

Antimony (Sb) is a trace element widely distributed throughout the environment as a result of both natural processes and anthropogenic activities. The biogeochemistry of Sb has long been an understudied topic, even though it is toxic and its use dates back several thousand years (Sundar and Chakravarty 2010, Anderson 2012). Under oxic and anoxic conditions, thermodynamics predict that Sb should occur primarily as oxyanions of antimonate [Sb(V)] and antimonite [Sb(III)], respectively (Wilson *et al.* 2010). In spite of these predictions, significant concentrations of thermodynamically unstable species have been measured in the environment and biological activity has been invoked as a possible source (Filella *et al.* 2002).

A number of aerobic and anaerobic Sb(III)-oxidizing bacteria have already been isolated (Lyalikova 1972, Lehr *et al.* 2007, Hamamura *et al.* 2013, Li *et al.* 2013, Nguyen and Lee 2015, Terry *et al.* 2015). All of the Sb(III)-oxidizers identified thus far belong to the *Proteobacteria* or *Actinobacteria*, with the γ-*Proteobacteria* accounting for 49% of strains (Li *et al.* 2016). With respect to the reductive side of the cycle, the first unequivocal evidence for microbial Sb(V) reduction came from experiments with anoxic sediments collected from an abandoned Sb mining site (Kulp *et al.* 2014). Subsequently, a chemolithoautotrophic microbial consortium dominated by *Rhizobium* spp. was shown to reduce Sb(V) using H_2 as the electron donor (Lai *et al.* 2016). Currently, only two Sb(V)-reducing bacteria exist in pure culture (Abin and Hollibaugh 2014, Nguyen and Lee 2014). One of these isolates, strain MLFW-2^T, was capable of respiring Sb(V) using lactate as the electron donor. Reduction of Sb(V) by strain MLFW-2^T was accompanied by the precipitation of Sb(III) as a mixture of cubic and orthorhombic microcrystals of antimony trioxide (Sb_2O_3). Here, we describe the morphological, physiological, and chemotaxanomic

characteristics of strain MLFW-2^T and demonstrate that it represents a novel species of the genus *Desulfuribacillus*.

RESULTS AND DISCUSSION

Strain MLFW-2^T was isolated from arsenic-rich anoxic sediments collected from the drainage area of a geothermal spring adjacent to Mono Lake, CA, USA (37°56'28.7" N, 119°1'22.4" W) (Abin and Hollibaugh 2014). A lactate-oxidizing, Sb(V)-reducing enrichment culture was established under anoxic conditions in a basal salts medium (BSM-1; Table 3.S1) supplemented with 1 mM lactate and 2 mM Sb(V). A pure culture of strain MLFW-2^T was obtained on agar media as previously described (Abin and Hollibaugh 2013).

Cell morphology during growth on Sb(V) was examined using a Leica DM RXA optical light microscope (Leica Microsystems), Zeiss 1450EP scanning electron microscope (Carl Zeiss), and Tecnai F20 transmission electron microscope (FEI). Cells of strain MLFW-2^T were motile and consisted of curved rods typically 0.3 – 0.5 μm wide and 2.0 – 11.0 μm long (Figure 3.1A). During the stationary phase of growth, cells formed ellipsoidal endospores in terminal, swollen sporangia (Figure 3.S1). The Gram stain and KOH string test were performed on mid-exponential phase cells as previously described (Gregersen 1978, Gerhardt *et al.* 1994). Strain MLFW-2^T stained Gram-negative and cell lysis occurred following incubation in 3% KOH. However, no outer membrane was apparent in ultra-thin sections (Figure 3.1B). It should be noted that strain MLFW-2^T was erroneously described as Gram-positive by Abin and Hollibaugh (2013).

Genomic DNA was extracted from a cell pellet using the PureLink Genomic DNA Mini Kit (Invitrogen). A fragment of the 16S rRNA gene was amplified by PCR with universal

bacterial primers 27F (5'-AGAGTTTGATCCTGGCTCAG-3') and 1492R (5'-GGTTACCTTGTTACGACTT-3') (Lane 1991). The amplicons were sequenced directly using the BigDye Terminator v3.1 Cycle Sequencing Kit (Applied Biosystems) and an Applied Biosystems 3730xl DNA Analyzer. The forward and reverse primers listed above were used for sequencing from both directions. The consensus 16S rRNA gene sequence of strain MLFW-2^T was compared with reference sequences in Genbank and the Ribosomal Database Project Release 11.4 using the BLASTn (Altschul *et al.* 1990) and RDP Classifier (Wang *et al.* 2007) algorithms, respectively. Sequence data from strain MLFW-2^T and its closest relatives were aligned using MUSCLE (Edgar 2004). The MEGA6 software package (Tamura *et al.* 2013) was used to generate phylogenetic trees using the neighbor-joining (Saitou and Nei 1987), maximum-parsimony (Fitch 1971), and maximum-likelihood (Felsenstein 1981) algorithms with Jukes-Cantor evolutionary distances (Jukes and Cantor 1969). Tree topologies were evaluated by bootstrap analysis (Felsenstein 1985) with 1,000 replicates.

A nearly full length 16S rRNA gene sequence (1,446 nucleotides) was obtained from strain MLFW-2^T. Taxonomic analysis by the RDP Classifier revealed that strain MLFW-2^T was a member of the order *Bacillales*, although it did not cluster with any established families at a 90% confidence threshold. The closest phylogenetic relative of strain MLFW-2^T was *Desulfuribacillus alkaliarsenatis* AHT28^T, with a sequence similarity of 93.9%. *D. alkaliarsenatis* AHT28^T was a Gram-positive, obligately anaerobic, dissimilatory sulfur- and arsenate-reducing haloalkaliphile isolated from soda lake sediments collected in the Kulunda Steppe, Altai, Russia (Sorokin *et al.* 2012). Strain MLFW-2^T only shared a maximum of 90.6% 16S rRNA gene sequence similarity with other type strains of the *Bacillales*. The 16S rRNA gene was also related to uncultured bacterial clones retrieved from an anaerobic aquifer

(Genbank accession number KC166752; similarity value 94.7%), alkaline, hypersaline lake (DQ206424 and DQ206425; 92.8% and 92.7%, respectively), municipal compost pile (FN667347; 92.7%), and landfill leachate sediment (HQ183747; 91.6%). Phylogenetic trees depicting the evolutionary relationship between strain MLFW-2^T and the most closely related type strains of the *Bacillales* are presented in Figures 3.2, 3.S2, and 3.S3. Strain MLFW-2^T consistently shared a branching node with *D. alkaliarsenatis* AHT28^T regardless of the algorithm used. In each case, the node was supported by a bootstrap value of 100%.

All growth experiments designed to characterize the physiological properties of strain MLFW-2^T were carried out in duplicate at 30°C under an atmosphere of 5% H_2 + 95% N_2, except where noted. Tests for the use of electron donors and acceptors were performed in BSM-1. Growth was assessed by monitoring cell density using acridine orange staining and epifluorescence microscopy (Hobbie *et al.* 1977). For a positive result, growth had to reach a level of at least two-fold that of the negative control and had to maintain that threshold for three consecutive transfers.

The range of terminal electron acceptors used by strain MLFW-2^T was investigated with 10 mM lactate as the electron donor. The following electron acceptors were tested, all at a concentration of 5 mM (unless stated otherwise): nitrate, nitrite (2 mM), amorphous Fe(III) oxyhydroxide (5 g l^{-1}), Fe(III) citrate, colloidal MnO_2 (5 g L^{-1}), sulfate, sulfite (2 mM), tetrathionate, thiosulfate, elemental sulfur (5 g L^{-1}), arsenate, selenate, selenite, chromate, vanadate, molybdate, fumarate, dimethylsulfoxide (DMSO), and trimethylamine-N-oxide (TMAO). All electron acceptors were added from anoxic, filter-sterilized stock solutions. The ability to grow aerobically (~21% O_2) was tested in a 200 mL Erlenmeyer flask open to the atmosphere. The capacity for microaerophilic growth was tested in a stoppered glass serum

bottle into which sterile air was injected to give final O_2 concentrations of 0.5, 1.0, and 2.0% (v/v) in the headspace.

Amorphous Fe(III) oxyhydroxide and colloidal MnO_2 were prepared as described previously (Lovley and Phillips 1986, 1988). Nitrate, nitrite, and ammonium were measured by the cadmium-copper reduction (Wood *et al.* 1967), Greiss (Bendschneider and Robinson 1952), and phenol-hypochlorite (Weatherburn 1967) methods, respectively. Arsenate, arsenite, and selenite were quantified using high-performance liquid chromatography (Fisher *et al.* 2007). Total dissolved selenium was measured using a Thermo Jarrell-Ash 965 inductively-coupled argon plasma spectrometer following filtration of the culture medium with a 0.22 μm nylon filter (Nalgene). Selenate and elemental selenium were quantified by subtracting the concentration of selenite and dissolved selenium, respectively, from the initial amount of dissolved selenium present at the start of the incubation.

In addition to Sb(V), strain MLFW-2^T was able to grow using DMSO, nitrate, nitrite, arsenate, selenate, and selenite as terminal electron acceptors. The growth rate was highest when arsenate was provided as the electron acceptor (data not shown). Strain MLFW-2^T reduced nitrate and nitrite to ammonium. Selenate and selenite were reduced to a red allotrope of elemental selenium. Nitrate and selenate reduction were sequential processes involving the transient accumulation of nitrite and selenite, respectively, in the culture medium. No growth was observed in the presence of O_2, indicating that strain MLFW-2^T was an obligate anaerobe. *D. alkaliarsenatis* AHT28^T was also a strict anaerobe capable of respiring arsenate, although elemental sulfur and thiosulfate could support growth as well. Another key difference between the two strains lies in the inability of *D. alkaliarsenatis* AHT28^T to grow using DMSO, nitrate, nitrite, selenate, or selenite as electron acceptors (Sorokin *et al.* 2012).

The ability of strain MLFW-2^T to grow using a range of electron donors was tested with 5 mM arsenate as the electron acceptor under an N_2 atmosphere. The following substrates were tested, all at a concentration of 10 mM (unless stated otherwise): acetate, pyruvate, formate (± 2 mM acetate), fumarate, malate, succinate, maleate, oxalate, ascorbate, citrate, tartrate, glycolate, propionate, D-glucose, D-galactose, D-fructose, ethanol, methanol, glycerol, D-sorbitol, L-glycine, L-glutamate, L-serine, and 100% (v/v) H_2 (± 2 mM acetate). In addition to lactate, strain MLFW-2^T was able to grow using formate, pyruvate, and H_2 as electron donors. No fermentative growth on these substrates was observed when arsenate was omitted from the medium. Growth on formate and H_2 was only possible when acetate was provided as a carbon source, indicating that strain MLFW-2^T was incapable of autotrophic growth.

For all growth optimum experiments, lactate and arsenate were used as the electron donor and acceptor, respectively. The influence of salinity on the growth rate of strain MLFW-2^T was assessed in BSM-2 (Table 3.S1). The final NaCl concentration (w/v) of the medium was adjusted to 0, 0.25, 0.50, 0.75, 1.0, 1.5, 2.0, 2.5, 3.0, 3.5, 4.0, 4.5, and 5.0%. The pH tolerance was determined in BSM-3 and BSM-4 (Table 3.S1) from pH 7 – 10 (at intervals of 0.25 pH units). Buffers comprised of NaH_2PO_4/Na_2HPO_4 (BSM-3; pH 7.0 – 8.0) and $NaHCO_3/Na_2CO_3$ (BSM-4; pH 8.25 – 10.0) were added to a final concentration of 50 mM to maintain a stable pH. The temperature tolerance was tested in BSM-5 (Table 3.S1) at 10, 15, 20, 25, 30, 32, 34, 36, 38, 40, 42, and 43°C. Optimal growth of strain MLFW-2^T occurred at 34°C (range 10 - 43°C), pH 8.25 – 8.50 (range 7.0 – 10.0), and 0.75% NaCl (range 0 – 5.0%).

Oxidase activity was tested using XeroStrips (Biorex Labs). Catalase activity was assessed by checking for the production of gas bubbles after the addition of a drop of 3% (v/v) H_2O_2 to a smeared pellet of freshly cultured cells. Strain MLFW-2^T was catalase-positive and

oxidase-negative. This is in slight contrast to *D. alkaliarsenatis* AHT28^{T}, which was both catalase- and oxidase-negative (Sorokin *et al*. 2012).

For chemotaxonomic analyses, cells were cultivated in BSM-5 at 34°C using lactate and arsenate as the electron donor and acceptor, respectively. Cellular fatty acids were analyzed as the methyl ester derivatives prepared from 20 mg of wet cellular biomass. Gas chromatographic analysis of fatty acid methyl esters (FAMEs) was performed by Microbial ID, Inc. (Newark, DE, USA), using the Sherlock Microbial Identification System. Only saturated, unsaturated, and branched fatty acids were detected in the fatty acid profile of strain MLFW-2^{T} (Table 3.1). The dominant fatty acids were $C_{18:1}\omega 7c$ (35.4%), $C_{16:0}$ (21.7%), $C_{16:1}\omega 9c$ (14.1%), $C_{16:1}\omega 7c$ (13.9%), and $C_{18:1}\omega 9c$ (7.3%). The same major components were detected in *D. alkaliarsenatis* AHT28^{T}, although $C_{18:1}\omega 7c$ and $C_{16:1}\omega 9$ only accounted for 20.7% and 6.6% of total cellular fatty acids, respectively, while $C_{16:1}\omega 7c$ was present in higher abundance (Sorokin *et al*. 2012). Both strains lacked the C_{15} fatty acids normally prominent in members of the phylum *Firmicutes* (Kämpfer 2002).

Polar lipids and respiratory lipoquinones were analyzed by the Identification Service of the Deutsche Sammlung von Mikroorganismen und Zellkulturen (DSMZ; Braunschweig, Germany). The polar lipid profile of strain MLFW-2^{T} was dominated by phosphatidylglycerol and phosphatidylethanolamine (Figure 3.S4). Moderate amounts of two unknown phospholipids (PL1 and PL2) and two unknown polar lipids (L2 and L3) were also present, as well as minor amounts of other unknown polar lipids (L1, L4 – L7). The only respiratory lipoquinone detected was menaquinone-7 (MK-7).

To test the sensitivity of strain MLFW-2^{T} to various antibiotics, cells were grown to the late exponential phase in BSM-5 and inoculated into a series of Hungate tubes containing fresh

BSM-5 supplemented with ampicillin, kanamycin, rifampicin, chloramphenicol, erythromycin, gentamicin, streptomycin, or nalidixic acid at concentrations of 5, 10, 25, 50, 75, and 100 μg mL^{-1}. The tubes were prepared in triplicate and scored for positive growth after an incubation period of 96 hours at 34°C. Strain MLFW-2^T was only able to grow in the presence of 5 μg mL^{-1} chloramphenicol, 5 – 25 μg mL^{-1} kanamycin, and 5 – 75 μg mL^{-1} nalidixic acid.

The genome of strain MLFW-2^T was sequenced using the Illumina Miseq platform with 250 bp paired-end reads. Genomic DNA from strain MLFW-2^T was sheared using a Covaris E220 Evolution Focused-ultrasonicator to generate an average fragment size of 696 bp. Paired-end DNA libraries were prepared using the TruSeq DNA LT Sample Prep Kit (Illumina) and indexed with TruSeq DNA LT single index adapters (Illumina). The library was sequenced for 500 cycles using a MiSeq Reagent Kit v2 (Illumina). The reads were randomly subsampled to an approximate 85-fold median coverage with seqtk version 1.0-r63 (https://github.com/lh3/seqtk). Read cleaning and *de novo* assembly was performed using the A5-Miseq pipeline (Coil *et al.* 2015). Genome annotation was performed using the RAST server (Aziz *et al.* 2008). Genome completeness was assessed using AMPHORA2 (Wu and Scott, 2012).

The genome assembly yielded 40 contigs, with maximum and N_{50} contig sizes of 400,702 bp and 233,716 bp, respectively. The total length of the draft genome was 3,119,699 bp with a G+C content of 38.2%. Genome annotation revealed 3,028 coding sequences and 63 tRNA genes. The draft genome was nearly complete, as it contained all 31 phylogenetic marker genes essential in bacteria. The size and G+C content of the draft genome were very similar to the values of 3,106,435 bp and 37.5%, respectively, reported for the draft genome of *D. alkaliarsenatis* AHT28^T (Abin and Hollibaugh 2016). It should be noted that the thermal

denaturation method yielded a G+C content of 39.1% for the genome of *D. alkaliarsenatis* AHT28^T in the original description of the type strain (Sorokin *et al*. 2012).

To further refine the phylogenetic relationship between strain MLFW-2^T and *D. alkaliarsenatis* AHT28^T, the average nucleotide identity (ANI), average amino acid identity (AAI), and percent of conserved proteins (POCP) between both strains were determined. For species delineation, ANI and AAI values ≥95% derived from whole or draft genome sequences have been shown to correlate well with the recommended threshold of ≥70% genomic relatedness based on DNA-DNA hybridization (DDH) (Konstantinidis and Tiedje 2005, Goris *et al.* 2007). Similarly, a POCP of ≥50% has been proposed as a robust genomic parameter for delimiting the prokaryotic genus boundary (Qin *et al.* 2014). The ANI and AAI were calculated using EzGenome (http://www.ezbiocloud.net/ezgenome/ani) and the Kostas Lab AAI Calculator (http://enve-omics.ce.gatech.edu/aai/), respectively. The POCP analysis was performed as described by Qin *et al*. (2014). The ANI, AAI, and POCP values of strain MLFW-2^T with *D. alkaliarsenatis* AHT28^T were 69.07%, 65.43%, and 66.58%, respectively. These values suggest that the novel isolate and *D. alkaliarsenatis* AHT28^T are two distinct species that belong to the same genus.

On the basis of the morphological, physiological, chemotaxanomic, and phylogenomic data presented here, strain MLFW-2^T merits recognition as a novel species of the genus *Desulfuribacillus*, for which the name *Desulfuribacillus stibiiarsenatis* is proposed. While strain MLFW-2^T shares many phenotypic traits with the only other existing member of the genus *Desulfuribacillus*, *D. alkaliarsenatis* AHT28^T, it is possible to distinguish between them using the characteristics shown in Table 3.2.

Emended description of the genus Desulfuribacillus

Cells are motile, curved rods that stain Gram–positive or –negative and produce terminal endospores. Oxidase-negative. Mesophilic. Obligately anaerobic with an exclusively respiratory catabolism. Hydrogen, formate, lactate, and pyruvate can serve as electron donors. Arsenate can serve as an electron acceptor. Incapable of chemoautotrophic growth. The major cellular fatty acids are $C_{16:0}$, $C_{16:1}\omega9$, $C_{16:1}\omega7c$, $C_{18:1}\omega9$, and $C_{18:1}\omega7c$. The major respiratory lipoquinone is MK-7. The DNA G+C content is 37.5 – 38.2 mol%. The type species is *Desulfuribacillus alkaliarsenatis*.

Description of Desulfuribacillus stibiiarsenatis sp. nov.

Desulfuribacillus stibiiarsenatis (sti.bi.i.ar.se.na'tis. L. n. *stibium*, antimony; N.L. n. *arsenas -atis*, arsenate; N.L. gen. n. *stibiiarsenatis*, of antimony (and) arsenate, referring to the ability of the strain to use antimonate and arsenate as electron acceptors).

In addition to the characteristics listed in the genus description above, cells are approximately 0.3 – 0.5 x 2.0 – 11.0 μm and produce ellipsoidal endospores. Gram-stain-negative and lysis occurs upon treatment with 3% KOH. No outer membrane is present. Growth is observed from 10 – 43°C (optimum 34°C), pH 7.0 – 10.0 (optimum 8.25 – 8.50), and with 0 – 5% (w/v) NaCl (optimum 0.75%). Catalase-positive. Nitrate, nitrite, DMSO, antimonate, selenate, and selenite can serve as terminal electron acceptors for anaerobic respiration. Sulfate, sulfite, tetrathionate, thiosulfate, elemental sulfur, chromate, vanadate, amorphous Fe(III) oxyhydroxide, Fe(III) citrate, colloidal MnO_2, molybdate, fumarate, and TMAO cannot be used as electron acceptors. Growth on formate and H_2 as electron donors requires supplementation

with acetate as a carbon source. Acetate, fumarate, malate, succinate, maleate, oxalate, ascorbate, citrate, tartrate, glycolate, propionate, D-glucose, D-galactose, D-fructose, ethanol, methanol, glycerol, D-sorbitol, L-glycine, L-glutamate, and L-serine cannot serve as electron donors. The major polar lipids are phosphatidylglycerol and phosphatidylethanolamine. Two unknown phospholipids (PL1 and PL2) and seven unknown polar lipids (L1 – L7) are also produced. Cells are resistant to chloramphenicol, kanamycin, and nalidixic acid, but highly sensitive to ampicillin, rifampicin, erythromycin, gentamicin, and streptomycin.

The type strain, MLFW-2^T (=DSM 28709^T =JCM 30866^T), was isolated from anoxic sediments collected from the drainage area of a geothermal spring adjacent to the southern shore of Mono Lake, CA, USA (37° 56’ 28.7” N, 119° 1’ 22.4” W). The DNA G+C content of the type strain is 38.2 mol%.

ACKNOWLEDGEMENTS

We thank the editor and three anonymous reviewers for constructive comments that helped improve the manuscript. We also thank Dr. John Shields for assistance with electron microscopy. DNA library preparation and Illumina sequencing was performed by the Georgia Genomics Facility at the University of Georgia in Athens, GA, USA. This work was supported by National Science Foundation grants EAR 09-52271 (JTH) and DGE-0903734 (CAA). Additional funding was provided by a Minority Ph.D. Program scholarship from the Alfred P. Sloan Foundation (CAA).

REFERENCES

Abin CA, Hollibaugh JT (2014). Dissimilatory antimonate reduction and production of antimony trioxide microcrystals by a novel microorganism. *Environ Sci Technol* **48:** 681-688.

Abin CA, Hollibaugh JT (2016). Draft genome sequence of the type strain *Desulfuribacillus alkaliarsenatis* AHT28, an obligately anaerobic, sulfidogenic bacterium isolated from Russian soda lake sediments. *Genome Announc* **4:** e01244-16.

Altschul SF, Gish W, Miller W, Myers EW, Lipman DJ (1990). Basic local alignment search tool. *J Mol Biol* **215:** 403-410.

Anderson CG (2012). The metallurgy of antimony. *Chem Erde-Geochem* **72:** 3-8.

Aziz R, Bartels D, Best A, DeJongh M, Disz T, Edwards R *et al.* (2008). The RAST Server: rapid annotations using subsystems technology. *BMC Genomics* **9:** 75.

Bendschneider K, Robinson RJ (1952). A new spectrophotometric method for the determination of nitrite in sea water. *J Marine Res* **11:** 87-96.

Coil D, Jospin G, Darling AE (2015). A5-miseq: an updated pipeline to assemble microbial genomes from Illumina MiSeq data. *Bioinformatics* **31:** 587-589.

Edgar RC (2004). MUSCLE: multiple sequence alignment with high accuracy and high throughput. *Nucl Acids Res* **32:** 1792-1797.

Felsenstein J (1981). Evolutionary trees from DNA sequences: a maximum likelihood approach. *J Mol Evol* **17:** 368-376.

Felsenstein J (1985). Confidence limits on phylogenies: an approach using the bootstrap. *Evolution* **39:** 783-791.

Filella M, Belzile N, Chen YW (2002). Antimony in the environment: a review focused on natural waters: I. Occurrence. *Earth-Sci Rev* **57:** 125-176.

Fisher JC, Wallschläger D, Planer-Friedrich B, Hollibaugh JT (2007). A new role for sulfur in arsenic cycling. *Environ Sci Technol* **42:** 81-85.

Fitch WM (1971). Toward defining the course of evolution: minimum change for a specific tree topology. *Syst Biol* **20:** 406-416.

Gerhardt P, Murray RGE, Wood WA, Krieg NR (1994). *Methods for General and Molecular Bacteriology*. Washington, D.C.: American Society for Microbiology.

Goris J, Konstantinidis KT, Klappenbach JA, Coenye T, Vandamme P, Tiedje JM (2007). DNA–DNA hybridization values and their relationship to whole-genome sequence similarities. *Int J Syst Evol Microbiol* **57:** 81-91.

Gregersen T (1978). Rapid method for distinction of Gram-negative from Gram-positive bacteria. *Euro J Appl Microbiol Biotechnol* **5:** 123-127.

Hamamura N, Fukushima K, Itai T (2013). Identification of antimony- and arsenic-oxidizing bacteria associated with antimony mine tailing. *Microbes Environ* **28:** 257-263.

Hobbie JE, Daley RJ, Jasper S (1977). Use of nuclepore filters for counting bacteria by fluorescence microscopy. *Appl Environ Microbiol* **33:** 1225-1228.

Jukes TH, Cantor CR (1969). Evolution of protein molecules. In *Mammalian Protein Metabolism*. New York, NY: Academic Press.

Kämpfer P (2002). Whole-cell fatty acid analysis in the systematics of *Bacillus* and related genera. In *Applications and Systematics of Bacillus and Relatives*. Oxford, UK: Blackwell Science.

Konstantinidis KT, Tiedje JM (2005). Towards a genome-based taxonomy for prokaryotes. *J Bacteriol* **187:** 6258-6264.

Kulp TR, Miller LG, Braiotta F, Webb SM, Kocar BD, Switzer Blum J *et al.* (2014). Microbiological reduction of Sb(V) in anoxic freshwater sediments. *Environ Sci Technol* **48:** 218-226.

Lai C, Wen L, Zhang Y, Luo S, Wang Q, Luo Y *et al.* (2016). Autotrophic antimonate bio-reduction using hydrogen as the electron donor. *Water Res* **88:** 467-474.

Lane DJ (1991). 16S/23S rRNA sequencing. In *Nucleic Acid Techniques in Bacterial Systematics*. New York, NY: John Wiley and Sons.

Lehr CR, Kashyap DR, McDermott TR (2007). New insights into microbial oxidation of antimony and arsenic. *Appl Environ Microbiol* **73:** 2386-2389.

Li J, Wang Q, Oremland RS, Kulp TR, Rensing C, Wang G (2016). Microbial antimony biogeochemistry: enzymes, regulation, and related metabolic pathways. *Appl Environ Microbiol* **82:** 5482-5495.

Li J, Wang Q, Zhang S, Qin D, Wang G (2013). Phylogenetic and genome analyses of antimony-oxidizing bacteria isolated from antimony mined soil. *Int Biodeterior Biodegrad* **76:** 76-80.

Lovley DR, Phillips EJP (1986). Organic matter mineralization with reduction of ferric iron in anaerobic sediments. *Appl Environ Microbiol* **51:** 683-689.

Lovley DR, Phillips EJP (1988). Novel mode of microbial energy metabolism: organic carbon oxidation coupled to dissimilatory reduction of iron or manganese. *Appl Environ Microbiol* **54:** 1472-1480.

Lyalikova NN (1972). Oxidation of trivalent antimony up to higher oxides as an energy source for the development of a new autotrophic organism, *Stibiobacter* gen. nov. *Dokl Akad Nauk SSSR* **205:** 1228-1229.

Nguyen VK, Lee JU (2014). Isolation and characterization of antimony-reducing bacteria from sediments collected in the vicinity of an antimony factory. *Geomicrobiol J* **31:** 855-861.

Nguyen VK, Lee JU (2015). Antimony-oxidizing bacteria isolated from antimony-contaminated sediment – a phylogenetic study. *Geomicrobiol J* **32:** 50-58.

Oremland RS, Switzer Blum J, Culbertson CW, Visscher PT, Miller LG, Dowdle P *et al.* (1994). Isolation, growth, and metabolism of an obligately anaerobic, selenate-respiring bacterium, strain SES-3. *Appl Environ Microbiol* **60:** 3011-3019.

Qin QL, Xie BB, Zhang XY, Chen XL, Zhou BC, Zhou J *et al.* (2014). A proposed genus boundary for the prokaryotes based on genomic insights. *J Bacteriol* **196:** 2210-2215.

Saitou N, Nei M (1987). The neighbor-joining method: a new method for reconstructing phylogenetic trees. *Mol Biol Evol* **4:** 406-425.

Sorokin DY, Tourova TP, Sukhacheva MV, Muyzer G (2012). *Desulfuribacillus alkaliarsenatis* gen. nov. sp. nov., a deep-lineage, obligately anaerobic, dissimilatory sulfur and arsenate-reducing, haloalkaliphilic representative of the order *Bacillales* from soda lakes. *Extremophiles* **16:** 597-605.

Sundar S, Chakravarty J (2010). Antimony toxicity. *Int J Environ Res Public Health* **7:** 4267-4277.

Tamura K, Stecher G, Peterson D, Filipski A, Kumar S (2013). MEGA6: molecular evolutionary genetics analysis version 6.0. *Mol Biol Evol* **30:** 2725-2729.

Terry LR, Kulp TR, Wiatrowski H, Miller LG, Oremland RS (2015). Microbiological oxidation of antimony(III) with oxygen or nitrate by bacteria isolated from contaminated mine sediments. *Appl Environ Microbiol* **81:** 8478-8488.

Wang Q, Garrity GM, Tiedje JM, Cole JR (2007). Naïve Bayesian classifier for rapid assignment of rRNA sequences into the new bacterial taxonomy. *Appl Environ Microbiol* **73:** 5261-5267.

Weatherburn MW (1967). Phenol-hypochlorite reaction for determination of ammonia. *Anal Chem* **39:** 971-974.

Widdel F, Kohring GW, Mayer F (1983). Studies on dissimilatory sulfate-reducing bacteria that decompose fatty acids. III. Characterization of the filamentous gliding *Desulfonema limnicola* gen. nov., sp. nov., and *Desulfonema magnum* sp. nov. *Arch Microbiol* **134:** 286-294.

Wilson SC, Lockwood PV, Ashley PM, Tighe M (2010). The chemistry and behaviour of antimony in the soil environment with comparisons to arsenic: a critical review. *Environ Pollut* **158:** 1169-1181.

Wood ED, Armstrong FAJ, Richards FA (1967). Determination of nitrate in sea water by cadmium-copper reduction to nitrite. *J Mar Biol Assoc UK* **47:** 23-31.

Wu M, Scott AJ (2012). Phylogenomic analysis of bacterial and archaeal sequences with AMPHORA2. *Bioinformatics* **28:** 1033-1034.

Table 3.1. Cellular fatty acid content of strain MLFW-2^T and *D. alkaliarsenatis* AHT28^T. Data for *D. alkaliarsenatis* AHT28^T were taken from Sorokin *et al*. (2012). Values are percentages of total fatty acids. Only fatty acids representing ≥1% are shown. Fatty acids representing ≥5% of the total fatty acids are shown in bold. **—**, Not detected or <1%.

Fatty acid	**Strain MLFW-2^T**	***D. alkaliarsenatis* AHT28^T**
$C_{16:0}$	**21.7**	**24.6**
$C_{16:0}$ ALDE	**—**	2.8
$C_{16:1}\omega9$	**14.1***	**6.6**
$C_{16:1}\omega9$ ALDE	**—**	2.3
$C_{16:1}\omega7$ ALDE	**—**	1.3
$C_{16:1}\omega7c$	**13.9**	**20.0**
$C_{16:1}\omega5$	1.3*	3.5
i-$C_{17:0}$	**—**	1.1
$C_{18:0}$	1.2	1.4
$C_{18:1}\omega9$	**7.3***	**6.0**
$C_{18:1}\omega9$ ALDE	**—**	1.0
$C_{18:1}\omega7$ ALDE	**—**	4.1
$C_{18:1}\omega7c$	**35.4**	**20.7**
$C_{18:1}\omega5$	1.5*	1.4

*Only *cis* stereoisomer detected.

Table 3.2. Phenotypic comparison between strain MLFW-2^T and its closest phylogenetic relative, *D. alkaliarsenatis* AHT28^T. Data for *D. alkaliarsenatis* AHT28^T were taken from Sorokin *et al*. (2012) and Abin and Hollibaugh (2016). +, Positive; -, negative; ND, not determined. Both strains are positive for: curved, rod-shaped cells; terminal endospores; motility; MK-7 as the dominant respiratory lipoquinone; use of arsenate as an electron acceptor; and use of formate, lactate, pyruvate, and H_2 as electron donors. Both strains are negative for: cytochrome oxidase; use of acetate, fumarate, propionate, malate, succinate, ethanol, glucose, and fructose as electron donors; and use of oxygen, sulfate, sulfite, fumarate, amorphous Fe(III) oxyhydroxide, and colloidal MnO_2 as electron acceptors.

Characteristic	**Strain MLFW-2^T**	***D. alkaliarsenatis* AHT28^T**
Isolation source	Anoxic sediments	Soda lake sediments
Cell width (μm)	0.3 – 0.5	0.4
Cell length (μm)	2.0 – 11.0	2.0 – 7.0
Gram stain	-	+
Endospore shape	Ellipsoidal	Round or ellipsoidal
Catalase	+	-
Temperature (°C)		
Range (Optimum)	10 – 43 (34)	ND – 43 (35)
pH		
Range (Optimum)	7.0 – 10.0 (8.25 – 8.50)	8.5 – 10.6 (10.2)
NaCl concentration (%)		
Range (Optimum)	0 – 5.0 (0.75)	1.2 – 14.6 (3.5 – 4.7)
Electron acceptors		
Nitrite	+	-
Nitrate	+	-
Elemental Sulfur	-	+
Thiosulfate	-	+
Antimonate	+	ND
Selenite	+	-
Selenate	+	-
DMSO	+	-
Major polar lipids	PG, PE*	ND
DNA G+C content (mol%)[‡]	38.2	37.5

*PG, phosphatidylglycerol; PE, phosphatidylethanolamine.
[‡]Values derived from the draft genome sequences.

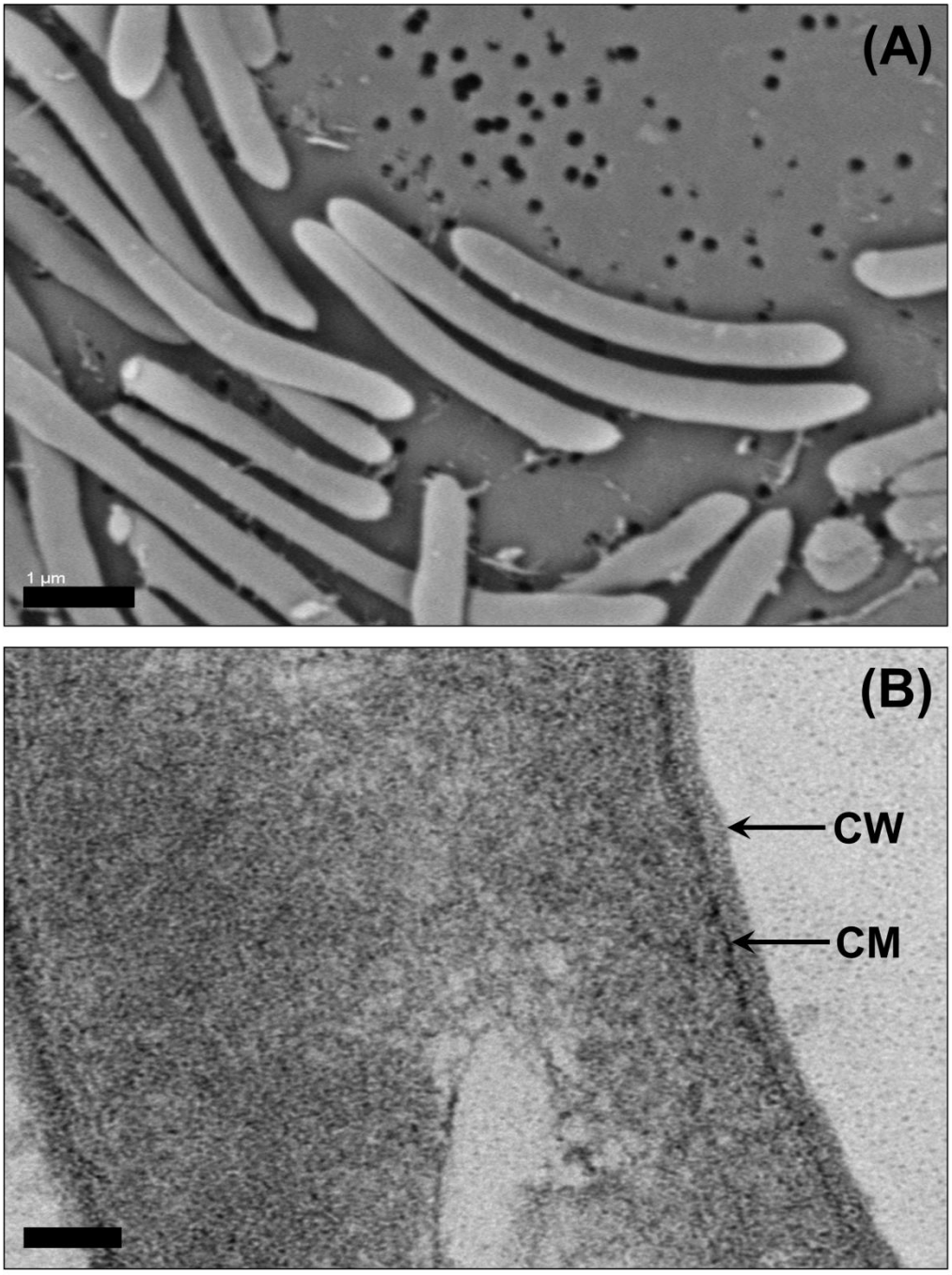

Figure 3.1. Cellular morphology and ultrastructure of strain MLFW-2^T. (A) Scanning electron micrograph of cells grown in BSM-1 with lactate and Sb(V) as the electron donor and acceptor, respectively. Scale bar, 1 µm. (B) Transmission electron micrograph showing a magnified ultra-thin section of the cell envelope of a cell grown in BSM-5 with lactate and arsenate. Scale bar, 40 nm. CM, cytoplasmic membrane; CW, cell wall.

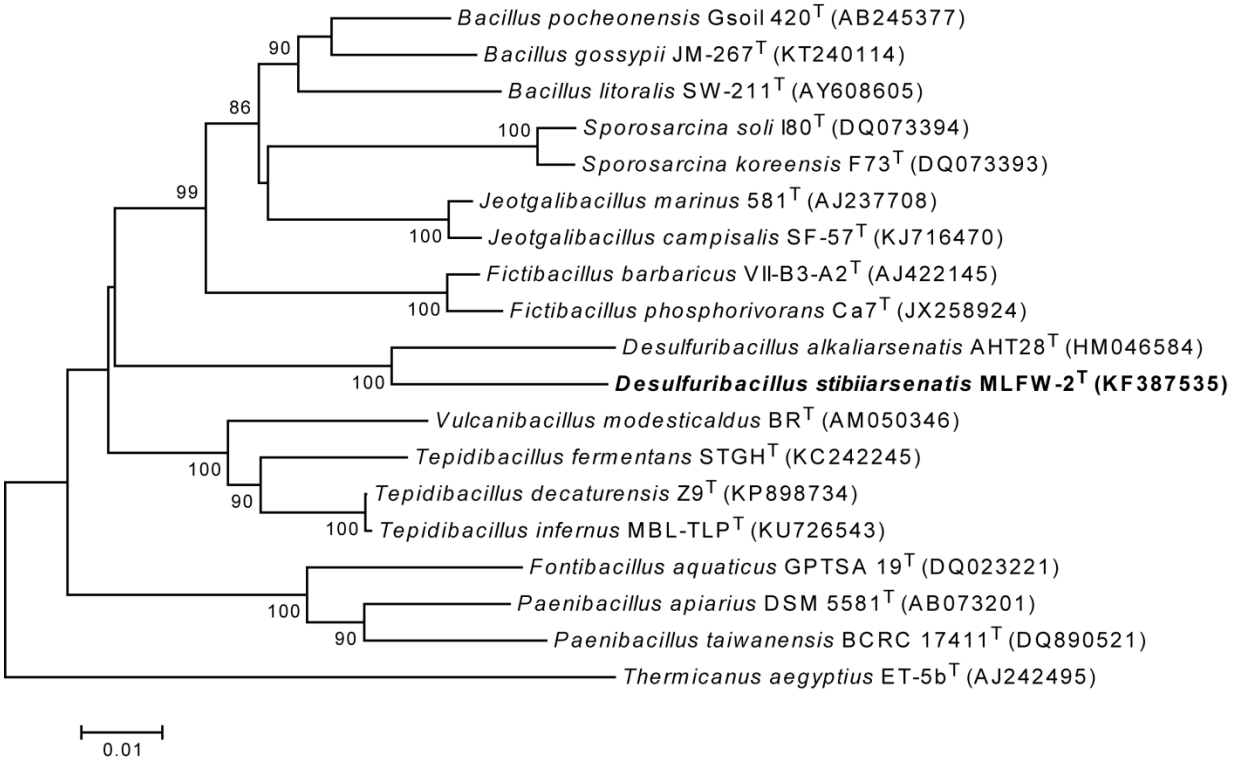

Figure 3.2. Neighbor-joining phylogenetic tree based on 16S rRNA gene sequences showing the relationship between strain MLFW-2^T and the most closely related type strains of the *Bacillales*. Bootstrap values (≥70%) based on 1,000 re-samplings are shown at the nodes. *Thermicanus aegyptius* ET-5b^T was used as an outgroup. GenBank accession numbers are given in parentheses. Bar, 0.01 substitutions per nucleotide position.

CHAPTER 4

IDENTIFICATION OF COMPLEX IRON-SULFUR MOLYBDOENZYMES FUNCTIONING AS POSSIBLE ANAEROBIC RESPIRATORY REDUCTASES IN *DESULFURIBACILLUS STIBIIARSENATIS* MLFW-2[T3]

[3]Abin C.A. and J.T. Hollibaugh. To be submitted to *MBio*.

ABSTRACT

The dimethyl sulfoxide reductase (DMSOR) family is an important class of enzymes that supports the respiratory diversity of anaerobic prokaryotes. Members of this family possess a molybdenum- or tungsten-containing cofactor and catalyze two-electron redox reactions that are pivotal to the dissimilatory metabolism of organic and inorganic compounds containing nitrogen, sulfur, arsenic, selenium, and chlorine. *Desulfuribacillus stibiiarsenatis* MLFW-2^T is an obligately anaerobic bacterium that grows by respiring a variety of terminal electron acceptors, several of which [DMSO, nitrate, Se(VI), and As(V)] are known substrates for members of the DMSOR family. The draft genome of MLFW-2^T contains fourteen genes that are predicted to encode the catalytic subunits of enzymes belonging to the DMSOR family. In order to assign putative functions to some of these genes, RT-qPCR was used to quantify their relative transcription during growth on nitrate, Se(VI), As(V), and Sb(V), with growth on nitrite serving as a control. Genes BHU72_03635, BHU72_07355, and BHU72_10330 appear to encode the catalytic subunits of a periplasmic nitrate reductase (NapA), membrane-bound Se(VI) reductase (SrdA), and respiratory As(V) reductase (ArrA), respectively. Transcription of BHU72_07145 was markedly increased in the presence of Sb(V), indicating that the product of this gene may play a role in dissimilatory Sb(V) reduction. The physiological response of MLFW-2^T to growth on Sb(V) and As(V) was assessed by analyzing the transcriptomes of cultures grown on these electron acceptors. In comparison to As(V), Sb(V) was found to induce the transcription of genes involved in oxidative stress, including those involved in repairing or degrading damaged biomolecules and scavenging reactive oxygen species.

INTRODUCTION

Bacteria and Archaea thrive in diverse environments characterized by extremes of redox potential, temperature, pH, salinity, pressure, and ionizing radiation. A key factor that contributes to the ability of these organisms to colonize such environments is their remarkable metabolic versatility. Prokaryotic genomes encode a multitude of respiratory electron transfer chain enzymes that allow for growth on a variety of terminal electron donors and acceptors. An important group of enzymes that contributes to this respiratory versatility is the dimethyl sulfoxide reductase (DMSOR) family of the complex iron-sulfur molybdoenzyme (CISM) superfamily, members of which exploit the versatility of a molybdenum- or tungsten-containing cofactor to catalyze two-electron redox reactions (McEwan *et al.* 2002, Rothery *et al.* 2008). Enzymes of the DMSOR family have been implicated in the dissimilatory reduction of DMSO, trimethylamine N-oxide (TMAO), (per)chlorate, nitrate, arsenate [As(V)], selenate [Se(VI)], elemental sulfur/polysulfide, thiosulfate, and tetrathionate. In addition, several members are responsible for the dissimilatory oxidation of substrates such as formate, dimethyl sulfide (DMS), arsenite [As(III)], and nitrite (Grimaldi *et al.* 2013).

The molecular organization of enzymes of the DMSOR family is remarkably varied, with the only common feature being the catalytic subunit. Enzymes of this family can occur as monomeric, dimeric, or trimeric protein complexes localized to the periplasm or cytoplasm, or bound to the cell membrane by an integral membrane subunit. An archetypal enzyme contains three subunits: a catalytic subunit, an electron transfer subunit (ETS), and an electron entry/exit subunit (EES) (Grimaldi *et al.* 2013). The catalytic subunit contains a molybdenum/tungsten-*bis*(pyranopterin guanine dinucleotide) (Mo/W-*bis*PGD) cofactor in which the central Mo/W atom transfers between the +4,+5, and +6 oxidation states during enzyme turnover (Rothery *et*

al. 2008, Schwarz *et al.* 2009). In the majority of cases, the catalytic subunit also contains a [4Fe-4S] cluster that functions to transfer electrons to the site of catalysis. The ETS is usually a ferredoxin that contains four [4Fe-4S] clusters and functions to shuttle electrons from the EES to the [4Fe-4S] cluster of the catalytic subunit. Lastly, the EES serves to link the complex to the electron transport chain. In the majority of cases, the EES is an integral membrane protein that serves as the site of quinone-reduction or quinol-oxidation. The EES can be a transmembrane cytochrome b, a soluble cytochrome c, or an NrfD family transmembrane protein devoid of any cofactors (Grimaldi *et al.* 2013).

The significance of the role that enzymes of the DMSOR family play in supporting prokaryotic metabolisms cannot be understated. These enzymes catalyze redox reactions that account for important steps in the global C, N, S, As, Se, and Cl cycles. Moreover, phylogenetic analyses based on 3D structures have revealed that several members of the family, including polysulfide reductase (Psr), formate dehydrogenase (Fdh), respiratory nitrate reductase (Nar), and aerobic As(III) oxidase (Aio) were most likely present in the last universal common ancestor (LUCA) to all life on Earth (Schoepp-Cothenet *et al.* 2012). In spite of this, relatively little is known about this family of enzymes and the exact manner by which they are integrated into energy-conserving respiratory chains. Indeed, BLAST searches of prokaryotic genomes reveal many new and distinct subfamilies whose functions are currently unknown. The study of their potential function, molecular properties, and evolutionary relationships will be essential to further our understanding of this ancient group of enzymes and the roles that they have played in supporting the metabolic evolution of microbial life on Earth.

Desulfuribacillus stibiiarsenatis MLFW-2^{T} is an obligately anaerobic bacterium that was isolated from anoxic sediments along the southern shore of Mono Lake, CA (Abin and

Hollibaugh 2014, Abin and Hollibaugh 2017). It is capable of respiring several terminal electron acceptors, including DMSO, nitrate, nitrite, Se(VI), Se(IV), and As(V), many of which are known substrates for anaerobic respiratory reductases of the DMSOR family. MLFW-2^T is also capable of using the toxic oxyanion antimonate [Sb(V)] as an electron acceptor for growth, converting it to antimonite [Sb(III)] (Abin and Hollibaugh 2014). Based on the chemical similarities between Sb and As, coupled with the fact that dissimilatory Sb(V) reduction involves a two-electron redox reaction, it is likely that the terminal Sb(V) reductase is a member of the DMSOR family. Indeed, recent evidence has shown that the Aio systems of *Agrobacterium tumefaciens* 5A and *Rhizobium* sp. strain NT-26 are capable of catalyzing the oxidation of not only As(III), but Sb(III) as well (Wang *et al.* 2015).

Therefore, MLFW-2^T presents a unique opportunity to study novel enzymes of the DMSOR family and the function(s) that they play in anaerobic respiration. In this study, genes encoding the catalytic subunits of members of the DMSOR family were identified within the draft genome of MLFW-2^T. The relative transcription of these genes during growth on nitrate, Se(VI), As(V), and Sb(V) was monitored, using growth on nitrite as a control. The goal of this work was to identify the respiratory reductases used by MLFW-2^T during growth on nitrate, Se(VI), and As(V), as well as to determine if any DMSOR family genes were upregulated during growth on Sb(V). In addition, RNA sequencing (RNA-seq) was used to compare the physiological response of MLFW-2^T to growth on Sb(V) and As(V), two electron acceptors that share similar chemistry, yet elicit very different effects on growth.

MATERIALS & METHODS

Media preparation and culture conditions

Strain MLFW-2^T was grown anaerobically with nitrite, nitrate, Se(VI), As(V), and Sb(V) as terminal electron acceptors. Lactate was provided in stoichiometric excess as the electron donor. Growth experiments involving nitrite, nitrate, Se(VI), and As(V) were performed in a mineral salts medium (MS-NSeAs) containing the following ingredients per liter of deionized water: 4.2 g $NaHCO_3$, 3.62 g NaCl, 0.261 g K_2HPO_4, 0.075 g NH_4Cl, 0.050 g Na_2SO_4, 0.5 g tryptone, 0.2 g yeast extract, 10 mL vitamin solution (Oremland *et al.* 1994), and 1 mL SL-10 trace metals solution (Widdel *et al.* 1983) modified by the addition of 2.85 g/L $MgCl_2$ x $6H_2O$ and 0.103 g/L $CaCl_2$ x $2H_2O$. The pH of the medium was adjusted to 8.2 with KOH and the medium was filter sterilized into sterile glass media bottles using a Steritop filter unit (MilliporeSigma, Burlington, MA). For growth experiments involving Sb(V), MLFW-2^T was grown in a mineral salts medium (MS-Sb) containing the following ingredients per liter of deionized water: 0.084 g $NaHCO_3$, 0.203 g K_2HPO_4, 0.075 g NH_4Cl, 0.05 g Na_2SO_4, and 10 mL and 1 mL, respectively, of the vitamin and trace metals solutions described above. The pH of the medium was adjusted to 7.0 with HCl and the medium was filter sterilized as above.

The caps of the bottles containing the sterile media were loosened and the media were allowed to deoxygenate in an anaerobic chamber (Coy Laboratory Products, Grass Lake, MI) containing an atmosphere of 95% N_2 + 5% H_2 for at least 7 days prior to use. Sterile stock solutions of ACS reagent grade sodium L-lactate, sodium nitrite ($NaNO_2$), sodium nitrate ($NaNO_3$), sodium selenate (Na_2SeO_4), sodium arsenate dibasic heptahydrate (Na_2HAsO_4 x $7H_2O$), potassium hexahydroxoantimonate [$KSb(OH)_6$], and sodium sulfide nonahydrate (Na_2S x $9H_2O$) were prepared and allowed to deoxygenate in the anaerobic chamber for at least 4 days

prior to use. All stock solutions were used within 7 days of preparation. All further manipulations were made in the anaerobic chamber using sterile technique.

For growth experiments involving nitrite, nitrate, Se(VI), and As(V), anoxic MS-NSeAs medium was supplemented with 100 μM sulfide (as reducing agent and source of reduced sulfur) and the following concentrations of lactate and electron acceptor: 5 mM lactate + 2 mM nitrite, 14 mM lactate + 5 mM nitrate, 10 mM lactate + 5 mM Se(VI), and 5mM lactate + 5 mM As(V). A control experiment, in which MS-NSeAs medium was supplemented with 100 μM sulfide + 15 mM lactate + 5 mM As(V), was also prepared. The growth experiment involving Sb(V) used anoxic MS-Sb medium supplemented with 100 μM sulfide + 1 mM lactate + 1 mM Sb(V). A control experiment, in which MS-Sb medium was supplemented with 100 μM sulfide + 5 mM lactate + 5 mM As(V), was also prepared. In all cases, 98 mL of the as-prepared medium was dispensed into fifteen sterile, 160 mL glass serum bottles (Wheaton, Millville, NJ). Three of the bottles served as replicate samples for the quantification of cells and dissolved oxyanions. The remaining twelve bottles were split into two groups of six (three replicates, with two bottles per replicate) to be grown in parallel and used for RNA extraction during the early- and late-log phases of growth. The serum bottles were closed with sterile butyl rubber stoppers (Geo-Microbial Technologies, Ochelata, OK) and crimp-sealed with aluminum caps (Wheaton). The headspace within each bottle was the same as the gas mixture in the anaerobic chamber.

The inoculum for the nitrite, nitrate, Se(VI), and As(V) growth experiments [including the control with 15 mM lactate + 5 mM As(V)] was 2 mL of a culture of MLFW-2^T that was grown in the presence of lactate and the respective electron acceptor for at least six transfers (1:50 dilution per transfer). This practice was used to ensure that only the desired electron

acceptor was present in the medium at the start of the experiment. The serum bottles were incubated at 34°C in the dark and without shaking.

The inoculum for the growth experiment involving Sb(V) consisted of cells that were grown on 3 mM lactate + 500 μM As(V) + 1 mM Sb(V) for at least eight transfers (1:20 dilution per transfer), washed, grown once on 1 mM lactate + 1 mM Sb(V), and then washed again prior to inoculation. Cells were prepared for washing by passing 300 mL of culture through a 0.22 μm Sterivex syringe filter unit (MilliporeSigma). Cells trapped on the filter were washed by passing ~30 mL of sterile, anoxic MS-Sb medium supplemented with 100 μM sulfide + 1 mM lactate through the filter unit using a syringe. The washed cells were recovered from the filter unit using a syringe and re-suspended in a total volume of 30 mL of the wash medium. Two mL of this suspension was inoculated into each of the serum bottles. The inoculum for the control experiment with 5 mM lactate + 5 mM As(V) in MS-Sb medium was 2 mL of a culture grown in the presence of lactate and As(V) for at least six transfers (1:50 dilution each transfer) and then washed as described above, with the exception that only 80 mL of culture was filtered. Serum bottles were incubated at 30°C in the dark and without shaking for both of these experiments.

In all cases, a syringe was used to remove a ~2.2 mL sample of culture from replicate serum bottles for each treatment at certain time points. One mL of this sample was sterilized using a 0.22 μm syringe filter (Thermo Fisher Scientific, Waltham, MA) and subsequently used to quantify organic acids and dissolved oxyanions. A second 1 mL sample was used to enumerate cells.

Chemical and biological analyses

Lactate, acetate, As(V), As(III), and selenite [Se(IV)] were quantified using high performance liquid chromatography (HPLC) with 0.016 N H_2SO_4 as the mobile phase (Hoeft *et al.* 2004, Fisher *et al.* 2007). As(V), As(III), and Se(IV) were detected at a wavelength of 200 nm, while lactate and acetate were detected at 210 nm. Total dissolved Se was quantified using a Thermo Jarrell-Ash 965 inductively coupled argon plasma optical emission spectrometer (ICP-OES) (Thermo Jarrell-Ash, Franklin, MA) at the Center for Applied Isotope Studies at the University of Georgia (Athens, GA). Se(VI) and Se(0) were quantified by difference, as described previously (Abin and Hollibaugh 2017). Total dissolved Sb and Sb(V) were measured using ICP-OES after selective removal of Sb(III) by liquid-liquid extraction (Abin and Hollibaugh 2014). The concentration of Sb(III) was then calculated as the difference between total dissolved Sb and Sb(V). Nitrite was measured colorimetrically following reaction with the Greiss reagent (Bendschneider and Robinson 1952). Copperized cadmium filings were used to reduce nitrate to nitrite quantitatively, followed by reaction of nitrite with the Greiss reagent (Wood *et al.* 1967). Nitrate was calculated as the difference between these two nitrite measurements. Ammonium was measured colorimetrically by the phenol-hypochlorite method (Weatherburn 1967). Cells were enumerated using a Leica DM RXA epifluorescence microscope (Leica, Wetzlar, Germany) after being fixed in 5% formalin and stained with 0.01% acridine orange.

Phylogenetic Methods

The amino acid sequences of the catalytic subunits of well characterized enzymes of the DMSOR family were used as queries to search the MLFW-2^T draft genome using the Basic

Local Alignment Search Tool (BLAST) (Altschul *et al.* 1990). Once identified, the products of target genes were analyzed using InterProScan v5 (Jones *et al.* 2014) to confirm the presence of a Mo/W-*bis*PGD-binding domain. MetalPredator (Valasatava *et al.* 2016), TargetS (Yu *et al.* 2013), and the ScanProsite tool (de Castro *et al.* 2006) were also used to analyze protein sequences for potential ligand-binding domains. The TatP v1.0 (Bendtsen *et al.* 2005) and SignalP v4.1 (Petersen *et al.* 2011) servers were used to predict the presence of signal peptide cleavage sites in protein sequences. Transmembrane helix prediction was performed using the TMHMM Server v2.0 (Krogh *et al.* 2001). Multiple sequence alignments were performed using MUSCLE (Edgar 2004). Phylogenetic trees were constructed using MEGA v6.06 (Tamura *et al.* 2013). Evolutionary histories were inferred using the neighbor-joining method (Saitou and Nei 1987) with Jukes-Cantor evolutionary distances (Jukes and Cantor 1969). The confidence limits for the branch points on each tree were estimated from 1,000 bootstrap replications (Felsenstein 1985).

RNA extraction

Total RNA was extracted from two sets of triplicate samples of early- and late-log phase cultures (for a total of six samples per treatment). All manipulations of cells prior to harvesting were performed in the anaerobic chamber. At each time point, the contents of two serum bottles for each replicate (200 mL total volume) were emptied into a sterile, 250 mL polycarbonate centrifugation bottle with a rubber gasket (Thermo Fisher Scientific) and immediately placed on ice. The cells were then harvested by centrifugation at 10,000x*g* for 10 minutes at 4°C. The supernatant was decanted and total RNA was extracted from the cell pellet using a ZR Fungal/Bacterial RNA MiniPrep Kit (Zymo Research, Irvine, CA) according to the

manufacturer's instructions. Genomic DNA was removed from the RNA extracts using a TURBO DNA-free Kit (Thermo Fisher Scientific), increasing the incubation time to 1 hour at 37°C. The quantity and purity of the RNA in each sample was assessed after each procedure using a NanoDrop 2000 UV-Vis spectrophotometer (Thermo Fisher Scientific).

Primer design

The software package Geneious v8.1.8 (Kearse *et al.* 2012) was used to design gene-specific PCR primers to amplify an internal region (103-198 bp) of fourteen different target genes in the MLFW-2^T draft genome that were expected to encode the catalytic subunits of enzymes of the DMSOR family. A PCR primer set designed to amplify a 148 bp internal region of the housekeeping gene *gyrB*, encoding the beta subunit of DNA gyrase, was also developed. Information about each of the fifteen qPCR primer sets used in this study is presented in Table 4.S1.

Reverse transcription – quantitative PCR (RT-qPCR)

RT-qPCRs were performed in Hard-Shell 96-well PCR plates (Bio-Rad, Hercules, CA) using a CFX96 Touch Real-Time PCR Detection System (Bio-Rad). Reactions were prepared in a total volume of 20 μL using the iTaq Universal SYBR Green One-Step Kit (Bio-Rad), with forward and reverse primers supplied at a concentration of 0.4 μM each and using 30 ng of RNA template. All reactions were performed with three technical replicates per biological replicate. The thermocycle profile was identical for all samples and consisted of the following steps: 50 °C for 10 min (cDNA synthesis), 95 °C for 1 min, 40 cycles of 95 °C for 45 sec, 55 °C for 30 sec,

72 °C for 30 sec, and a final incremental denaturation cycle from 62-95°C to evaluate the melt curves of the PCR products.

The melt curve of each of the fifteen PCR products revealed only a single peak at the expected temperature, indicating that the desired template was amplified in each case. The PCR products were electrophoresed on a 1.5% agarose gel and compared with a Quick-Load 100 bp DNA Ladder (New England Biolabs, Ipswich, MA) to confirm that they were of the correct length. An aliquot of each DNase-treated extract used in this study was also subjected to PCR using primers targeting the *gyrB* gene to rule out DNA contamination.

The RT-qPCR amplification efficiency of each primer set was determined using DNase-treated RNA extracted from late-log phase cells of MLFW-2^T grown in MS-NSeAs medium containing 100 μM sulfide + 5 mM lactate + 5 mM As(V). The RNA was serially diluted (1:2) nine times and RT-qPCRs were performed on the samples from the dilution series. The amplification efficiency (E) of each primer set was then calculated from the slope of the C_T vs. log(RNA input) curve according to the equation: $E = (10^{(-1/slope)} - 1) \times 100$ (Pfaffl 2001). The mean amplification efficiency for all fifteen primer sets was 94.1% (range: 92.4% – 97.6%) with all linear correlation coefficients (R^2) ≥ 0.99 (Table 4.S1).

The raw C_T values obtained from RT-qPCR were corrected for amplification efficiency using the formula: $C_{T(adj)} = C_{T(raw)}[Log(1+E)/Log(2)]$ (Ståhlberg *et al.* 2013). For each treatment, the ΔC_T for a gene was calculated by subtracting the average $C_{T(adj)}$ for that gene by the average $C_{T(adj)}$ for *gyrB*. Relative changes in gene transcription between treatments were calculated using the $2^{-\Delta\Delta CT}$ method (Livak and Schmittgen 2001), with growth on nitrite as the calibrator. Statistically significant changes in relative gene transcription were assessed by Student's t-test,

for which a p-value ≤ 0.05 was considered significant. Genes were considered to be differentially transcribed if they had a |fold change| ≥ 2 and a p-value ≤ 0.05.

RNA-seq

RNA-seq was performed on the twelve DNA-free RNA samples extracted from early- and late-log phase cultures of MLFW-2^T grown on Sb(V) and As(V) in MS-Sb medium (six samples per treatment). Ribosomal RNA (rRNA) depletion, library construction, and sequencing were performed at the Georgia Genomics Facility at the University of Georgia. A Ribo-zero rRNA Removal Kit (Illumina, San Diego, CA) was used to deplete 16S and 23S rRNA from the samples, according to the manufacturer's instructions. The quality of the depleted RNA was assessed on an Agilent 2100 Bioanalyzer (Agilent, Santa Clara, CA) using an Agilent RNA 6000 Pico Kit. RNA fragmentation, first- and second-strand cDNA synthesis, A-tailing, adapter ligation, and library amplification were performed using the KAPA Stranded RNA-Seq Library Preparation Kit (Kapa Biosystems, Wilmington, MA), according to the manufacturer's instructions. The size and quality of the resulting libraries was assessed using a Fragment Analyzer Automated CE System (Advanced Analytical Technologies, Ankeny, IA). The concentration of DNA in each library was determined using a Qubit 2.0 fluorometer (Invitrogen, Carlsbad, CA). Paired-end (2 x 75 bp) sequencing was performed using the Miseq platform (Illumina) with a MiSeq Reagent Kit v3 (Illumina). The RNA-seq data have been deposited in the NCBI Sequence Read Archive under the project accession number SRP136324.

Bioinformatic analysis of RNA-seq data

The raw reads obtained from each of the sequencing runs were trimmed and filtered using Trimmomatic v0.36 (Bolger *et al.* 2014). Reads were mapped to the MLFW-2^T draft genome (Genbank accession no. NZ_MJAT00000000) using Bowtie2 v2.2.1 (Langmead and Salzberg 2012). The number of reads that mapped to each annotated coding sequence was determined using HTSeq-count v0.6.1 (Anders *et al.* 2015). Genes that were differentially transcribed between the two conditions were determined using the R package DESeq2 (Love *et al.* 2014), correcting for multiple testing using the method of Benjamini and Hochberg (1995). Genes were considered to be differentially transcribed if they had a |fold change| ≥ 2 and an adjusted *p*-value ≤ 0.05. Functional annotation of differentially transcribed genes was performed using the eggNOG-mapper (Huerta-Cepas *et al.* 2017), which assigns functional orthology based on homology to sequences in the EggNOG 4.5.1 (Huerta-Cepas *et al.* 2016), Kyoto Encyclopedia of Genes and Genomes (KEGG) (Kanehisa and Goto 2000), Gene Ontology (GO) (Ashburner *et al.* 2000), and Clusters of Orthologous Groups (COG) (Tatusov *et al.* 2000) databases.

RESULTS

Identification of genes encoding enzymes of the DMSOR family in MLFW-2^T

We queried the draft genome of MLFW-2^T to search for genes encoding proteins with homology to the catalytic subunits of well characterized members of the DMSOR family, including DorA (Knäblein *et al.* 1996), DmsA (Bilous *et al.* 1988), NarG (Blasco *et al.* 1989), NapA (Thomas *et al.* 1999), PsrA (Krafft *et al.* 1992), SrdA (Kuroda *et al.* 2011), SerA (Krafft *et al.* 2000), TtrA (Hensel *et al.* 1999), FdhA (Raaijmakers *et al.* 2002), and ArrA (Saltikov and Newman 2003). We identified seventeen genes that encode putative members of the DMSOR

family using this approach. The products of three of these genes (BHU72_04285, BHU72_05685, and BHU72_10655) were expected to encode the catalytic subunits of aldehyde oxidases/xanthine dehydrogenases of the xanthine oxidase (XO) family of CISMs. All three proteins possessed a molybdenum-pyranopterin cytosine dinucleotide (Mo-PCD)-binding domain as well as the a/b hammerhead domain found in all members of the XO family (Schwarz *et al.* 2009). These genes were excluded from further analysis, as they were not expected to encode components of anaerobic respiratory chains.

The proteins encoded by the remaining fourteen genes all contained the Mo/W-*bis*PGD-binding domain found in enzymes of the DMSOR family. The genes and their products are listed in Table 4.1. All but three of these genes (BHU72_01065, BHU72_03930, and BHU72_07925) encode proteins predicted to be secreted across the membrane by the twin arginine translocation (TAT) pathway. A phylogenetic tree showing the evolutionary relationship between each of the expected gene products and well-characterized members of the DMSOR family is provided in Figure 4.1. The products of seven genes (BHU72_01065, BHU72_01090, BHU72_04760, BHU72_07145, BHU72_07340, BHU72_07925, and BHU72_09285) did not cluster closely with any of the known subfamilies. BHU72_03930 and BHU72_06270 may encode the catalytic subunits of formate dehydrogenases, which catalyze the oxidation of formate to CO_2, typically donating the liberated electrons to the quinone pool or to other electron shuttles (Maia *et al.* 2017). The product of BHU72_03930 is a selenocysteine-containing protein that shared 33% sequence identity and 52% sequence similarity to YrhE and YjgC, the catalytic subunits of two putative formate dehydrogenases from *Bacillus subtilis*. BHU72_06270 encodes another selenocysteine-containing protein that shared significant homology with the catalytic subunits of the tungsten-containing formate dehydrogenase of

Desulfovibrio gigas (FdhA; 47% identity and 63% similarity) and the nitrate-inducible formate dehydrogenase of *Escherichia coli* (FdnG; 44% identity and 62% similarity).

The product of BHU72_03635 clustered well with NapA, the catalytic subunit of periplasmic nitrate reductase. The Nap complex is responsible for the reduction of nitrate to nitrite, passing electrons from the quinone pool through an integral membrane quinol dehydrogenase and a soluble cytochrome c (Stewart *et al.* 2002, Brondijk *et al.* 2004). The product of BHU72_03635 was 47% identical and 64% similar to the well characterized NapA from *Desulfovibrio desulfuricans*. BHU72_07355 encodes a protein with a high degree of homology (66% identity and 80% similarity) to SrdA, the catalytic subunit of the membrane-bound Se(VI) reductase from *Bacillus selenatarsenatis*. This complex catalyzes the reduction of Se(VI) to Se(IV) and is anchored to the membrane by an NrfD family EES, as opposed to the soluble Se(VI) reductase (Ser) from *Thauera selenatis* (Kuroda *et al.* 2011). The product of BHU72_07375 shared a modest degree of homology with the well-studied TtrA from *Salmonella enterica* ser. Typhimurium (31% identity and 49% similarity). TtrA serves as the catalytic subunit for a membrane-bound tetrathionate reductase complex that catalyzes the reduction of tetrathionate to thiosulfate (Hensel *et al.* 1999).

BHU72_10220 and BHU72_10330 both encode proteins with significant homology to ArrA, the catalytic subunit of respiratory As(V) reductase. This complex reduces As(V) to As(III) and can function as a soluble (ArrAB) or membrane-linked (ArrABC) module (van Lis *et al.* 2013). The product of BHU72_10220 shared 54% identity/69% similarity and 50% identity/67% similarity, respectively, with the purified ArrA from *Bacillus selenitireducens* and *Shewanella* sp. ANA-3. Likewise, the protein encoded by BHU72_10330 shared 49%

identity/64% similarity and 49% identity/65% similarity, respectively, with ArrA from the same two organisms listed above.

Relative transcription of DMSOR family genes during growth on different electron acceptors

To assign putative functions to some of the DMSOR family genes, their transcription relative to the housekeeping gene *gyrB* was monitored by RT-qPCR during exponential growth on nitrate, Se(VI), As(V), and Sb(V). For these experiments, growth on nitrite was used to normalize relative changes in gene transcription. Nitrite reduction was chosen because it is not known to be performed by any member of the DMSOR family. The Sb(V) treatment was performed in a modified medium (MS-Sb; MS-NSeAs for all other experiments) with a low sodium content because Sb(V) combines with sodium to form the sparingly soluble compound $NaSb(OH)_6$ ($Ksp = 8.89 \times 10^{-6}$) (Diemar *et al.* 2009). No precipitation of Sb(V) was observed in MS-Sb medium in abiotic controls (data not shown). In addition, the inoculum for the Sb(V) treatment consisted of cells that had been washed with fresh medium prior to transfer. This was done because reproducible growth on Sb(V) could only be achieved if highly toxic Sb(III) was removed from culture supernatants prior to transfer.

Growth curves and growth rates of MLFW-2^T on each electron acceptor are presented in Figures 4.S1-S5 and Table 4.2, respectively. Relative transcription data for all fourteen DMSOR family genes during growth on each electron acceptor are provided in Figure 4.2 and Table 4.S2. In each case, lactate was provided as the electron donor in stoichiometric excess relative to the electron acceptor. Control experiments demonstrated that there were no statistically significant differences in the relative transcription of DMSOR family genes when MLFW-2^T was grown in MS-NSeAs medium with varying amounts of lactate, or when the cells were washed and grown

in MS-Sb medium (Figure 4.S6 and Table 4.S3). Growth curves for the control experiments are provided in Figure 4.S7.

As first reported by Abin and Hollibaugh (2017), MLFW-2^T is capable of dissimilatory nitrate/nitrite reduction to ammonium (DNRA). When provided with nitrate as the electron acceptor, nitrite is produced transiently before it is reduced to ammonium. The nitrite concentration in the nitrate treatment reached a maximum of 1.3 mM at 13.5 h (Figure 4.S2). Both species appeared to be reduced simultaneously, rather than sequentially. The reduction of ~5 mM nitrate led to an approximate 200-fold increase in the abundance of cells, while ~2 mM nitrite supported an 80-fold increase (Figures 4.S1 and S2). The observed molar ratio of electron acceptor reduced to lactate oxidized was 1:1.6 and 1:2.5 for growth on nitrite and nitrate, respectively. These values are similar to the theoretical molar ratios of 1:1.5 and 1:2 for nitrite and nitrate reduction, respectively, coupled to lactate oxidation.

Four DMSOR family genes (BHU72_01090, BHU72_03635, BHU72_04760, and BHU72_09285) were upregulated when nitrate was provided as the electron acceptor (Figure 4.2 and Table 4.S2). There was a 3-fold increase in the transcription of BHU72_01090 relative to the Se(VI) and Sb(V) treatments. There was a 2-fold increase in transcription relative to the As(V) treatment, but the change was not statistically significant. BHU72_09285 was modestly upregulated, with a 4- to 6-fold increase relative to each of the other treatments. The transcription of BHU72_03635 and BHU72_04760 was highly upregulated in the presence of nitrate. BHU72_03635 was transcribed at a level 84- to 514-fold greater than each of the other treatments, while BHU72_04760 was 60- to 434-fold upregulated.

Dissimilatory reduction of Se(VI) by MLFW-2^T also involved the transient formation of Se(IV), which was further reduced to yield a red allotrope of Se(0). Unlike the case with growth

on nitrate and nitrite, however, Se(VI) and Se(IV) reduction did not proceed simultaneously. The consumption of ~5 mM Se(VI) was completed within 17.6 h without appreciable accumulation of elemental Se (Figure 4.S3). At 17.6 h, Se(IV) reached a maximum concentration of ~4 mM and was subsequently consumed over the next ~7 h, resulting in the precipitation of Se(0) in an amount that was approximately equivalent to the amount of Se(VI) originally present in the medium. The reduction of ~5 mM Se(VI) resulted in an approximate 320-fold increase in the abundance of cells, with a 1:1.8 ratio of Se(VI) reduced to lactate oxidized. This ratio is similar to the expected ratio of 1:1.5 based on theoretical calculations.

Two genes, BHU72_07355 and BHU72_07375, were highly upregulated when MLFW-2^T was grown with Se(VI) as the electron acceptor (Figure 4.2 and Table 4.S2). The transcription of BHU72_07355 was 211- and 216-fold greater in the presence of Se(VI) than nitrate and As(V), respectively. Transcription of this gene also increased 8-fold relative to the Sb(V) treatment. The expression of BHU72_07375 showed a similar pattern, with 35- to 167-fold upregulation relative to each of the other treatments.

Dissimilatory reduction of As(V) by MLFW-2^T proceeded rapidly, with complete conversion of ~5 mM As(V) to As(III) within 13.8 h, accompanied by an 85-fold increase in the abundance of cells (Figure 4.S4). There was good agreement between the observed (1.8:1) and theoretical (2:1) molar ratios of the amount of As(V) reduced relative to lactate oxidized. Growth on As(V) yielded the shortest doubling time and the fastest cellular rate of electron acceptor reduction, even though thermodynamic considerations ranked As(V) as the least favorable electron acceptor tested (Table 4.2). This phenomenon has been observed previously in the obligate anaerobe *Desulfurispirillum indicum* S5, which grows preferentially on As(V)

over less toxic and more thermodynamically favorable electron acceptors such as nitrate (Rauschenbach *et al.* 2012).

The transcription of BHU72_10330 was highly upregulated when As(V) was provided as the terminal electron acceptor (Figure 4.2 and Table 4.S2). The transcription of this gene increased 36- to 61-fold relative to each of the other treatments. Transcription of BHU72_07145 also increased approximately 2-fold during growth on As(V) relative to the nitrate and Se(VI) treatments. However, BHU72_07145 was transcribed at a level 350-fold lower than in the Sb(V) treatment.

Growth of MLFW-2^T on ~1.2 mM Sb(V) was poor relative to the other electron acceptors, with only a 4-fold increase in cells over a period of 23 h (Figure 4.S5). Even though the doubling time of MLFW-2^T on Sb(V) was the longest of any electron acceptor tested, the cellular rate of Sb(V) reduction was higher than that observed for both nitrate and nitrite reduction (Table 4.2). The concentration of dissolved Sb remained relatively stable until 16.3 h, at which point the Sb(III) concentration had reached ~0.8 mM. Between 16.3 h and 24.3 h, the concentration of dissolved Sb decreased by ~0.5 mM due to the precipitation of Sb(III). The observed molar ratio of Sb(V) reduced to lactate oxidized was 2.3:1, a value in close agreement with the expected ratio of 2:1.

The transcription of four genes (BHU72_03930, BHU72_07145, BHU72_07355, and BHU72_07375) was elevated when Sb(V) was provided as the electron acceptor (Figure 4.2 and Table 4.S2). BHU72_03930 was 2-fold upregulated relative to each of the other treatments. BHU72_07145 was highly upregulated in the presence of Sb(V), with transcription increasing 350- to 786-fold relative to each of the other treatments. The transcription of BHU72_07355 and BHU72_07375 was upregulated relative to the nitrate and As(V) treatments, but not the Se(VI)

treatment. In the case of BHU72_07355, transcription increased 25- and 26-fold relative to the nitrate and As(V) treatments, respectively, but was 8-fold lower relative to the Se(VI) treatment. The transcription of BHU72_07375 increased 2- and 5-fold relative to the nitrate and As(V) treatments, respectively. However, this gene was transcribed at a level 35-fold lower than in the presence of Se(VI).

Genomic context of upregulated DMSOR family genes

The chromosomal regions immediately surrounding each of the four genes upregulated during dissimilatory nitrate reduction by MLFW-2^T are presented in Figure 4.3. The gene with the most significant increase in relative transcription, BHU72_03635, most likely encodes the catalytic subunit, NapA, of the periplasmic nitrate reductase in this organism. A phylogenetic tree showing the evolutionary relationship between BHU72_03635 and other NapA proteins is presented in Figure 4.S8. The presumptive *nap* operon of MLFW-2^T shares synteny with the unusual *nap* operon of *Bacillus azotoformans*. Both operons lack genes encoding the cytoplasmic maturation factors NapF and NapL, as well as the integral-membrane quinol dehydrogenase NapC (Heylen and Keltjens 2012). However, genes encoding two distinct copies of NapG (BHU72_03615 and BHU72_03630) are present, as well as genes encoding NapH (BHU72_03620), the cytoplasmic chaperone NapD (BHU72_03625), and a diheme *c*-type cytochrome resembling NapB (BHU72_03640). NapG2 and NapH likely form an integral-membrane quinol dehydrogenase that shuttles electrons from the quinone pool to the NapAB catalytic module (Brondijk *et al.* 2004). It is thought that in *B. azotoformans*, NapG1 may substitute for the absent NapF to assure proper assembly of the [4Fe-4S] cluster of the NapA subunit (Heylen and Keltjens 2012).

BHU72_04760 was also highly upregulated in the presence of nitrate. Immediately upstream of this locus are genes encoding a histidine kinase (BHU72_04740), a TusA-like sulfurtransferase (BHU72_04745), a LysR family transcriptional regulator (BHU72_04750), and a membrane protein involved in the transport of sulfur-containing compounds (BHU72_04755) (Figure 4.3B). Downstream of BHU72_04760 are genes encoding a 4[4Fe-4S] ETS (BHU72_04765), NrfD family EES (BHU72_04770), and TorD family cytoplasmic chaperone (BHU72_04775).

The other two genes associated with nitrate reduction, BHU72_09285 and BHU72_01090, were only modestly upregulated. Downstream of BHU72_09285 are genes encoding a 4[4Fe-4S] ETS (BHU72_09280), NrfD family EES (BHU72_09275), and TorD family cytoplasmic chaperone (BHU72_09270) (Figure 4.3C). Immediately upstream of BHU72_09285, and on the opposite strand, is a gene encoding a LysR family transcriptional regulator (BHU72_09290). BHU72_01090 exists in a potential operon that lacks an EES, but contains genes encoding a TorD family cytoplasmic chaperone (BHU72_01085) and a 4[4Fe-4S] ETS (BHU72_01095) (Figure 4.3D).

Dissimilatory Se(VI) reduction was associated with the upregulation of two genes, BHU72_07355 and BHU72_07375, located very close to each other on the MLFW-2^T chromosome. BHU72_07355 most likely encodes SrdA, the catalytic subunit of a membrane-bound Se(VI) reductase. Two genes, *srdB* (BHU72_07345) and *srdC* (BHU72_07350), encoding the ETS and EES subunits, respectively, of the Srd complex are located immediately upstream of BHU72_07355 (Fig. 4.4A). The orientation of genes in the presumptive *srd* operon of MLFW-2^T is the same as that found in *B. selenatarsenatis*, the only other organism known to encode a membrane-bound Se(VI) reductase (Kuroda *et al.* 2011). A gene encoding a 4[4Fe-4S]

ETS (BHU72_07370) is found upstream of BHU72_07375, while three downstream genes (BHU72_07380, BHU72_07385, and BHU72_07390) encode a periplasmic phosphonate-binding protein, histidine kinase, and a LuxR family transcriptional regulator, respectively (Fig. 4.4B). Phylogenetic analysis of BHU72_07355 and BHU72_07375 revealed that they belong to two separate clades related to, but distinct from, tetrathionate reductases (Figure 4.S9).

The transcription of BHU72_10330 was highly upregulated in the presence of As(V), and this gene likely encodes the ArrA catalytic subunit of the respiratory As(V) reductase in MLFW-2^T. Phylogenetic analysis showed that BHU72_10330 clustered well with ArrA proteins from other As(V)-respiring bacteria (Figure 4.S10). The potential *arr* operon of MLFW-2^T also contains genes encoding the 4[4Fe-4S] ETS ArrB (BHU72_10325), the TorD family cytoplasmic chaperone ArrD (BHU72_10320), and the 4[4Fe-4S] ferredoxin ArrB' (BHU72_10315), but it lacks a gene for ArrC, the NrfD family EES that links the complex to the quinone pool in some bacteria (van Lis *et al.* 2013) (Figure 4.5A). Although the function of *arrB'* gene product is currently unknown, it may play a role in the maturation of the Arr complex because it always occurs directly downstream of *arrD*. The *arr* operons of several bacteria, including *Desulfuribacillus alkaliarsenatis*, *Anaerobacillus arceniciselenatis*, *B. selenatarsenatis*, *D. indicum*, *Alkaliphilus* spp., and *Geobacter* spp. contain at least one copy of *arrB*'.

Interestingly, the transcription of BHU72_10220 was not upregulated in the presence of As(V), even though it clustered well with ArrA proteins from other As(V)-respiring bacteria (Figure 4.S10) and it is located upstream of the *acr3* (BHU72_10200), *arsA* (BHU72_10195), and *arsD* (BHU72_10185) genes involved in As resistance (Figure 4.5B). Five genes directly upstream of BHU72_10220 encode a periplasmic phosphonate-binding protein (BHU72_10245), histidine kinase (BHU72_10240), LuxR family transcriptional regulator (BHU72_10235), sec-

independent protein translocase (TatA) (BHU72_10230), and ArrC (BHU72_10225). A gene encoding ArrB (BHU72_10215) is found directly downstream of BHU72_10220. As with the *arr* operons of *Shewanella* spp. (van Lis *et al.* 2013), a gene encoding ArrD is absent from this potential operon.

Dissimilatory Sb(V) reduction was associated with increased transcription of four genes, BHU72_03930, BHU72_07145, BHU72_07355, and BHU72_07375. BHU72_03930 is unusual in that genes encoding an ETS, EES, or a TorD family cytoplasmic chaperone could not be found nearby. It occurs directly downstream and upstream of genes involved in tryptophan and peptidoglycan biosynthesis, respectively. These observations, coupled to the fact that BHU72_03930 clusters fairly well with the catalytic subunits of formate dehydrogenases from other members of the *Bacillales*, leads us to conclude that this enzyme does not function as an anaerobic respiratory reductase in MLFW-2^{T}. On the other hand, the potential operon containing BHU72_07145 displays all of the classic features of an operon encoding an enzyme of the DMSOR family (Figure 4.6A). Upstream of BHU72_07145 are two genes encoding a diheme *c*-type cytochrome (BHU72_07135) and a 4[4Fe-4S] ETS (BHU72_07140). Directly downstream are five genes encoding a TorD family cytoplasmic chaperone (BHU72_07150), ArrB'-like 4[4Fe-4S] ferredoxin (BHU72_07155), periplasmic phosphonate-binding protein (BHU72_07160), histidine kinase (BHU72_07165), and LuxR family transcriptional regulator (BHU72_07170). As with the presumptive *arr* operon, a gene encoding an NrfD family EES is absent.

A BLAST search with BHU72_07145 as query revealed the presence of homologs in members of six described and two candidate phyla, including representatives from both prokaryotic domains of life (Figure 4.7). The potential operon occurred in seven different

orientations in these organisms, as shown in Figure 4.6B – G. The only other potential operon to contain a diheme *c*-type cytochrome belonged to a Euryarchaeon recovered from a sub-seafloor sulfide deposit metagenome (Kato *et al.* 2018). Additionally, there was a great deal of phylogenetic diversity with respect to the genes encoding ETSs, EESs, histidine kinases, and transcriptional regulators. For example, a gene encoding an EES was absent from potential operons in MLFW-2^{T}, δ-*Proteobacteria, Denitrovibrio acetiphilus*, *Nitrospirae*, and Archaeon BMS3Abin16. The ETS and EES encoded by members of the *Chloroflexi* were most closely related to SrdB and SrdC from membrane-bound Se(VI) reductases, while the ETS encoded by all other phyla was most closely related to TtrB from tetrathionate reductases (data not shown). Moreover, the two-component signal transduction system encoded in potential operons from *Denitrovibrio acetiphilus*, *Nitrospirae*, and δ-*Proteobacteria* consisted of a ZraS-like histidine kinase and an NtrC family transcriptional regulator, while all other phyla encoded a PAS/PAC-type histidine kinase and a LuxR family transcriptional regulator.

Transcriptional response of MLFW-2^{T} to Sb(V) and As(V)

MLFW-2^{T} has been grown using lactate and As(V) as the electron donor and acceptor, respectively, since its initial isolation and characterization. As(V) is the preferred electron acceptor for growth, as demonstrated by the fact that the highest growth rate was achieved on this substrate (Table 4.2). Additionally, viable cryogenic stocks for long-term storage could not be generated from cultures that had been grown using Sb(V) as the electron acceptor. After several transfers on As(V), MLFW-2^{T} no longer grew on Sb(V) beyond a single transfer without a wash step to remove toxic Sb(III) prior to inoculation.

It was noticed that amending cultures with As(III) rescued growth on Sb(V) and alleviated the need to wash between transfers. The "rescue" regimen involved amendment with ~150 μM As(III) for ~5 transfers, at which point the As(III) concentration was gradually decreased over a span of several transfers until it reached a negligible concentration (i.e. equivalent to background levels of As in the environment). Using this approach, reproducible growth on Sb(V) could be achieved for >10 transfers (1:5 dilution each transfer) in the absence of both As(III) and washing. In spite of this, we found that, in the absence of washing, As(III)-rescued growth on Sb(V) could only be achieved at a maximum temperature of ~30°C, while washed cells were capable of growth at 34°C.

The potential effects of As and Sb on global gene transcription in MLFW-2^T were investigated by comparing transcriptomes obtained by shotgun sequencing of the RNA harvested from cultures grown on Sb(V) and As(V). A summary of the characteristics of each transcriptome is provided in Table 4.S4. The relative levels of transcription of all fourteen DMSOR family genes examined individually by RT-qPCR were highly correlated with the RNA-seq estimates of transcription for those same genes. The Pearson correlation coefficient (R) and linear coefficient of determination (R^2) between the two data sets were 0.988 and 0.976, respectively (Figure 4.S11), indicating that both approaches provided similar assessments of the transcriptional responses of MLFW-2^T to growth on As(V) and Sb(V).

A total of 594 genes were differentially transcribed when Sb(V) versus As(V) served as the electron acceptor, with 294 (49.5%) and 300 (50.5%) genes being up- and downregulated, respectively (Tables 4.S5 and 4.S6). The three most highly represented COG functional categories for upregulated genes (excluding those with unknown functions) were amino acid transport and metabolism (16.8%), signal transduction mechanisms (10.6%), and energy

production and conversion (8.7%) (Figure 4.S8). Genes in COG functional categories for translation/ribosomal structure and biogenesis (14.2%), signal transduction mechanisms (13.3%), and inorganic ion transport and metabolism (9.1%) were most highly represented in the downregulated data set.

Among the most highly upregulated genes were those that made up a potential operon with BHU72_07145, encoding an enzyme of the DMSOR family likely involved in Sb(V) reduction. A potential operon consisting of four genes (BHU72_10075 – BHU72_10090) was also highly upregulated in response to Sb(V). BHU72_10075 and BHU72_10085 encode proteins containing N-terminal signal sequences, suggesting that they are exported across the cell membrane by a sec-dependent pathway. The product of BHU72_10075 is expected to be a soluble protein while that of BHU72_10085 is predicted to be attached to the membrane by a single transmembrane helix. The products of BHU72_10080 and BHU72_10090 are integral-membrane proteins containing 8 and 9 transmembrane helices, respectively. BHU72_10090 contains a binding site for a [4Fe-4S] cluster, indicating a potential role in electron transfer. Genes homologous to BHU72_10085 and BHU72_10090 were only found in the genomes of members of the *Bacillales*, *Clostridiales*, and *Actinomycetales*, three bacterial orders that lack a true outer membrane. Among other genes potentially involved in electron transport, two genes (BHU72_04210 and BHU72_04215) encoding soluble pentaheme *c*-type cytochromes were each upregulated approximately 33-fold in the presence of Sb(V).

Genes involved in various stress response pathways were also upregulated. Among the most abundant were genes typically activated by oxidative stress, such as those involved in histidine biosynthesis (*hisZDK*), Fe-S cluster biosynthesis and repair (*csd*, *iscS*, and *nifU*), biosynthesis of thiol-containing cofactors (*coaBC*, *moaB*, *moeA*), purine biosynthesis

(*purBDHFKT*), proline biosynthesis (*proABC*), maintenance of cellular redox homeostasis (*cysK* and *yyaL*), detoxification of reactive oxygen and nitrogen species (ROS/RNS) (*hcp*, *katG*, *ridA*, and BHU72_01310), and repair of oxidized protein thiols and thioethers (*bdbCD* and *msrB*). Genes encoding a cobalt transporter (*cbiQ*) and proteins involved in cobalamin biosynthesis (*cbiEG* and *cobQ*) were also upregulated in response to Sb(V).

Other stress-responsive genes were also upregulated, including those involved in stress-induced signal transduction (BHU72_02080 and BHU72_14260), DNA damage repair (*addAB*, *ligA*, *recA*, *ung*, *uvrCD*, BHU72_13325, and BHU72_13855), cell wall biosynthesis and repair (*dacF*, *ftsW*, *mnaA*, and *mreBC*), flagellar biosynthesis and modification (*flaG*, *fliSO*, *pseBHI*, and BHU72_06760), degradation of damaged proteins (BHU72_14255), alkaline pH tolerance (*asp*), heavy metal/metalloid resistance (*acr3*, *arsA*, *cadA*, *copA*, *ctpC*, and *zitB*), and antibiotic resistance (*mprF*, BHU72_04190, BHU72_04915, BHU72_10700, BHU72_12980, BHU72_14315, and BHU72_14320). Interestingly, three genes (*dctMPQ*) encoding a tripartite ATP-independent periplasmic (TRAP) dicarboxylate transport system and one gene (BHU72_14430) encoding a tricarboxylate transporter were also upregulated in the presence of Sb(V).

The three genes most downregulated in the presence of Sb(V) (*opuA*, *opuB*, and *gbuC*) were all involved in the uptake of quaternary amines such as glycine betaine, choline, and carnitine. These low molecular weight osmolytes typically function as osmoprotectants under conditions of osmotic stress (Kempf and Bremer 1995, Ko and Smith 1999). As expected, the *arrABD* genes of the active *arr* operon in MLFW-2^T were also highly downregulated. However, the *arrB*' gene, encoding a 4[4Fe-4S] ferredoxin with unknown function, was not differentially expressed between the two treatments. Genes encoding a possible tungsten-containing formate

dehydrogenase (*fdoGHI*) were downregulated 11- to 18-fold in the presence of Sb(V). As a possible consequence of poor growth yields on Sb(V) relative to As(V), the majority of downregulated genes were involved in protein synthesis. These included genes of the *rpm*, *rps*, and *rpl* gene families encoding structural components of the 30S and 50S ribosomal subunits, as well as those involved in ribosome maturation (*era*, *rbgA*, *rimO*, *rsmAI*, *yabOR*, and BHU72_08100), translation initiation (*infC*), elongation (*efp*, *tsf* and *lepA*), and termination (*frr*). Genes encoding subunits of ATP synthase (*atpBEFI*) were also downregulated, as were genes involved in iron transport (*feoB*, BHU72_11385, and BHU72_11390) and storage (*ftnA*).

There were several stress response genes that were more highly transcribed when As(V) was provided as the electron acceptor. These included genes involved in stress-related signal transduction (BHU72_01030, BHU72_01040, BHU72_02460, and BHU72_04615), DNA damage repair (*mutY*, *recR*, and *ssb*), detoxification of ROS/RNS (*ahpC*, *hcp*, BHU72_03065, and BHU72_07175), cellular redox homeostasis (trxA and BHU72_09130), prevention and/or correction of protein misfolding (*clpB*, *groS*, and *htpG*), low temperature tolerance (BHU72_04065), viral defense (*bglII*, *cas2*, *nfo*, BHU72_06035, and BHU72_13280), and antibiotic resistance (BHU72_07595, BHU72_08095, BHU72_11685, and BHU72_13360).

DISCUSSION

The data presented here suggest that a potential operon consisting of BHU72_03615 – BHU72_03640 encodes a periplasmic nitrate reductase consisting of an integral membrane quinol dehydrogenase (NapG2H), a putative maturation factor (NapG1), and a soluble catalytic module (NapAB). Other genes, including BHU72_01090, BHU72_04760, and BHU72_09285, were also upregulated when nitrate was provided as the electron acceptor. Only one of these

genes, BHU72_04760, was upregulated at a level equivalent to *napA*. This gene exists in a potential operon (BHU72_04740 – BHU72_04775) encoding an unknown enzyme of the DMSOR family. The presence of genes encoding a sulfur transferase (BHU72_04745), sulfur transporter (BHU72_04755), and rhodanese proteins (BHU72_04785, BHU72_04790, BHU72_04795, and BHU72_04805) within or directly downstream of the potential operon lead us to speculate that the unknown enzyme may be involved in sulfur metabolism.

Dissimilatory Se(VI) reduction in MLFW-2^T was associated with the upregulation of two genes, BHU72_07355 and BHU72_07375, encoding proteins phylogenetically related to TtrA, the catalytic subunit of tetrathionate reductase. The product of only one of these genes, BHU72_07355, shared significant homology with SrdA, the catalytic subunit of the membrane-bound Se(VI) reductase from *B. selenatarsenatis*. The potential *srd* operon in MLFW-2^T consisted of three genes, *srdBCA* (BHU72_07345 – BHU72_07355), arranged in the same order as the *srd* operon of *B. selenatarsenatis* (Kuroda *et al.* 2011), thus providing further evidence that this complex is responsible for dissimilatory Se(VI) reduction. The discovery of a membrane-bound Se(IV) reductase in MLFW-2^T is significant because it represents only the second such enzyme to be reported in the literature. Using SrdA from *B. selenatarsenatis* and MLFW-2^T as queries, a BLAST search revealed that a third *srdBCA* operon encoded by BKP35_08575 – BKP35_08585 is present in the draft genome of *A. arceniciselenatis*, an obligately anaerobic, As(V)- and Se(VI)-reducing haloalkaliphile isolated from Mono Lake, CA (Switzer Blum *et al.* 1998). The function of the other enzyme of the DMSOR family significantly upregulated by Se(VI), and encoded by BHU72_07370 – BHU72_07390, is currently unknown. However, the downstream presence of *selD* (BHU72_07395 and BHU72_07475) and *selA* (BHU72_07470), two genes involved in selenocysteine biosynthesis

(Leinfelder *et al.* 1990) and selenocysteinyl-tRNA charging (Forchhammer *et al.* 1991), respectively, indicate that this enzyme may play a role in assimilatory Se metabolism.

The respiratory As(V) reductase in MLFW-2^T is most likely encoded by BHU72_10315 – BHU72_10330. A gene encoding ArrC, the NrfD-type EES that connects the rest of the complex to the electron transport chain, was absent from the *arr* operon of MLFW-2^T. The *arr* operons of several other phylogenetically-diverse As(V)-reducing bacteria also do not contain a copy of *arrC*. In these organisms, it is thought that a membrane-anchored tetraheme *c*-type cytochrome of the NapC/NirT/NrfH family links the catalytic module to the quinone pool (Grimaldi *et al.* 2013). In *Shewanella* spp., for example, CymA functions as the electron donor to water soluble periplasmic oxidoreductases such as ArrAB (Murphy and Saltikov 2007) and NapAB (Gao *et al.* 2009). The MLFW-2^T draft genome contains two genes (BHU72_01505 and BHU72_06155) that encode tetraheme *c*-type cytochromes of the NapC/NirT/NrfH family. It is possible that the product of one or both of these genes serves a similar function in MLFW-2^T as CymA in *Shewanella* spp.

Interestingly, BHU72_10220, encoding a second ArrA-like protein, was not upregulated in the presence of As(V) or any other electron acceptor. This gene occurs in a potential operon (BHU72_10215 – BHU72_10245) encoding all of the necessary regulatory and structural components for a membrane-bound respiratory As(V) reductase, except the cytoplasmic chaperone ArrD. The fact that the transcription of this *arr*-like operon was not upregulated during dissimilatory As(V) reduction indicates that it serves some other function in the physiology of this organism besides As metabolism. Alternatively, the regulatory network responsible for modulating the transcription of this potential operon may have lost the ability to

sense As in the environment. Further study will be required to determine the nature of the product of this potential operon.

Dissimilatory Sb(V) reduction in MLFW-2^T was associated with elevated transcription of three genes, BHU72_07145, BHU72_07355, and BHU72_07375. As mentioned above, the products of BHU72_07355 and BHU72_07375 most likely play roles in Se metabolism, working in concert to convert Se(VI) into reduced forms required for selenocysteine biosynthesis. Selenocysteine has been shown to be a potent antioxidant in cells, capable of reacting with ROS/RNS at a rate 10- to 100-fold faster than its sulfur analog, cysteine (Padmaja *et al.* 1998, Skaff *et al.* 2009, Skaff *et al.* 2012). In addition, selenoproteins such as glutathione peroxidase, thioredoxin reductase, and methionine sulfoxide reductase are key components of the oxidative stress response in bacteria (Rahmanto and Davies, 2012). Therefore, we speculate that the products of BHU72_07355 and BHU72_07375 are not involved in dissimilatory Sb(V) reduction, but rather in mitigating the oxidative stress placed on cells by Sb.

The transcription of BHU72_07145 was markedly enhanced in the presence of Sb(V), indicating that this gene may encode the catalytic subunit of a dissimilatory Sb(V) reductase. Homologs of this protein were found in a number of phylogenetically-diverse microorganisms, including six described and two candidate phyla across both prokaryotic domains of life. These organisms were recovered from environments possibly enriched in Sb, including the terrestrial subsurface (Anantharaman *et al.* 2016, Bagnoud *et al.* 2016, Probst *et al.* 2018), hot springs (Sekiguchi *et al.* 2003, Dodsworth *et al.* 2014), municipal sludge (Madsen and Licht 1992), paddy soil (Li *et al.* 2018), soils and sediments contaminated with chlorinated hydrocarbons (Suyama *et al.* 2001, De Wildeman *et al.* 2003), mine tailings (Mardanov *et al.* 2016), an As-rich lake (Hoeft *et al.* 2004), and deep-sea massive sulfide deposits (Kato *et al.* 2018). If this gene

was inherited from a common ancestor rather than through horizontal gene transfer, it implies that dissimilatory Sb(V) reduction is an ancient process that would have been important for sustaining life in Sb-rich environments on the early Earth.

The potential operon harboring BHU72_07145 is unusual because it encodes a soluble DMSOR family enzyme lacking a discernible EES subunit, but containing an additional ETS in the form of a diheme *c*-type cytochrome. Other enzymes of the DMSOR family are known to interact with multiple ETSs, including the periplasmic nitrate reductase, perchlorate reductase, periplasmic Se(VI) reductase, and the soluble formate dehydrogenases of *D. vulgaris* and *D. desulfuricans* (Grimaldi *et al.* 2013). As with the respiratory As(V) reductase of MLFW-2^T and other organisms, this enzyme may be linked to the quinone pool by a member of the NapC/NirT/NrfH family of proteins.

Finally, RNA-seq was used to compare the physiological response of MLFW-2^T to growth using Sb(V) versus As(V) as terminal electron acceptors. The primary motivation for this experiment was to try to understand why growth of MLFW-2^T on Sb(V) was poor relative to As(V). It was hoped that RNA-seq would also shed light on why amending cultures with As(III) "rescued" growth on Sb(V) and alleviated the need for washing between transfers.

Transcription of genes involved in stress response pathways was enhanced when MLFW-2^T was grown on Sb(V) versus As(V). Most of these differentially transcribed genes were involved in the oxidative stress response, including those responsible for repairing oxidized biomolecules or scavenging ROS/RNS. Several genes involved in cobalt import and cobalamin biosynthesis were also upregulated in response to Sb(V). Cobalamin has shown to be an important intracellular antioxidant contributing to the survival of cells exposed to oxidative stress from ROS (Birch *et al.* 2009, Ferrer *et al.* 2016).

The toxicity of Sb, and especially Sb(III), is largely due to its affinity for binding thiol groups, leading to depletion of cytosolic pools of antioxidants and generating ROS (Tirmenstein *et al.* 1997, Hashemzaei *et al.* 2015, Jiang *et al.* 2016). Binding of Sb to thiol groups in proteins can cause loss of function by interfering with the coordination of active site residues (Baiocco *et al.* 2009), disrupting disulfide bridges that maintain tertiary structure (Tamás *et al.* 2014), or by displacing thiol-coordinated cofactors such as metal ions, Fe-S clusters, and heme (Tamás 2016). For example, Sb is known to cause DNA damage by disrupting the function of enzymes of the nucleotide excision pathway, binding to cysteine residues that normally coordinate zinc atoms in these proteins (Demicheli *et al.* 2008, Grosskopf *et al.* 2010). In addition, both Sb(III) and Sb(V) form highly stable complexes with molecules containing adjacent carboxylic or hydroxyl groups such as free ribonucleosides, RNA, and various central metabolites (Demicheli *et al.* 2002, Hansen and Pergantis 2006, Hansen and Pergantis 2006, Tella and Pokrovski 2008, Tella and Pokrovski 2009). The upregulation of genes involved in di- and tricarboxylate transport by MLFW-2^T may represent a novel strategy to detoxify Sb by forming stable chelates that sequester both Sb(V) and Sb(III). Alternatively, import of these compounds may simply be a mechanism to replenish cytosolic pools depleted as a result of sequestration by Sb.

Several genes involved in resistance to heavy metals/metalloids and antibiotics were more highly transcribed when Sb(V) was provided as the electron acceptor. Surprisingly, the *arsA* and *acr3* genes conferring resistance to As and Sb were more highly transcribed in the presence of Sb(V) than in the presence of As(V), even though Sb(V) was provided at a concentration of 1 mM versus 5 mM for As(V). In several bacteria, transcription of the *ars* operon can be activated by both As(III) and Sb(III) (Ji and Silver 1992, Wu and Rosen 1993, Cai *et al.* 1998, Sato and Kobayashi 1998, López-Maury *et al.* 2003). The ATP-driven As(III) efflux

pump, encoded by *arsA* and *arsB* (or *acr3*), can also pump Sb(III) out of the cell (Carlin *et al.* 1995, Meng *et al.* 2004). The ability of As(III) to rescue Sb(V)-dependent growth of MLFW-2^T may be due to enhanced initial stimulation of the *ars* operon by the combined effects of As(III) and Sb(III), leading to a greater capacity to rid the cytoplasm of Sb(III). However, the exact mechanism by which the cells are able to maintain growth in the presence of high levels of Sb(III) even after complete removal of As(III) will require further investigation.

Growth on Sb(V) induced the transcription of several genes possibly involved in electron transport. A potential operon encoding a set of four periplasmically-oriented and membrane-associated proteins was considerably upregulated in response to Sb(V). Homologs of two of the genes (BHU72_10085 and BHU72_10090) co-occur in many members of the *Firmicutes* and *Actinobacteria*. However, homologs of the two proteins encoded by BHU72_10075 and BHU72_10085 could not be found in any genetic database. While one can only speculate on the function of these proteins, they may form a complex that participates in electron transfer with the quinone pool, as predicted by the presence of a binding site for a [4Fe-4S] cluster on the transmembrane protein encoded by BHU72_10090. Therefore, these proteins may play a role in linking the potential dissimilatory Sb(V) reductase encoded by BHU72_07135 – BHU72_07170 to the rest of the electron transport chain. This function would be analogous to that of the integral membrane quinol dehydrogenases of the NapC/NirT/NrfH family. Alternatively, they may play a role in Sb detoxification or may be directly involved in dissimilatory Sb(V) reduction. However, the conspicuous absence of homologs of two of the gene products from genetic databases suggests that they do not constitute the dissimilatory Sb(V) reductase, as Sb(V) reduction has been linked to a phylogenetically diverse array of microorganisms (Abin and Hollibaugh 2014, Nguyen and Lee 2014, Lai *et al.* 2016, Nguyen *et al.* 2018, Zhu *et al.* 2018).

As expected from low growth yields on Sb(V) versus As(V), most of the genes that were downregulated in the presence of Sb(V) were involved in ribosome maturation and protein synthesis. Noteworthy, however, was the observation that, relative to growth on Sb(V), growth on As(V) was associated with highly elevated transcription of the *opuAB* and *gbuC* genes involved in the uptake of tertiary amines, such as glycine betaine and choline, that typically serve as osmo- and thermo-protectants in bacteria (Caldas *et al.* 1999, Sleator and Hill 2002). Some plants have been known to accumulate glycine betaine in response to heavy metal stress (Bergmann *et al.* 2001, Bera *et al.* 2017). In these species, glycine betaine is an important osmolyte that alleviates the toxic effects of heavy metals by stimulating the antioxidant defense system and stabilizing proteins, nucleic acids, and membranes (Islam *et al.* 2009, Chen and Murata 2011, Rasheed *et al.* 2014, Ali *et al.* 2015). It is likely that tertiary amines play a similar role in mitigating the toxic effects of As in MLFW-2^T and other microbes as well. Lastly, a set of three genes involved in iron uptake and storage were downregulated during growth on Sb(V) versus As(V). This may constitute an effort to limit ROS formation by reducing the amount of free cytosolic iron that can participate in the Fenton reaction (Winterbourn 1995).

The results of this study further our understanding of the enzymes of the DMSOR family and the roles that they play in the global N, Se, As, and Sb cycles. Evidence presented here strongly implicates BHU72_03635, BHU72_07355, BHU72_10330, and BHU72_07145 as encoding the catalytic subunits of the anaerobic respiratory reductases for nitrate, Se(VI), As(V), and Sb(V), respectively, in MLFW-2^T. Further work in molecular genetics and enzymology will need to be performed to confirm these predictions. For instance, the potential operon containing BHU72_07145 may be cloned into a suitable host and evaluated for the ability to confer an Sb(V) reduction phenotype. A similar approach was successfully applied in *E. coli* to investigate

the product of the *srd* operon of *B. selenatarsenatis* (Kuroda *et al.* 2011). Despite the progress of the last two decades, relatively little is known about the potential substrates and biochemistry of enzymes of this vast family. A greater understanding of these proteins will provide insight into the evolution of prokaryotic metabolisms on Earth, as well as potentially allow for their catalytic properties to be harnessed for bioremedial and biotechnological applications.

ACKNOWLEDGEMENTS

We would like to thank Christian Edwardson, Bradley Tolar, Julian Damashek, Shalabh Sharma, and Courtney Thomas for providing advice about experimental design and assistance with bioinformatics. Jelani Cheek performed the nitrate, nitrite, and ammonium analyses on our culture samples from the nitrate and nitrite treatments. We are also grateful to Mary Ann Moran for providing some of the equipment necessary to extract and process RNA from our cultures. This research was supported by two awards from the National Science Foundation, EAR 09-52271 (JTH) and DGE-0903734 (CAA), as well as a Minority PhD program scholarship from the Alfred P. Sloan Foundation (CAA).

REFERENCES

Abin CA, Hollibaugh JT (2014). Dissimilatory antimonate reduction and production of antimony trioxide microcrystals by a novel microorganism. *Environ Sci Technol* **48:** 681-688.

Abin CA, Hollibaugh JT (2017). *Desulfuribacillus stibiiarsenatis* sp. nov., an obligately anaerobic, dissimilatory antimonate- and arsenate-reducing bacterium isolated from anoxic sediments, and emended description of the genus *Desulfuribacillus*. *Int J Syst Evol Microbiol* **67:** 1011-1017.

Ali S, Chaudhary A, Rizwan M, Anwar HT, Adrees M, Farid M *et al.* (2015). Alleviation of chromium toxicity by glycinebetaine is related to elevated antioxidant enzymes and suppressed chromium uptake and oxidative stress in wheat (*Triticum aestivum* L.). *Environ Sci Pollut Res* **22:** 10669-10678.

Altschul SF, Gish W, Miller W, Myers EW, Lipman DJ (1990). Basic local alignment search tool. *J Mol Biol* **215:** 403-410.

Anantharaman K, Brown CT, Hug LA, Sharon I, Castelle CJ, Probst AJ *et al.* (2016). Thousands of microbial genomes shed light on interconnected biogeochemical processes in an aquifer system. *Nat Commun* **7:** 13219.

Anders S, Pyl PT, Huber W (2015). HTSeq—a Python framework to work with high-throughput sequencing data. *Bioinformatics* **31:** 166-169.

Ashburner M, Ball CA, Blake JA, Botstein D, Butler H, Cherry JM *et al.* (2000). Gene Ontology: tool for the unification of biology. *Nat Genet* **25:** 25-29.

Bagnoud A, Chourey K, Hettich RL, de Bruijn I, Andersson AF, Leupin OX *et al.* (2016). Reconstructing a hydrogen-driven microbial metabolic network in Opalinus Clay rock. *Nat Commun* **7:** 12770.

Baiocco P, Colotti G, Franceschini S, Ilari A (2009). Molecular basis of antimony treatment in Leishmaniasis. *J Med Chem* **52:** 2603-2612.

Bard AJ, Parsons R, Jordan J (1985). *Standard Potentials in Aqueous Solutions*. New York, NY: Marcel Dekker.

Bendschneider K, Robinson RJ (1952). A new spectrophotometric method for the determination of nitrite in sea water. *J Marine Res* **11:** 87-96.

Bendtsen JD, Nielsen H, Widdick D, Palmer T, Brunak S (2005). Prediction of twin-arginine signal peptides. *BMC Bioinformatics* **6:** 167.

Benjamini Y, Hochberg Y (1995). Controlling the false discovery rate: a practical and powerful approach to multiple testing. *J Royal Stat Soc Ser B Methodol* **57:** 289-300.

Bera S, De AK, Adak MK (2017). Modulation of glycine betaine accumulation with oxidative stress induced by aluminium toxicity in rice. *Proc Natl Acad Sci India Sec B: Biol Sci*.

Bergmann H, Machelett B, Lippmann B, Friedrich Y (2001). Influence of heavy metals on the accumulation of trimethylglycine, putrescine and spermine in food plants. *Amino Acids* **20:** 325-329.

Bilous PT, Cole ST, Anderson WF, Weiner JH (1988). Nucleotide sequence of the *dmsABC* operon encoding the anaerobic dimethylsulphoxide reductase of *Escherichia coli*. *Mol Microbiol* **2:** 785-795.

Birch CS, Brasch NE, McCaddon A, Williams JHH (2009). A novel role for vitamin B12: cobalamins are intracellular antioxidants in vitro. *Free Radic Biol Med* **47:** 184-188.

Blasco F, Iobbi C, Giordano G, Chippaux M, Bonnefoy V (1989). Nitrate reductase of *Escherichia coli*: completion of the nucleotide sequence of the *nar* operon and reassessment of the role of the α and β subunits in iron binding and electron transfer. *Mol Gen Genet* **218:** 249-256.

Bolger AM, Lohse M, Usadel B (2014). Trimmomatic: a flexible trimmer for Illumina sequence data. *Bioinformatics* **30:** 2114-2120.

Brondijk THC, Nilavongse A, Filenko N, Richardson DJ, Cole JA (2004). NapGH components of the periplasmic nitrate reductase of *Escherichia coli* K-12: location, topology and physiological roles in quinol oxidation and redox balancing. *Biochem J* **379:** 47-55.

Cai J, Salmon K, DuBow MS (1998). A chromosomal *ars* operon homologue of *Pseudomonas aeruginosa* confers increased resistance to arsenic and antimony in *Escherichia coli*. *Microbiol* **144:** 2705-2729.

Caldas T, Demont-Caulet N, Ghazi A, Richarme G (1999). Thermoprotection by glycine betaine and choline. *Microbiol* **145:** 2543-2548.

Carlin A, Shi W, Dey S, Rosen BP (1995). The *ars* operon of *Escherichia coli* confers arsenical and antimonial resistance. *J Bacteriol* **177:** 981-986.

Chen THH, Murata N (2011). Glycinebetaine protects plants against abiotic stress: mechanisms and biotechnological applications. *Plant Cell Environ* **34:** 1-20.

de Castro E, Sigrist CJA, Gattiker A, Bulliard V, Langendijk-Genevaux PS, Gasteiger E *et al.* (2006). ScanProsite: detection of PROSITE signature matches and ProRule-associated functional and structural residues in proteins. *Nucleic Acids Res* **34:** W362-W365.

De Wildeman S, Diekert G, Van Langenhove H, Verstraete W (2003). Stereoselective microbial dehalorespiration with vicinal dichlorinated alkanes. *Appl Environ Microbiol* **69:** 5643-5647.

Demicheli C, Frézard F, Lecouvey M, Garnier-Suillerot A (2002). Antimony(V) complex formation with adenine nucleosides in aqueous solution. *Biochim Biophys Acta - Gen Subj* **1570:** 192-198.

Demicheli C, Frezard F, Mangrum JB, Farrell NP (2008). Interaction of trivalent antimony with a CCHC zinc finger domain: potential relevance to the mechanism of action of antimonial drugs. *Chem Comm* **39:** 4828-4830.

Diemar GA, Filella M, Leverett P, Williams PA (2009). Dispersion of antimony from oxidizing ore deposits. *Pure Appl Chem* **81:** 1547-1553.

Dodsworth JA, Gevorkian J, Despujos F, Cole JK, Murugapiran SK, Ming H *et al.* (2014). *Thermoflexus hugenholtzii* gen. nov., sp. nov., a thermophilic, microaerophilic, filamentous bacterium representing a novel class in the *Chloroflexi*, *Thermoflexia classis* nov., and description of *Thermoflexaceae* fam. nov. and *Thermoflexales* ord. nov. *Int J Syst Evol Microbiol* **64:** 2119-2127.

Edgar RC (2004). MUSCLE: multiple sequence alignment with high accuracy and high throughput. *Nucleic Acids Res* **32:** 1792-1797.

Felsenstein J (1985). Confidence limits on phylogenies: an approach using the bootstrap. *Evolution* **39:** 783-791.

Ferrer A, Rivera J, Zapata C, Norambuena J, Sandoval Á, Chávez R *et al.* (2016). Cobalamin protection against oxidative stress in the acidophilic iron-oxidizing bacterium *Leptospirillum* Group II CF-1. *Front Microbiol* **7:** 748.

Fisher JC, Wallschläger D, Planer-Friedrich B, Hollibaugh JT (2007). A new role for sulfur in arsenic cycling. *Environ Sci Technol* **42:** 81-85.

Forchhammer K, Leinfelder W, Boesmiller K, Veprek B, Böck A (1991). Selenocysteine synthase from *Escherichia coli*. Nucleotide sequence of the gene (selA) and purification of the protein. *J Biol Chem* **266:** 6318-6323.

Gao H, Yang ZK, Barua S, Reed SB, Romine MF, Nealson KH *et al.* (2009). Reduction of nitrate in *Shewanella oneidensis* depends on atypical NAP and NRF systems with NapB as a preferred electron transport protein from CymA to NapA. *ISME J* **3:** 966-976.

Grimaldi S, Schoepp-Cothenet B, Ceccaldi P, Guigliarelli B, Magalon A (2013). The prokaryotic Mo/W-bisPGD enzymes family: A catalytic workhorse in bioenergetics. *Biochim Biophys Acta - Bioenerg* **1827:** 1048-1085.

Grosskopf C, Schwerdtle T, Mullenders LHF, Hartwig A (2010). Antimony impairs nucleotide excision repair: XPA and XPE as potential molecular targets. *Chem Res Toxicol* **23:** 1175-1183.

Hansen H, Pergantis S (2006). Mass spectrometric identification and characterization of antimony complexes with ribose-containing biomolecules and an RNA oligomer. *Anal Bioanal Chem* **385:** 821-833.

Hansen HR, Pergantis SA (2006). Investigating the formation of an Sb(V)-citrate complex by HPLC-ICP-MS and HPLC-ES-MS(/MS). *J Anal At Spectrom* **21:** 1240-1248.

Hashemzaei M, Pourahmad J, Safaeinejad F, Tabrizian K, Akbari F, Bagheri G *et al.* (2015). Antimony induces oxidative stress and cell death in normal hepatocytes. *Toxicol Environ Chem* **97:** 256-265.

Hensel M, Hinsley AP, Nikolaus T, Sawers G, Berks BC (1999). The genetic basis of tetrathionate respiration in *Salmonella typhimurium*. *Mol Microbiol* **32:** 275-287.

Heylen K, Keltjens J (2012). Redundancy and modularity in membrane-associated dissimilatory nitrate reduction in *Bacillus*. *Front Microbiol* **3:** 371.

Hoeft SE, Kulp TR, Stolz JF, Hollibaugh JT, Oremland RS (2004). Dissimilatory arsenate reduction with sulfide as electron donor: experiments with Mono Lake water and isolation of strain MLMS-1, a chemoautotrophic arsenate respirer. *Appl Environ Microbiol* **70:** 2741-2747.

Huerta-Cepas J, Forslund K, Coelho LP, Szklarczyk D, Jensen LJ, von Mering C *et al.* (2017). Fast genome-wide functional annotation through orthology assignment by eggNOG-Mapper. *Mol Biol Evol* **34:** 2115-2122.

Huerta-Cepas J, Szklarczyk D, Forslund K, Cook H, Heller D, Walter MC *et al.* (2016). eggNOG 4.5: a hierarchical orthology framework with improved functional annotations for eukaryotic, prokaryotic and viral sequences. *Nucleic Acids Res* **44:** D286-D293.

Islam MM, Hoque MA, Okuma E, Banu MNA, Shimoishi Y, Nakamura Y *et al.* (2009). Exogenous proline and glycinebetaine increase antioxidant enzyme activities and confer tolerance to cadmium stress in cultured tobacco cells. *J Plant Physiol* **166:** 1587-1597.

Ji G, Silver S (1992). Regulation and expression of the arsenic resistance operon from *Staphylococcus aureus* plasmid pI258. *J Bacteriol* **174:** 3684-3694.

Jiang X, An Z, Lu C, Chen Y, Du E, Qi S *et al.* (2016). The protective role of Nrf2-Gadd45b against antimony-induced oxidative stress and apoptosis in HEK293 cells. *Toxicol Lett* **256:** 11-18.

Jones P, Binns D, Chang HY, Fraser M, Li W, McAnulla C *et al.* (2014). InterProScan 5: genome-scale protein function classification. *Bioinformatics* **30:** 1236-1240.

Jukes TH, Cantor CR (1969). Evolution of protein molecules. In *Mammalian Protein Metabolism*. New York, NY: Academic Press.

Kanehisa M, Goto S (2000). KEGG: Kyoto encyclopedia of genes and genomes. *Nucleic Acids Res* **28:** 27-30.

Kato S, Shibuya T, Takaki Y, Hirai M, Nunoura T, Suzuki K (2018). Genome-enabled metabolic reconstruction of dominant chemosynthetic colonizers in deep-sea massive sulfide deposits. *Environ Microbiol* **20:** 862-877.

Kearse M, Moir R, Wilson A, Stones-Havas S, Cheung M, Sturrock S *et al.* (2012). Geneious Basic: An integrated and extendable desktop software platform for the organization and analysis of sequence data. *Bioinformatics* **28:** 1647-1649.

Kempf B, Bremer E (1995). OpuA, an osmotically regulated binding protein-dependent transport system for the osmoprotectant glycine betaine in *Bacillus subtilis*. *J Biol Chem* **270:** 16701-16713.

Knäblein J, Mann K, Ehlert S, Fonstein M, Huber R, Schneider F (1996). Isolation, cloning, sequence analysis and localization of the operon encoding dimethyl sulfoxide/trimethylamine N-oxide reductase from *Rhodobacter capsulatus*. *J Mol Biol* **263:** 40-52.

Ko R, Smith LT (1999). Identification of an ATP-driven, osmoregulated glycine betaine transport system in *Listeria monocytogenes*. *Appl Environ Microbiol* **65:** 4040-4048.

Krafft T, Bokranz M, Klimmek O, Schröder I, Fahrenholz F, Kojro E *et al.* (1992). Cloning and nucleotide sequence of the *pstA* gene of *Wolinella succinogenes* polysulphide reductase. *Eur J Biochem* **206:** 503-510.

Krafft T, Bowen A, Theis F, Macy JM. (2000). Cloning and sequencing of the genes encoding the periplasmic-cytochrome b-containing selenate reductase of *Thauera selenatis*. *DNA Seq* **10:** 365-377.

Krogh A, Larsson B, von Heijne G, Sonnhammer ELL (2001). Predicting transmembrane protein topology with a hidden markov model: application to complete genomes. *J Mol Biol* **305:** 567-580.

Kuroda M, Yamashita M, Miwa E, Imao K, Fujimoto N, Ono H *et al.* (2011). Molecular cloning and characterization of the srdBCA operon, encoding the respiratory selenate reductase complex, from the selenate-reducing bacterium *Bacillus selenatarsenatis* SF-1. *J Bacteriol* **193:** 2141-2148.

Lai C, Wen L, Zhang Y, Luo S, Wang Q, Luo Y *et al.* (2016). Autotrophic antimonate bio-reduction using hydrogen as the electron donor. *Water Res* **88:** 467-474.

Langmead B, Salzberg SL (2012). Fast gapped-read alignment with Bowtie 2. *Nat Methods* **9:** 357-359.

Leinfelder W, Forchhammer K, Veprek B, Zehelein E, Böck A (1990). In vitro synthesis of selenocysteinyl-tRNA(UCA) from seryl-tRNA(UCA): involvement and characterization of the *selD* gene product. *Proc Natl Acad Sci* **87:** 543-547.

Li GX, Chen XP, Wang XN, Chen Z, Bao P (2018). Sulfur redox cycling dependent abiotic ferrihydrite reduction by a *Desulfitobacterium hafniense*. *ACS Earth Space Chem* (Accepted manuscript).

Livak KJ, Schmittgen TD (2001). Analysis of relative gene expression data using real-time quantitative PCR and the $2^{-\Delta\Delta CT}$ method. *Methods* **25:** 402-408.

López-Maury L, Florencio FJ, Reyes JC (2003). Arsenic sensing and resistance system in the cyanobacterium *Synechocystis* sp. strain PCC 6803. *J Bacteriol* **185:** 5363-5371.

Love MI, Huber W, Anders S (2014). Moderated estimation of fold change and dispersion for RNA-seq data with DESeq2. *Genome Biol* **15:** 550.

Madsen T, Licht D (1992). Isolation and characterization of an anaerobic chlorophenol-transforming bacterium. *Appl Environ Microbiol* **58:** 2874-2878.

Maia LB, Moura I, Moura JJG (2017). Molybdenum and tungsten-containing formate dehydrogenases: aiming to inspire a catalyst for carbon dioxide utilization. *Inorg Chim Acta* **455:** 350-363.

Mardanov AV, Panova IA, Beletsky AV, Avakyan MR, Kadnikov VV, Antsiferov DV *et al.* (2016). Genomic insights into a new acidophilic, copper-resistant *Desulfosporosinus* isolate from the oxidized tailings area of an abandoned gold mine. *FEMS Microbiol Ecol* **92:** fiw111.

McEwan AG, Ridge JP, McDevitt CA, Hugenholtz, P (2002). The DMSO reductase family of microbial molybdenum enzymes; molecular properties and role in the dissimilatory reduction of toxic elements. *Geomicrobiol J* **19:** 3-21.

Meng YL, Liu Z, Rosen BP (2004). As(III) and Sb(III) uptake by GlpF and efflux by ArsB in *Escherichia coli*. *J Biol Chem* **279:** 18334-18341.

Murphy JN, Saltikov CW (2007). The *cymA* gene, encoding a tetraheme c-type cytochrome, is required for arsenate respiration in *Shewanella* species. *J Bacteriol* **189:** 2283-2290.

Nguyen VK, Choi W, Park Y, Yu J, Lee T (2018). Characterization of diversified Sb(V)-reducing bacterial communities by various organic or inorganic electron donors. *Bioresour Technol* **250:** 239-246.

Nguyen VK, Lee JU (2014). Isolation and characterization of antimony-reducing bacteria from sediments collected in the vicinity of an antimony factory. *Geomicrobiol J* **31:** 855-861.

Nordstrom DK, Archer DG (2003). Arsenic thermodynamic data and environmental geochemistry. In *Arsenic in Ground Water: Geochemistry and Occurrence*. Boston, MA: Springer.

Oremland RS, Switzer Blum J, Culbertson CW, Visscher PT, Miller LG, Dowdle P *et al.* (1994). Isolation, growth, and metabolism of an obligately anaerobic, selenate-respiring bacterium, strain SES-3. *Appl Environ Microbiol* **60:** 3011-3019.

Padmaja S, Squadrito GL, Pryor WA (1998). Inactivation of glutathione peroxidase by peroxynitrite. *Arch Biochem Biophys* **349:** 1-6.

Petersen TN, Brunak S, von Heijne G, Nielsen H (2011). SignalP 4.0: discriminating signal peptides from transmembrane regions. *Nat Methods* **8:** 785-786.

Pfaffl MW (2001). A new mathematical model for relative quantification in real-time RT–PCR. *Nucleic Acids Res* **29:** e45.

Rauschenbach I, Bini E, Häggblom MM, Yee N (2012). Physiological response of *Desulfurispirillum indicum* S5 to arsenate and nitrate as terminal electron acceptors. *FEMS Microbiol Ecol* **81:** 156-162.

Probst AJ, Ladd B, Jarett JK, Geller-McGrath DE, Sieber CMK, Emerson JB *et al.* (2018). Differential depth distribution of microbial function and putative symbionts through sediment-hosted aquifers in the deep terrestrial subsurface. *Nat Microbiol* **3:** 328-336.

Rahmanto AS, Davies MJ (2012). Selenium-containing amino acids as direct and indirect antioxidants. *IUBMB Life* **64:** 863-871.

Raaijmakers H, Macieira S, Dias JM, Teixeira S, Bursakov S, Huber R *et al.* (2002). Gene sequence and the 1.8 Å crystal structure of the tungsten-containing formate dehydrogenase from *Desulfovibrio gigas*. *Structure* **10:** 1261-1272.

Rasheed R, Ashraf MA, Hussain I, Haider MZ, Kanwal U, Iqbal M (2014). Exogenous proline and glycinebetaine mitigate cadmium stress in two genetically different spring wheat (*Triticum aestivum* L.) cultivars. *Braz J Bot* **37:** 399-406.

Rothery RA, Workun GJ, Weiner JH (2008). The prokaryotic complex iron–sulfur molybdoenzyme family. *Biochim Biophys Acta - Biomem* **1778:** 1897-1929.

Saitou N, Nei M (1987). The neighbor-joining method: a new method for reconstructing phylogenetic trees. *Mol Biol Evol* **4:** 406-425.

Saltikov CW, Newman DK (2003). Genetic identification of a respiratory arsenate reductase. *Proc Natl Acad Sci* **100:** 10983-10988.

Sato T, Kobayashi Y (1998). The *ars* operon in the *skin* element of *Bacillus subtilis* confers resistance to arsenate and arsenite. *J Bacteriol* **180:** 1655-1661.

Sekiguchi Y, Yamada T, Hanada S, Ohashi A, Harada H, Kamagata Y (2003). *Anaerolinea thermophila* gen. nov., sp. nov. and *Caldilinea aerophila* gen. nov., sp. nov., novel filamentous thermophiles that represent a previously uncultured lineage of the domain *Bacteria* at the subphylum level. *Int J Syst Evol Microbiol* **53:** 1843-1851.

Skaff O, Pattison DI, Davies MJ (2009). Hypothiocyanous acid reactivity with low-molecular-mass and protein thiols: absolute rate constants and assessment of biological relevance. *Biochem J* **422:** 111-117.

Skaff O, Pattison DI, Morgan PE, Bachana R, Jain VK, Priyadarsini KI *et al.* (2012). Selenium-containing amino acids are targets for myeloperoxidase-derived hypothiocyanous acid: determination of absolute rate constants and implications for biological damage. Biochem J **441:** 305-316.

Schoepp-Cothenet B, Van Lis R, Philippot P, Magalon A, Russell MJ, Nitschke W (2012). The ineluctable requirement for the trans-iron elements molybdenum and/or tungsten in the origin of life. *Sci Rep* **2:** 263.

Schwarz G, Mendel RR, Ribbe MW (2009). Molybdenum cofactors, enzymes and pathways. *Nature* **460:** 839-847.

Sleator RD, Hill C (2002). Bacterial osmoadaptation: the role of osmolytes in bacterial stress and virulence. *FEMS Microbiol Rev* **26:** 49-71.

Suyama A, Iwakiri R, Kai K, Tokunaga T, Sera N, Furukawa K (2001). Isolation and characterization of *Desulfitobacterium* sp. strain Y51 capable of efficient dehalogenation of tetrachloroethene and polychloroethanes. *Biosci Biotechnol Biochem* **65:** 1474-1481.

Ståhlberg A, Rusnakova V, Forootan A, Anderova M, Kubista, M. (2013). RT-qPCR work-flow for single-cell data analysis. *Methods* **59:** 80-88.

Stewart V, Lu Y, Darwin AJ (2002). Periplasmic nitrate reductase (NapABC enzyme) supports anaerobic respiration by *Escherichia coli* K-12. *J Bacteriol* **184:** 1314-1323.

Switzer Blum J, Burns Bindi A, Buzzelli J, Stolz JF, Oremland RS (1998). *Bacillus arsenicoselenatis*, sp. nov., and *Bacillus selenitireducens*, sp. nov.: two haloalkaliphiles from Mono Lake, California that respire oxyanions of selenium and arsenic. *Arch Microbiol* **171:** 19-30.

Tamás, M. J. (2016). Cellular and molecular mechanisms of antimony transport, toxicity and resistance. Environ Chem **13:** 955-962.

Tamás M, Sharma S, Ibstedt S, Jacobson T, Christen P (2014). Heavy metals and metalloids as a cause for protein misfolding and aggregation. *Biomolecules* **4:** 252-267.

Tamura K, Stecher G, Peterson D, Filipski A, Kumar S (2013). MEGA6: molecular evolutionary genetics analysis version 6.0. *Mol Biol Evol* **30:** 2725-2729.

Tatusov RL, Galperin MY, Natale DA, Koonin EV (2000). The COG database: a tool for genome-scale analysis of protein functions and evolution. *Nucleic Acids Res* **28:** 33-36.

Tella M, Pokrovski GS (2008). Antimony(V) complexing with O-bearing organic ligands in aqueous solution: an x-ray absorption fine structure spectroscopy and potentiometric study. *Mineral Mag* **72:** 205-209.

Tella M, Pokrovski GS (2009). Antimony(III) complexing with O-bearing organic ligands in aqueous solution: an x-ray absorption fine structure spectroscopy and solubility study. *Geochim Cosmochim Acta* **73:** 268-290.

Thauer RK, Jungermann K, Decker K (1977). Energy conservation in chemotrophic anaerobic bacteria. *Bacteriol Rev* **41:** 100-180.

Thomas G, Potter L, Cole JA (1999). The periplasmic nitrate reductase from *Escherichia coli*: a heterodimeric molybdoprotein with a double-arginine signal sequence and an unusual leader peptide cleavage site. *FEMS Microbiol Lett* **174:** 167-171.

Tirmenstein MA, Mathias PI, Snawder JE, Wey HE, Toraason M (1997). Antimony-induced alterations in thiol homeostasis and adenine nucleotide status in cultured cardiac myocytes. *Toxicology* **119:** 203-211.

Valasatava Y, Rosato A, Banci L, Andreini C (2016). MetalPredator: a web server to predict iron–sulfur cluster binding proteomes. *Bioinformatics* **32:** 2850-2852.

van Lis R, Nitschke W, Duval S, Schoepp-Cothenet B (2013). Arsenics as bioenergetic substrates. *Biochim Biophys Acta Bioenerg* **1827:** 176-188.

Wang Q, Warelow TP, Kang YS, Romano C, Osborne TH, Lehr CR *et al.* (2015). Arsenite oxidase also functions as an antimonite oxidase. *Appl Environ Microbiol* **81:** 1959-1965.

Weatherburn MW (1967). Phenol-hypochlorite reaction for determination of ammonia. *Anal Chem* **39:** 971-974.

Widdel F, Kohring GW, Mayer F (1983). Studies on dissimilatory sulfate-reducing bacteria that decompose fatty acids. III. Characterization of the filamentous gliding *Desulfonema limnicola* gen. nov., sp. nov., and *Desulfonema magnum* sp. nov. *Arch Microbiol* **134:** 286-294.

Winterbourn CC (1995). Toxicity of iron and hydrogen peroxide: the Fenton reaction. *Toxicol Lett* **82-83:** 969-974.

Wood ED, Armstrong FAJ, Richards FA (1967). Determination of nitrate in sea water by cadmium-copper reduction to nitrite. *J Mar Biol Assoc UK* **47:** 23-31.

Wu J, Rosen BP (1993). Metalloregulated expression of the *ars* operon. *J Biol Chem* **268:** 52-58.

Yu DJ, Hu J, Yang J, Shen HB, Tang J, Yang JY (2013). Designing template-free predictor for targeting protein-ligand binding sites with classifier ensemble and spatial clustering. *IEEE/ACM Trans Comp Biol Bioinform* **10:** 994-1008.

Zhu Y, Wu M, Gao N, Chu W, An N, Wang Q *et al.* (2018). Removal of antimonate from wastewater by dissimilatory bacterial reduction: role of the coexisting sulfate. *J Hazard Mater* **341:** 36-45.

Zotov AV, Shikina ND, Akinfiev NN (2003). Thermodynamic properties of the Sb(III) hydroxide complex $Sb(OH)_{3(aq)}$ at hydrothermal conditions. *Geochim Cosmochim Acta* **67:** 1821-1836.

Table 4.1. Genes encoding enzymes of the DMSOR family found in the draft genome of MLFW-2^T.

Locus Tag	Protein Accession #	Length (AA)	Genbank Annotation[a]
BHU72_01065	WP_069700761	686	MO
BHU72_01090	WP_069700766	737	DMSOR
BHU72_03635	WP_069701962	772	NR
BHU72_03930	WP_069702010	904[b]	FD
	WP_069702011		
BHU72_04760	WP_069702231	728	D
BHU72_06270	WP_083248387	1,013	FDN
BHU72_07145	WP_069702695	942	D
BHU72_07340	WP_083248419	753	HP
BHU72_07355	WP_069702733	1,046	HP
BHU72_07375	WP_069702735	1,029	HP
BHU72_07925	WP_083248445	687	MOFP
BHU72_09285	WP_069703115	734	HP
BHU72_10220	WP_069700989	871	D
BHU72_10330	WP_069701007	845	D

[a]Abbreviations are as follows: D, dehydrogenase; DMSOR, dimethyl sulfoxide reductase; FD, formate dehydrogenase; FDN, formate dehydrogenase N; HP, hypothetical protein; MO; molybdopterin oxidoreductase; MOFP, molybdopterin oxidoreductase family protein; NR, nitrate reductase.
[b]Reflects the actual length of the protein, as RefSeq counts a selenocysteine residue at position 361 of WP_069702010 as a stop codon.

Table 4.2. Rates of growth and electron acceptor reduction by MLFW-2^T

Electron Acceptor (EA)	$\Delta G^{\circ\prime}$ (kJ mol^{-1} EA)[a,b]	Specific Growth Rate, μ (h^{-1})	Doubling Time, t_d (h)	EA Reduction Rate (fmol h^{-1} $cell^{-1}$)
Nitrate	-608.2[c]	0.37 ± 0.01	1.88 ± 0.04	2.58 ± 0.33
Nitrite	-443.2[c]	0.33 ± 0.01	2.10 ± 0.09	2.05 ± 0.02
Se(VI)	-433.8[d]	0.44 ± 0.04	1.60 ± 0.14	5.39 ± 0.71
Sb(V)	-99.9	0.16 ± 0.01	4.29 ± 0.29	2.80 ± 0.13
As(V)	-85.8	0.54 ± 0.04	1.30 ± 0.10	7.59 ± 0.55

[a]Standard Gibbs free energy change for the reduction of electron acceptor coupled to the oxidation of lactate to acetate and HCO_3^-, assuming a midpoint condition (i.e. $[EA_{ox}] = [EA_{red}]$).
[b]Calculated using thermodynamic values provided by Thauer *et al.* (1977), Bard *et al.* (1985), Nordstrom and Archer (2003), Zotov *et al.* (2003), and Diemar *et al.* (2009).
[c]Calculation based on ammonium as end product.
[d]Calculation based on Se(0) as end product.

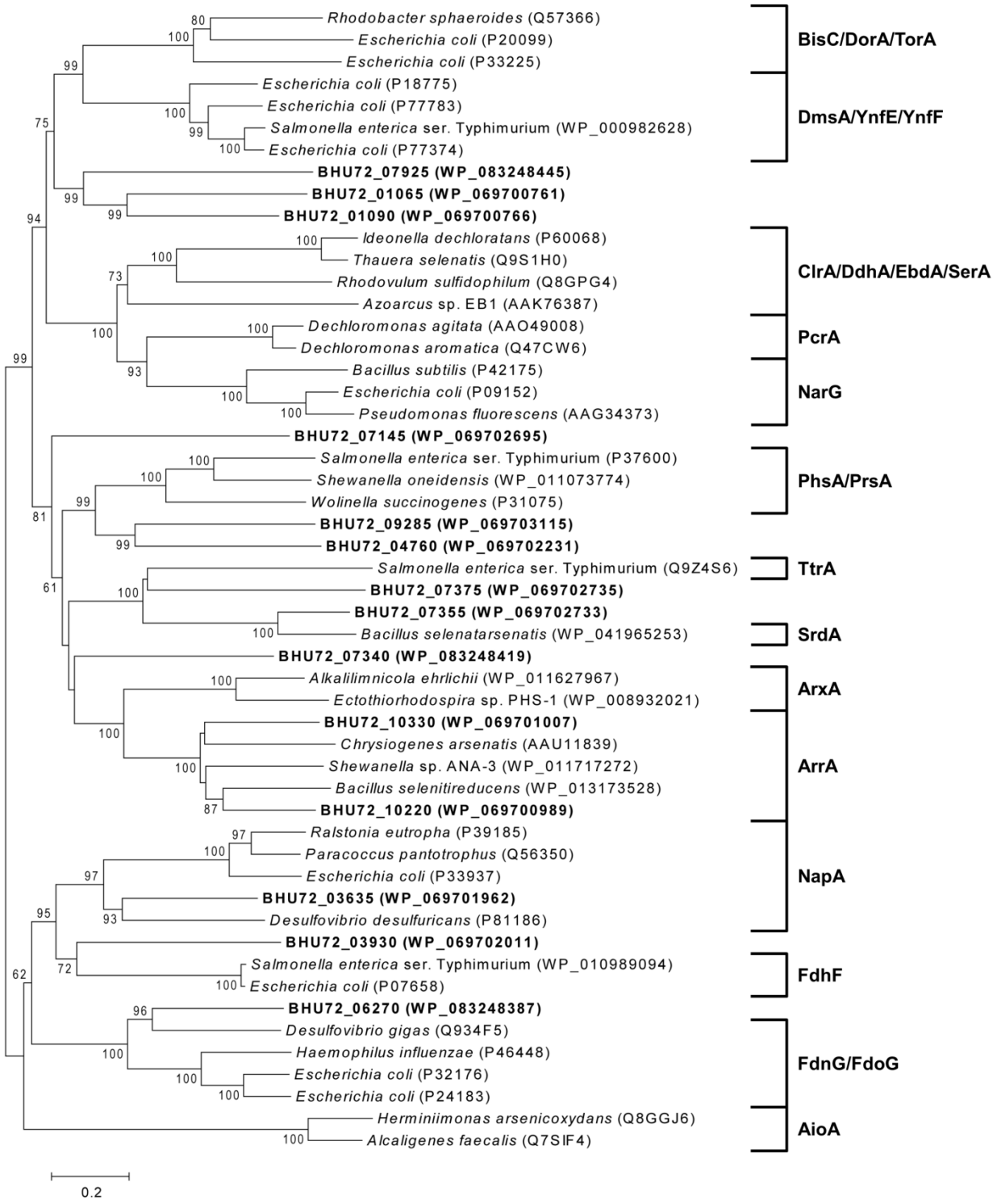
Rhodobacter sphaeroides (Q57366)
Escherichia coli (P20099)
Escherichia coli (P33225)
Escherichia coli (P18775)
Escherichia coli (P77783)
Salmonella enterica ser. Typhimurium (WP_000982628)
Escherichia coli (P77374)
BHU72_07925 (WP_083248445)
BHU72_01065 (WP_069700761)
BHU72_01090 (WP_069700766)
Ideonella dechloratans (P60068)
Thauera selenatis (Q9S1H0)
Rhodovulum sulfidophilum (Q8GPG4)
Azoarcus sp. EB1 (AAK76387)
Dechloromonas agitata (AAO49008)
Dechloromonas aromatica (Q47CW6)
Bacillus subtilis (P42175)
Escherichia coli (P09152)
Pseudomonas fluorescens (AAG34373)
BHU72_07145 (WP_069702695)
Salmonella enterica ser. Typhimurium (P37600)
Shewanella oneidensis (WP_011073774)
Wolinella succinogenes (P31075)
BHU72_09285 (WP_069703115)
BHU72_04760 (WP_069702231)
Salmonella enterica ser. Typhimurium (Q9Z4S6)
BHU72_07375 (WP_069702735)
BHU72_07355 (WP_069702733)
Bacillus selenatarsenatis (WP_041965253)
BHU72_07340 (WP_083248419)
Alkalilimnicola ehrlichii (WP_011627967)
Ectothiorhodospira sp. PHS-1 (WP_008932021)
BHU72_10330 (WP_069701007)
Chrysiogenes arsenatis (AAU11839)
Shewanella sp. ANA-3 (WP_011717272)
Bacillus selenitireducens (WP_013173528)
BHU72_10220 (WP_069700989)
Ralstonia eutropha (P39185)
Paracoccus pantotrophus (Q56350)
Escherichia coli (P33937)
BHU72_03635 (WP_069701962)
Desulfovibrio desulfuricans (P81186)
BHU72_03930 (WP_069702011)
Salmonella enterica ser. Typhimurium (WP_010989094)
Escherichia coli (P07658)
BHU72_06270 (WP_083248387)
Desulfovibrio gigas (Q934F5)
Haemophilus influenzae (P46448)
Escherichia coli (P32176)
Escherichia coli (P24183)
Herminiimonas arsenicoxydans (Q8GGJ6)
Alcaligenes faecalis (Q7SIF4)
0.2
BisC/DorA/TorA
DmsA/YnfE/YnfF
ClrA/DdhA/EbdA/SerA
PcrA
NarG
PhsA/PrsA
TtrA
SrdA
ArxA
ArrA
NapA
FdhF
FdnG/FdoG
AioA

Figure 4.1. Unrooted, neighbor-joining phylogenetic tree based on inferred amino acid sequences showing the evolutionary relationship between the catalytic subunits of enzymes of the DMSOR family. Bootstrap values (≥ 50%) based on 1,000 replicates are shown at the nodes. Proteins encoded by MLFW-2^T are shown in bold. GenBank, RefSeq, or UniProtKB/Swiss-Prot accession numbers are provided in parentheses. Abbreviation for proteins are as follows: AioA, aerobic arsenite oxidase; ArrA, respiratory arsenate reductase; ArxA, anaerobic arsenite oxidase; BisC, biotin sulfoxide reductase; ClrA, chlorate reductase; DdhA, dimethyl sulfide dehydrogenase; DmsA, membrane-bound dimethyl sulfoxide reductase; DorA, periplasmic dimethyl sulfoxide reductase; EbdA, ethylbenzene dehydrogenase; FdhF, formate dehydrogenase; FdnG, formate dehydrogenase; FdoG, formate dehydrogenase; NapA, periplasmic nitrate reductase; NarG, membrane-bound nitrate reductase; PcrA, perchlorate reductase; PhsA, thiosulfate reductase; PsrA, polysulfide reductase; SerA, periplasmic selenate reductase; SrdA, membrane-bound selenate reductase; TorA, trimethylamine-N-oxide reductase; TtrA, tetrathionate reductase; YnfE, selenate reductase; YnfF, selenate reductase. Scale bar, 0.2 substitutions per position.

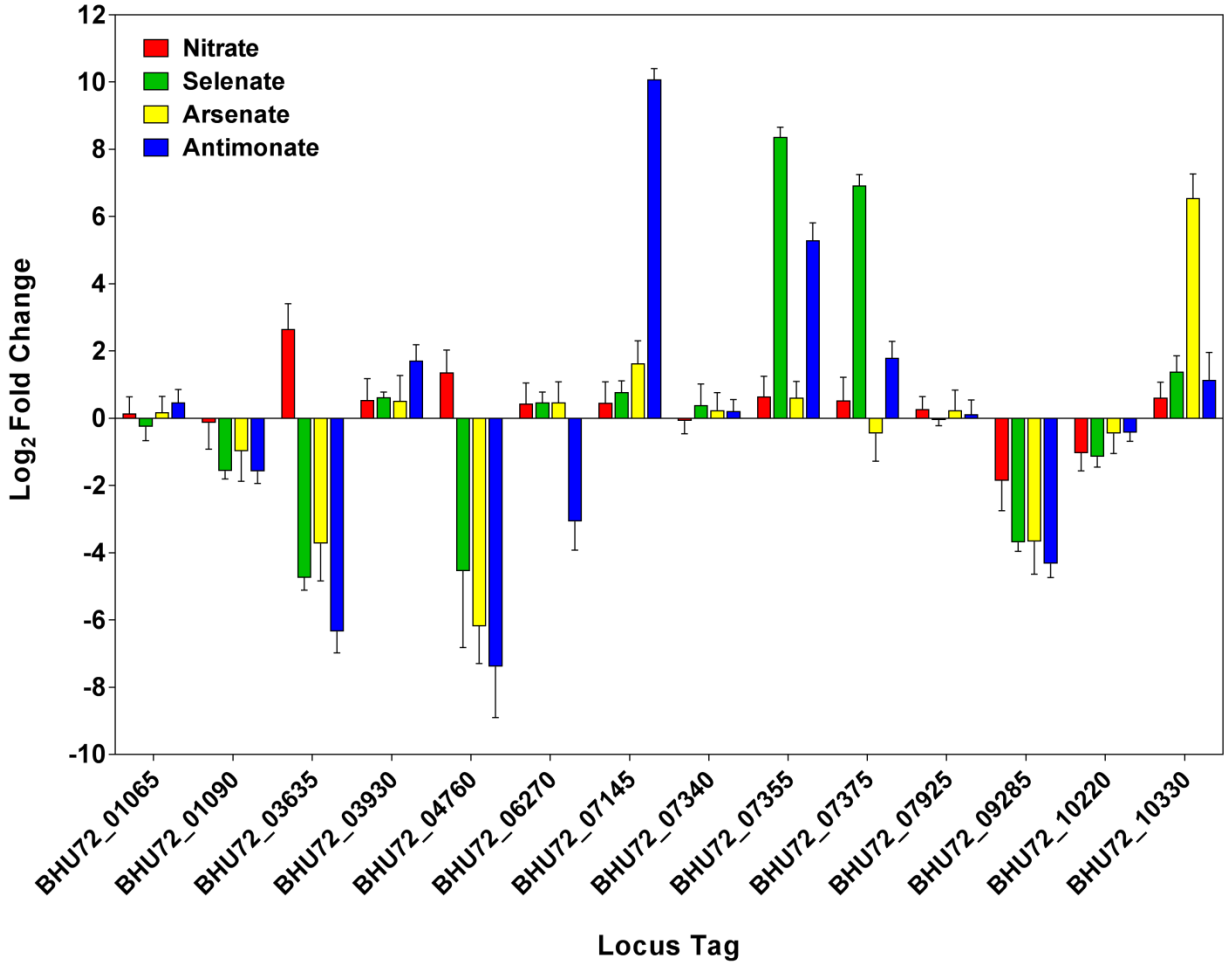

Figure 4.2. Relative transcription of genes encoding the catalytic subunits of enzymes of the DMSOR family during exponential growth of MLFW-2^T on different terminal electron acceptors. Transcription of each gene was normalized to the housekeeping gene *gyrB*, using growth on nitrite as a calibrator.

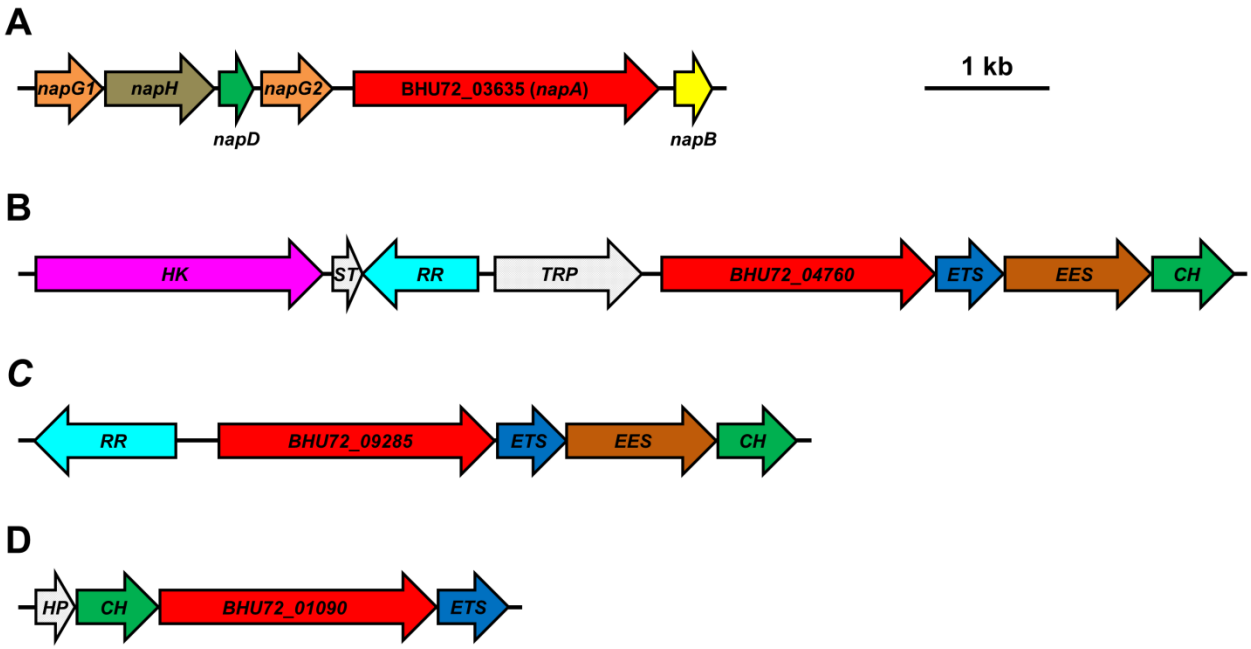

Figure 4.3. Organization of hypothetical operons harboring DMSOR family genes upregulated during growth of MLFW-2^T on nitrate as the terminal electron acceptor. The locus tags for genes encoding catalytic subunits (red) are provided. Abbreviations for annotations are as follows: *CH*, TorD-family cytoplasmic chaperone; *EES*, electron entry/exit subunit; *ETS*, electron transfer subunit; *HK*, histidine kinase; *HP*, hypothetical protein; *napA*, catalytic subunit of periplasmic nitrate reductase; *napB*, diheme *c*-type cytochrome ETS of periplasmic nitrate reductase; *napD*, cytoplasmic chaperone; *napG1*, putative cytoplasmic chaperone; *napG2*, integral membrane quinol dehydrogenase; *napH*, integral membrane quinol dehydrogenase; *RR*, response regulator; *ST*, sulfurtransferase; *TRP*, putative transporter for sulfur-containing compounds.

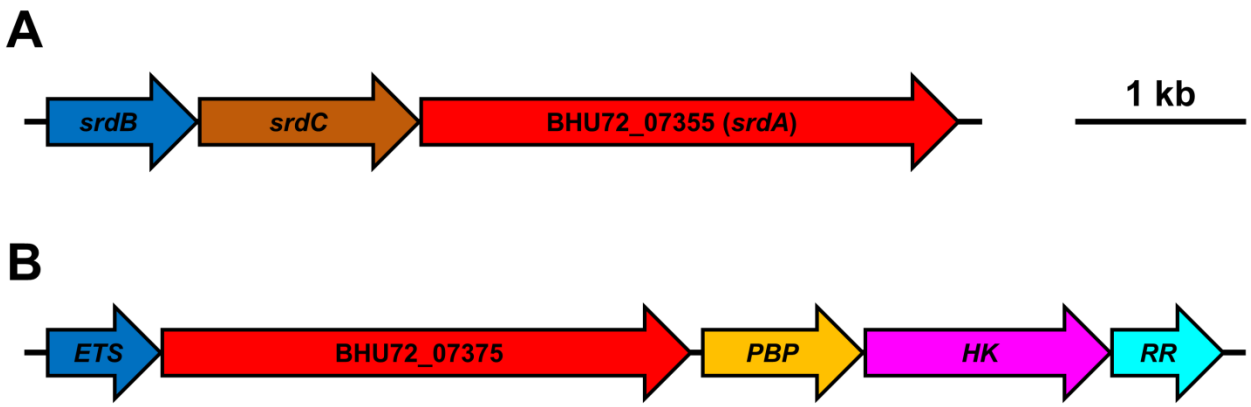

Figure 4.4. Organization of hypothetical operons harboring DMSOR family genes upregulated during growth of MLFW-2^T on Se(VI) as the terminal electron acceptor. The locus tags for genes encoding catalytic subunits (red) are provided. Abbreviations for annotations are as follows: *ETS*, electron transfer subunit; *HK*, histidine kinase; *PBP*, periplasmic phosphonate-binding protein; *RR*, response regulator; *srdA*, catalytic subunit of membrane-bound Se(VI) reductase; *srdB*, ETS for membrane-bound Se(VI) reductase; *srdC*, EES of membrane-bound Se(VI) reductase.

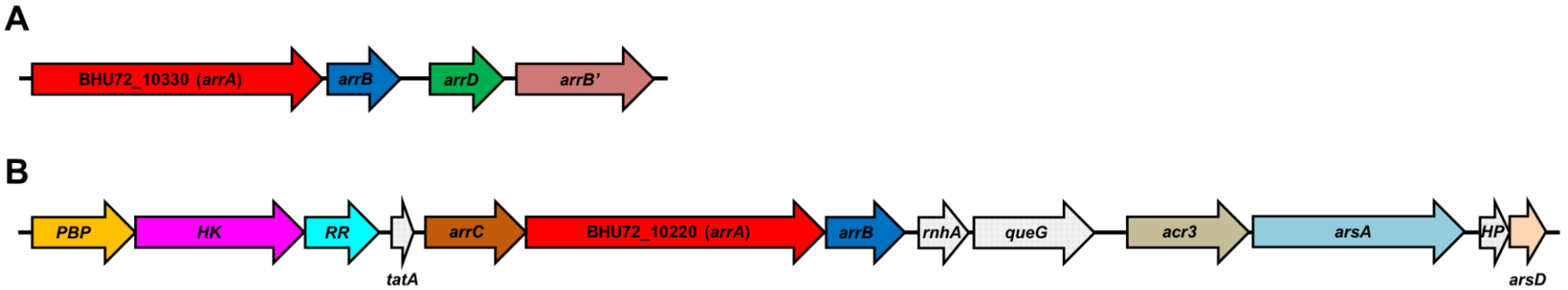

Figure 4.5. Organization of hypothetical operons harboring DMSOR family genes upregulated during growth of MLFW-2^T on As(V) as the terminal electron acceptor. The locus tags for genes encoding catalytic subunits (red) are provided. Abbreviations for annotations are as follows: *acr3*, As(III) efflux pump; *arrA*, catalytic subunit of respiratory As(V) reductase; *arrB*, ETS of respiratory As(V) reductase; *arrB'*, 4[4Fe-4S] ferredoxin; *arrC*, EES of respiratory As(V) reductase; *arrD*, TorD-family cytoplasmic chaperone; *arsA*, As(III) efflux pump-driving ATPase; *arsD*, *ars* operon repressor; *HK*, histidine kinase; *HP*, hypothetical protein; *PBP*, periplasmic phosphonate-binding protein; *queG*, epoxyqueuosine reductase; *rnhA*, ribonuclease H; *RR*, response regulator; *tatA*, protein translocase.

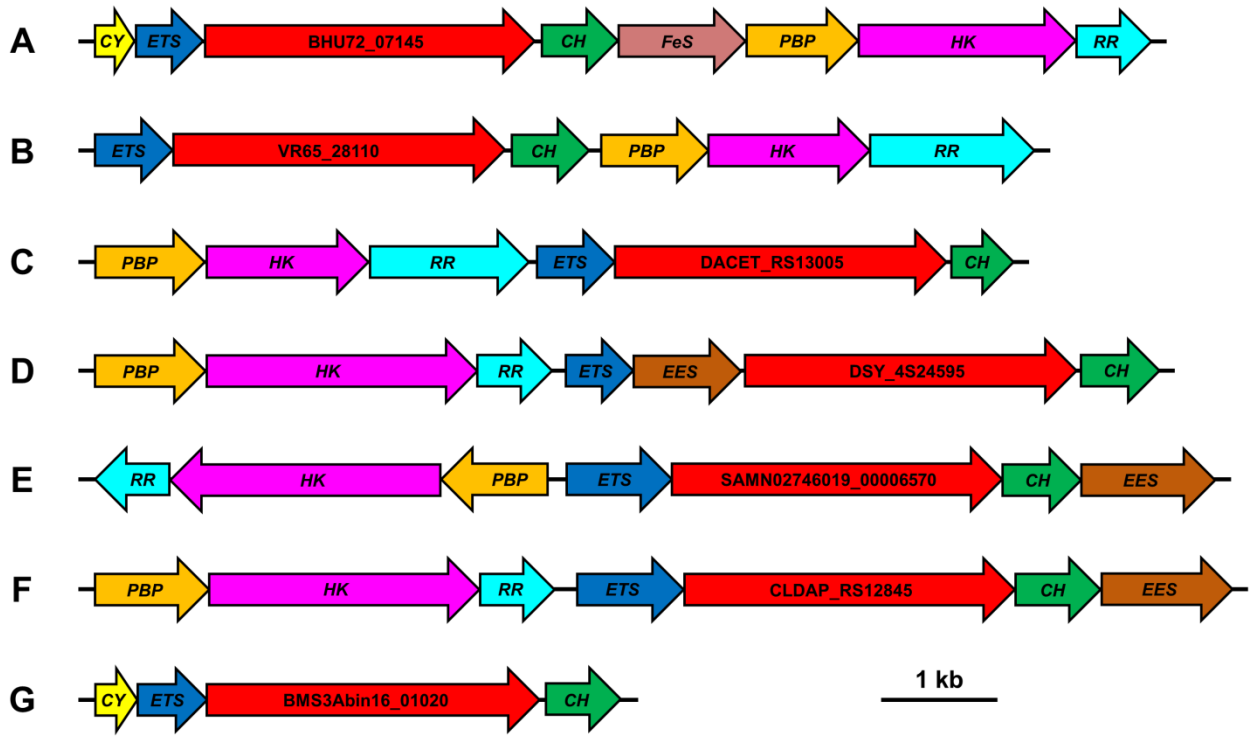

Figure 4.6. Organization of hypothetical operons possibly encoding dissimilatory Sb(V) reductases in phylogenetically-diverse microorganisms. **(A)** Hypothetical operon harboring DMSOR family gene upregulated during growth of MLFW-2^T on Sb(V) as the terminal electron acceptor. **(B-G)** Hypothetical operons encoding a protein with significant homology (≥50% amino acid identity and ≥90% coverage) to BHU72_07145. The letters correspond to the following taxa: B, *Deltaproteobacteria*; C, *Denitrovibrio acetiphilus* and *Nitrospirae*; D, *Clostridiales*; E, *Thermoflexus hugenholtzii*; F, *Caldilinea aerophila*; G, Euryarcheon BMS3Abin16. The locus tags for genes encoding catalytic subunits (red) are provided. Abbreviations for annotations are as follows: *CH*, TorD-family cytoplasmic chaperone; *CY*, diheme c-type cytochrome; *EES*, electron entry/exit subunit; *ETS*, electron transfer subunit; *FeS*, 4[4Fe-4S] ferredoxin; *HK*, histidine kinase; *PBP*, periplasmic phosphonate-binding protein; *RR*, response regulator.

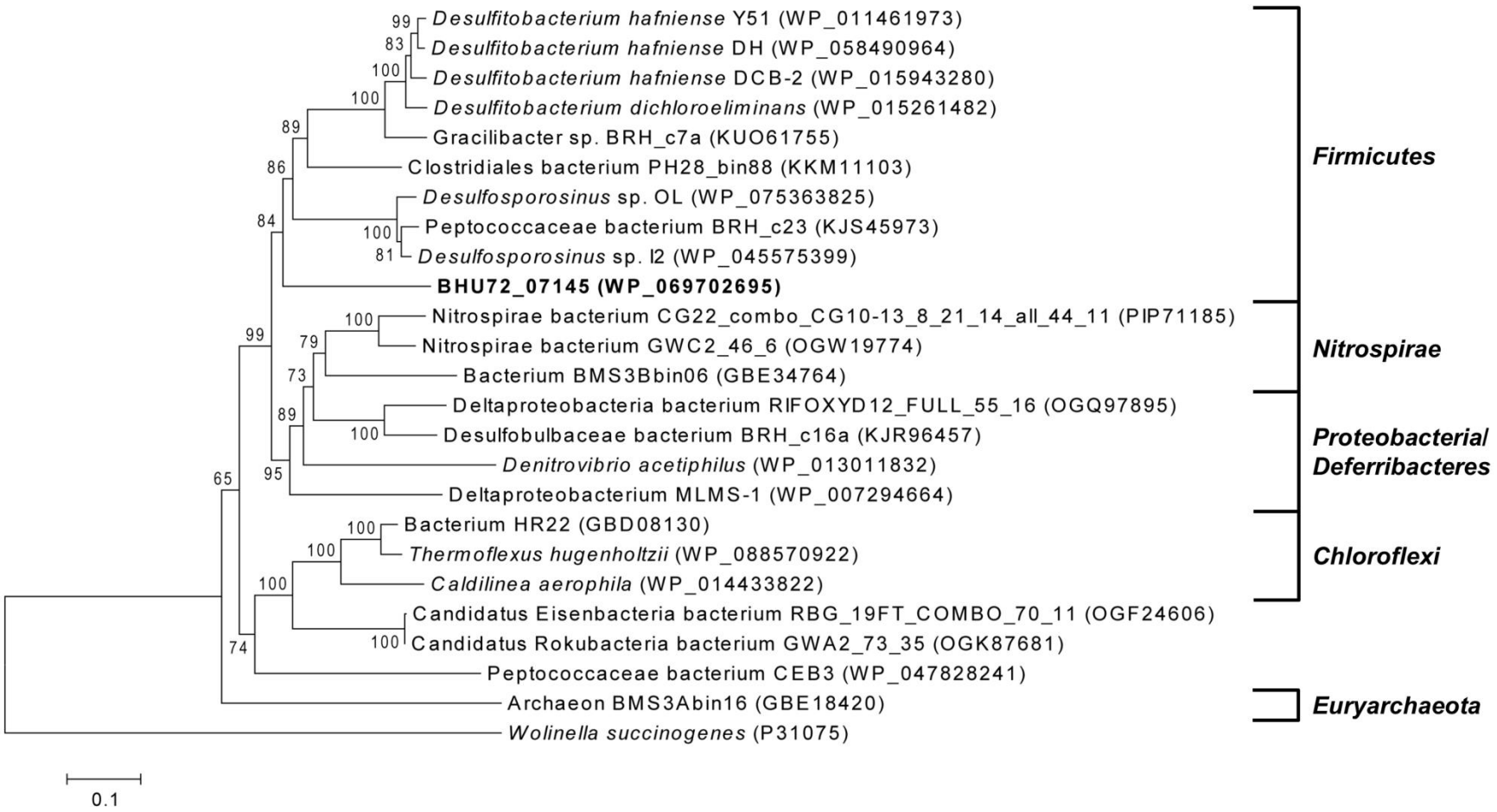

Figure 4.7. Neighbor-joining phylogenetic tree based on inferred amino acid sequences showing the evolutionary relationship between the product of BHU72_07145 (bold) and closely related proteins found in other organisms. Only those amino acid sequences with significant homology (≥ 50% identity and ≥ 90% coverage) to BHU72_07145 are included in the tree. Bootstrap values (≥ 50%) based on 1,000 replicates are shown at the nodes. GenBank, RefSeq, or UniProtKB/Swiss-Prot accession numbers are provided in parentheses. PsrA from *Wolinella succinogenes* was used as the outgroup. Scale bar, 0.1 substitutions per position.

CHAPTER 5

CONCLUSIONS

The preceding chapters present the isolation and characterization of the first dissimilatory Sb(V)-reducing microorganism to be discovered. The genome of the isolate was sequenced and genes encoding terminal anaerobic respiratory reductases belonging to the complex iron-sulfur molybdoenzyme superfamily were identified. Putative functions were assigned to several of these genes based on their relative transcription during growth of the isolate on different terminal electron acceptors. Lastly, a transcriptomics approach was used to study the physiological response of the isolate to Sb(V) and As(V), two species with similar chemistry but eliciting markedly different effects on cellular growth.

The first unequivocal evidence for dissimilatory Sb(V) reduction by a microorganism was presented in Chapter 2. A lactate-oxidizing, Sb(V)-reducing enrichment culture was established from anoxic sediments collected from the drainage area of a geothermal spring near the southern shore of Mono Lake, CA. The enrichment culture was maintained over a period of several months, until it became dominated by a single morphotype consisting of motile, curved, rod-shaped cells. A pure culture of the microorganism, referred to as strain MLFW-2^T, was obtained and shown to grow on lactate using Sb(V) as the terminal electron acceptor. Growth on Sb(V) was accompanied by the precipitation of white microcrystals of Sb_2O_3, as demonstrated by energy-dispersive X-ray spectroscopy and X-ray diffraction. The crystals were made up of two polymorphs, a dominant orthorhombic phase and a less common cubic phase. The orthorhombic phase, also known as valentinite, consisted of bowtie-shaped crystals with flat blades radiating

out from a central bundle. The cubic phase was made up of octahedral crystals and was consistent with the mineral sénarmontite.

The discovery that Sb(V) reduction by MLFW-2^T was accompanied by Sb(III) precipitation was significant for several reasons. First, it provided a novel strategy for the synthesis of semiconducting Sb_2O_3 microcrystals for potential applications in solar cells and other optoelectronic nanodevices. Currently, chemical synthesis methods are employed for the controlled synthesis of Sb_2O_3 nano- and microcrystals of varying morphologies, but these methods often require high temperatures and pressures or harsh chemicals. The precipitation of Sb_2O_3 by MLFW-2^T may present a unique approach to produce crystals with similar shapes and properties in a cost-effective and sustainable manner. Secondly, Sb(V) reduction may serve as a viable method to remove toxic Sb from contaminated soils, sediments, and groundwaters, such as those occurring around past or present mining sites, Sb-processing factories, and shooting ranges. Dissimilatory Sb(V) reduction converts soluble Sb(V) into insoluble Sb(III), which precipitates as Sb_2S_3 or Sb_2O_3 in sulfidic and non-sulfidic environments, respectively. Sb(III) can also be removed from the aqueous phase by adsorption onto the surface of iron, manganese, and aluminum (hydr)oxides.

The morphological, physiological, chemotaxonomic, and phylogenetic properties of MLFW-2^T were presented in Chapter 3. Cells of MLFW-2^T were found to stain Gram-negative. The curved rods formed terminal endospores during the stationary phase of growth. The observation that cells stained Gram-negative was interesting, given that an outer membrane was not present in transmission electron micrographs. Cells were catalase positive and oxidase negative, consistent with the inability of MLFW-2^T to grow in the presence of oxygen. The production of catalase may explain why MLFW-2^T is able to grow in media containing only a

small amount of sulfide as reducing agent (i.e. characterized by a higher redox potential). MLFW-2^T was able to grow on several electron acceptors, including nitrate, nitrite, DMSO, Se(VI), Se(IV), As(V), and Sb(V) using lactate as the electron donor and carbon source. The growth rate was highest when As(V) was the provided as the terminal electron acceptor, a phenomenon previously reported for the arsenate-respiring bacterium *Desulfurispirillum indicum*. MLFW-2^T could use H_2, formate, lactate, and pyruvate as electron donors with As(V) as the electron acceptor. However, growth with H_2 and formate was only possible if acetate was provided as a carbon source, indicating that MLFW-2^T was unable to grow autotrophically. MLFW-2^T was a mesophilic, slightly alkaliphilic, and halotolerant bacterium, with maximal growth occurring at a temperature of 34 °C, pH of 8.25 – 8.50, and salinity of 0.75% NaCl. These growth optima are consistent with the characteristics of the environment from which MLFW-2^T was isolated – freshwater sediments receiving seasonal inputs of alkaline, hypersaline water from Mono Lake.

The genome of MLFW-2^T was sequenced to generate a draft genome with a total length of 3.1 Mbp and a G+C content of 38.2%. The genome contained 3,028 coding sequences and was nearly complete, as demonstrated by the presence of 31 out of 31 phylogenetic marker genes essential in bacteria. A phylogenetic analysis of the 16S rRNA gene of MLFW-2^T revealed that it was a member of the order *Bacillales* of the phylum *Firmicutes*. The closest phylogenetic relative was *Desulfuribacillus alkaliarsenatis* AHT28^T, an obligately anaerobic, dissimilatory arsenate- and sulfur-reducing haloalkaliphile isolated from a Russian soda lake. The draft genome of *D. alkaliarsenatis* was very similar in length and G+C content to that of MLFW-2^T, with values of 3.1 Mbp and 37.5%, respectively. A set of three *in silico* analyses were conducted to refine the phylogenetic relationship between the two strains. The results of ANI, AAI, and

POCP analyses suggested that both strains belonged to different species within the same genus. Based on the available evidence, MLFW-2^T merited recognition as a novel species within the genus *Desulfuribacillus*, for which the name *Desulfuribacillus stibiiarsenatis* sp. nov. was proposed.

Genes potentially involved in anaerobic respiration in MLFW-2^T were examined in Chapter 4. Genes encoding components of terminal anaerobic respiratory reductases of the DMSOR family of complex iron-sulfur molybdoenzymes were of particular interest because some of the electron acceptors respired by MLFW-2^T [DMSO, nitrate, Se(VI), and As(V)] were known substrates for members of this family. Given that Sb and As share similar chemistry and Sb(V) reduction involves a two-electron redox reaction, the terminal Sb(V) reductase was likely to be a member of the DMSOR family. A search of the MLFW-2^T draft genome uncovered a total of fourteen genes encoding the catalytic subunits of enzymes of the DMSOR family, with the products of only seven of them clustering tightly within established subfamilies. RT-qPCR was used to monitor the relative transcription of each of these fourteen genes during growth on several different electron acceptors. Strong evidence was presented that four of these genes encode the catalytic subunits of the respiratory nitrate, Se(VI), As(V), and Sb(V) reductases in MLFW-2^T. Most notably, homologs of the gene identified as most likely encoding the catalytic subunit of the dissimilatory Sb(V) reductase were found in eight different phyla, including two candidate phyla, from both prokaryotic domains of life. These results suggest that Sb(V) reduction may be an ancient process – one that could have played an important role in sustaining life in Sb-rich environments on the early Earth.

Growth of MLFW-2^T on Sb(V) could only be re-established with great difficulty after growing the isolate on As(V) as the electron acceptor. Robust growth on Sb(V) could only be re-

established if toxic Sb(III) was removed by washing the cells between transfers. RNA-seq was used to study the physiological response of MLFW-2^T to growth on Sb(V) and As(V) as electron acceptors, with the primary motivation to find out why the former species was significantly more toxic than the latter. It was thought that RNA-seq could provide information about the cellular functions and types of biomolecules most impacted by Sb toxicity. Transcriptome data showed that Sb(V) elicited a stronger oxidative stress response than As(V), with the cytoplasmic pool of free- and protein-bound thiols and thioethers, Fe-S clusters, and DNA serving as the main targets for oxidative damage. For instance, genes involved in the biosynthesis of three important antioxidants (cysteine, coenzyme A, and cobalamin) were more highly transcribed when Sb(V) versus As(V) was provided as the electron acceptor. Greater amounts of ROS and RNS were produced during growth on Sb(V) relative to As(V), as evidenced by the upregulation of genes involved in their detoxification.

There were several interesting observations arising from these studies that merit further discussion. Firstly, the potential Sb(V) reductase encoded by BHU72_07135 – BHU72_07170 does not contain an obvious EES subunit, so it is unknown how the complex connects to the rest of the electron transport chain. Four genes (BHU72_10075 – BHU72_10090) encoding proteins possibly involved in electron transport were highly upregulated when Sb(V) was provided as the electron acceptor. It is possible that these four proteins form a complex that functions as a quinol dehydrogenase in MLFW-2^T, shuttling electrons from the quinone pool to the dissimilatory Sb(V) reductase. This function would be analogous to the one played by proteins of the NapC/NirT/NrfH family in organisms such as *Shewanella* spp. that encode a large number of soluble, periplasmic oxidoreductases. Secondly, Sb(V), rather than As(V), induced greater transcription of the *arsA* and *acr3* genes encoding an ATP-driven As(III) efflux pump involved

in As detoxification. Although Sb(III) has been previously shown to induce the expression of chromosomal and plasmid-borne arsenic resistance (*ars*) operons in organisms from diverse phyla, this result was surprising because Sb(V) was provided at a significantly lower concentration than As(V). Thirdly, Sb(V) caused the upregulation of several genes involved in the uptake of di- and tricarboxylates, compounds which are known to be strong chelators of Sb oxyanions. This may represent a novel mechanism for Sb detoxification by which reactive Sb(V) and Sb(III) are removed from the cytoplasm through complexation with organic ligands. Lastly, As(V) induced the upregulation of genes involved in uptake of tertiary amines such as glycine betaine and choline. These osmo- and thermoprotectants may play important roles in mitigating the toxic effects of As, perhaps by stimulating components of the antioxidant defense system or by stabilizing proteins and nucleic acids.

In summary, this work has increased the understanding of the global biogeochemical cycling of Sb by demonstrating that microorganisms can use Sb(V) as an electron acceptor to support growth. Through their metabolism, Sb(V)-reducing microorganisms can produce nano- and microcrystals of Sb_2O_3 useful for a number of industrial applications. Moreover, *in situ* Sb(V) reduction may represent a viable alternative for the removal of toxic Sb from contaminated soils, sediments, and groundwaters. By identifying a set of genes possibly encoding a dissimilatory Sb(V) reductase, this work has laid the foundation for future experiments to uncover the molecular machinery underlying this novel mode of anaerobic respiration. The transcriptomics work presented here also provided a detailed picture of the exact mechanisms by which Sb elicits its toxic effects on cells.

APPENDIX A

SUPPLEMENTARY CHAPTER 1: DRAFT GENOME SEQUENCE OF THE TYPE STRAIN *DESULFURIBACILLUS ALKALIARSENATIS* AHT28, AN OBLIGATELY ANAEROBIC, SULFIDOGENIC BACTERIUM ISOLATED FROM RUSSIAN SODA LAKE SEDIMENTS[4]

[4]Abin C.A. and J.T. Hollibaugh. 2016. *Genome Announc*. 4(6): e01244-16. Reprinted here with permission of publisher.

ABSTRACT

Desulfuribacillus alkaliarsenatis AHT28^{T} is an obligately anaerobic, sulfur- and arsenate-reducing haloalkaliphile that was isolated from Russian soda lake sediments. Here, we present the 3.1 Mbp draft genome sequence for this strain, consisting of 36 contigs with a G+C content of 37.5% and 2,978 protein-coding sequences.

Sulfidogenesis is the process by which sulfide is produced through microbial reduction of oxidized sulfur compounds such as sulfate, sulfite, thiosulfate, and elemental sulfur. Elemental sulfur reduction appears to be widespread in alkaline (pH 9 – 11), hypersaline (>3.5% salt) soda lakes, with activities having been observed to surpass that of sulfate reduction under conditions of salt saturation (Sorokin *et al.* 2010). Even though sulfur reduction is a potentially important biogeochemical process in soda lakes, relatively little is known about the phylogeny and physiology of sulfur-respiring haloalkaliphiles. To date, five bacterial and two archaeal strains have been isolated and described (Sorokin *et al.* 2015). Publicly available genome sequences exist for only *Halarsenatibacter silvermanii* SLAS-1^T (Oremland *et al.* 2005, Switzer Blum *et al.* 2009) and two strains of *Halanaeroarchaeum sulfurireducens* (Messina *et al.* 2016, Sorokin *et al.* 2016).

Desulfuribacillus alkaliarsenatis AHT28^T was isolated from a composite of sediment samples collected from a series of six different soda lakes in the Kulunda Steppe, Altai, Russia (Sorokin *et al.* 2012). It is an obligately anaerobic, alkaliphilic, and moderately halotolerant strain with a respiratory metabolism involving the use of elemental sulfur, thiosulfate, or arsenate as electron acceptors. Pure extracts of *D. alkaliarsenatis* AHT28^T genomic DNA were obtained from the Leibniz Institute German Collection of Microorganisms and Cell Cultures (DSMZ, Braunschweig, Germany) and quantified using a Qubit fluorometer (Thermo Fisher Scientific, Waltham, MA, USA). Genome sequencing was performed using the MiSeq platform (Illumina, San Diego, CA, USA) with 250 bp paired-end reads.

A total of 7,186,040 reads were generated, providing about 536-fold median coverage of the genome. The reads were randomly subsampled to an approximate 85-fold coverage with seqtk version 1.0-r63 (https://github.com/lh3/seqtk). Sequence processing and *de novo* assembly

was performed using the A5-miseq pipeline (Coil *et al.* 2015). The assembly yielded 36 contigs, with maximum and N_{50} contig sizes of 689,966 bp and 235,557 bp, respectively. The genome size was 3,106,435 bp with a G+C content of 37.5%, slightly lower than the value of 39.1% previously obtained by the thermal denaturation method (Sorokin *et al.* 2012). The genome was annotated using the RAST server (Aziz *et al.* 2008), which identified 2,978 protein-coding sequences and 60 tRNA genes. A total of 1,392 coding sequences (47%) were assigned to subsystems. Genome completeness was assessed using AMPHORA2 (Wu and Scott 2012), which confirmed the presence of all 31 phylogenetic marker genes essential in prokaryotes.

The genome of *D. alkaliarsenatis* AHT28^T contained several features associated with an anaerobic respiratory metabolism involving the reduction of sulfur and arsenic compounds. Two operons were found to encode complex iron-sulfur molybdoenzymes (CISMs) related to polysulfide reductase (Psr) and thiosulfate reductase (Phs). Operons encoding a respiratory arsenate reductase (Arr) and a downstream arsenical resistance system (Ars) were also found. Interestingly, the genome encoded a nitrogenase (Nif), suggesting that *D. alkaliarsenatis* AHT28^T is capable of converting nitrogen (N_2) to ammonia (NH_3). This draft genome will enable further study of bacterial sulfur, arsenic, and nitrogen transformations under haloalkaliphilic conditions.

Nucleotide sequence accession number(s)

This whole-genome shotgun project has been deposited at DDBJ/ENA/GenBank under the accession MIJE00000000. The version described in this paper is the first version, MIJE01000000.

ACKNOWLEDGEMENTS

DNA library preparation and Illumina sequencing was performed at the Georgia Genomics Facility at the University of Georgia (Athens, GA, USA). We thank Christian Edwardson, Roger Nilsen, Katherine Sandlin, and Cathrin Spröer for technical assistance. This work was supported by an award (EAR-0952271) to JTH and a Graduate Research Fellowship (DGE-0903734) to CAA from the National Science Foundation. Additional funding was provided by a Minority Ph.D. Program Scholarship to CAA from the Alfred P. Sloan Foundation.

REFERENCES

Aziz R, Bartels D, Best A, DeJongh M, Disz T, Edwards R *et al.* (2008). The RAST Server: rapid annotations using subsystems technology. *BMC Genomics* **9:** 75.

Coil D, Jospin G, Darling AE (2015). A5-miseq: an updated pipeline to assemble microbial genomes from Illumina MiSeq data. *Bioinformatics* **31:** 587-589.

Messina E, Sorokin DY, Kublanov IV, Toshchakov S, Lopatina A, Arcadi E *et al.* (2016). Complete genome sequence of '*Halanaeroarchaeum sulfurireducens*' M27-SA2, a sulfur-reducing and acetate-oxidizing haloarchaeon from the deep-sea hypersaline anoxic lake Medee. *Stand Genomic Sci* **11:** 1-15.

Oremland RS, Kulp TR, Blum JS, Hoeft SE, Baesman S, Miller LG *et al.* (2005). A microbial arsenic cycle in a salt-saturated, extreme environment. *Science* **308:** 1305-1308.

Sorokin DY, Banciu HL, Muyzer G (2015). Functional microbiology of soda lakes. *Curr Opin Microbiol* **25:** 88-96.

Sorokin DY, Kublanov IV, Yakimov MM, Rijpstra WIC, Sinninghe Damsté JS (2016). *Halanaeroarchaeum sulfurireducens* gen. nov., sp. nov., the first obligately anaerobic sulfur-respiring haloarchaeon, isolated from a hypersaline lake. *Int J Syst Evol Microbiol* **66:** 2377-2381.

Sorokin DY, Rusanov II, Pimenov NV, Tourova TP, Abbas B, Muyzer G (2010). Sulfidogenesis under extremely haloalkaline conditions in soda lakes of Kulunda Steppe (Altai, Russia). *FEMS Microbiol Ecol* **73:** 278-290.

Sorokin DY, Tourova TP, Sukhacheva MV, Muyzer G (2012). *Desulfuribacillus alkaliarsenatis* gen. nov. sp. nov., a deep-lineage, obligately anaerobic, dissimilatory sulfur and arsenate-reducing, haloalkaliphilic representative of the order *Bacillales* from soda lakes. *Extremophiles* **16:** 597-605.

Switzer Blum J, Han S, Lanoil B, Saltikov C, Witte B, Tabita FR *et al.* (2009). Ecophysiology of "*Halarsenatibacter silvermanii*" strain SLAS-1^T, gen. nov., sp. nov., a facultative chemoautotrophic arsenate respirer from salt-saturated Searles Lake, California. *Appl Environ Microbiol* **75:** 1950-1960.

Wu M, Scott AJ (2012). Phylogenomic analysis of bacterial and archaeal sequences with AMPHORA2. *Bioinformatics* **28:** 1033-1034.

APPENDIX B

SUPPLEMENTARY CHAPTER 2: DRAFT GENOME FOR THE TYPE STRAIN *VULCANIBACILLUS MODESTICALDUS* BR, A STRICTLY ANAEROBIC, MODERATELY THERMOPHILIC, AND NITRATE-REDUCING BACTERIUM ISOLATED FROM DEEP-SEA HYDROTHERMAL VENTS OF THE MID-ATLANTIC RIDGE[5]

[5]Abin C.A. and J.T. Hollibaugh. 2016. *Genome Announc*. 4(6): e01246-16. Reprinted here with permission of publisher.

ABSTRACT

Vulcanibacillus modesticaldus BR^T was isolated from calcite-rich, metalliferous core samples collected at the Rainbow deep-sea hydrothermal vent field on the Mid-Atlantic Ridge. Here, we report the 2.2 Mbp draft genome sequence for this strain, consisting of 100 contigs with a G+C content of 33.6% and 2,227 protein-coding sequences.

Vulcanibacillus modesticaldus BR^T was isolated from core samples collected at the Rainbow hydrothermal vent field on the Mid-Atlantic Ridge (MAR) (36° 14' N, 33° 54' W) (L'Haridon *et al.* 2006). The Rainbow vent field is located at a depth of ~2,300 meters on the western flank of a non-volcanic ridge of the MAR southwest of the Azores Archipelago (Fouquet *et al.* 1997). Active chimneys emit acidic (pH 2.8), high temperature (365°C) fluids enriched in H_2, CO_2, CO, CH_4, metals, and rare earth elements (Charlou *et al.* 2002, Douville *et al.* 2002). *V. modesticaldus* BR^T was able to grow at temperatures from 37 – 60° C, pH values of 6.0 – 8.5, and salinities of 1 – 4%. The strain grew chemoheterotrophically with organic acids, carbohydrates, and complex proteinaceous substrates as electron donors with nitrate as the sole electron acceptor. Nitrite produced from dissimilatory nitrate reduction was not reduced further to ammonium or to N_2, indicating that the strain was unable to perform dissimilatory nitrate reduction to ammonium (DNRA) or denitrification (L'Haridon *et al.* 2006).

Pure genomic DNA from *V. modesticaldus* BR^T was obtained from the Leibniz Institute German Collection of Microorganisms and Cell Cultures (DSMZ, Braunschweig, Germany) and quantified using a Qubit fluorometer (Thermo Fisher Scientific, Waltham, MA, USA). Genome sequencing was performed using the Illumina MiSeq platform with 250 bp paired-end reads. A total of 2,728,778 reads were generated, providing about 287-fold median coverage of the genome. The sequence processing toolkit seqtk version 1.0-r63 (https://github.com/lh3/seqtk) was used to randomly subsample the reads to an approximate 85-fold median coverage. Adapter removal, quality trimming, error correction, and *de novo* assembly was performed using the A5-miseq pipeline (Coil *et al.* 2015). The assembly yielded 100 contigs with a total genome size of 2,224,341 bp. The maximum and N_{50} contig sizes were 161,986 bp and 50,162 bp, respectively. The G+C content was 33.6%, a value slightly lower than the 34.5% previously obtained by

reversed-phase HPLC (L'Haridon *et al.* 2006). Genome annotation was performed by the Rapid Annotations using Subsystems Technology (RAST) server (Aziz *et al.* 2008). A total of 2,227 protein-coding sequences and 64 tRNA genes were predicted. Fifty-two percent (1,156) of the coding sequences were assigned to subsystems. Phylogenomic analysis by AMPHORA2 (Wu and Scott 2012) was used to estimate genome completeness. All 31 phylogenetic marker genes essential in bacteria were found to be present in the draft genome.

The genome of *V. modesticaldus* BR^T encodes multiple pathways involved in the metabolism of carbohydrates and organic acids. The full assortment of genes required for glycolysis and the tricarboxylic acid cycle is present, which is consistent with the ability of the strain to grow using acetate, pyruvate, and several mono- and polysaccharides as electron donors. The genome also contains an operon encoding a membrane-bound dissimilatory nitrate reductase (Nar) as well as two nitrate/nitrite transporters. The knowledge obtained from this draft genome will help shed light on the evolution and physiology of moderately thermophilic bacteria inhabiting deep sea hydrothermal vent ecosystems.

Nucleotide sequence accession number(s)

This whole-genome shotgun project has been deposited at DDBJ/ENA/GenBank under the accession MIJF00000000. The version described in this paper is the first version, MIJF01000000.

ACKNOWLEDGEMENTS

Library preparation and sequencing was performed at the Georgia Genomics Facility at the University of Georgia (Athens, GA, USA). We thank Christian Edwardson, Roger Nilsen, Katherine Sandlin, and Cathrin Spröer for technical assistance. This work was supported by a grant (EAR-0952271) to JTH and a Graduate Research Fellowship (DGE-0903734) to CAA from the National Science Foundation. Additional funding was provided by a Minority Ph.D. Program Scholarship to CAA from the Alfred P. Sloan Foundation.

REFERENCES

Aziz R, Bartels D, Best A, DeJongh M, Disz T, Edwards R *et al.* (2008). The RAST Server: rapid annotations using subsystems technology. *BMC Genomics* **9:** 75.

Charlou JL, Donval JP, Fouquet Y, Jean-Baptiste P, Holm N (2002). Geochemistry of high H_2 and CH_4 vent fluids issuing from ultramafic rocks at the Rainbow hydrothermal field (36°14′N, MAR). *Chem Geol* **191:** 345-359.

Coil D, Jospin G, Darling AE (2015). A5-miseq: an updated pipeline to assemble microbial genomes from Illumina MiSeq data. *Bioinformatics* **31:** 587-589.

Douville E, Charlou JL, Oelkers EH, Bienvenu P, Jove Colon CF, Donval JP *et al.* (2002). The rainbow vent fluids (36°14′N, MAR): the influence of ultramafic rocks and phase separation on trace metal content in Mid-Atlantic Ridge hydrothermal fluids. *Chem Geol* **184:** 37-48.

Fouquet Y, Charlou JL, Ondreas H, Radford-Knoery J, Donval JP, Douville E *et al.* (1997). Discovery and first submersible investigations on the Rainbow hydrothermal field on the MAR (36 14′ N). *Eos Trans AGU* **78:** F832.

L'Haridon S, Miroshnichenko ML, Kostrikina NA, Tindall BJ, Spring S, Schumann P *et al.* (2006). *Vulcanibacillus modesticaldus* gen. nov., sp. nov., a strictly anaerobic, nitrate-reducing bacterium from deep-sea hydrothermal vents. *Int J Syst Evol Microbiol* **56:** 1047-1053.

Wu M, Scott AJ (2012). Phylogenomic analysis of bacterial and archaeal sequences with AMPHORA2. *Bioinformatics* **28:** 1033-1034.

APPENDIX C

SUPPORTING INFORMATION FOR CHAPTER 2

Table 2.S1. Concentrations of selected metal(loid)s in subsurface (5 – 10 cm depth) sediments receiving hydrological inputs from the NBWS and comparison to mean abundance in the upper continental crust.

Element	Concentration (ppm)	
	NBWS-1 Sediments[a]	**Upper Continental Crust**[b]
As	38.91 ± 0.52	2.00
Zn	9.71 ± 0.95	52.0
Cu	7.24 ± 4.49	14.3
Ni	2.58 ± 0.12	18.6
Mo	1.86 ± 0.12	1.40
Cr	1.36 ± 0.03	35.0
Pb	0.85 ± 0.11	17.0
Sb	0.77 ± 0.05	0.31
Co	0.67 ± 0.09	11.6
Se	0.24 ± 0.05	0.083
Te	0.09 ± 0.03	0.027[c]
Cd	0.09 ± 0.01	0.102

[a]Average ± SD for three replicate samples.
[b]Data from Wedepohl (1995).
[c]Value from Hu and Gao (2008).

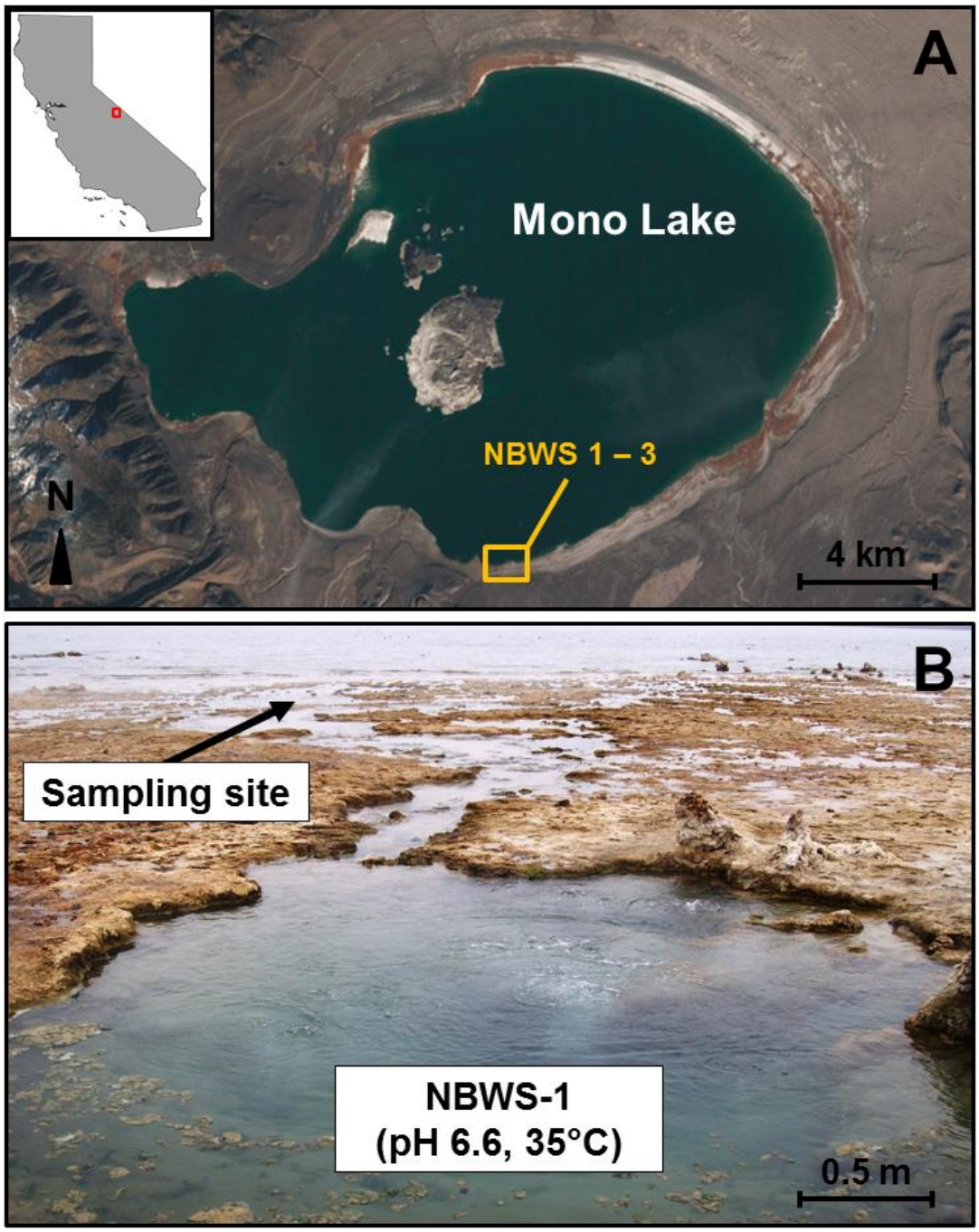

Figure 2.S1. Location of the sampling site within the Mono Basin in California. **(A)** Satellite image of Mono Lake indicating the location of the NBWS along the southern shore of Mono Lake. The inset shows the location of Mono Lake (red square) within the state of California. Image courtesy of the NASA Earth Observatory. **(B)** View of NBWS-1 (37°56'28.7" N, -119°1'22.4" W) and the site of sample collection. Photograph courtesy of Matthew Lee High.

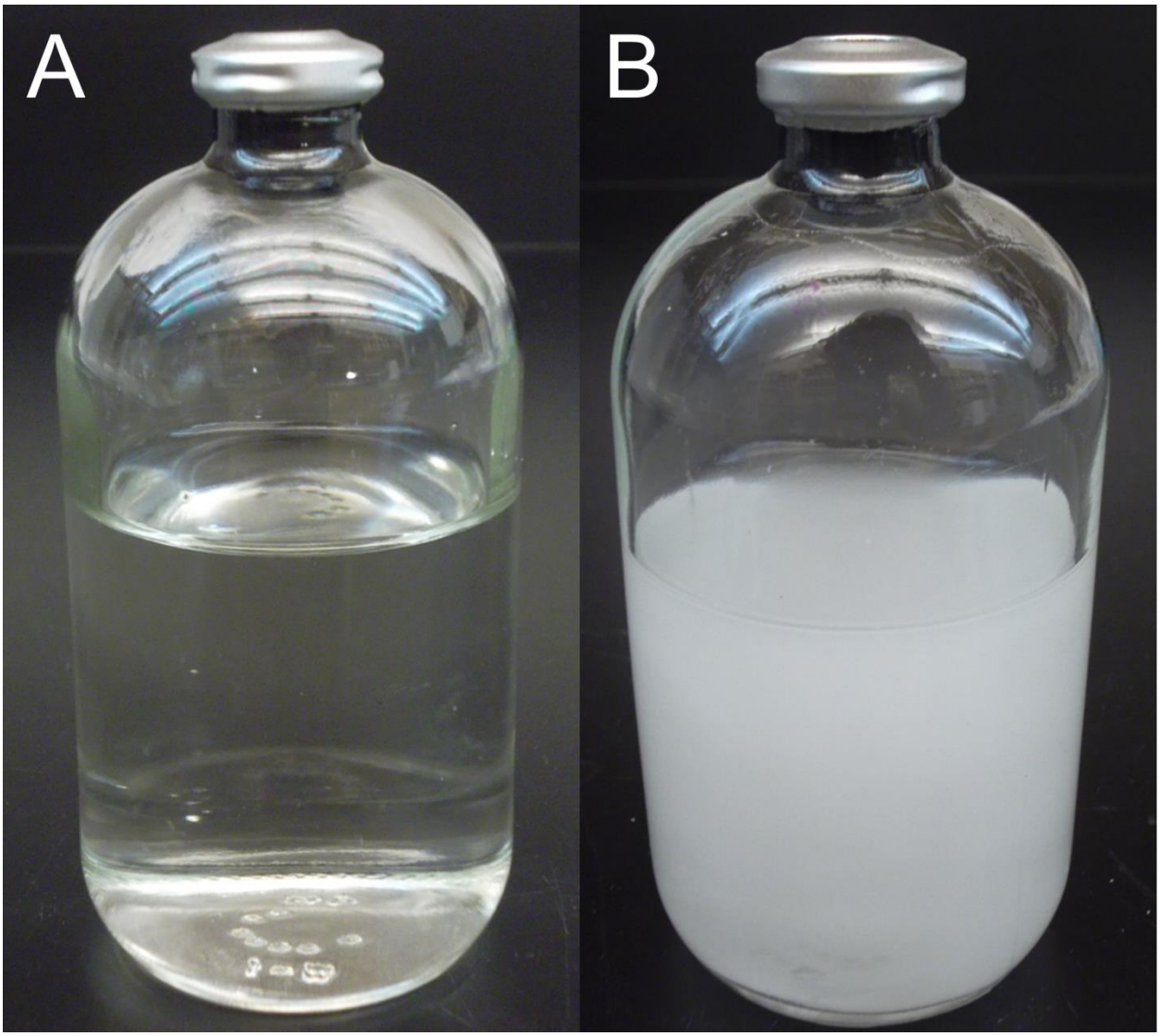

Figure 2.S2. Precipitation of a white, crystalline compound following growth of strain MLFW-2 on Sb(V). Photographs show the appearance of the medium **(A)** before and **(B)** after growth.

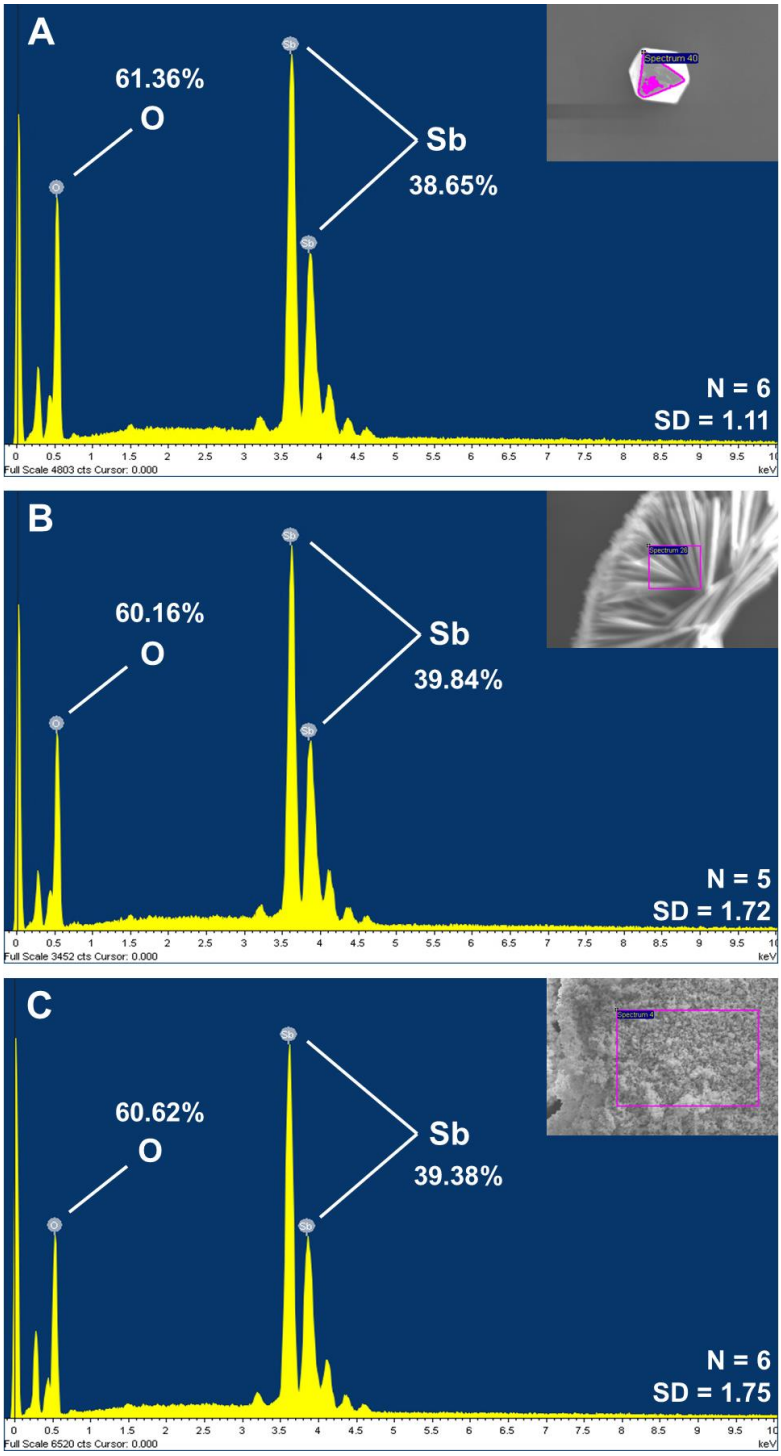

Figure 2.S3. EDS spectra of the **(A)** octahedral and **(B)** bowtie-shaped microcrystals produced by strain MLFW-2 during dissimilatory Sb(V) reduction. **(C)** EDS spectrum of >99.9% powdered Sb_2O_3. The insets show the specific areas analyzed. "N" refers to the total number of random fields or individual microcrystals analyzed, while "SD" corresponds to the standard deviation associated with the average atomic percentages obtained for Sb and O in each case.

APPENDIX D

SUPPORTING INFORMATION FOR CHAPTER 3

Table 3.S1. Liquid media used for the cultivation of strain MLFW-2^T.

Component	Amount per Liter of Medium				
	BSM-1	**BSM-2**	**BSM-3**	**BSM-4**	**BSM-5**
NaCl	—	Variable	Variable[c]	Variable[c]	3.62 g
$NaHCO_3$	—	—	—	Variable[d]	4.20 g
Na_2CO_3	—	—	—	Variable[d]	—
K_2CO_3 x $1.5H_2O$	0.240 g	—	—	—	—
NaH_2PO_4	—	—	Variable[e]	—	—
Na_2HPO_4	—	—	Variable[e]	—	—
KH_2PO_4	0.100 g	0.100 g	—	—	—
K_2HPO_4	0.150 g	0.150 g	—	0.262 g	0.262 g
NH_4Cl	0.075 g	—	0.075 g	0.075 g	0.075 g
NH_4HCO_3	—	0.115 g	—	—	—
Na_2SO_4	—	—	0.050 g	0.050 g	0.050 g
Na_2HAsO_4 x $7H_2O$	—	—	—	—	1.560 g
KH_2AsO_4	—	0.901 g	0.901 g	0.901 g	—
Sodium L-lactate	—	0.560 g	1.120 g	1.120 g	1.120 g
Yeast extract	—	—	0.200 g	0.200 g	0.200 g
Vitamin solution[a]	10 mL	10 mL	10 mL	10 mL	10 mL
Trace minerals solution[b]	1 mL	1 mL	1 mL	1 mL	1 mL
500 mM Na_2S solution	0.2 mL	0.2 mL	0.2 mL	0.2 mL	0.2 mL
Final pH	7.0 – 7.5	7.0 – 7.5	7.0 – 8.0	8.25 – 10.0	8.2 – 8.5

[a]Oremland *et al.* (1994).
[b]Trace element solution SL-10 of Widdel *et al.* (1983) modified by addition of 14 mM $MgCl_2$ and 700 μM $CaCl_2$.
[c]Final amount varied to achieve $[Na^+]_{tot}$ = 125 mM.
[d]$[HCO_3^-] + [CO_3^{2-}]$ = 50 mM.
[e]$[H_2PO_4^-] + [HPO_4^{2-}]$ = 50 mM.

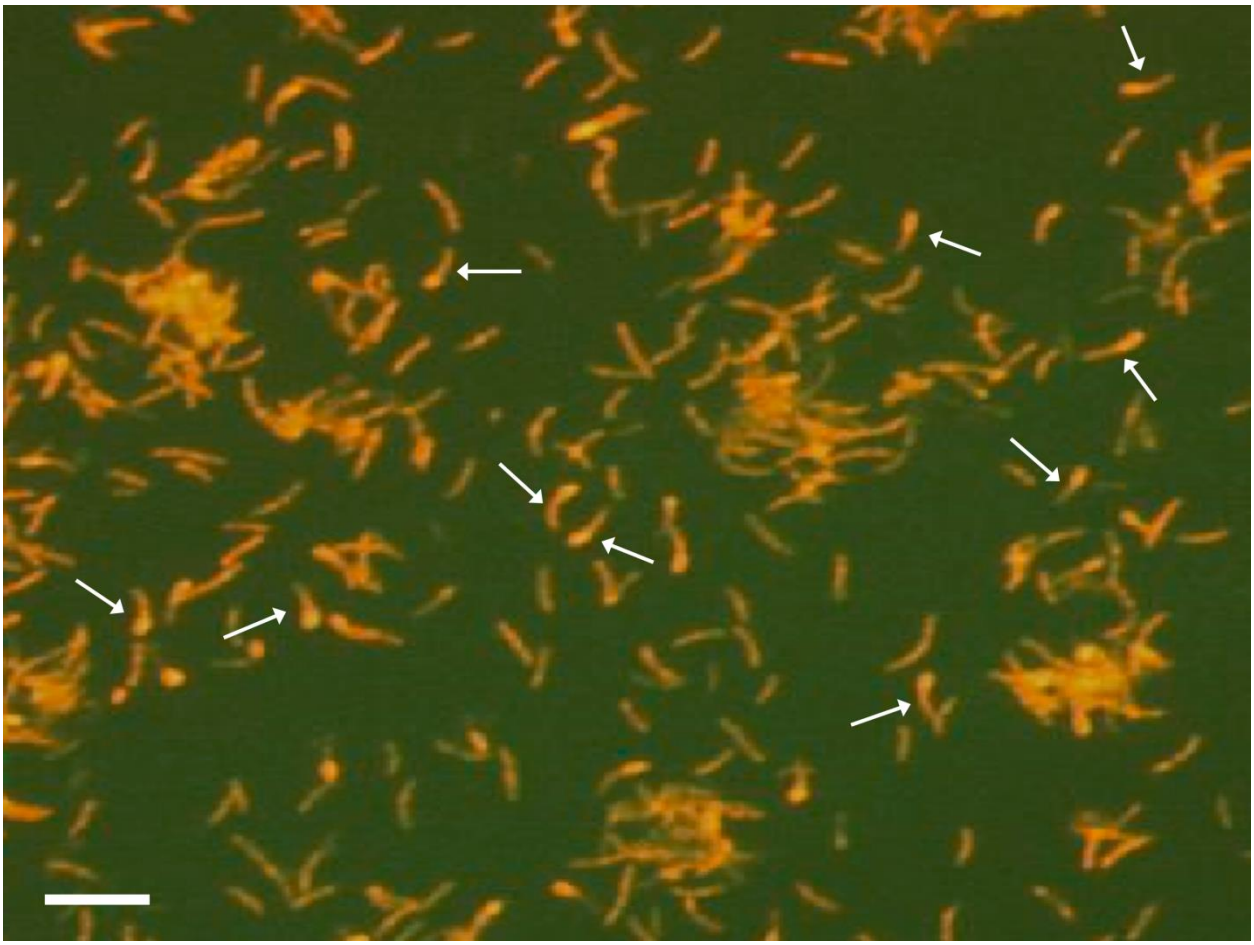

Figure 3.S1. Epifluorescence micrograph of stationary phase cells of strain MLFW-2^T stained with acridine orange. Sporulating cells are indicated with arrows. Scale bar, 5 μm.

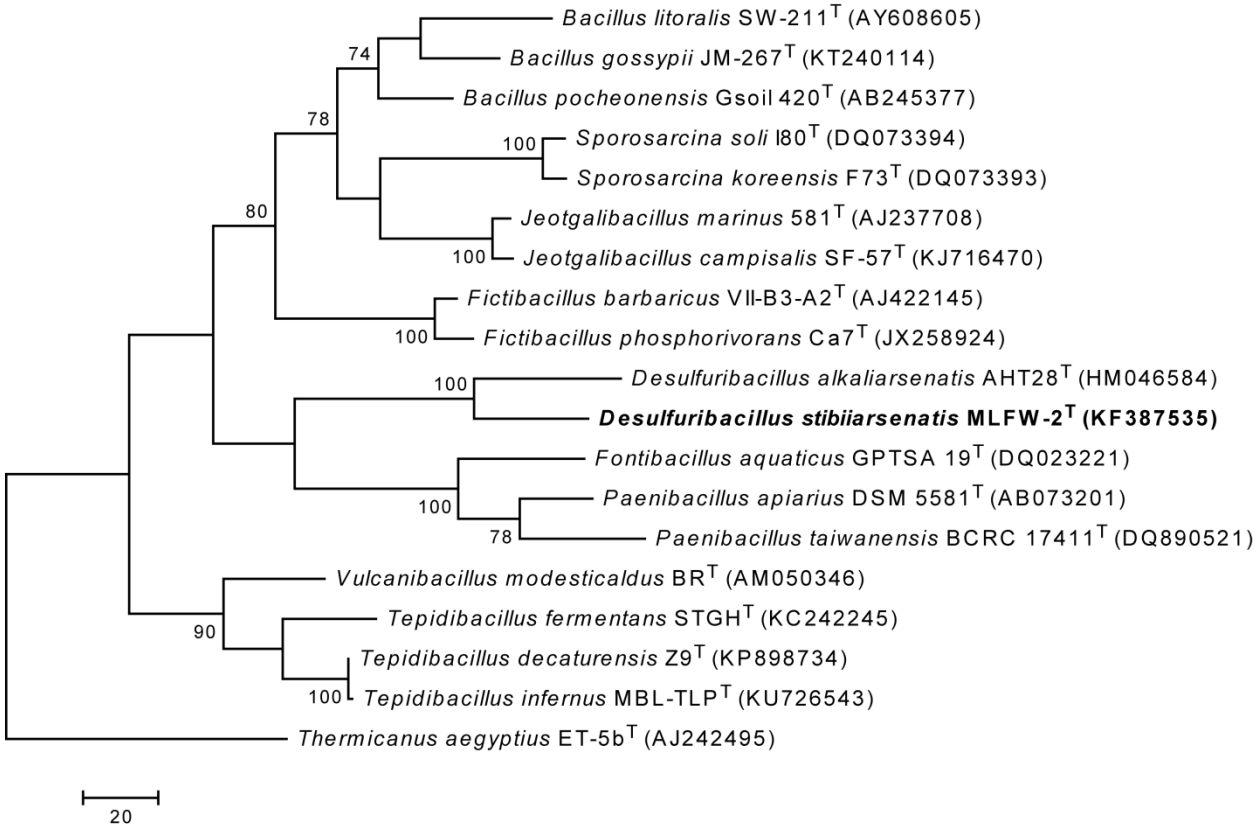

Figure 3.S2. Maximum-parsimony phylogenetic tree based on partial 16S rRNA gene sequences showing the relationship between strain MLFW-2^T and the most closely related type strains of the *Bacillales*. Bootstrap values are expressed as percentages of 1,000 replications; only values ≥70% are shown at branch nodes. *Thermicanus aegyptius* ET-5b^T was used as an outgroup. GenBank accession numbers are provided in parentheses. Scale bar, 20 substitutions.

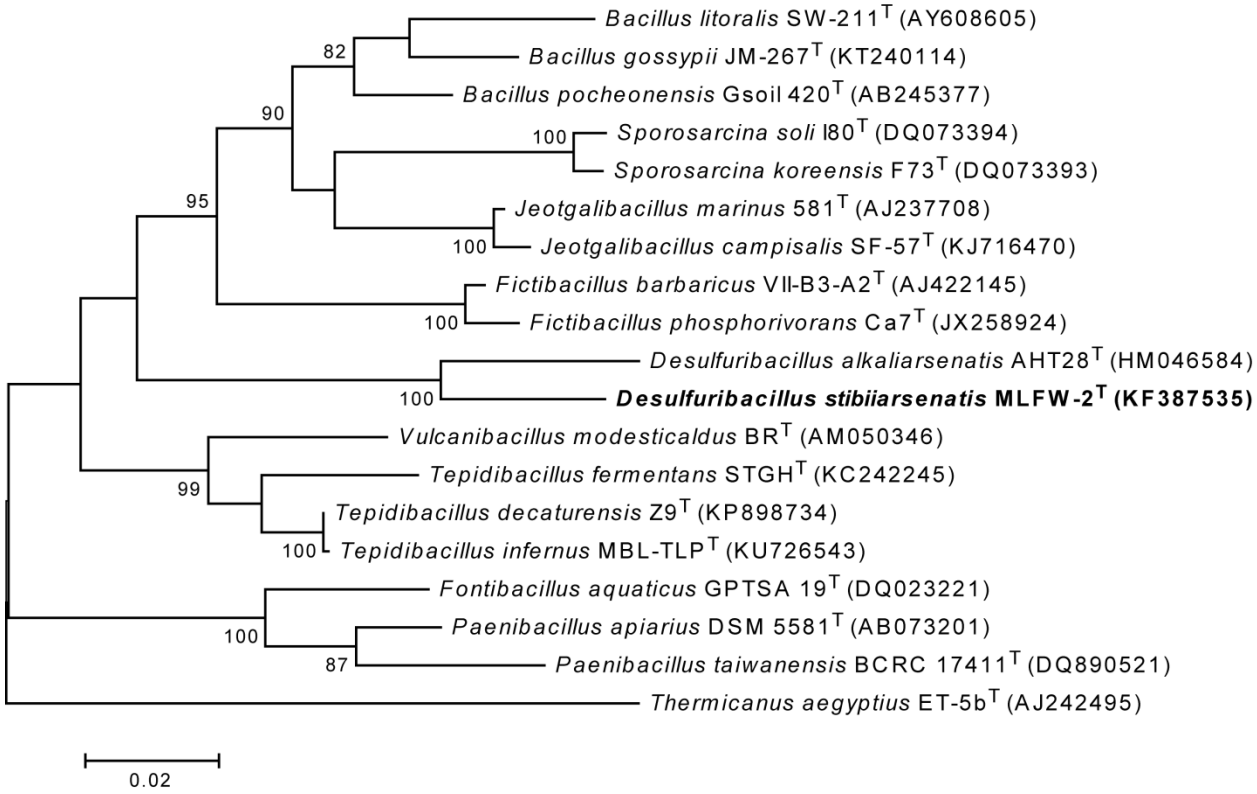

Figure 3.S3. Maximum-likelihood phylogenetic tree based on partial 16S rRNA gene sequences showing the relationship between strain MLFW-2^T and the most closely related type strains of the *Bacillales*. Bootstrap values are expressed as percentages of 1,000 replications; only values ≥70% are shown at branch nodes. *Thermicanus aegyptius* ET-5b^T was used as an outgroup. GenBank accession numbers are provided in parentheses. Scale bar, 0.02 substitutions per nucleotide position.

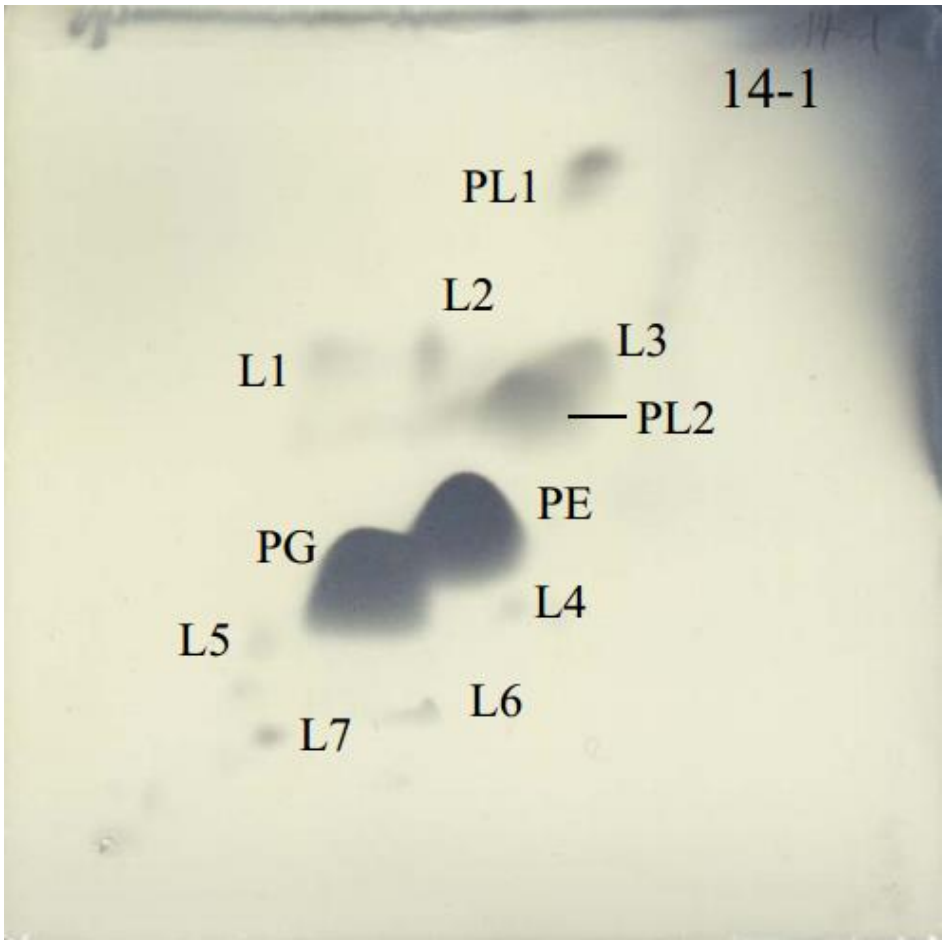

Figure 3.S4. Two-dimensional thin-layer chromatogram of polar lipids from strain MLFW-2^{T}. PG, phosphatidylglycerol; PE, phosphatidylethanolamine; PL, unknown phospholipid; L, unknown polar lipid.

APPENDIX E

SUPPORTING INFORMATION FOR CHAPTER 4

Table 4.S1. List of oligonucleotide primers used for RT-qPCR in this study.

Target	Sequence (5'– 3')	Position	Tm (°C)	Amplicon Length (bp)	Amplification Efficiency (%)
BHU72_01065	F: TACAACTCAGGCTATTGGTTCG	528 – 549	54.6	168	94.8
	R: ATAAACGGCATACTATGGACGG	674 – 695	54.5		
BHU72_01090	F: GCATGGTGCTCGGTTCATTC	676 – 695	56.9	103	95.1
	R: CCTTTGATGCTGTTGCCGTC	759 – 778	57.1		
BHU72_03635	F: GAAACCCCGGCACAATCTCAACC	88 – 110	60.7	167	94.7
	R: TTTACCGTGTTGTCAGGATCGCC	232 – 254	59.5		
BHU72_03930	F: AACACCACAGAAGCCCATCC	1,189 – 1,208	57.7	138	94.9
	R: ACCAGGCTTTAACGCGATCC	1,307 – 1,326	57.8		
BHU72_04760	F: GGACTCCGTACTCTGGGTAGA	402 – 422	57.2	156	92.8
	R: GCTAAAGAATCGCCGACCATCT	536 – 557	57.2		
BHU72_06270	F: ACTATAAGGCTTGCCGTCGC	2,213 – 2,232	57.6	184	93.5
	R: TCACCATTCCACCAGATTGACG	2,375 – 2,396	57.2		
BHU72_07145	F: CCGAAACCTGAAGGCTGATAAGG	2,082 – 2,104	57.7	150	93.2
	R: CCGATTTCCTTTAATCCCGGTGG	2,209 – 2,231	58.0		
BHU72_07340	F: TTGTCCGCTGTTAAATGGTCACA	610 – 632	57.1	177	92.4
	R: AATTACATGGGCCATAGCAAGGG	764 – 786	57.5		
BHU72_07355	F: GGAATCCGTCCAGGTGTAATAGG	2,908 – 2,930	56.8	166	93.0
	R: GAGTTCCGTTCAGATGCTCATCC	3,051 – 3,073	57.6		
BHU72_07375	F: AGATGCATGTCAGCTAGGATGG	744 – 765	56.7	148	97.6
	R: ACCTATTAACCCAGGCTTTCCG	870 – 891	56.9		
BHU72_07925	F: CACCGCTCAAAAGAATCGGGA	191 – 211	57.7	154	93.1
	R: CCCATTGTGCCAGCGTAACTAA	323 – 344	57.7		
BHU72_09285	F: AGCATCAGTCACAGTTGGCAC	57 – 77	57.9	170	93.6
	R: GATTTCCTTTCGCTCTCCACAC	205 – 226	56.0		
BHU72_10220	F: GGATTCGACCAGGAACTATTGC	2,420 – 2,441	55.7	179	94.3
	R: TACTCTAGTTACCCCACCATGACG	2,575 – 2,598	57.5		
BHU72_10330	F: GTTCGTAGGTGACTTCAAGGATGG	885 – 908	57.2	198	92.4
	R: CCCATTTCAGTAGCTACACGAACG	1,059 – 1,082	57.6		
BHU72_12715 (*gyrB*)	F: TTGAAGAGAACCCAAGCACAGC	1,088 – 1,109	57.9	148	95.7
	R: CAATCCGCTAACTTACCAGGCAG	1,213 – 1,235	57.8		

Table 4.S2. Relative fold changes in transcription of DMSOR family genes during exponential growth of MLFW-2^{T} on different terminal electron acceptors.

Locus Tag	Electron Acceptor	Relative Transcription (Fold Change)[a,b]				
		vs. Nitrite	vs. Nitrate	vs. Se(VI)	vs. As(V)	vs. Sb(V)
BHU72_01065	Nitrite	—	-1.1	1.2	-1.1	-1.4
	Nitrate	1.1	—	1.3	1.0	-1.3
	Se(VI)	-1.2	-1.3	—	-1.3	-1.7*
	As(V)	1.1	1.0	1.3	—	-1.2
	Sb(V)	1.4	1.3	1.7*	1.2	—
BHU72_01090	Nitrite	—	1.1	**3.0*****	2.0	**3.0****
	Nitrate	-1.1	—	**2.7****	1.8	**2.7****
	Se(VI)	**-3.0*****	**-2.7****	—	-1.5	1.0
	As(V)	-2.0	-1.8	1.5	—	1.5
	Sb(V)	**-3.0****	**-2.7****	1.0	-1.5	—
BHU72_03635	Nitrite	—	**-6.3*****	**26.9*****	**13.3*****	**81.5*****
	Nitrate	**6.3*****	—	**169.5*****	**83.6*****	**514.2*****
	Se(VI)	**-26.9*****	**-169.5*****	—	-2.0	**3.0****
	As(V)	**-13.3*****	**-83.6*****	2.0	—	**6.1****
	Sb(V)	**-81.5*****	**-514.2*****	**-3.0****	**-6.1****	—
BHU72_03930	Nitrite	—	-1.5	-1.5*	-1.4	**-3.3*****
	Nitrate	1.5	—	-1.1	1.0	**-2.2***
	Se(VI)	1.5*	1.1	—	1.1	**-2.1****
	As(V)	1.4	1.0	-1.1	—	**-2.3***
	Sb(V)	**3.3*****	**2.2***	**2.1****	**2.3***	—

Locus Tag	Electron Acceptor	Relative Transcription (Fold Change)[a,b]				
		vs. Nitrite	vs. Nitrate	vs. Se(VI)	vs. As(V)	vs. Sb(V)
BHU72_04760	Nitrite	—	**-2.6***	**23.4****	**72.9*****	**168.0*****
	Nitrate	**2.6***	—	**60.4*****	**188.2*****	**433.6*****
	Se(VI)	**-23.4****	**-60.4*****	—	3.1	**7.2***
	As(V)	**-72.9*****	**-188.2*****	-3.1	—	2.3
	Sb(V)	**-168.0*****	**-433.6*****	**-7.2***	-2.3	—
BHU72_06270	Nitrite	—	-1.3	-1.4	-1.4	**8.4*****
	Nitrate	1.3	—	1.0	1.0	**11.4*****
	Se(VI)	1.4	1.0	—	1.0	**11.7*****
	As(V)	1.4	1.0	1.0	—	**11.7*****
	Sb(V)	**-8.4*****	**-11.4*****	**-11.7*****	**-11.7*****	—
BHU72_07145	Nitrite	—	-1.4	-1.7*	**-3.1****	**-1,083.1*****
	Nitrate	1.4	—	-1.2	**-2.2***	**-785.6*****
	Se(VI)	1.7*	1.2	—	-1.8*	**-633.3*****
	As(V)	**3.1****	**2.2***	1.8*	—	**-349.7*****
	Sb(V)	**1,083.1*****	**785.6*****	**633.3*****	**349.7*****	—
BHU72_07340	Nitrite	—	1.1	-1.3	-1.2	-1.2
	Nitrate	-1.1	—	-1.4	-1.3	-1.2
	Se(VI)	1.3	1.4	—	1.1	1.1
	As(V)	1.2	1.3	-1.1	—	1.0
	Sb(V)	1.2	1.2	-1.1	1.0	—

Locus Tag	Electron Acceptor	Relative Transcription (Fold Change)[a,b]				
		vs. Nitrite	vs. Nitrate	vs. Se(VI)	vs. As(V)	vs. Sb(V)
BHU72_07355	Nitrite	—	-1.6	**-329.4*****	-1.5	**-39.2*****
	Nitrate	1.6	—	**-210.7*****	1.0	**-25.1*****
	Se(VI)	**329.4*****	**210.7*****	—	**216.2*****	**8.4*****
	As(V)	1.5	1.0	**-216.2*****	—	**-25.7*****
	Sb(V)	**39.2*****	**25.1*****	**-8.4*****	**25.7*****	—
BHU72_07375	Nitrite	—	-1.4	**-121.5*****	1.4	**-3.5****
	Nitrate	1.4	—	**-83.8*****	2.0	**-2.4***
	Se(VI)	**121.5*****	**83.8*****	—	**166.8*****	**35.0*****
	As(V)	-1.4	-2.0	**-166.8*****	—	**-4.8*****
	Sb(V)	**3.5****	**2.4***	**-35.0*****	**4.8*****	—
BHU72_07925	Nitrite	—	-1.2	1.0	-1.2	-1.1
	Nitrate	1.2	—	1.3	1.0	1.1
	Se(VI)	1.0	-1.3	—	-1.2	-1.1
	As(V)	1.2	1.0	1.2	—	1.1
	Sb(V)	1.1	-1.1	1.1	-1.1	—
BHU72_09285	Nitrite	—	**3.6***	**12.9*****	**12.7*****	**20.1*****
	Nitrate	**-3.6***	—	**3.6****	**3.5***	**5.5*****
	Se(VI)	**-12.9*****	**-3.6****	—	1.0	1.6*
	As(V)	**-12.7*****	**-3.5***	1.0	—	1.6
	Sb(V)	**-20.1*****	**-5.5*****	-1.6*	-1.6	—

Locus Tag	Electron Acceptor	Relative Transcription (Fold Change)[a,b]				
		vs. Nitrite	vs. Nitrate	vs. Se(VI)	vs. As(V)	vs. Sb(V)
BHU72_10220	Nitrite	—	**2.1***	**2.2****	1.4	1.3
	Nitrate	**-2.1***	—	1.1	-1.5	-1.5*
	Se(VI)	**-2.2****	-1.1	—	-1.6*	-1.7**
	As(V)	-1.4	1.5	1.6*	—	1.0
	Sb(V)	-1.3	1.5*	1.7**	1.0	—
BHU72_10330	Nitrite	—	-1.5	**-2.6***	**-93.7*****	-2.2
	Nitrate	1.5	—	-1.7*	**-61.4*****	-1.4
	Se(VI)	**2.6***	1.7*	—	**-35.9*****	1.2
	As(V)	**93.7*****	**61.4*****	**35.9*****	—	**42.4*****
	Sb(V)	2.2	1.4	-1.2	**-42.4*****	—

[a]Average fold change in mRNA transcript abundance relative to *gyrB*. Postive values indicate upregulation while negative values indicate downregulation. Negative values were calculated by taking the negative reciprocal of the decimal fold change.
[b]Statistically significant changes in relative transcription (i.e. |fold change| ≥ 2 and $p \leq 0.05$) are indicated in bold.
*Indicates a statistically significant difference in relative transcription, with $0.01 \leq p \leq 0.05$.
**Indicates a statistically significant difference in relative transcription, with $0.001 \leq p < 0.01$.
***Indicates a statistically significant difference in relative transcription, with $p < 0.001$.

Table 4.S3. Relative fold changes in transcription of DMSOR family genes during exponential growth of MLFW-2^T on As(V) in control experiments.

Locus Tag	Control Experiment[a]	Relative Transcription (Fold change)[b]		
		vs. #1	vs. #2	vs. #3
BHU72_01065	#1	—	1.1	-1.2
	#2	-1.1	—	-1.4
	#3	1.2	1.4	—
BHU72_01090	#1	—	1.1	1.6
	#2	-1.1	—	1.5
	#3	-1.6	-1.5	—
BHU72_03635	#1	—	1.2	1.0
	#2	-1.2	—	-1.2
	#3	1.0	1.2	—
BHU72_03930	#1	—	-1.2	-1.3
	#2	1.2	—	-1.1
	#3	1.3	1.1	—
BHU72_04760	#1	—	-1.1	1.3
	#2	1.1	—	1.4
	#3	-1.3	-1.4	—
BHU72_06270	#1	—	-1.1	-1.3
	#2	1.1	—	-1.2
	#3	1.3	1.2	—

Locus Tag	Control Experiment[a]	Relative Transcription (Fold change)[b]		
		vs. #1	vs. #2	vs. #3
BHU72_07145	#1	—	1.3	1.5
	#2	-1.3	—	1.2
	#3	-1.5	-1.2	—
BHU72_07340	#1	—	1.1	1.2
	#2	-1.1	—	1.1
	#3	-1.2	-1.1	—
BHU72_07355	#1	—	1.3	1.1
	#2	-1.3	—	-1.2
	#3	-1.1	1.2	—
BHU72_07375	#1	—	-1.1	-1.4
	#2	1.1	—	-1.2
	#3	1.4	1.2	—
BHU72_07925	#1	—	-1.3	-1.2
	#2	1.3	—	1.1
	#3	1.2	-1.1	—
BHU72_09285	#1	—	-1.2	-1.2
	#2	1.2	—	1.0
	#3	1.2	1.0	—
BHU72_10220	#1	—	-1.1	-1.1
	#2	1.1	—	1.0
	#3	1.1	1.0	—

Locus Tag	Control Experiment[a]	Relative Transcription (Fold change)[b]		
		vs. #1	vs. #2	vs. #3
BHU72_10330	#1	—	1.2	1.3
	#2	-1.2	—	1.1
	#3	-1.3	-1.1	—

[a]The control experiments were as follows: Control experiment #1, 5 mM As(V) + 5 mM lactate in MS-NSeAs medium; Control experiment #2, 5 mM As(V) + 15 mM lactate in MS-NSeAs medium; Control experiment #3, 5 mM As(V) + 5 mM lactate in MS-Sb medium with an inoculum of washed cells.

[b]Average fold change in mRNA transcript abundance relative to *gyrB*. Postive values indicate upregulation while negative values indicate downregulation. Negative values were calculated by taking the negative reciprocal of the decimal fold change.

Table 4.S4. Summary data characterizing the transcriptomes analyzed in this study.

Sample[a]	Number of Raw Reads	Number of Quality Reads	Average Quality Read Length (bases)	Number of Quality Reads that Mapped[b]	Percentage of Quality Reads that Mapped[b]
As(V) #1	2,866,448	2,381,778	73.3 ± 5.7	1,990,744	83.6
As(V) #2	2,463,950	2,063,233	73.5 ± 5.5	1,667,137	80.8
As(V) #3	2,441,236	2,128,634	73.9 ± 5.0	1,761,282	82.7
As(V) #4	2,763,577	2,496,739	74.2 ± 4.5	2,220,334	88.9
As(V) #5	1,643,140	1,492,594	74.2 ± 4.5	1,332,486	89.3
As(V) #6	2,125,700	1,906,512	74.1 ± 4.6	1,693,073	88.8
Sb(V) #1	2,429,610	2,185,492	74.2 ± 4.5	1,924,609	88.1
Sb(V) #2	2,122,769	1,872,090	74.2 ± 4.5	1,623,336	86.7
Sb(V) #3	2,263,764	2,035,104	74.2 ± 4.4	1,812,821	89.1
Sb(V) #4	2,737,912	2,396,785	74.0 ± 4.8	2,104,161	87.8
Sb(V) #5	2,661,280	2,285,597	73.9 ± 4.9	2,070,831	90.6
Sb(V) #6	2,805,715	2,510,147	74.2 ± 4.6	2,149,011	85.6

[a]Samples 1,2, and 3 were collected during the early log phase of growth; Samples 4,5, and 6 were collected during the late log phase of growth.
[b]Reads were mapped to the *D. stibiiarsenatis* MLFW-2^T draft genome.

Table 4.S5. List of genes upregulated during exponential growth of MLFW-2^T on Sb(V) relative to As(V).

Locus ID	Description	Gene Name	COG Category[a]	Fold Change
BHU72_00010	SLH domain protein		S	3.1
BHU72_00045	Phosphoglucomutase	*pgm*	G	2.1
BHU72_00385	Flagellar protein	*flaG*	N	2.7
BHU72_00390	Flagellar secretion chaperone	*fliS*	N	2.7
BHU72_00395	Protein of unknown function		S	5.8
BHU72_00485	Acetylornithine/succinyldiaminopimelate aminotransferase	*argD*	E	4.2
BHU72_00490	Carbamoyl-phosphate synthase, small subunit	*carA*	F	2.8
BHU72_00495	Carbamoyl-phosphate synthase, large subunit	*carB*	F	3.1
BHU72_00500	Ornithine carbamoyltransferase	*argF*	E	3.3
BHU72_00625	ATP phosphoribosyltransferase regulatory subunit	*hisZ*	E	4.6
BHU72_00635	Histidinol dehydrogenase	*hisD*	E	6.0
BHU72_00665	Histidinol phosphate phosphatase	*hisK*	E	5.7
BHU72_00685	Nucleotide-binding protein		S	2.0
BHU72_00705	Cytochrome c-type biogenesis protein	*ccdA*	O	2.0
BHU72_00710	Glyceraldehyde-3-phosphate dehydrogenase	*gapA*	G	2.2
BHU72_00720	2,3-bisphosphoglycerate-independent phosphoglycerate mutase	*gpmI*	G	2.1
BHU72_00755	[4Fe-4S] ferredoxin		C	5.0
BHU72_00760	Aldehyde:ferredoxin oxidoreductase		C	3.5

Locus ID	Description	Gene Name	COG Category[a]	Fold Change
BHU72_01005	ArsR family transcriptional regulator		K,T	2.2
BHU72_01010	Cadmium-exporting P-type ATPase	*cadA*	P,V	2.2
BHU72_01145	Anaerobic ribonucleoside-triphosphate reductase		F	3.5
BHU72_01180	Aminopeptidase		E	2.2
BHU72_01310	2-nitropropane dioxygenase-like protein		C	2.2
BHU72_01325	AsnC family transcriptional regulator		K,T	2.9
BHU72_01330	Cysteine desulfurase	*iscS*	E	5.5
BHU72_01335	Iron-sulfur cluster assembly scaffold protein	*nifU*	C	3.6
BHU72_01340	U32 family peptidase		O	11.3
BHU72_01410	Citramalate synthase		E	5.0
BHU72_01425	LytTR-type response regulator		T	2.8
BHU72_01445	Indolepyruvate oxidoreductase	*iorA*	C	5.1
BHU72_01450	Phenylacetate-coenzyme A ligase	*paaK*	Q	9.3
BHU72_01455	C4-dicarboxylate ABC transporter, permease protein	*dctM*	G,P	9.3
BHU72_01460	Tripartite ATP-independent periplasmic transporter	*dctQ*	G,P	7.6
BHU72_01465	C4-dicarboxylate ABC transporter, periplasmic protein	*dctP*	G,P	5.4
BHU72_01470	Amino acid-binding protein		E	2.6
BHU72_01475	Phenylacetate-coenzyme A ligase	*paaK*	Q	3.3
BHU72_01510	Tryptophan synthase, beta subunit	*trpB*	E	5.4

Locus ID	Description	Gene Name	COG Category[a]	Fold Change
BHU72_01800	Vitamin B12-dependent methione synthase		E	3.3
BHU72_01805	5-methyltetrahydrofolate--homocysteine methyltransferase	*metH*	E	4.4
BHU72_01810	Methylenetetrahydrofolate reductase		E	3.4
BHU72_01815	UvrABC system protein C	*uvrC*	L	5.6
BHU72_01830	Succinate dehydrogenase, flavoprotein subunit	*sdhA*	C	2.2
BHU72_01850	Protein of unknown function		S	4.4
BHU72_02015	Metal-dependent phosphohydrolase		T	3.8
BHU72_02080	Anti-anti-sigma factor		T	6.0
BHU72_02185	Chemotaxis response regulator, protein-glutamate methylesterase	*cheB*	N,T	2.0
BHU72_02210	Aminomethyltransferase	*gcvT*	E	3.6
BHU72_02220	Glycine dehydrogenase (decarboxylating), subunit I	*gcvPA*	E	12.3
BHU72_02225	Glycine dehydrogenase (decarboxylating), subunit II	*gcvPB*	E	18.6
BHU72_02230	Protein of unknown function		S	8.4
BHU72_02235	Radical SAM domain protein		H	14.1
BHU72_02250	Vitamin B12-dependent ribonucleotide reductase	*nrdJ*	F	3.1
BHU72_02350	Alkaline-shock protein	*asp*	O,T	2.4
BHU72_02360	Integral membrane protein of unknown function		S	2.3
BHU72_02370	M22 family peptidase		O	5.4
BHU72_02405	Protein of unknown function		S	2.8

Locus ID	Description	Gene Name	COG Category[a]	Fold Change
BHU72_02455	Peptide-methionine (R)-S-oxide reductase	*msrB*	O	3.2
BHU72_02485	Aminotransferase		E,H	2.6
BHU72_02550	Phosphopentomutase	*deoB*	G	2.4
BHU72_02915	Coenzyme A biosynthesis bifunctional protein	*coaBC*	H	2.6
BHU72_02990	PEP-dependent dihydroxyacetone kinase, ADP-binding subunit	*dhaL*	S	2.1
BHU72_03225	Voltage-gated sodium channel		P	2.5
BHU72_03360	Flagellar biosynthesis protein	*fliO*	N	3.0
BHU72_03575	Dipicolinate synthase, beta subunit	*dpaB*	H	2.4
BHU72_03580	Aspartate-semialdehyde dehydrogenase	*asd*	E	3.1
BHU72_03585	Aspartokinase	*dapG*	E	5.1
BHU72_03590	4-hydroxy-tetrahydrodipicolinate synthase	*dapA*	E	2.9
BHU72_03595	Arsenical pump protein	*acr3*	P,V	2.2
BHU72_03710	Protein RecA	*recA*	L	2.8
BHU72_03875	Chorismate synthase	*aroC*	E	3.6
BHU72_03890	Anthranilate phosphoribosyltransferase	*trpD*	E	2.1
BHU72_03895	Indole-3-glycerol phosphate synthase	*trpC*	E	2.3
BHU72_03900	N-(5'-phosphoribosyl)anthranilate isomerase	*trpF*	E	2.2
BHU72_03905	Tryptophan synthase, beta subunit	*trpB*	E	2.6
BHU72_04070	CAP family transcriptional regulator (cNMP-binding)		T	2.3

Locus ID	Description	Gene Name	COG Category[a]	Fold Change
BHU72_04075	Formate-dependent phosphoribosylglycinamide formyltransferase	*purT*	F	3.0
BHU72_04100	Protein of unknown function		S	2.9
BHU72_04130	Glutamate synthase, large subunit	*gltB*	E	3.5
BHU72_04135	Glutamate synthase, small subunit	*gltD*	E	7.1
BHU72_04165	Copper-exporting P-type ATPase	*copA*	P,V	3.3
BHU72_04180	RarD family transporter		S	2.2
BHU72_04185	Rnd family efflux pump		V	2.3
BHU72_04190	Acriflavin resistance protein		V	2.7
BHU72_04210	Pentaheme c-type cytochrome		C	33.0
BHU72_04215	Pentaheme c-type cytochrome		C	33.3
BHU72_04240	Protein of unknown function		S	3.7
BHU72_04250	Homoserine O-acetyltransferase	*metA*	E	2.9
BHU72_04385	Protein of unknown function		S	2.1
BHU72_04390	Integral membrane metalloprotease	*htpX*	O	2.6
BHU72_04430	CheY superfamily transcriptional regulator		T	3.4
BHU72_04505	Protein of unknown function		S	2.8
BHU72_04510	Integral membrane protein of unknown function		S	2.0
BHU72_04520	ATP-dependent helicase/deoxyribonuclease, beta subunit	*addB*	L	3.1
BHU72_04525	ATP-dependent helicase/deoxyribonuclease, alpha subunit	*addA*	L	2.4

Locus ID	Description	Gene Name	COG Category[a]	Fold Change
BHU72_04535	Serine protease		O	2.4
BHU72_04545	Methyl-accepting chemotaxis transducer		N,T	2.9
BHU72_04700	Arginine-tRNA ligase	*argS*	J	3.6
BHU72_04710	Protein of unknown function		S	3.0
BHU72_04715	CheY superfamily transcriptional regulator		T	2.2
BHU72_04720	PAS domain response regulator		T	4.7
BHU72_04725	Histidine kinase		T	12.9
BHU72_04730	CheY superfamily transcriptional regulator		T	2.5
BHU72_04870	Peptide chain release factor 1	*prfA*	J	2.4
BHU72_04905	Methyl-accepting chemotaxis transducer		N,T	2.2
BHU72_04915	Aminoglycoside 3-N-acetyltransferase-like protein		V	4.4
BHU72_04920	Serine hydroxymethyltransferase	*glyA*	E	2.1
BHU72_04930	UDP-N-acetylglucosamine 2-epimerase	*mnaA*	M	2.1
BHU72_05095	SLH domain protein		S	2.4
BHU72_05190	UDP-N-acetylglucosamine 4,6-dehydratase (Inverting)	*pseB*	M	2.1
BHU72_05210	N-acetylneuraminate synthase	*pseI*	M	2.1
BHU72_05215	GNAT family N-acetyltransferase	*pseH*	M	2.0
BHU72_05240	DegT/DnrJ/EryC1/StrS aminotransferase		E	4.0
BHU72_05620	Glutamine synthetase	*glnA*	E	2.1

Locus ID	Description	Gene Name	COG Category[a]	Fold Change
BHU72_05625	Integral membrane protein of unknown function		S	3.9
BHU72_05630	Zinc efflux pump	*zitB*	P,V	5.6
BHU72_05635	ArsR family transcriptional regulator		K,T	5.0
BHU72_05710	Transketolase	*tkt*	G	2.5
BHU72_05750	Pyruvate carboxylase	*pyc*	C	2.2
BHU72_05800	Integral membrane protein of unknown function		S	5.0
BHU72_05805	Hydroxylamine reductase	*hcp*	C	3.0
BHU72_05810	Redox-active disulfide protein 2		O	2.0
BHU72_05850	Protein of unknown function		S	3.3
BHU72_05965	Tyrosine--tRNA ligase	*tyrS*	J	3.1
BHU72_06110	Glutamyl-tRNA(Gln) amidotransferase, alpha subunit	*gatA*	J	3.3
BHU72_06135	DNA ligase	*ligA*	L	2.2
BHU72_06145	ATP-dependent DNA helicase	*uvrD*	L	2.2
BHU72_06195	Phosphoribosylamine-glycine ligase	*purD*	F	3.4
BHU72_06200	Bifunctional purine biosynthesis protein	*purH*	F	4.2
BHU72_06215	Amidophosphoribosyltransferase	*purF*	F	5.0
BHU72_06225	Adenylosuccinate lyase	*purB*	F	3.2
BHU72_06230	N5-carboxyaminoimidazole ribonucleotide synthase	*purK*	F	3.1
BHU72_06305	Sec-independent protein translocase protein	*tatC*	U	2.2

Locus ID	Description	Gene Name	COG Category[a]	Fold Change
BHU72_06310	Sec-independent protein translocase protein	*tatA*	U	2.1
BHU72_06315	Redox-sensing transcriptional repressor	*rex*	K,T	2.5
BHU72_06320	Molybdopterin-guanine dinucleotide biosynthesis protein	*moeA*	H	2.5
BHU72_06325	Molybdopterin-guanine dinucleotide biosynthesis protein	*moaB*	H	4.7
BHU72_06375	tRNA N6-adenosine threonylcarbamoyltransferase	*tsaD*	O	2.9
BHU72_06435	Probable manganese/zinc-exporting P-type ATPase	*ctpC*	P,V	2.0
BHU72_06760	FlaG-like flagellar protein		N	2.1
BHU72_06820	ABC transporter, permease protein		P	3.2
BHU72_06840	Histidine kinase		T	14.6
BHU72_06885	Histidine kinase		T	2.2
BHU72_07115	Molybdate ABC transporter, substrate-binding protein	*modA*	P	2.5
BHU72_07120	Molybdenum ABC transporter, permease subunit	*modB*	P	2.0
BHU72_07135	Diheme c-type cytochrome		C	498.8
BHU72_07140	4[4Fe-4S] ferredoxin, CISM ETS Subunit		C	682.3
BHU72_07145	Mo-*bis*MGD-containing CISM catalytic subunit		C	549.8
BHU72_07150	TorD family cytoplasmic chaperone		O	92.2
BHU72_07155	4[4Fe-4S] ferredoxin		C	5.2
BHU72_07160	ABC transporter, periplasmic phosphonate-binding protein		P	5.3
BHU72_07165	Histidine kinase		T	6.4

Locus ID	Description	Gene Name	COG Category[a]	Fold Change
BHU72_07170	LuxR family transcriptional regulator		T	7.3
BHU72_07200	2-hydroxyglutaryl-CoA dehydratase		I	2.5
BHU72_07215	Integral membrane protein of unknown function		S	3.3
BHU72_07225	Phosphatidylglycerol lysyltransferase	*mprF*	V	2.2
BHU72_07230	ABC transporter, substrate-binding protein		P	2.5
BHU72_07290	Asparagine synthase (glutamine-hydrolyzing)	*asnB*	E	2.7
BHU72_07345	Membrane-bound selenate reductase, ETS subunit	*srdB*	C	41.0
BHU72_07350	Membrane-bound selenate reductase, EES subunit	*srdC*	C	56.1
BHU72_07355	Membrane-bound selenate reductase, catalytic subunit	*srdA*	C	25.1
BHU72_07365	Polysaccharide deacetylase		G	2.8
BHU72_07375	Mo-*bis*MGD-containing CISM catalytic subunit		C	2.1
BHU72_07400	LysR family transcriptional regulator		K,T	2.2
BHU72_07510	Branched chain amino acid ABC transporter, ATP-binding protein	*livF*	E,P	2.1
BHU72_07695	Peptidoglycan glycosyltransferase	*ftsW*	D,M	5.5
BHU72_07805	Bifunctional protein PyrR	*pyrR*	F	3.6
BHU72_07810	Uracil permease	*pyrP*	F	4.0
BHU72_07815	Dihydroorotase	*pyrC*	F	7.4
BHU72_07820	Carbamoyl-phosphate synthase, small subunit	*carA*	F	8.5
BHU72_07825	Carbamoyl-phosphate synthase, large subunit	*carB*	F	8.9

Locus ID	Description	Gene Name	COG Category[a]	Fold Change
BHU72_07830	Dihydroorotate dehydrogenase B (NAD^+), electron transfer subunit	*pyrK*	C	9.6
BHU72_07835	Dihydroorotate dehydrogenase	*pyrD*	F	8.4
BHU72_07840	Orotidine 5'-phosphate decarboxylase	*pyrF*	F	7.1
BHU72_07845	Orotate phosphoribosyltransferase	*pyrE*	F	5.4
BHU72_07850	Integral membrane 2[4Fe-4S] ferredoxin		C	2.2
BHU72_07880	Cystathionine gamma-synthase	*metB*	E	2.4
BHU72_07935	Precorrin-6y C5,15-methyltransferase	*cbiE*	H	2.1
BHU72_07950	Cobalt-precorrin-5A hydrolase	*cbiG*	H	2.3
BHU72_07985	Cobyric acid synthase	*cobQ*	H	2.6
BHU72_08165	RNA-binding protein	*hfq*	O,T	2.3
BHU72_08435	Histidine kinase		T	2.8
BHU72_08450	Protein of unknown function		S	25.3
BHU72_08515	Branched-chain amino acid aminotransferase	*ilvE*	E	2.7
BHU72_08520	Epimerase family protein	*yfhF*	M	7.1
BHU72_08550	Protein of unknown function		S	4.2
BHU72_08560	EAL- and GGDEF-domain signaling protein		T	2.5
BHU72_08600	S-adenosylmethionine:tRNA ribosyltransferase-isomerase	*queA*	J	3.1
BHU72_08830	Integral membrane protein of unknown function		S	3.8
BHU72_08910	U32 family peptidase		O	3.3

Locus ID	Description	Gene Name	COG Category[a]	Fold Change
BHU72_08970	Alpha-1,4 glucan phosphorylase	*glgP*	G	2.9
BHU72_08975	4-alpha-glucanotransferase	*malQ*	G	2.1
BHU72_09005	Plasmid segregation protein	*stbA*	O	3.1
BHU72_09180	Leucine--tRNA ligase	*leuS*	J	2.4
BHU72_09185	ComEA-like competence protein		L	2.5
BHU72_09300	3-Isopropylmalate dehydrogenase	*leuB*	C	2.9
BHU72_09305	3-isopropylmalate dehydratase, small subunit	*leuD*	E	3.2
BHU72_09310	3-isopropylmalate dehydratase, large subunit	*leuC*	E	3.1
BHU72_09315	2-Isopropylmalate synthase	*leuA*	E	5.5
BHU72_09320	Ketol-acid reductoisomerase ($NADP^+$)	*ilvC*	E	2.6
BHU72_09325	Acetolactate synthase, small subunit	*ilvH*	E	3.1
BHU72_09330	Acetolactate synthase, large subunit	*ilvB*	E	4.0
BHU72_09335	Dihydroxy-acid dehydratase	*ilvD*	E,G	2.9
BHU72_09340	Prephenate dehydratase	*pheA*	E	2.2
BHU72_09345	pyrroline-5-carboxylate reductase	*proC*	E	4.1
BHU72_09350	Gamma-glutamyl phosphate reductase	*proA*	E	3.8
BHU72_09355	Glutamate 5-kinase	*proB*	E	3.3
BHU72_09395	Allophanate hydrolase, subunit II	*kipA*	E	4.9
BHU72_09600	Phosphate import system, ATP-binding protein	*pstB*	P	3.7

Locus ID	Description	Gene Name	COG Category[a]	Fold Change
BHU72_09605	Phosphate import system, permease protein	*pstA*	P	4.0
BHU72_09610	Phosphate import system, permease protein	*pstC*	P	4.5
BHU72_09615	Phosphate-binding protein	*pstS*	P	3.8
BHU72_09640	Methyl-accepting chemotaxis transducer		N,T	8.8
BHU72_09645	Fumarate hydratase	*fumB*	C	2.2
BHU72_09680	Membrane protein	*fxsA*	V	2.7
BHU72_09690	Pyruvate kinase	*pyk*	G	2.9
BHU72_09700	Acetyl-coenzyme A carboxylase, alpha subunit	*accA*	I	2.1
BHU72_09800	Reactive intermediate/imine deaminase	*ridA*	J	2.0
BHU72_10060	Integral membrane protein of unknown function		S	7.6
BHU72_10075	Protein of unknown function		S	428.8
BHU72_10080	Integral membrane protein of unknown function		S	554.9
BHU72_10085	Integral membrane protein of unknown function		S	593.1
BHU72_10090	Integral membrane [4Fe-4S] ferredoxin		C	637.8
BHU72_10180	Protein of unknown function		S	17.0
BHU72_10190	Protein of unknown function		S	2.4
BHU72_10195	Arsenical pump ATPase	*arsA*	P,V	3.3
BHU72_10200	Arsenical pump protein	*acr3*	P,V	2.5
BHU72_10335	Protein of unknown function		S	2.7

Locus ID	Description	Gene Name	COG Category[a]	Fold Change
BHU72_10385	EAL-,CBS-, and GGDEF-domain signaling protein		T	5.7
BHU72_10440	L-serine dehydratase, alpha subunit	*sdaA*	E	2.3
BHU72_10445	L-serine dehydratase, beta subunit	*sdaB*	E	3.2
BHU72_10490	Catalase-peroxidase	*katG*	P,V	2.8
BHU72_10560	Disulfide bond formation protein D	*bdbD*	O	2.8
BHU72_10565	Disulfide bond formation protein C	*bdbC*	O	3.8
BHU72_10600	Zinc-finger domain protein		S	2.2
BHU72_10620	Inosine-5'-monophosphate dehydrogenase	*guaB*	F	2.7
BHU72_10630	D-alanyl-D-alanine carboxypeptidase	*dacF*	M	3.5
BHU72_10655	Xanthine dehydrogenase	*xdhA*	C	3.5
BHU72_10685	Pyridoxal-5'-phosphate-dependent protein, beta subunit		E	2.7
BHU72_10700	Small multidrug export protein		V	3.0
BHU72_10705	L-lactate dehydrogenase	*ldh*	C	3.1
BHU72_10850	Selenium-dependent molybdenum hydroxylase system protein	*yqeB*	O	2.5
BHU72_10975	Orn/Lys/Arg decarboxylase		E	2.2
BHU72_11200	L-aspartate oxidase	*nadB*	H	2.8
BHU72_11260	Cysteine synthase	*cysK*	E	3.9
BHU72_11420	Ribosomal protein L11 methyltransferase	*prmA*	J	3.6
BHU72_11500	Integral membrane metal-dependent phosphohydrolase		T	2.0

Locus ID	Description	Gene Name	COG Category[a]	Fold Change
BHU72_11545	Putative pyruvate, phosphate dikinase regulatory protein		T	2.1
BHU72_11575	Integral membrane protein of unknown function		S	3.7
BHU72_11580	tRNA (adenine(22)-N(1))-methyltransferase	*trmK*	J	2.1
BHU72_11775	Resolvase/invertase-type recombinase		L	6.2
BHU72_11785	Integral membrane protein of unknown function		S	2.1
BHU72_11955	Terminase		L	2.3
BHU72_11975	Protein of unknown function		S	4.1
BHU72_12435	Dihydrofolate synthase/folylpolyglutamate synthase	*folC*	H	2.7
BHU72_12475	Type II secretion system protein		U	2.1
BHU72_12530	Integral membrane protein of unknown function		S	2.1
BHU72_12535	Integral membrane protein of unknown function		S	2.1
BHU72_12580	Rod shape-determining protein	*mreB*	D,M	2.4
BHU72_12585	Cell shape-determining protein	*mreC*	D,M	3.7
BHU72_12600	Probable septum site-determining protein	*minC*	D	2.7
BHU72_12770	tRNA uridine 5-carboxymethylaminomethyl modification enzyme	*mnmG*	D	2.2
BHU72_12795	Cysteine desulfurase	*csd*	E	4.2
BHU72_12830	Pyridinium-3,5-bisthiocarboxylic acid mononucleotide, Ni insertion protein	*larC*	O	2.1
BHU72_12835	1-(5-phosphoribosyl)-5-amino-4-imidazole-carboxylate carboxylase		F	2.5
BHU72_12915	GGDEF-domain signaling protein		T	2.1

Locus ID	Description	Gene Name	COG Category[a]	Fold Change
BHU72_12960	Histidine kinase		T	3.0
BHU72_12980	Metallo-beta-lactamase		V	3.4
BHU72_12990	Serine protease		O	2.2
BHU72_13325	DNA alkylation repair protein		L	2.9
BHU72_13440	Uracil-DNA glycosylase	*ung*	L	3.0
BHU72_13500	Protein of unknown function		S	3.3
BHU72_13510	PAS- and GGDEF-domain signaling protein		T	2.4
BHU72_13550	YD repeat protein		S	2.7
BHU72_13605	ABC transporter, permease protein		P	2.1
BHU72_13640	DEAD/DEAH box helicase		L	2.4
BHU72_13670	Sodium-dependent bicarbonate transporter family protein		P	2.4
BHU72_13675	Nitrogen regulatory protein PII	*glnB*	E	2.7
BHU72_13855	Type I DNA topoisomerase		L	2.2
BHU72_13865	Cysteine--tRNA ligase	*cysS*	J	2.2
BHU72_14140	Cobalt ABC transporter, permease protein	*cbiQ*	P	2.8
BHU72_14255	Ubiquitin-like protein		O	64.6
BHU72_14260	OmpR family transcriptional regulator		T	39.3
BHU72_14265	Histidine kinase		T	21.3
BHU72_14315	Macrolide export system, ATP-binding protein		V	2.4

Locus ID	Description	Gene Name	COG Category[a]	Fold Change
BHU72_14320	Macrolide export system, permease protein		V	2.1
BHU72_14385	Oxaloacetate decarboxylase, alpha subunit	*oadA*	C	6.0
BHU72_14390	Glutaconyl-CoA decarboxylase, beta subunit	*gcdB*	C	3.5
BHU72_14395	Glutaconyl-CoA decarboxylase, gamma subunit	*gcdC*	I	3.3
BHU72_14400	Sodium ion-translocating decarboxylase		P	4.5
BHU72_14405	Acetyl-coenzyme A carboxylase		I	2.6
BHU72_14425	Aldehyde:ferredoxin oxidoreductase		C	3.0
BHU72_14430	Tricarboxylate transporter		P	2.0
BHU72_14630	Protein of unknown function		S	2.1
BHU72_15190	Transposase IS66		L	2.7

[a]Letters correspond to the following COG functional categories: C, Energy production and conversion; D, Cell cycle control, cell division, and chromosome partitioning; E, Amino acid transport and metabolism; F, Nucleotide transport and metabolism; G, Carbohydrate transport and metabolism; H, Coenzyme transport and metabolism; I, Lipid transport and metabolism; J, Translation/ Ribosomal structure and biogenesis; K, Transcription; L, Replication, recombination, and repair; M, Cell wall, membrane, and envelope biogenesis; N, Cell motility; O, Post-translational modification, protein turnover, and chaperones; P, Inorganic ion transport and metabolism; Q, Secondary metabolites biosynthesis, transport, and catabolism; S, Function unknown; T, Signal transduction mechanisms; U, Intracellular trafficking, secretion, and vesicular transport; V, Defense mechanisms.

Table 4.S6. List of genes downregulated during exponential growth of MLFW-2^T on Sb(V) relative to As(V).

Locus ID	Description	Gene Name	COG Category[a]	Fold Change
BHU72_00020	Integral membrane protein of unknown function		S	-6.2
BHU72_00080	Polysaccharide pyruvyl transferase	*csaB*	M	-2.2
BHU72_00355	Protein of unknown function		S	-2.8
BHU72_00360	XRE family transcriptional regulator		K,T	-4.0
BHU72_00405	Amino acid ABC transporter, permease protein		E,P	-9.0
BHU72_00410	Amino acid ABC transporter, ATP-binding protein		E,P	-7.5
BHU72_00415	Ribosome hibernation promoting factor	*hpf*	J	-2.5
BHU72_00420	Integral membrane protein of unknown function		S	-2.4
BHU72_00460	Transketolase		G	-2.2
BHU72_00465	Integral membrane c-type cytochrome		C	-3.2
BHU72_00525	Flagellar export chaperone	*fliS*	N,O	-3.5
BHU72_00530	Flagellin	*fliC*	N	-3.1
BHU72_00565	CheW-like signal transduction protein		N,T	-2.5
BHU72_00730	Component of protein translocation complex	*secG*	U	-4.8
BHU72_00790	Protein of unknown function		S	-2.3
BHU72_00795	Protein of unknown function		S	-2.4
BHU72_00805	Protein of unknown function		S	-2.7
BHU72_00815	FtsW/RodA family cell division protein		D	-4.6

Locus ID	Description	Gene Name	COG Category[a]	Fold Change
BHU72_00830	Putative ATP-binding protein		S	-3.6
BHU72_00860	Methylated-DNA--protein-cysteine methyltransferase	*adaB*	L	-2.8
BHU72_00980	Rrf2 family transcriptional regulator		K,T	-4.6
BHU72_01030	Universal stress protein		T	-3.0
BHU72_01035	Sodium-independent sulfate transporter		P	-5.6
BHU72_01040	Universal stress protein		T	-4.8
BHU72_01045	Pentaheme c-type cytochrome		C	-6.2
BHU72_01055	GGDEF- and EAL-domain signaling protein		T	-5.7
BHU72_01195	Alkyl hydroperoxide reductase	*ahpC*	V	-5.5
BHU72_01205	Metallophosphoesterase		S	-2.3
BHU72_01305	Integral membrane protein of unknown function		S	-2.9
BHU72_01505	Integral membrane tetraheme c-type cytochrome		C	-3.0
BHU72_01560	Protein of unknown function		S	-3.2
BHU72_01740	MarR family transcriptional regulator		K,T	-3.5
BHU72_01790	Disulfide oxidoreductase		C	-4.3
BHU72_01900	Protein of unknown function		S	-2.6
BHU72_01985	Membrane protein TraX	*traX*	U	-4.0
BHU72_02010	Methyl-accepting chemotaxis signal transducer		N,T	-2.7
BHU72_02265	Elongation factor P	*efp*	J	-2.3

Locus ID	Description	Gene Name	COG Category[a]	Fold Change
BHU72_02450	Stage 0 sporulation protein A homolog		D,T	-2.8
BHU72_02460	Universal stress protein		T	-2.4
BHU72_02465	Hydroxylamine reductase	*hcp*	C	-4.5
BHU72_02535	Integral membrane c-type cytochrome		C	-2.4
BHU72_02740	Protein of unknown function		S	-3.0
BHU72_02835	6-carboxy-5,6,7,8-tetrahydropterin synthase	*queD*	H	-2.1
BHU72_02870	Sirohydrochlorin cobaltochelatase	*cbiX*	H	-2.5
BHU72_02980	50S ribosomal protein l28	*rpmB*	J	-7.3
BHU72_03040	Protein of unknown function		S	-11.9
BHU72_03045	50S ribosomal protein L32	*rpmF*	J	-3.1
BHU72_03050	FapR family transcriptional regulator		K,T	-2.6
BHU72_03065	2-nitropropane dioxygenase-like protein		I	-2.5
BHU72_03110	Transcriptional regulator		K,T	-4.2
BHU72_03115	Signal recognition particle protein	*ffh*	U	-5.0
BHU72_03120	30s ribosomal protein S16	*rpsP*	J	-13.8
BHU72_03125	Putative RNA-binding protein		S	-8.6
BHU72_03145	50S ribosomal protein L19	*rplS*	J	-14.3
BHU72_03150	Signal peptidase I	*lepB*	U	-2.2
BHU72_03155	Ribosome biogenesis GTPase A	*rbgA*	J	-2.6

Locus ID	Description	Gene Name	COG Category[a]	Fold Change
BHU72_03440	30S ribosomal protein S2	*rpsB*	J	-6.4
BHU72_03445	Elongation factor Ts	*tsf*	J	-4.4
BHU72_03450	Uridylate kinase	*pyrH*	F	-2.6
BHU72_03455	Ribosome recycling factor	*frr*	J	-3.4
BHU72_03540	30S ribosomal protein S15	*rpsO*	J	-7.6
BHU72_03635	Periplasmic nitrate reductase, catalytic subunit	*napA*	C	-3.3
BHU72_03640	Periplasmic nitrate reductase, diheme c-type cytochrome ETS	*napB*	C	-22.4
BHU72_03690	Ribosomal protein S12 methylthiotransferase	*rimO*	J	-2.1
BHU72_03715	Ribonuclease Y	*rny*	L	-2.1
BHU72_03720	Metallophosphoesterase		S	-2.2
BHU72_03725	Stage V sporulation protein S	*spoVS*	D	-2.3
BHU72_03745	Histone-like DNA-binding protein	*hup*	L	-6.7
BHU72_03790	Heptaprenyl diphosphate synthase, component 1	*hepS*	I	-2.1
BHU72_03825	Heptaprenyl diphosphate synthase, component 2	*hepT*	I	-2.0
BHU72_03830	Nucleoside diphosphate kinase	*ndk*	F	-7.0
BHU72_04015	CheY superfamily signal transducer		T	-2.5
BHU72_04025	ABC transporter, permease protein		P	-2.6
BHU72_04030	ABC transporter, ATP-binding protein		P	-5.3
BHU72_04060	DEAD/DEAH box RNA helicase		L	-2.8

Locus ID	Description	Gene Name	COG Category[a]	Fold Change
BHU72_04065	Cold-shock protein		K,T	-6.0
BHU72_04120	Histidine kinase		T	-2.5
BHU72_04270	DEAD/DEAH box RNA helicase		L	-2.3
BHU72_04275	ABC transporter, ATP-binding protein		P	-3.2
BHU72_04325	Major facilitator superfamily (MFS) transporter		P	-2.2
BHU72_04350	Sodium:proton antiporter		P	-5.8
BHU72_04405	GTP-binding protein	*typA*	T	-2.5
BHU72_04565	Protein of unknown function		S	-3.2
BHU72_04575	LysR family transcriptional regulator		K,T	-2.3
BHU72_04585	ABC transporter component		P	-2.0
BHU72_04615	Universal stress protein		T	-2.6
BHU72_04685	Pyruvoyl-dependent arginine decarboxylase	*pdaD*	E	-9.2
BHU72_04690	Polyamine aminopropyltransferase	*speE*	E	-5.1
BHU72_04855	50S ribosomal protein L31	*rpmE*	J	-2.2
BHU72_04860	YhcN/YlaJ-like spore lipoprotein		D	-11.1
BHU72_04865	Integral membrane protein of unknown function		S	-3.0
BHU72_04935	Integral membrane ATPase		S	-2.5
BHU72_04940	ATP synthase, subunit I	*atpI*	C	-3.6
BHU72_04945	ATP synthase, subunit A	*atpB*	C	-3.2

Locus ID	Description	Gene Name	COG Category[a]	Fold Change
BHU72_04950	ATP synthase, subunit C	*atpE*	C	-2.0
BHU72_04955	ATP synthase, subunit B	*atpF*	C	-2.2
BHU72_05000	NADH-quinone oxidoreductase, subunit D	*nuoD*	C	-2.3
BHU72_05400	YvtN family beta-propeller repeat protein		S	-4.4
BHU72_05405	Methyl-accepting chemotaxis signal transducer		N,T	-2.3
BHU72_05440	Integral membrane c-type cytochrome		C	-2.8
BHU72_05445	Integral membrane cytochrome		C	-2.3
BHU72_05450	Diheme c-type cytochrome		C	-2.4
BHU72_05485	Cupredoxin domain protein		P	-2.1
BHU72_05655	TetR family transcriptional regulator		K,T	-2.6
BHU72_05715	Chaperone protein	*htpG*	O	-2.2
BHU72_05770	TetR family transcriptional regulator		K,T	-4.6
BHU72_05775	Integral membrane protein of unknown function		S	-3.9
BHU72_05820	Transcriptional regulator		K,T	-4.2
BHU72_05825	Protein of unknown function		S	-8.6
BHU72_05910	Citrate synthase	*gltA*	C	-10.1
BHU72_05915	MarR family transcriptional regulator		K,T	-7.9
BHU72_05940	Transcriptional regulator		K,T	-2.9
BHU72_05945	Glycine betaine transporter, ATP-binding protein	*opuAA*	E	-412.7

Locus ID	Description	Gene Name	COG Category[a]	Fold Change
BHU72_05950	Glycine betaine transporter, permease protein	*opuAB*	E	-271.0
BHU72_05955	Glycine betaine transporter, substrate-binding protein	*gbuC*	E	-130.5
BHU72_05970	Type 12 Methyltransferase		S	-4.0
BHU72_05990	Polar amino acid ABC transporter, permease protein		E,P	-2.1
BHU72_05995	Polar amino acid ABC transporter, substrate-binding protein		E,P	-3.0
BHU72_06035	Restriction endonuclease		L,V	-4.4
BHU72_06040	Protein of unknown function		S	-2.1
BHU72_06120	[4Fe-4S] ferredoxin		C	-4.3
BHU72_06185	L-lysine 2,3-aminomutase	*kamA*	E	-9.1
BHU72_06260	Formate dehyrogenase, gamma subunit	*fdoI*	C	-18.4
BHU72_06265	Formate dehydrogenase, beta subunit	*fdoH*	C	-12.6
BHU72_06270	Formate dehydrogenase, alpha subunit	*fdoG*	C	-10.9
BHU72_06290	Chaperonin	*groS*	O	-3.7
BHU72_06415	GGDEF-domain signaling protein		T	-22.3
BHU72_06445	Protein of unknown function		S	-2.8
BHU72_06615	Glutamine--fructose-6-phosphate aminotransferase [isomerizing]	*glmS*	M	-2.2
BHU72_06700	CRISPR-associated endoribonuclease	*cas2*	L	-2.4
BHU72_06780	Integral membrane protein of unknown function		S	-2.1
BHU72_06810	Methyl-accepting chemotaxis signal transducer		N,T	-8.0

Locus ID	Description	Gene Name	COG Category[a]	Fold Change
BHU72_06875	Protein of unknown function		S	-2.8
BHU72_06950	SLH domain protein		S	-2.4
BHU72_07045	GGDEF-and EAL-domain signaling protein		T	-2.1
BHU72_07065	Integral membrane protein of unknown function		S	-2.6
BHU72_07070	Chaperone protein ClpB	*clpB*	O	-5.0
BHU72_07085	ABC transporter component		P	-3.9
BHU72_07100	Protein of unknown function		S	-20.8
BHU72_07105	CheY superfamily transcriptional regulator		T	-4.6
BHU72_07175	Rhodanese domain protein		P,V	-3.5
BHU72_07315	ABC transporter, periplasmic binding protein		P	-3.0
BHU72_07320	Histidine kinase		T	-2.3
BHU72_07460	Type 11 Methyltransferase		S	-11.9
BHU72_07465	Integral membrane protein of unknown function		S	-2.8
BHU72_07555	Protein of unknown function		S	-2.6
BHU72_07595	MATE family multidrug efflux transporter		V	-5.7
BHU72_07660	Cell division protein	*ftsL*	D	-4.0
BHU72_07895	Phosphoserine aminotransferase	*serC*	E	-2.1
BHU72_07900	Uridine kinase	*udk*	F	-2.1
BHU72_08045	Cytidylate kinase	*cmk*	F	-3.0

Locus ID	Description	Gene Name	COG Category[a]	Fold Change
BHU72_08050	Integral membrane protein of unknown function		S	-4.1
BHU72_08070	PDZ domain protein		S	-2.6
BHU72_08090	Phosphate propanoyltransferase	*pduL*	Q	-5.4
BHU72_08095	Metallo-beta-lactamase		V	-2.2
BHU72_08100	16S rRNA (Cytosine(1402)-N(4))-methyltransferase		J	-2.0
BHU72_08210	MerR family transcriptional regulator		K,T	-2.6
BHU72_08360	Integral membrane nucleotide cyclase		T	-2.5
BHU72_08380	Sodium-dependent transporter		P	-6.3
BHU72_08410	Integral membrane protein of unknown function		S	-6.3
BHU72_08420	[4Fe-4S] Ferredoxin		C	-2.3
BHU72_08430	SGNH hydrolase domain protein		S	-4.6
BHU72_08535	Protein of unknown function		S	-3.0
BHU72_08540	Pyrimidine/purine nucleoside phosphorylase		F	-3.1
BHU72_08585	Alkyl hydroperoxide reductase	*ahpC*	V	-3.3
BHU72_08800	tRNA cyclic N6-threonylcarbamoyladenosine(37) synthase	*tcdA*	H	-2.3
BHU72_09040	Fructose-1,6-bisphosphate aldolase, class II	*fbaA*	G	-2.6
BHU72_09055	Glutamine synthetase	*glnA*	E	-5.0
BHU72_09060	RNA-binding transcription antitermination regulator		T	-4.3
BHU72_09125	Protein of unknown function		S	-2.4

Locus ID	Description	Gene Name	COG Category[a]	Fold Change
BHU72_09130	Flavodoxin		C	-9.1
BHU72_09200	Thioredoxin	*trxA*	O	-2.1
BHU72_09380	Endonuclease IV	*nfo*	L	-2.4
BHU72_09480	50S ribosomal protein L20	*rplT*	J	-2.1
BHU72_09485	50S ribosomal protein L35	*rpmI*	J	-2.3
BHU72_09490	Translation initiation factor IF-3	*infC*	J	-2.8
BHU72_09495	Threonine--tRNA ligase	*thrS*	J	-2.7
BHU72_09500	Integral membrane protein of unknown function		S	-3.0
BHU72_09505	Monogalactosyldiacylglycerol synthase		M	-2.7
BHU72_09560	DNA-binding spore protein		O	-5.3
BHU72_09565	Glyceraldehyde-3-phosphate dehydrogenase	*gapA*	G	-2.1
BHU72_09740	GntR family transcriptional regulator		K,T	-2.3
BHU72_09780	Methyl-accepting chemotaxis signal transducer		N,T	-2.7
BHU72_09785	Ferritin	*ftnA*	P	-2.4
BHU72_09915	Protein of unknown function		S	-3.4
BHU72_09995	Integral membrane protein of unknown function		S	-2.1
BHU72_10100	Ferrous iron transporter B	*feoB*	P	-2.1
BHU72_10110	DtxR family transcriptional repressor		K,T	-3.2
BHU72_10140	1-acyl-sn-glycerol-3-phosphate acyltransferase	*plsC*	I	-2.7

Locus ID	Description	Gene Name	COG Category[a]	Fold Change
BHU72_10150	Magnesium transporter	*mgtE*	P	-4.8
BHU72_10155	Undecaprenyl-diphosphatase	*uppP*	V	-2.9
BHU72_10165	tRNA (cytidine(34)-2'-O)-methyltransferase	*trmL*	J	-4.3
BHU72_10235	LuxR family transcriptional regulator		T	-3.2
BHU72_10240	Histidine kinase		T	-2.2
BHU72_10245	ABC transporter, periplasmic binding protein		P	-2.2
BHU72_10255	ArsR family transcriptional regulator		K,T	-2.4
BHU72_10310	SLH domain protein		S	-3.7
BHU72_10320	TorD family cytoplasmic chaperone		O	-6.3
BHU72_10325	Respiratory arsenate reductase, ETS subunit	*arrB*	C	-30.3
BHU72_10330	Respiratory arsenate reductase, catalytic subunit	*arrA*	C	-28.6
BHU72_10355	Pyridoxal 5'-phosphate-dependent aminotransferase		E	-2.5
BHU72_10365	Hydrogenase maturation protease		O	-3.2
BHU72_10400	Rubrerythrin	*rbr*	C	-4.7
BHU72_10415	Hexaheme c-type cytochrome		C	-2.6
BHU72_10420	A/G-specific adenine glycosylase	*mutY*	L	-2.3
BHU72_10515	GNAT family N-acetyltransferase		M	-5.5
BHU72_10555	Ammonium transporter		P	-12.7
BHU72_10585	Integral membrane protein of unknown function		S	-3.9

Locus ID	Description	Gene Name	COG Category[a]	Fold Change
BHU72_10795	Integral membrane protein of unknown function		S	-2.0
BHU72_10835	Protein of unknown function		S	-2.1
BHU72_10875	c-type cytochrome biogenesis protein	*ccmH*	C	-3.2
BHU72_10925	Recombination protein RecR	*recR*	L	-2.0
BHU72_11005	Ribosomal RNA small subunit methyltransferase I	*rsmI*	J	-2.1
BHU72_11010	AbrB family transcriptional regulator		K,T	-3.5
BHU72_11035	Ribonuclease M5	*rnmV*	L	-2.1
BHU72_11040	Ribosomal RNA small subunit methyltransferase A	*rsmA*	J	-2.0
BHU72_11045	Veg protein	*veg*	T	-2.1
BHU72_11060	Putative septation protein	*spoVG*	D,M	-3.1
BHU72_11110	Histone-like DNA-binding protein	*hup*	L	-4.2
BHU72_11115	S4 RNA-binding domain protein	*yabO*	J	-4.2
BHU72_11135	S1 RNA-binding domain protein	*yabR*	J	-3.6
BHU72_11355	30S ribosomal protein S20	*rpsT*	J	-5.1
BHU72_11375	Elongation factor 4	*lepA*	J	-2.1
BHU72_11385	Ferric iron ABC transporter, substrate-binding protein		P	-8.2
BHU72_11390	Ferric iron ABC transporter, permease protein		P	-3.3
BHU72_11395	ABC transporter component		P	-2.1
BHU72_11400	Heat-inducible transcription repressor	*hrcA*	K,T	-3.3

Locus ID	Description	Gene Name	COG Category[a]	Fold Change
BHU72_11455	Histidine triad (HIT) family protein		F, G	-3.2
BHU72_11460	30S ribosomal protein S21	*rpsU*	J	-5.2
BHU72_11465	Aspartyl-tRNA amidotransferase		J	-5.9
BHU72_11515	GTPase Era	*era*	J	-3.9
BHU72_11685	Metallo-beta-lactamase		V	-2.7
BHU72_11695	Ktr potassium uptake system, protein D	*ktrD*	P	-2.5
BHU72_12155	Metal-dependent phosphohydrolase		T	-2.8
BHU72_12160	Protein of unknown function		S	-2.7
BHU72_12215	Protein of unknown function		S	-5.2
BHU72_12560	Protein of unknown function		S	-2.6
BHU72_12635	50S ribosomal protein L21	*rplU*	J	-5.5
BHU72_12640	Prp superfamily cysteine protease		O	-6.7
BHU72_12750	Ribonuclease P protein component	*rnpA*	J	-2.3
BHU72_12890	30S ribosomal protein S6	*rpsF*	J	-8.4
BHU72_12895	Single-stranded DNA-binding protein	*ssb*	L	-9.5
BHU72_12900	30S ribosomal protein S18	*rpsR*	J	-3.7
BHU72_13090	Integral membrane protein of unknown function		S	-8.6
BHU72_13095	RNA polymerase signa factor 70		K	-2.3
BHU72_13110	PAS domain phosphatase		T	-3.0

Locus ID	Description	Gene Name	COG Category[a]	Fold Change
BHU72_13210	Protein of unknown function		S	-2.6
BHU72_13235	Protein of unknown function		S	-3.2
BHU72_13240	2[4Fe-4S] ferredoxin		C	-3.2
BHU72_13280	Cytosine-specific methyltransferase		L	-2.9
BHU72_13285	Type-2 restriction enzyme BglII	*bglIIR*	L,V	-2.4
BHU72_13315	Protein of unknown function		S	-10.9
BHU72_13360	Quinolone resistance protein		V	-3.1
BHU72_13385	Phage recombinase	*xerC*	L	-3.0
BHU72_13600	Nickel ABC transporter, substrate-binding protein		P	-13.8
BHU72_13610	Peptide ABC transporter, permease protein		E,P	-2.4
BHU72_13620	Dipeptide ABC transporter, ATP-binding protein		E,P	-4.4
BHU72_13645	Protein of unknown function		S	-2.4
BHU72_13655	Heme ABC transporter, ATP-binding protein		P	-2.3
BHU72_13720	Peptidyl-prolyl cis-trans isomerase	*ppiB*	O	-2.9
BHU72_13750	ABC transporter, periplasmic component		P	-22.8
BHU72_13790	Transcriptional regulator CtsR	*ctsR*	K,T	-3.7
BHU72_13795	UVR domain protein	*yacH*	S	-2.2
BHU72_13835	Integral membrane protein of unknown function		S	-2.5
BHU72_13890	RNA polymerase sigma-H factor	*sigH*	K	-4.4

Locus ID	Description	Gene Name	COG Category[a]	Fold Change
BHU72_13895	Component of protein translocation complex	*secE*	U	-3.8
BHU72_13905	50S ribosomal protein L11	*rplK*	J	-2.9
BHU72_13910	50S ribosomal protein L1	*rplA*	J	-4.0
BHU72_13915	50S ribosomal protein L10	*rplJ*	J	-6.3
BHU72_13920	50S ribosomal protein L7/L12	*rplL*	J	-5.2
BHU72_13925	SAM-dependent methyltransferase		S	-6.6
BHU72_13940	50S ribosomal protein L7Ae-like protein	*rplGB*	J	-4.2
BHU72_13970	30S ribosomal protein S10	*rpsJ*	J	-3.5
BHU72_13975	50S ribosomal protein L3	*rplC*	J	-2.9
BHU72_13980	50S ribosomal protein L4	*rplD*	J	-2.4
BHU72_13990	50S ribosomal protein L2	*rplB*	J	-2.2
BHU72_14010	50S ribosomal protein L16	*rplP*	J	-2.2
BHU72_14015	50S ribosomal protein L29	*rpmC*	J	-2.2
BHU72_14020	30S ribosomal protein S17	*rpsQ*	J	-2.0
BHU72_14030	50S ribosomal protein L24	*rplX*	J	-2.0
BHU72_14125	50S ribosomal protein L17	*rplQ*	J	-2.0
BHU72_14150	50S ribosomal protein L13	*rplM*	J	-5.3
BHU72_14155	30S ribosomal protein S9	*rpsI*	J	-4.8
BHU72_14365	Integral membrane protein of unknown function		S	-2.3

Locus ID	Description	Gene Name	COG Category[a]	Fold Change
BHU72_14455	Integral membrane protein of unknown function		S	-2.5
BHU72_14525	Integral membrane protein of unknown function		S	-5.3
BHU72_14535	Protein of unknown function		S	-2.1
BHU72_14545	Protein of unknown function		S	-2.4
BHU72_14605	Protein of unknown function		S	-5.9
BHU72_14640	Integral membrane protein of unknown function		S	-2.2
BHU72_14650	XRE family transcriptional regulator		K,T	-3.7
BHU72_14655	Protein of unknown function		S	-7.0
BHU72_14670	Protein of unknown function		S	-2.2
BHU72_14675	Integral membrane protein of unknown function		S	-3.0
BHU72_14685	Protein of unknown function		S	-4.5
BHU72_14690	Protein of unknown function		S	-2.0
BHU72_14810	Putative DNA-binding protein		S	-2.5
BHU72_14960	Protein of unknown function		S	-2.4
BHU72_15090	Branched-chain amino acid ABC transporter, permease protein	*azlC*	E,P	-2.6
BHU72_15100	Protein of unknown function		S	-2.0

[a]Letters correspond to the following COG functional categories: C, Energy production and conversion; D, Cell cycle control, cell division, and chromosome partitioning; E, Amino acid transport and metabolism; F, Nucleotide transport and metabolism; G, Carbohydrate transport and metabolism; H, Coenzyme transport and metabolism; I, Lipid transport and metabolism; J, Translation/ Ribosomal structure and biogenesis; K, Transcription; L, Replication, recombination, and repair; M, Cell wall, membrane, and envelope biogenesis; N, Cell motility; O, Post-translational modification, protein turnover, and chaperones; P, Inorganic ion transport

and metabolism; Q, Secondary metabolites biosynthesis, transport, and catabolism; S, Function unknown; T, Signal transduction mechanisms; U, Intracellular trafficking, secretion, and vesicular transport; V, Defense mechanisms.

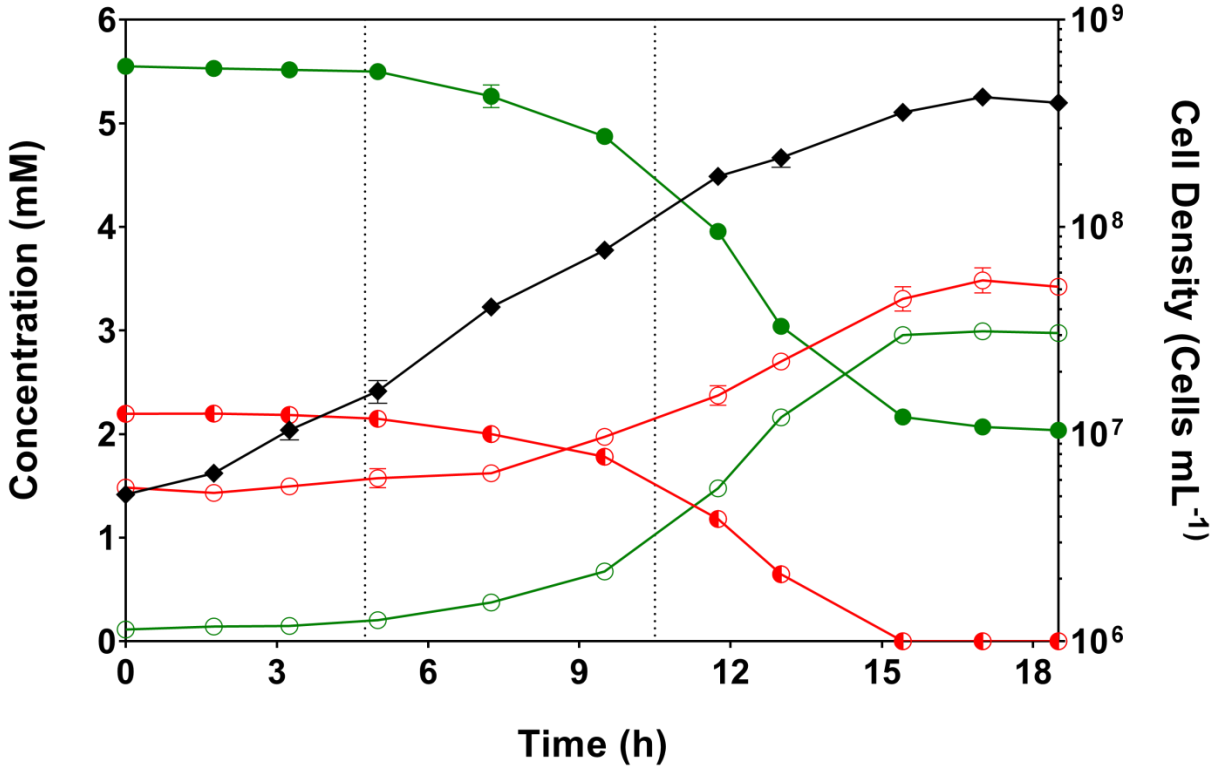

Figure 4.S1. Growth of MLFW-2^T on nitrite as the electron acceptor. Nitrite (◐); ammonium (○); lactate (●); acetate (○); cells (◆). Dotted vertical lines correspond to time points at which RNA was extracted from cultures.

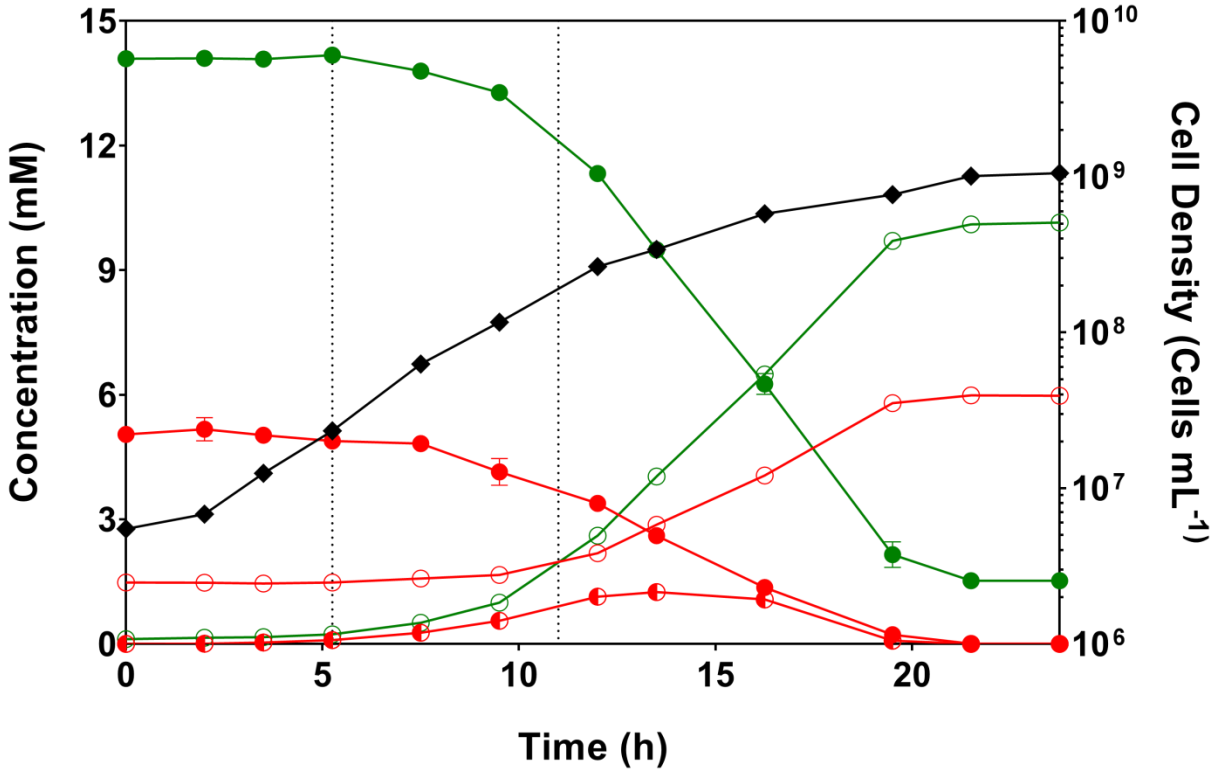

Figure 4.S2. Growth of MLFW-2^T on nitrate as the electron acceptor. Nitrate (●); nitrite (◐); ammonium (○); lactate (●); acetate (○); cells (◆). Dotted vertical lines correspond to time points at which RNA was extracted from cultures.

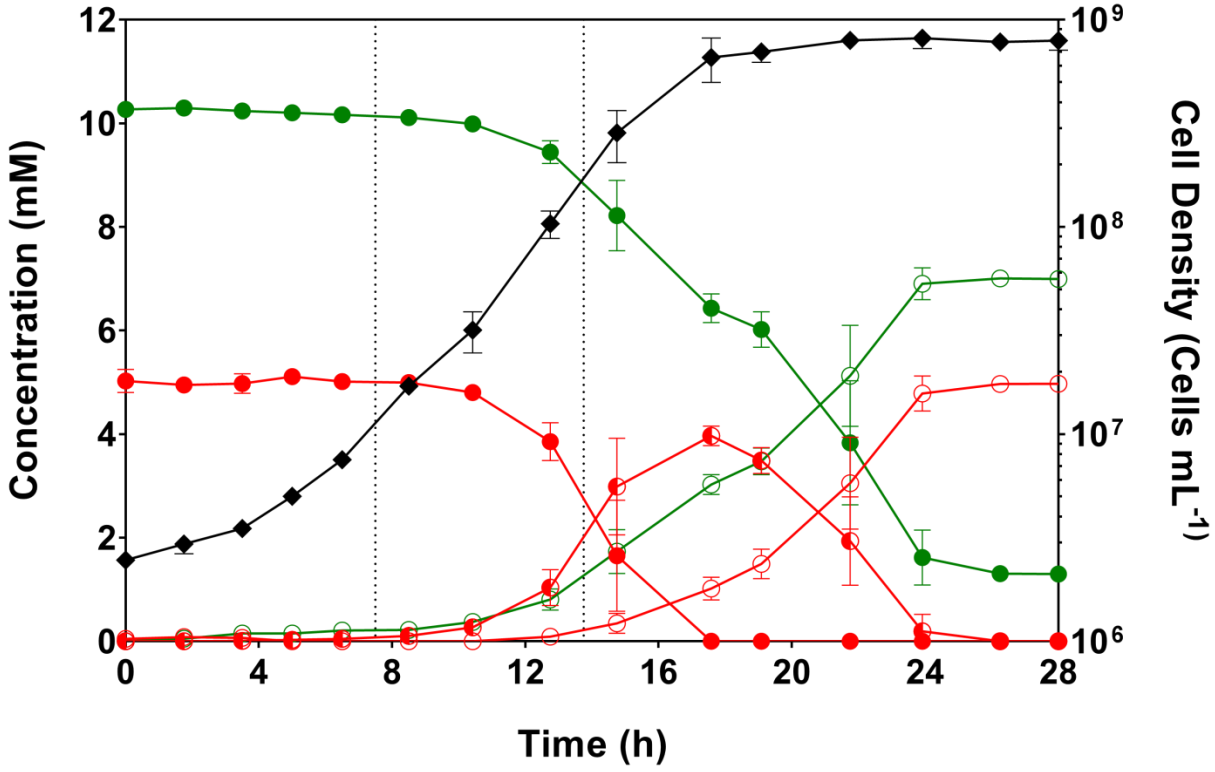

Figure 4.S3. Growth of MLFW-2^T on Se(VI) as the electron acceptor. Se(VI) (●); Se(IV) (◐); Se(0) (○); lactate (●); acetate (○); cells (◆). Dotted vertical lines correspond to time points at which RNA was extracted from cultures.

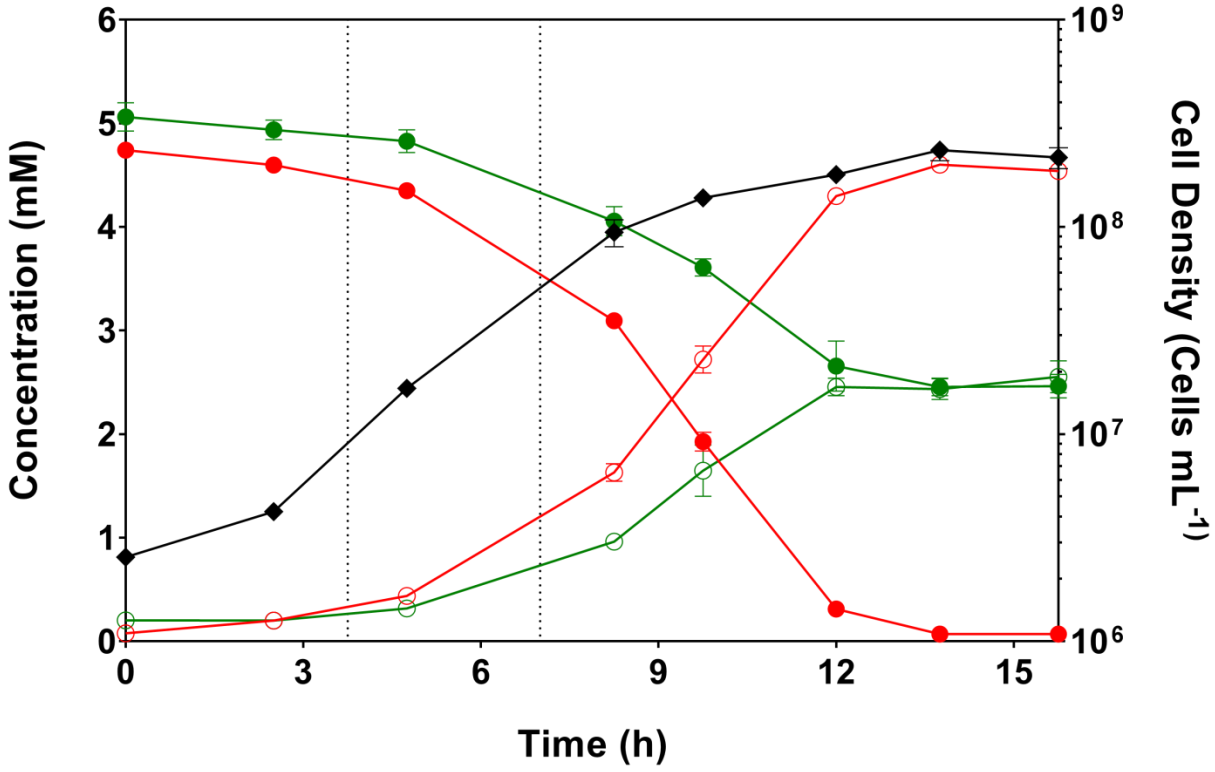

Figure 4.S4. Growth of MLFW-2^T on As(V) as the electron acceptor. As(V) (●); As(III) (○); lactate (●); acetate (○); cells (◆). Dotted vertical lines correspond to time points at which RNA was extracted from cultures.

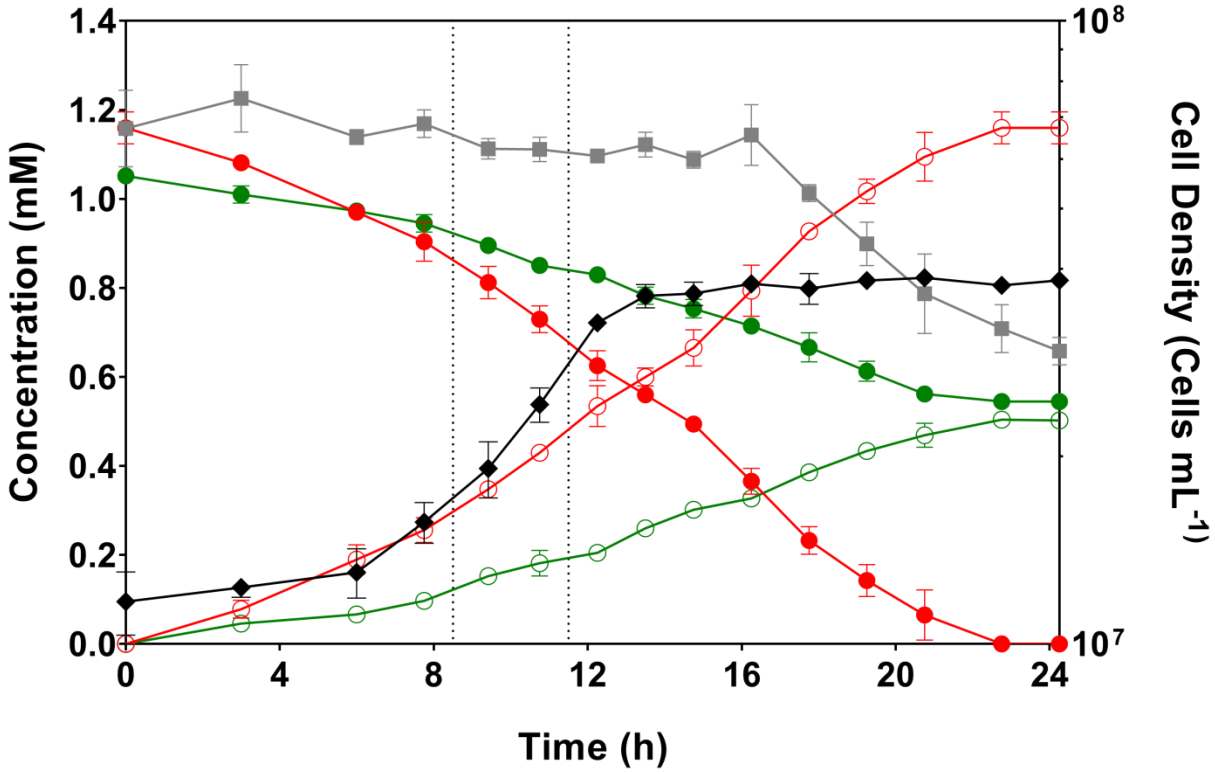

Figure 4.S5. Growth of MLFW-2^T on Sb(V) as the electron acceptor. Sb(V) (●); Sb(III) (○); total dissolved Sb (■); lactate (●); acetate (○); cells (◆). Dotted vertical lines correspond to time points at which RNA was extracted from cultures.

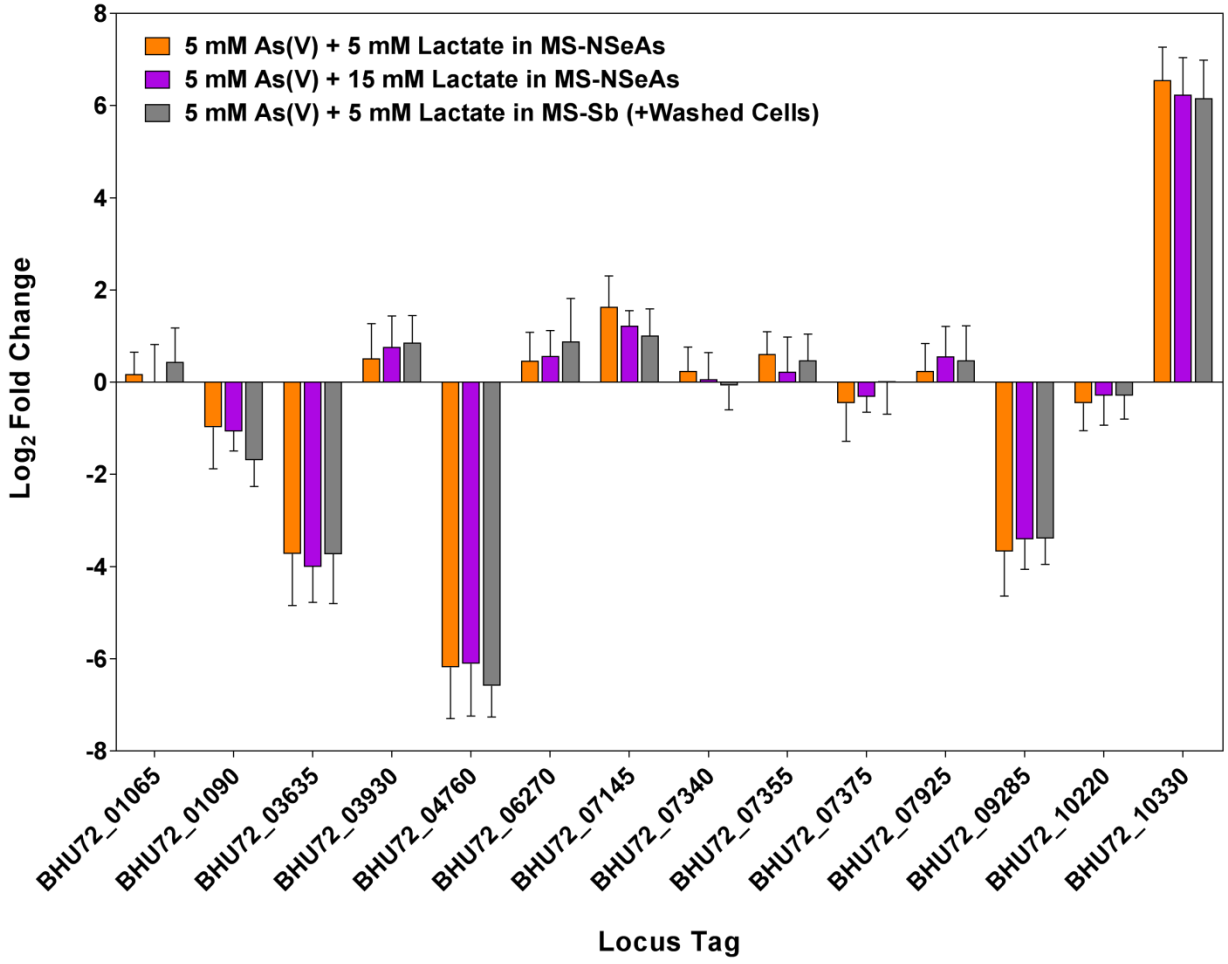

Figure 4.S6. Relative transcription of genes encoding the catalytic subunits of enzymes of the DMSOR family during exponential growth of MLFW-2^T on As(V) in control experiments. Transcription of each gene was normalized to the housekeeping gene *gyrB*, using growth on nitrite as a calibrator.

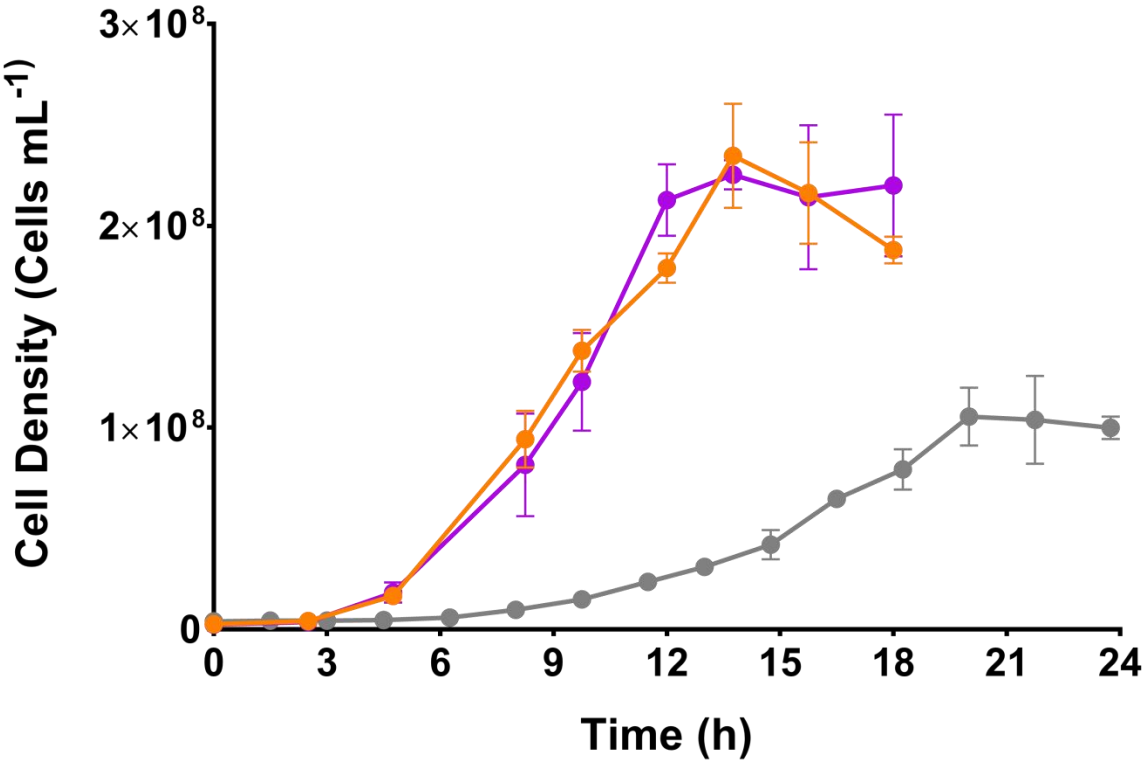

Figure 4.S7. Growth of MLFW-2^T on As(V) as the electron acceptor in control experiments. Control #1 [5 mM As(V) + 5 mM lactate in MS-NSeAs medium] (●); Control #2 [5 mM As(V) + 15 mM lactate in MS-NSeAs medium] (●); Control #3 [5 mM As(V) + 5 mM lactate in MS-Sb medium with an inoculum of washed cells] (●).

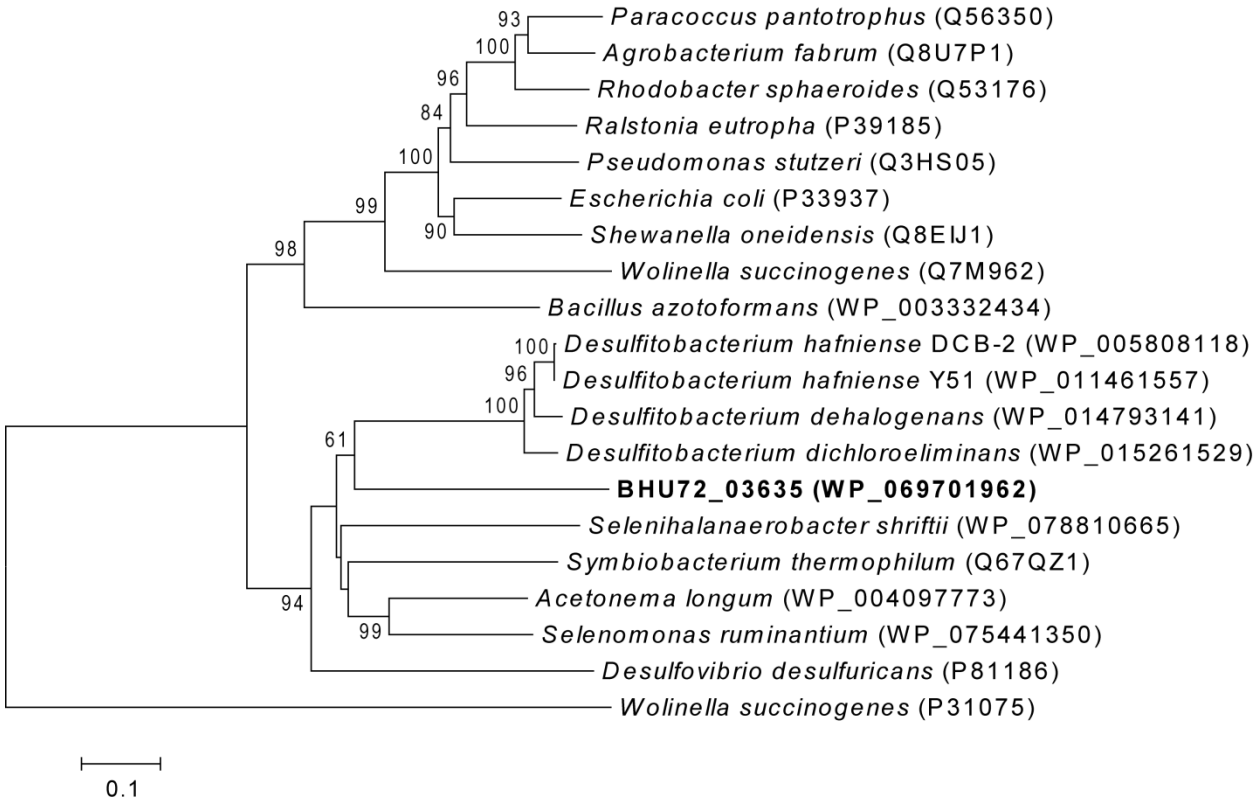

Figure 4.S8. Neighbor-joining phylogenetic tree based on inferred amino acid sequences showing the evolutionary relationship between the product of BHU72_03635 (bold) and NapA proteins from other organisms. Bootstrap values (≥ 50%) based on 1,000 replicates are shown at the nodes. RefSeq or UniProtKB/Swiss-Prot accession numbers are provided in parentheses. PsrA from *Wolinella succinogenes* was used as the outgroup. Scale bar, 0.1 substitutions per position.

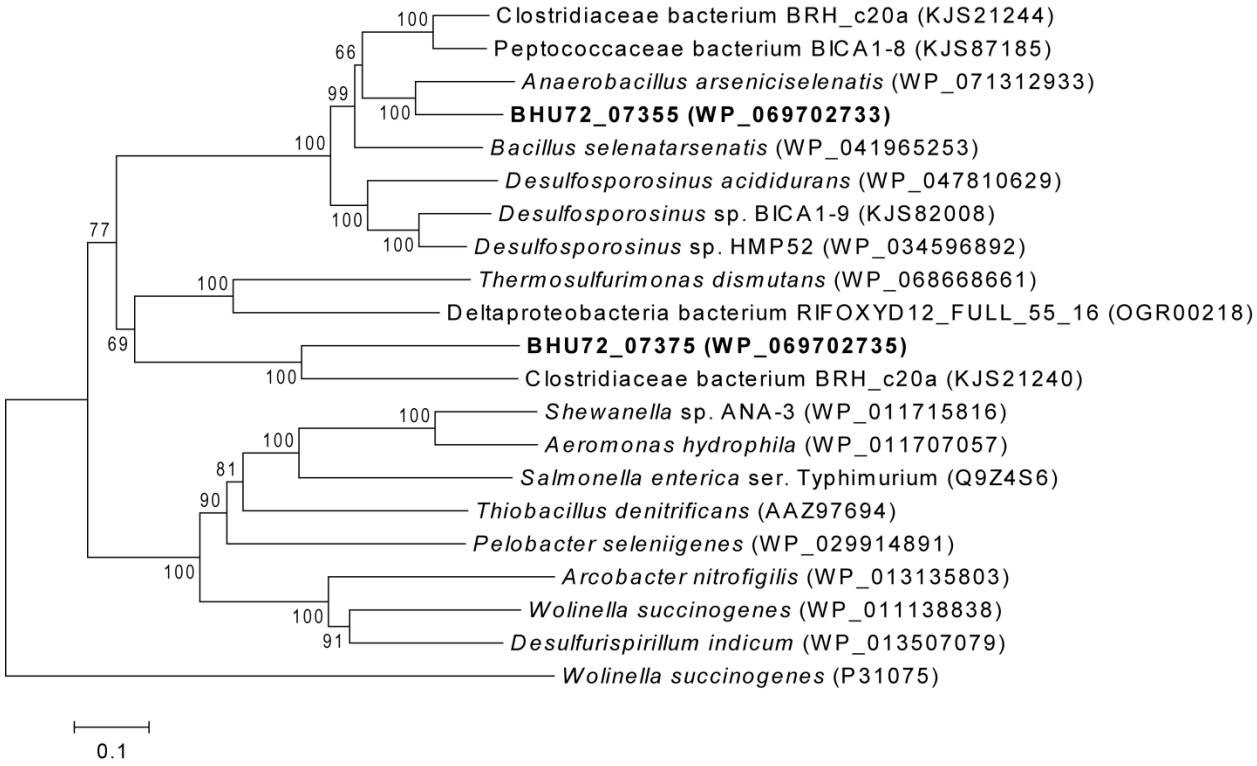

Figure 4.S9. Neighbor-joining phylogenetic tree based on inferred amino acid sequences showing the evolutionary relationship between the products of BHU72_07355 and BHU72_07375 (bold) and closely related proteins from other organisms. Bootstrap values (≥ 50%) based on 1,000 replicates are shown at the nodes. GenBank, RefSeq, or UniProtKB/Swiss-Prot accession numbers are provided in parentheses. PsrA from *Wolinella succinogenes* was used as the outgroup. Scale bar, 0.1 substitutions per position.

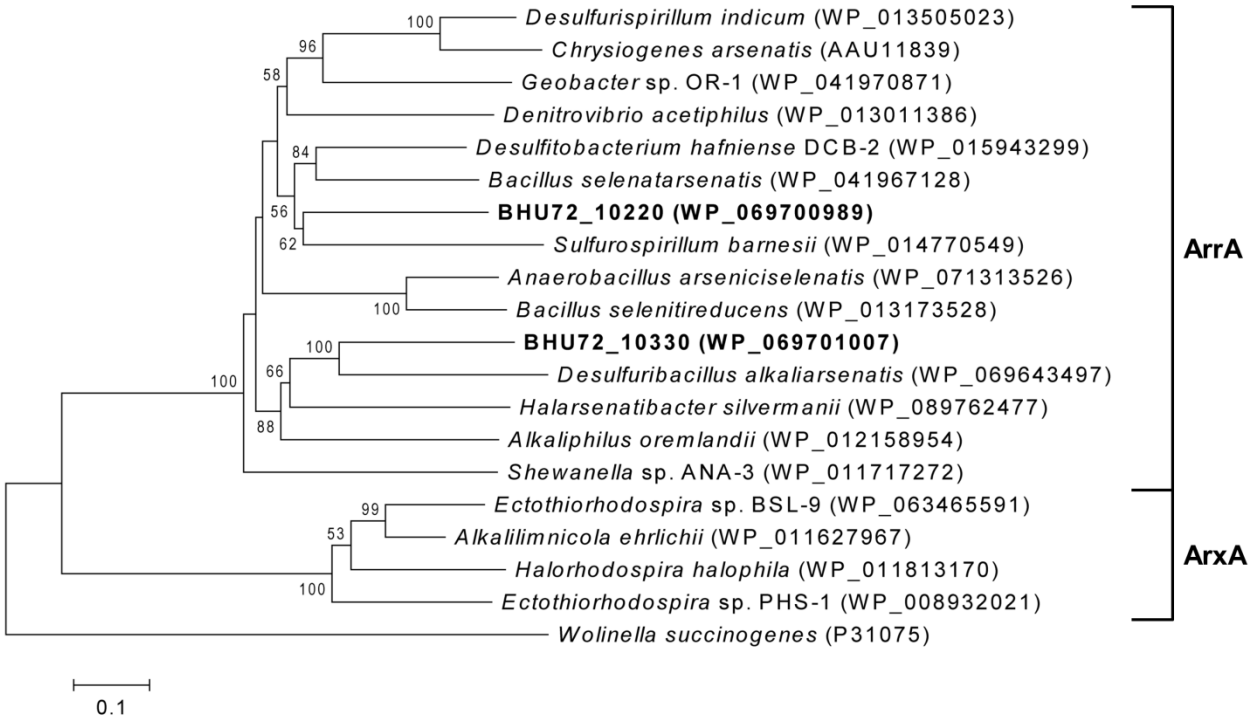

Figure 4.S10. Neighbor-joining phylogenetic tree based on inferred amino acid sequences showing the evolutionary relationship between the products of BHU72_10220 and BHU72_10330 (bold) and ArrA and ArxA proteins from other organisms. Bootstrap values (≥ 50%) based on 1,000 replicates are shown at the nodes. GenBank, RefSeq, or UniProtKB/Swiss-Prot accession numbers are provided in parentheses. PsrA from *Wolinella succinogenes* was used as the outgroup. Scale bar, 0.1 substitutions per position.

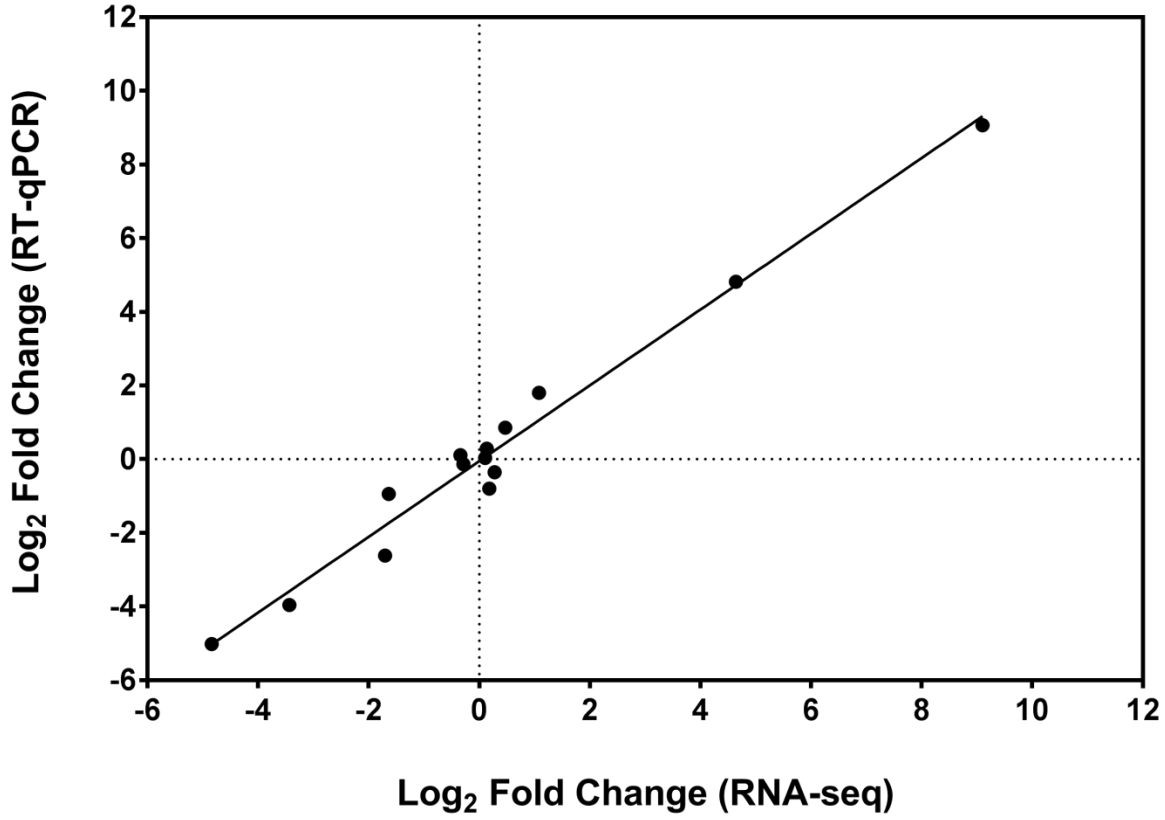

Figure 4.S11. Correlation between the RNA-seq and RT-qPCR data sets for all fourteen DMSOR family genes examined in this study. Relative transcription was assessed during exponential growth of MLFW-2^T on Sb(V) versus As(V) as electron acceptors.